

**FABRICATION OF BIOMEDICAL
COMPOSITE COATINGS BY
ELECTROPHORETIC DEPOSITION AND
DIP COATING METHODS**

**FABRICATION OF BIOMEDICAL
COMPOSITE COATINGS BY
ELECTROPHORETIC DEPOSITION AND DIP
COATING METHODS**

BY

ZHENGZHENG WANG, B.Eng., M.A.Sc.

A Thesis Submitted to the School of Graduate Studies in Partial
Fulfilment of the Requirements for the Degree Doctor of Philosophy

McMaster University © Copyright by Zhengzheng Wang, August 2024

Ph.D. Thesis – Zhengzheng Wang; McMaster University – Biomedical Engineering.

McMaster University DOCTOR OF PHILOSOPHY (2024) Hamilton, Ontario

(Biomedical Engineering)

TITLE: Fabrication of Biomedical Composite Coatings by Electrophoretic Deposition
and Dip Coating Methods

AUTHOR: Zhengzheng Wang

Master of Applied Science (McMaster University)

B.Eng. in Materials Science and Engineering (Zhengzhou University)

SUPERVISORS: Professor. Igor Zhitomirsky

Faculty of Engineering, McMaster University, Hamilton, Ontario, Canada

NUMBER OF PAGES: xxii, 229

Lay Abstract

There is a need to develop new coatings and manufacturing procedures for biomedical implant materials in order to extend the lifespan of orthopaedic implants used in clinical settings and avoid the need for expensive and unpleasant revision surgeries. Bioactive coatings enhance the durability of orthopaedic implants by reducing scar tissue formation and inflammation, while also increasing the chemical and physical bond between the synthetic implant and natural bone. As bone is a natural composite material, our goal in designing replacement materials is to replicate the inherent chemical composition and structure of human bone. Electrophoretic deposition (EPD) is a manufacturing technology that holds significant potential for creating composite coatings that imitate the structure of natural bone. This approach involves the application of an electric field to deposit charged materials onto a conductive substrate. The primary challenge in the manufacturing process of materials utilizing EPD is the tendency of particles in the precursor suspension to coagulate and distribute unevenly. This ultimately results in unwanted characteristics in the final coatings. An effective method to overcome this problem is by use dispersing agents, which are tiny molecules with either positive or negative charges that disperse particles in a suspension through electrostatic repulsion, physical separation, or a mix of both. Traditional dispersing agents have proven effective in various applications; nevertheless, their toxicity renders them unsuitable for the production of biological materials. This study presents the identification of novel dispersion agents, biomedical coatings, and manufacturing techniques for creating coatings that enhance the durability of implants and possess additional functionalities, such as biosensing for disease detection.

Abstract

It is essential to develop a new type of nanocomposite biomedical implant coatings that consist of bioactive ceramics and polymers, as well as customized surface characteristics. These coatings play a vital role in enhancing cell adhesion, proliferation, and interlocking at the interface between bone tissue and the implant. This development is crucial for prolonging the durability of orthopaedic implants. The utilization of combined colloidal and electrochemical processing techniques, specifically EPD and dip coating, enables the fabrication of these novel multi-component materials with relative simplicity. Additionally, they can be utilized to create nanostructures and surface topography that imitate the composition of human skeletal tissue on a nanoscale level. In addition, colloidal-electrochemical processing techniques can be easily scaled up for clinical product development and mass manufacture, unlike many regularly utilized nanotechnology processing techniques.

The absence of efficient and biocompatible dispersants and extractors is a significant obstacle to the widespread use of colloidal-electrochemical methods for fabricating novel biomaterials in EPD, as the success of this process relies on the utilization of a stable colloidal precursor. Biomimetics, sometimes known as gaining inspiration from the natural world, is one way to generating effective dispersion and extracting agents. Using this methodology, we identified novel extracting agents. These agents proved to be highly effective in extracting particles and forming composite films that combined organic and inorganic components, containing different sized of silica particles and polyvinylidene fluoride (PVDF). By extending the method, biomimetic inspiration was derived from the human digestive system, to use bile acid salts (BAS) as solubilizing, charging, dispersing and film-forming agents for the preparation of composite coatings, containing water insoluble drugs and proteins. These coatings have the potential to be

utilized for targeted administration of antibiotics, thereby preventing surgical infections after implantation. Furthermore, the inclusion of BAS surfactants enables the solubilization and dispersion of hydrophobic drugs and molecules, as well as the creation of composite films with functional properties using EPD. Moreover, a novel technique is devised for the anodic EPD of alginic acid polymer (AlgH) and composite films that contain drug molecules within the AlgH matrix. This approach entailed utilizing L-arginine as an alkalizing agent to enhance the solubility of medicines that have low solubility in water. AlgH and medication molecules are dissolved in water and then deposited via anodic EPD.

Dip coating remains a challenging task when it comes to depositing high concentrations of non-toxic solvents containing high molecular weight (M_w) polymers, such as poly(ethyl methacrylate) (PEMA) and poly(methyl methacrylate) (PMMA). In this study, we initially suggested the utilization of water-isopropanol as a co-solvent for dissolving high molecular weight PMMA at high concentrations. Additionally, we utilized an advanced dispersion agent to facilitate the solubilization of PEMA. It was discovered that water molecules can surround and solvate the carbonyl groups of the polymers. This technology avoided the use of noxious solvents and a protracted heating process for their elimination. In addition, these coatings have the potential to be integrated with advanced inorganic particles, such as drugs, diamond and HA, for use in biomedical applications.

Acknowledgements

I would like to express my deepest gratitude to my supervisor, Dr. Igor Zhitomirsky. Over the past seven years, he has been a constant source of guidance, support, patience, and understanding. His mentorship has been invaluable, not only in my academic journey but also in my personal growth. From the very beginning, when he gave me the opportunity to join his team as a graduate student, through to my doctoral studies, his unwavering belief in my potential has been a driving force behind my achievements. His encouragement and insightful advice have greatly shaped my research and helped me navigate the challenges of academia. Dr. Zhitomirsky is more than a supervisor; he is a mentor, a teacher, and a friend. Our long-standing relationship has been one of the most enriching experiences of my life. I am truly fortunate to have had the privilege of learning from him and working under his guidance.

I would also like to extend my heartfelt thanks to my committee members, Dr. Leyla Soleymani and Dr. Raja Gosh. Their advice and feedback at every stage of my doctoral journey have been crucial to the completion of my PhD. I am extremely fortunate to have had their support and guidance, and their insights have significantly contributed to my academic and research achievements.

Finally, I want to express my deepest appreciation to my family, including my parents, my husband, and my daughter. Their support has been invaluable throughout this unforgettable journey. I am especially grateful to my mother and my husband, whose unwavering presence and encouragement have given me the courage and strength to keep moving forward, no matter what challenges arose.

Table of Contents

Lay Abstract	ii
Abstract.....	iii
Acknowledgements	v
Table of Contents	vi
List of Figures and Tables	x
List of Abbreviations and Symbols.....	xix
Declaration of Academic Achievements	xxi
Chapter 1 Introduction.....	1
1.1. Background.....	1
1.2. Thesis Overview	5
1.3. References.....	8
Chapter 2 Literature Review	11
2.1. Orthopaedic Implant Materials	11
2.1.1. Metallic Materials for Orthopaedic Applications	11
2.1.2. Bioceramics and Bioactive Glasses	14
2.1.3. Polymers on Biomedical applications.....	22
2.2. Colloid Processing Techniques: Electrophoretic Deposition and Dip Coating	28
2.2.1. Fundamentals of Electrophoretic Deposition.....	28

2.2.2. Dip coating.....	45
2.3. Objectives	47
2.4. References.....	47
Chapter 3 Deposition of Organic-Inorganic Nanocomposite Coatings for Biomedical Applications	71
3.1. Abstract.....	71
3.2. Introduction.....	71
3.3. Experimental.....	73
3.4. Results and Discussion	74
3.5. Conclusions.....	85
3.6. Acknowledgements.....	86
3.7. References.....	86
Chapter 4 Surfactants for Electrophoretic Deposition of Polyvinylidene Fluoride–Silica Composites 96	
4.1. Abstract.....	96
4.2. Introduction.....	96
4.3. Experimental.....	98
4.4. Results and Discussion	100
4.5. Conclusions.....	109
4.6. Acknowledgements.....	109

4.7.	Supplementary data.....	110
4.8.	References.....	114
Chapter 5 Surfactant assisted dip-coating method for deposition of polyethylmethacrylate-diamond coatings..... 124		
5.1.	Abstract.....	124
5.2.	Introduction.....	125
5.3.	Experimental.....	128
5.4.	Results and Discussion	129
5.5.	Conclusions.....	141
5.6.	Acknowledgements.....	142
5.7.	References.....	142
Chapter 6 Bile Acid Salt as a Vehicle for Solubilization and Electrodeposition of Drugs and Functional Biomolecules for Surface Modification of Materials 148		
6.1.	Abstract.....	148
6.2.	Introduction.....	149
6.3.	Experimental.....	153
6.4.	Results and discussion	153
6.5.	Conclusions.....	164
6.6.	Acknowledgements.....	165
6.7.	References.....	165

Chapter 7 Application of Cyrene solvent for the fabrication of polymethyl methacrylate, polyethylmethacrylate and composite films containing hydroxyapatite and diamonds 173

7.1.	Abstract.....	173
7.2.	Introduction.....	173
7.3.	Experimental.....	177
7.4.	Results and Discussion	178
7.5.	Conclusion	188
7.6.	Acknowledgements.....	189
7.7.	References.....	189

Chapter 8 Strategies for alkali-free synthesis, surface modification and electrophoretic deposition of composite films for biomedical applications..... 197

8.1.	Abstract.....	197
8.2.	Introduction.....	198
8.3.	Experimental.....	202
8.4.	Results and Discussion	204
8.5.	Conclusion	215
8.6.	Acknowledgements.....	216
8.7.	References.....	216

Chapter 9 Conclusions and future work..... 226

List of Figures and Tables

Figure 2-1 Schematic illustration of electrophoretic deposition process. (a) Cathodic EPD and (b) anodic EPD[131] with permission from Elsevier.....	29
Figure 2-2 The force profiles (A) and the potential energy profiles (B) as functions of the separation distance between two particles, according to the DLVO theory[134], used with permission.	31
Figure 2-3 A simplified representation of the possible effects of polymer addition on the stability of colloidal system[142], used with permission.....	33
Figure 2-4 The schematic diagram of the electrical double layer associated with a positively charged surface in a liquid[141]	35
Figure 2-5 The electrical potential as a function of distance from the surface[141]	35
Figure 2-6 Schematic representation of steric stabilization of metal colloid particles[152], used with permission.....	37
Figure 2-7 Schematic representation of electrosteric stabilization of metal colloid particles[152], used with permission	38
Figure 2-8 Schematic diagram showing the polymer segments of poly(methacrylic acid) (PMAA) and poly(acrylic acid) (PAA)[154], used with permission	39
Figure 2-9 Schematic of mussel adsorption and chemical structure of catechol[156], used with permission.	41
Figure 2-10 Structure of molecules from catechol family[156], used with permission ...	42
Figure 2-11 Suggested adsorption mechanisms of caffeic acid: (a) bidentate chelating bonding, (b) bidentate bridging bonding (inner sphere), (c) bidentate bridging bonding (outer	

sphere) of catechol group, (d) adsorption, involving a carboxylic group[156], used with permission
 43

Figure 2-12 Graphical representation of dip coating technique[173], used with permission
 45

Figure 3-1 SEM images of PMMA coating: (A) as-deposited and room-temperature-dried,
 (B) annealed at 200 °C. 75

Figure 3-2 SEM images of (A,B) PMMA-Ag₂O, (C,D) PMMA-HA and PMMA-ZnO
 coatings, (A,C,E) as-deposited and room-temperature-dried, (B,D,F) annealed at 200 °C..... 77

Figure 3-3 SEM images of (A,B) PMMA-micron size composites and (C,D) PMMA-
 nanosilica composites, (A,C) as-deposited and room-temperature-dried, (B,D) annealed at 200 °C.
 78

Figure 3-4 X-ray diffraction patterns of (a) as-received PMMA, and composites (b)
 PMMA-ZnO, (c) PMMA-HA, (d) PMMA-Ag₂O and (e) PMMA-HAP-Ag₂O, ▼—JCPDS file 04-
 020-9583, ▲—JCPDS file 04-008-4759, ●—JCPDS file 00-041-1104, ◆—PMMA. 79

Figure 3-5 X-ray diffraction patterns of (a) PMMA, (b) micron size silica, (c) PMMA-
 micron size silica, (d) nanosilica and (e) PMMA-nanosilica (●—silica, ◆—PMMA). 80

Figure 3-6 TGA data for (A) PMMA-HA, (B) PMMA-Ag₂O, (C) PMMA-ZnO, (D)
 PMMA-micron size silica and (E) PMMA-nanosilica composites. 81

Figure 3-7 SEM images of as-deposited and room-temperature-dried coatings: (A) PMMA-
 ibuprofen, (B) PMMA-tetracycline and (C) PMMA-amoxicillin coatings. 82

Figure 3-8 X-ray diffraction patterns of (a) PMMA-amoxicillin, (b) PMMA-ibuprofen and
 (c) PMMA-tetracycline; major XRD peaks are labeled: ▲—peaks corresponding to JCPDS file 00-

039-1832 of amoxicillin, ●—peaks corresponding to JCPDS file 00-032-1723 of ibuprofen,◆—
peaks corresponding to JCPDS file 00-039-1985 of tetracycline. 83

Figure 3-9 FTIR spectra of (a) as-received PMMA (b) as-received ibuprofen, (c) PMMA-
ibuprofen, (d) asreceived tetracycline, (e) PMMA-tetracycline, (f) as-received amoxicillin and (g)
PMMA-amoxicillin. 84

Figure 4-1 TEM images of PVDF particles at (A,B) different magnifications. 100

Figure 4-2 Chemical structures of (A) THB, (B) CFA, (C) CA and (D) GA. 101

Figure 4-3 (A) Deposit mass achieved for different dispersants using 5 g L^{-1} PVDF
suspensions containing 1 g L^{-1} dispersants, (B) deposit mass versus PVDF concentration in
suspensions, containing 1 g L^{-1} dispersants for deposition time of 5 min and deposition voltage of
100 V. 104

Figure 4-4 SEM images of (A) as-deposited and (B) annealed PVDF films fabricated via
EPD from 5 g L^{-1} PVDF suspension containing 1 g L^{-1} GA as a dispersant. The films were obtained
at deposition time of 5 min and deposition voltage of 100 V. 104

Figure 4-5 Tafel plots for (a) uncoated substrate and (b) coated from 5 g L^{-1} PVDF
suspensions containing 1 g L^{-1} GA and annealed at $200 \text{ }^\circ\text{C}$. PVDF films were obtained at
deposition time of 5 min and deposition voltage of 100 V 105

Figure 4-6 Bode plots for (a) uncoated substrate and (b) coated from 5 g L^{-1} PVDF
suspensions containing 1 g L^{-1} GA and annealed at 200°C . PVDF films were obtained at deposition
time of 5 min and deposition voltage of 100V 106

Figure 4-7 SEM images at different magnifications for coatings deposited from 5 g L^{-1}
PVDF suspensions, containing 1 g L^{-1} GA and 1 g L^{-1} (A,B) nanosilica and (C,D) micron-size

silica and annealed at 200 °C. Deposition was performed during 5 min at a deposition voltage of 100 V. 107

Figure 4-8 Deposit mass versus silica concentration in 5 g L⁻¹ PVDF suspension containing 1 g L⁻¹ GA. Deposition was performed during 5 min at a deposition voltage of 100 V 108

Figure 4-9 Deposit mass achieved for different dispersants using 5 g L⁻¹ PVDF suspensions containing 1 g L⁻¹ dispersants for deposition time of 5 min and deposition voltage of 50V.....110

Figure 4-10 Deposit mass versus PVDF concentration in suspensions, containing 1 g L⁻¹ dispersants for deposition time of 5 min and deposition voltage of 50V.110

Figure 4-11 Deposit mass versus deposition time at a deposition voltage of 100 V for 5 g L⁻¹ PVDF suspensions.....111

Figure 4-12 Deposit mass versus deposition voltage for 5 g L⁻¹ PVDF suspensions at deposition time of 5 min.111

Figure 4-13 FTIR spectra of deposits, prepared from using 5 g L⁻¹ PVDF suspensions containing 1 g L⁻¹ dispersants: (a) THB, (b) CFA, (c) CA, (d) GA for deposition time of 5 min and deposition voltage of 100V and (e) as-received PVDF.112

Figure 4-14 Deposit mass versus nanosilica concentration in 5 g L⁻¹ PVDF suspension containing 2 g L⁻¹ GA at deposition time of 5 min at voltages of 50 V and 100 V.....113

Figure 4-15 SEM images of coatings, prepared from 5 g L⁻¹ PVDF solution, containing 1 g L⁻¹ GA (A) without silica, (B) with 1 g L⁻¹ nanosilica and (C) with 1 g L⁻¹ micron size silica deposited at a deposition voltage of 100V and deposition time of 5 min and annealed at 200°C for 1 h.....113

Figure 5-1 (A) Chemical structures of RLP: mono-RLP and di-RLP, (B) Chemical structure of GRA, (C) diamond suspensions in isopropanol without and with biosurfactants..... 131

Figure 5-2 SEM images of PEMA films prepared from 10 g L⁻¹ PEMA solutions, containing 2 g L⁻¹ (A) GRA and (B) RLP..... 131

Figure 5-3 Tafel plots for (a) uncoated stainless steel and coated with PEMA films prepared using (b) GRA and (c) RLP. Coated samples contained one dip-coated layer..... 133

Figure 5-4 EIS data presented in Bode plots for (a) uncoated stainless steel and coated with PEMA films prepared using (b) RLP and (c) GRA 133

Figure 5-5 Deposit mass of PEMA films versus number of deposited layers prepared from 10 g L⁻¹ PEMA solutions, containing 2 g L⁻¹ (a) GRA and (b) RLP..... 134

Figure 5-6 SEM images at different magnifications for films prepared from 10 g L⁻¹ PEMA solutions, containing 2 g L⁻¹ RLP and (A, B) 1 g L⁻¹ and (C,D) 3 g L⁻¹ microdiamond..... 136

Figure 5-7 SEM images at different magnifications for films prepared from 10 g L⁻¹ PEMA solutions, containing 2 g L⁻¹ RLP and (A, B) 1 g L⁻¹ and (C,D) 3 g L⁻¹ nanodiamond. 137

Figure 5-8 SEM images at different magnifications for films prepared from 10 g L⁻¹ PEMA solutions, containing 2 g L⁻¹ GRA and (A, B) 1 g L⁻¹ and (C,D) 3 g L⁻¹ microdiamond..... 138

Figure 5-9 SEM images at different magnifications for films prepared from 10 g L⁻¹ PEMA solutions, containing 2 g L⁻¹ GRA and (A, B) 1 g L⁻¹ and (C,D) 3 g L⁻¹ nanodiamond. 138

Figure 5-10 Film mass versus number of the deposited layers for films prepared from 10 g L⁻¹ PEMA solutions containing (A,B) microdiamonds and (C,D) nanodiamonds, prepared using (A,C) 2 g L⁻¹ GRA and (B,D) 2 g L⁻¹ RLP and diamonds concentrations of (a) 1 g L⁻¹ and (b) 3 g L⁻¹ 139

Figure 5-11 Film mass as a function of number of alternating (A) PEMA/PEMA-microdiamond and (B) PEMA/PEMA-nanodiamond layers, prepared from 10 g L⁻¹ PEMA/10 g L⁻¹ PEMA and 1 g L⁻¹ diamond media prepared using (a) 2 g L⁻¹ GRA and (b) 2 g L⁻¹ RLP. . 140

Figure 6-1 Chemical structures of (A) CHOLNa, (B) curcumin (C) hydrocortisone and (D) indomethacin.....	151
Figure 6-2 Schematics of electrophoresis (EP) and phenomena at the electrode surface for (A) CHOL- micelles, (B) proteins or enzymes (C) heparin and (D-F) CHOL- micelles with mixed micelles, containing CHOL- and (D) drugs, (E) Hb or BSA, F (HP). Formation of (A) pure CHOLH films and (D-E) composite films by EPD.	154
Figure 6-3 SEM images at different magnifications (A,B) of CHOLH films.	156
Figure 6-4 SEM images at different magnifications for films, prepared from CHOLNa solutions, containing (A,B) CCM, (C,D) HCS and (E,F) IDM.	157
Figure 6-5 XRD patterns for A(a) CCM, A(b) HCS, A(c) IDM, A(d) CHOLH, B(a) CHOLH-CCM, B(b) CHOLH-HCS, B(c) CHOLH-IDM, ●, ▲, ◆ - labels for peaks, corresponding to JCPDS files 66-1420, 15-1016 and 58-1737, respectively.	159
Figure 6-6 FTIR spectra for A(a) CCM, A(b) HCS, A(c) IDM, A(d) CHOLH, B(a) CHOLH-CCM, B(b) CHOLH-HCS, and B(c) CHOLH-IDM.....	159
Figure 6-7 SEM images at different magnifications for films prepared from CHOLNa solutions, containing (A,B) BSA, (C,D) Hb and (E,F) HP.	160
Figure 6-8 FTIR spectra of A(a) BSA, A(b) Hb, A(c) HP, B(a) CHOLH-BSA, B(b) CHOLH-Hb, B(c) CHOLH-HP.....	162
Figure 7-1 SEM images of (A) cross section (F-film) and (B) surface of as-deposited PEMA films, (C) cross section and (D) surface of annealed PMMA films, arrows show film cross section.	178
Figure 7-2 SEM images of as-deposited PEMA films: (A) cross section and (B) surface	179

Figure 7-3 Electrochemical impedance spectroscopy data presented in Bode plots (A) absolute value of impedance $|Z|$ and (B) phase angle φ for (a) uncoated stainless steel, and (b) coated with PMMA and (c) coated with PEMA. The films were annealed at 180°C for 1 h. 179

Figure 7-4 Tafel plots for (a) uncoated stainless steel and coated with (b) PMMA and (c) PEMA 180

Figure 7-5 (A,B) TEM images at different magnifications of HA nanoparticles synthesized using rutin as a capping agent..... 181

Figure 7-6 X-ray diffraction patterns of (A) starting materials: (a) PMMA, (b) PEMA, (c) microdiamond, (d) nanodiamond, (e) HA and (B) deposited composite materials (f) PMMA-HAp, (g) PEMA-HA, (h) PEMA-microdiamond, (i) PMMA-microdiamond, (j) PEMA-nanodiamond, (k) PMMA-nanodiamond (▼-peaks corresponding to JCPDS file 00-006-0675 of diamond, ▲ - peaks corresponding to JCPDS file 00-009-0432 of HA)..... 182

Figure 7-7 SEM images at different magnifications for films prepared from 50 g L⁻¹ PMMA solutions, containing (A,B) 5 g L⁻¹ and (C,D) 20 g L⁻¹ HA and 50 g L⁻¹ PEMA solutions, containing (E,F) 5 g L⁻¹ and (G,H) 20 g L⁻¹ HA. 184

Figure 7-8 SEM images at different magnifications for films prepared from 50 g L⁻¹ PMMA solutions, containing (A,B) 5 g L⁻¹ and (C,D) 20 g L⁻¹ microdiamond and 50 g L⁻¹ PEMA solutions, containing (E,F) 5 g L⁻¹ and (G,H) 20 g L⁻¹ microdiamond. 186

Figure 7-9 SEM images at different magnifications for films prepared from 50 g L⁻¹ PMMA solutions, containing (A,B) 5 g L⁻¹ and (C,D) 20 g L⁻¹ nanodiamond and 50 g L⁻¹ PEMA solutions, containing (E,F) 5 g L⁻¹ and (G,H) 20 g L⁻¹ nanodiamond..... 187

Figure 8-1 Chemical structures of (A) BPEI, (B) LPEI, (C) AlgH and (D) L-arginine. 200

Figure 8-2 X-ray diffraction patterns of (A) calcium phosphate materials, prepared (a) without pH adjustment, (b) using BPEI for pH adjustment, (c) using L-arginine for pH adjustment, (● - peaks corresponding to JCPDS file 04-013-3344 of brushite, ◆ - peaks corresponding to JCPDS file 00-009-0432 of HA; (B) (a,b) zirconia, (c,d) titania, (a,c) as-precipitated, (b,d) annealed at 400°C for 1 h, (▼ - peaks corresponding to JCPDS file 01-075-9646 of tetragonal zirconia, ▲ – peaks corresponding to JCPDS file 04-014-5762 of anatase titania prepared using BPEI; (C) (a,b,c) zirconia, (d,e,f) titania, (a,d) as-prepared, (b,e) annealed at 400°C for 1 h, (c,f) annealed at 600°C for 1 h, (▼ - peaks corresponding to JCPDS file 01-075-9646 of tetragonal zirconia, □ – peaks corresponding to JCPDS file 00-037-1484 of monoclinic zirconia, ▲ – peaks corresponding to JCPDS file 04-014-5762 of anatase titania) prepared using L-arginine. 204

Figure 8-3 . TEM images of precipitates obtained using (A-C) BPEI and (D-F) (L-arginine), (A) HA, (D) brushite, (B,E) titania, (C, F) zirconia..... 207

Figure 8-4 SEM images at different magnifications for composite films prepared by cathodic EPD using (A,B) as-precipitated HA, (C,D) titania annealed at 400°C for 1 h, (E,F) zirconia annealed at 400°C for 1 h, for materials synthesized using BPEI. 209

Figure 8-5 SEM images at different magnifications for composite films prepared by cathodic EPD using (A,B) as-precipitated brushite, (C,D) titania annealed at 600°C for 1 h, (E,F) zirconia annealed at 600°C for 1 h, for materials synthesized using L-arginine. 210

Figure 8-6 (A) chemical structure of ibuprofen, (B) X-ray diffraction patterns of (a) deposited AlgH, (b) as-received ibuprofen and (c) co-deposited AlgH and ibuprofen (◆-peaks corresponding to JCPDS file 00-032-1723 of ibuprofen)..... 212

Figure 8-7 SEM images of films at different magnifications: (A,B) AlgH and (C,D) AlgH-
ibuprofen 213

Figure 8-8 FTIR spectra of (A) (a) as-received L-arginine, (b) as-received AlgH, (c)
deposited AlgH; (B) (a) as-received ibuprofen, (b) deposited AlgH-ibuprofen. 214

List of Abbreviations and Symbols

Abbr.	Full Description	Abbr.	Full Description
EPD	Electrophoretic deposition	YSZ	Yttria-Stabilized Zirconia
PVDF	Polyvinylidene fluoride	ZTA	Zirconia Toughened Alumina
BAS	Bile acid salts	ATZ	Alumina Toughened Zirconia
AlgH	Alginic acid	NP	Nanoparticle
PMMA	Poly methyl methacrylate	TCP	Tricalcium phosphate
PEMA	Poly ethyl methacrylate	DOPA	Dihydroxyphenylalanine
Hap	Hydroxyapatite	CFA	Caffeic acid
CaP	Calcium phosphate	DHB	Dihydroxybenzoic acid
CHIT	Chitosan	DHP	Dihydroxyphenylacetic acid
ALG	Alginates	DHC	Dihydroxyhydrocinnamic acid
HLA	Hyaluronic acid	GA	Gallic acid
GRA	18 β -glycyrrhetic acid	CA	Cholic acid
RLP	Rhamnolipids	THB	2,3,4 trihydroxybenzoic acid
CHOLNa	Sodium cholate	DLC	Diamond-like carbon
PEI	Polyethylenimine	CHOLH	Cholic acid
SS	Stainless steel	EP	Electrophoresis
THA	Total hip arthroplasty	CCM	Curcumin
SMA	Shape memory alloy	HCS	Hydrocortisone
SMM	Shape memory materials	IDM	Indomethacin

Abbr.	Full Description	Abbr.	Full Description
BSA	Bovine serum albumin	HP	Heparin
Hb	Hemoglobin	LPEI	Linear polyethylenimine
BPEI	Branched polyethylenimine		

Declaration of Academic Achievements

I, Zhengzheng Wang, declare that this thesis is my own work and was written to fulfill the requirements for a PhD degree in the Department of Biomedical Engineering at McMaster University. All of the experiments were conducted from September 2020 to August 2024 and adhered to the research policy and procedures from McMaster University. This dissertation contains six published, peer-reviewed journal papers in which I am the first author and the main contributor under the supervision of Dr. Zhitomirsky. To the best of my knowledge, the contents of this thesis do not infringe on anyone else's copyright and have not been submitted or published previously or anywhere else for the award of any other academic degree or diploma.

The six first-authored, peer-reviewed journal papers are the following:

1. Wang, Zhengzheng, and Igor Zhitomirsky. "Deposition of organic-inorganic nanocomposite coatings for biomedical applications." *Solids* 3, no. 2 (2022): 271-281.
2. Wang, Zhengzheng, and Igor Zhitomirsky. "Surfactants for Electrophoretic Deposition of Polyvinylidene Fluoride–Silica Composites." *Surfaces* 5, no. 2 (2022): 308-317.
3. Wang, Zhengzheng, and Igor Zhitomirsky. "Surfactant assisted dip-coating method for deposition of polyethylmethacrylate-diamond coatings." *Advances in Applied Ceramics* 122, no. 3-4 (2023): 226-235.
4. Wang, Zhengzheng, and Igor Zhitomirsky. "Bile Acid Salt as a Vehicle for Solubilization and Electrodeposition of Drugs and Functional Biomolecules for

Surface Modification of Materials." *Biomedical Materials & Devices* 2, no. 1 (2024): 397-406.

5. Wang, Zhengzheng, and Igor Zhitomirsky. "Application of Cyrene solvent for the fabrication of polymethyl methacrylate, polyethyl methacrylate and composite films containing hydroxyapatite and diamonds." *Journal of Applied Polymer Science*: e56002.
6. Wang, Zhengzheng, and Igor Zhitomirsky. "Strategies for alkali-free synthesis, surface modification and electrophoretic deposition of composite films for biomedical applications" *Colloids and Surfaces A: Physicochemical and Engineering Aspects* (2024): 135150.

Chapter 1 Introduction

1.1. Background

Bone is a specialized kind of connective tissue that serves as the structural framework of the human body and is essential for several physiological processes. The main components of bone are calcium phosphate (CaP) apatite crystals and collagen. Crystals of apatite exist in the collagen matrix. Bone is classified into two types based on density: cortical bone, which is dense, and cancellous (or trabecular) bone, which is highly porous and houses bone marrow. Bone tissue is continuously remodeled by cells: osteoblasts make bone, osteoclasts resorb it, and osteocytes are mature osteoblasts that have become inactive. The structure has a hierarchical organization, ranging from lamellae to individual collagen fibrils, with diameters in the nanoscale. Hydroxyapatite (HA), a mineral found in bones, is architecture down to few hundred nanometers. Osteoblasts work in coordination to maintain structural integrity and help regenerate diseased bone tissue. However, in some situations like tumour removal or critical-sized flaws, the natural healing process may not be enough. In such circumstances, bone grafting is necessary to stimulate regeneration[1].

Polymers play an important role in bone tissue engineering field[2, 3]. Current research endeavours to improve the longevity and efficiency of these materials when used in the human body. Initially used to replace connective tissue, polymers now hold promise in tissue engineering, supporting the regeneration of bone tissue and other implants[4]. Polymers like poly(methyl methacrylate (PMMA)[5], polyvinylidene fluoride (PVDF)[6] as well as poly(ethyl) methacrylate

(PEMA)[7] are extensively used in biomedical applications, especially as implants in bone tissue engineering[4].

PMMA is highly sought after for a range of applications, including biomedical implants, biosensors, optical devices, solar cells, and energy storage. This is because it has exceptional thermal and chemical stability, biocompatibility, and improved mechanical qualities. Composites that include inorganic components such as ZnO, TiO₂, and Al₂O₃ in the PMMA matrix have superior mechanical and optical characteristics, biocompatibility, and improved thermal and dimensional stability[8].

PEMA composites also show potential for biomedical applications, including bio-cements with improved mechanical properties and biocompatibility, shape memory composites for biomedical devices, and composites for bone healing and tissue engineering[9]. PEMA is particularly useful in dentistry, orthopedic applications, craniofacial implants, and biosensors[9].

PVDF is a chemically inert polymer that exhibits excellent resistance to inorganic and organic acids, a wide range of solvents, and other chemicals. This polymer demonstrates ferroelectric and piezoelectric characteristics, as well as high mechanical strength and low flammability. The PVDF films and coatings have been applied in many applications.. Thin films were employed in the fabrication of piezoelectric actuators and transducers, pyroelectric sensors, as well as electrical insulators and capacitors[10]. PVDF films have garnered considerable attention for their use in water treatment, pollutant removal, gas separation membranes, polymer fuel cells, and batteries. PVDF applications in various biosensors are particularly intriguing. Researchers are currently studying PVDF films for potential use in implantable biomedical devices[10]. Polyvinylidene fluoride (PVDF) and PVDF-silica composites have garnered considerable attention in the field of biological tissue engineering[10].

Although PMMA, PEMA and PVDF are promising polymers in bio-implants fields, they have their limitations when they are being processed. PMMA was dissolved using a range of solvents including toluene, benzene, methyl ethyl ketone, and other organic solvents. These solvents are known to be carcinogenic and poisonous. Utilizing these solvents for biological purposes is challenging due to the tendency of solvent molecules to adhere to the surface or inside of the PMMA coatings[11]. PEMA also exhibits solubility in hazardous solvents, including tetrahydrofuran, chloroform, dimethyl formamide, benzene, and toluene. These solvents have been often employed in previous studies for the creation of coatings using casting and spin coating processes[12]. Due to the use of toxic solvent, the biomedical applications of PMMA and PEMA are extremely restricted. This research developed new methodologies for processing PMMA and PEMA in environmentally and biologically safe solvents, paving the way for broader biomedical use. In addition, PVDF is a chemically inert and hydrophobic polymer[13] which is unsuitable for film processing by electrophoretic deposition (EPD). Thus, a biomimetic approach using bile acids as natural surfactants was developed.

EPD is an important method to deposit a wide range of materials and composites from colloidal suspensions or solutions containing macromolecules. It has the benefits of a high rate of deposition and the potential for creating a homogenous coating on substrates with a large surface area. EPD enables precise manipulation of film thickness and deposition rate. It can be used for deposition of thin films, patterned films, and thick coatings. EPD is an economical and adaptable method used to deposit a wide range of polymers, ceramics, metals, hydroxides, and other organic and inorganic compounds. EPD is particularly important for biomedical applications because of the exceptional purity of the deposits and the ability to evenly coat substrates with intricate forms. EPD of multilayer films, which consist of individual layers with precisely controlled thickness and

composition, is very significant for biomedical applications. In addition, EPD enables the creation of films with varying composition and precise morphological control. Another advantage of EPD for many biomedical applications is the ability to deposit different organic and inorganic composites at ambient temperature[14].

While EPD has been used to create organic-inorganic nanocomposite biomaterials, there is a need to enhance the adhesion of the coating when exposed to body fluid. Biopolymers such as chitosan (CHIT), alginates (ALG), and hyaluronic acid (HLA) have been chemically modified using catechol, a functional group present in the byssal plaque of mussels. This modification was motivated by the mussel's capacity to adhere to seawalls in challenging maritime environments[15]. The objective is to improve the bonding of coatings to inorganic surfaces, nanoparticles, and the mucosal layer in mammals[16].

Therefore, it is crucial to create a novel type of nanocomposite coatings for biomedical implants that incorporate important functional elements, such as biopolymers, bioceramics, antibacterial agents, morphogenic proteins, and enzymes. Advancements in this field will lead to the avoidance of expensive and excruciating modifications, while also prolonging the durability of orthopedic implants. Organic-inorganic nanocomposite coatings have the ability to serve as biomedical implant coatings and thin-film biosensors. This is because they incorporate functional nanomaterials and biological molecules, making them multi-functional. My work explores innovative methods for creating new biomaterials by combining organic and inorganic components at the nanoscale. Additionally, I investigate sophisticated approaches for applying multi-functional coatings in biomedical settings using colloidal-electrochemical processes. Through my scientific methods and approach, I have been able to bring about innovation in the areas of electrochemistry, colloidal science, biomaterials, and nanotechnology.

1.2. Thesis Overview

A summary of the remaining chapters included in this thesis are as follows:

Chapter 2 is a literature review, which covers the introduction of the orthopaedic implant materials and the colloid processing techniques in this research. In the part of orthopaedic implant materials, it describes some commonly used biomedical materials such as metallic materials, bioceramics and polymers. In the other part of processing techniques, it describes the principles of EPD and dip coating

Chapter 3 is based on the paper “Deposition of Organic-Inorganic Nanocomposite Coatings for Biomedical Applications”. It states that the development of composite coatings for biomedical applications benefits from eliminating toxic solvents for PMMA processing. Instead of hazardous solvents, water-isopropanol was used to synthesize PMMA and composite coatings. Dip coating is a versatile method for making composite coatings with bioceramics, antimicrobials, and drugs. PMMA coatings with hydroxyapatite and silica could improve bioactivity and biocompatibility of biomedical implants. Composite coatings can become antimicrobial by co-depositing Ag_2O and ZnO with PMMA. Drug delivery is possible with PMMA-drug composite coatings. Simple and inexpensive, dip coating is ideal for multiple layer processing. Thus, improving this technique can create intricate microstructures with multiple layers of functional materials. Advances in this technique may lead to more coatings with functional biomaterials for various purposes.

Chapter 4 is based on the paper “Surfactants for Electrophoretic Deposition of Polyvinylidene Fluoride–Silica Composites”. It describes new dispersing agents for charging chemically inert PVDF particles for EPD. The deposition yields of PVDF with different surfactants are different and some agents can be used for the co-deposition with nano-silica and micron-size

silica and the fabrication of composite films. The film composition can be varied by the variation of silica concentration in suspensions for EPD. The use of different surfactants as a charging co-dispersant for materials of different types paves the way for the deposition of advanced organic–inorganic composites.

Chapter 5 is based on the paper “Surfactant assisted dip-coating method for deposition of polyethylmethacrylate-diamond coatings”. It demonstrates that 18 β -glycyrrhetic acid (GRA) and rhamnolipids (RLP) can solubilize PEMA eliminating the need in toxic solvents. We dissolved high molecular mass PEMA and obtained concentrated solutions in isopropanol. These findings helped to develop a dip coating method for PEMA film deposition, which is versatile. The deposited films protected stainless steel from corrosion. GRA-PEMA films protected against corrosion better than RLP-PEMA films. PEMA films can be deposited as monolayers or multilayers. GRA and RLP could solubilize PEMA and disperse chemically inert diamonds, enabling composite PEMA-diamond coatings. Diamond suspension concentration affects film composition. The analysis of film morphologies showed that GRA and RLP chemical structures affect their interactions with PEMA and diamonds. GRA composite films had no diamond-PEMA interface defects, unlike RLP films.

Chapter 6 is based on the paper “Bile Acid Salt as a Vehicle for Solubilization and Electrodeposition of Drugs and Functional Biomolecules for Surface Modification of Materials”. It describes a methodology based on sodium cholate (CHOLNa) as a solubilizing, micelle-forming and gel-forming agent for the fabrication of composite films. The use of CHOLNa represents a versatile EPD strategy for biomolecules of various types that cannot be deposited independently due to poor solubility, electrical neutrality, charge reversal at isoelectric points, and strong pH-independent charge. Traditional charging agents for EPD are toxic and unsuitable for biomedical

applications. Natural bile acid salts can be used as multifunctional biosurfactants for deposition from aqueous solutions.

Chapter 7 is based on paper “Application of Cyrene solvent for the fabrication of polymethyl methacrylate, polyethylmethacrylate and composite films containing hydroxyapatite and diamonds”. It presents the feasibility studies of solubilization of PMMA and PEMA in Cyrene. Cyrene is a promising biodegradable solvent that could replace toxic, carcinogenic solvents. Dip coating of PMMA and PEMA films required the ability to form relatively concentrated solutions of high molecular mass polymers. The use of Cyrene facilitates the fabrication stable HA, microdiamond, and nanodiamond suspensions. This approach was based on the use of a biocompatible dispersant for the dispersion of chemically inert diamond particles. As a chelating catecholate-type capping agent, rutin produced smaller HA nanorods. HA, microdiamond, and nanodiamond were co-deposited with PMMA or PEMA. The results of this work are promising for the fabrication of films with advanced functionality for biomedical and other applications.

Chapter 8 is based on the paper “Strategies for alkali-free synthesis, surface modification and electrophoretic deposition of composite films for biomedical applications”. It builds a new methodology that branched-polyethylenimine (BPEI) and L-arginine can be used as organic alkalizers-capping agents for synthesis hydroxyapatite, zirconia and titania. Alkalizers-capping agents allow for the synthesis of smaller nanoparticles in a simple, environmentally friendly process. Cathodic EPD produced linear-polyethylenimine (LPEI)-bioceramic composite films. Anodic EPD with L-arginine as an alkalizer facilitated the fabrication of alginic acid (AlgH) films for the first time, enabling AlgH solution fabrication. Composite films were made using L-arginine as an alkalizer to solubilize AlgH and ibuprofen. This study's methods can be used to synthesize

other materials and to perform anodic EPD of advanced biopolymers with drugs, bioceramics, and other functional materials.

Chapter 9 provides a concise summary of the important discoveries and notable contributions made in this study, along with outlining potential future research.

1.3. References

- [1] S. Saravanan, R. S. Leena, and N. Selvamurugan, "Chitosan based biocomposite scaffolds for bone tissue engineering," (in en), *International Journal of Biological Macromolecules*, vol. 93, pp. 1354-1365, 2016/12// 2016, doi: 10.1016/j.ijbiomac.2016.01.112.
- [2] N. Ingwattanapok, Y. Sakunrak, and N. Tangboriboon, "Bio composite of porous hydroxyapatite and collagen extracted from eggshell membrane and *Oreochromis niloticus* fish skin for bone tissue applications," *Journal of Applied Polymer Science*, vol. 140, no. 41, 2023, doi: 10.1002/app.54527.
- [3] R. Sikkema, B. Keohan, and I. Zhitomirsky, "Alginate Acid Polymer-Hydroxyapatite Composites for Bone Tissue Engineering," (in en), *Polymers*, vol. 13, no. 18, p. 3070, 2021/01// 2021, doi: 10.3390/polym13183070.
- [4] D. Banoriya, R. Purohit, and R. K. Dwivedi, "Advanced Application of Polymer based Biomaterials," (in en), *Materials Today: Proceedings*, vol. 4, no. 2, pp. 3534-3541, 2017 2017, doi: 10.1016/j.matpr.2017.02.244.
- [5] U. Ali, K. J. B. A. Karim, and N. A. Buang, "A Review of the Properties and Applications of Poly (Methyl Methacrylate) (PMMA)," (in en), *Polymer Reviews*, vol. 55, no. 4, pp. 678-705, 2015/10/02/ 2015, doi: 10.1080/15583724.2015.1031377.

- [6] P. Saxena and P. Shukla, "A comprehensive review on fundamental properties and applications of poly(vinylidene fluoride) (PVDF)," *Adv Compos Hybrid Mater*, vol. 4, pp. 8-26, 2021, doi: 10.1007/s42114-021-00217-0.
- [7] S. Rawal, "Poly (Ethyl Methacrylate) (PEMA) and its Composites for Various Applications: Background, Recent Progress, and Future challenges," *Macromolecular Symposia*, vol. 413, no. 1, 2024, doi: 10.1002/masy.202300096.
- [8] X. Li and I. Zhitomirsky, "Deposition of poly(methyl methacrylate) and composites containing bioceramics and bioglass by dip coating using isopropanol-water co-solvent," (in en), *Progress in Organic Coatings*, vol. 148, p. 105883, 2020/11// 2020, doi: 10.1016/j.porgcoat.2020.105883.
- [9] K. Baker and I. Zhitomirsky, "Biomimetic approach to poly(ethyl methacrylate) solubilization, deposition, and coating loading with functional biomaterials," (in en), *Colloid and Polymer Science*, vol. 300, no. 6, pp. 599-607, 2022/06// 2022, doi: 10.1007/s00396-022-04971-5.
- [10] Z. Wang and I. Zhitomirsky, "Surfactants for Electrophoretic Deposition of Polyvinylidene Fluoride–Silica Composites," *Surfaces*, vol. 5, no. 2, pp. 308-317, 2022/05// 2022, doi: 10.3390/surfaces5020022.
- [11] Z. Wang and I. Zhitomirsky, "Deposition of Organic-Inorganic Nanocomposite Coatings for Biomedical Applications," *Solids*, vol. 3, no. 2, pp. 271-281, 2022, doi: 10.3390/solids3020019.
- [12] X. Liu, S. Veldhuis, R. Mathews, and I. Zhitomirsky, "Dip coating of poly(ethyl methacrylate) and composites from solutions in isopropanol-water co-solvent," *Colloids*

- and Surfaces A: Physicochemical and Engineering Aspects*, vol. 631, 2021, doi: 10.1016/j.colsurfa.2021.127703.
- [13] G. Vitola, R. Mazzei, E. Fontananova, and L. Giorno, "PVDF membrane biofunctionalization by chemical grafting," *J. Membr. Sci.*, vol. 476, pp. 483-489, 2015/02// 2015, doi: 10.1016/j.memsci.2014.12.004.
- [14] R. Sikkema, K. Baker, and I. Zhitomirsky, "Electrophoretic deposition of polymers and proteins for biomedical applications," (in en), *Advances in Colloid and Interface Science*, vol. 284, p. 102272, 2020/10// 2020, doi: 10.1016/j.cis.2020.102272.
- [15] K. Gulati *et al.*, "Anodized 3D–printed titanium implants with dual micro- and nano-scale topography promote interaction with human osteoblasts and osteocyte-like cells," *Journal of tissue engineering and regenerative medicine*, vol. 11, no. 12, pp. 3313-3325, 2017.
- [16] A. R. Boccaccini, S. Keim, R. Ma, Y. Li, and I. Zhitomirsky, "Electrophoretic deposition of biomaterials," *J R Soc Interface*, vol. 7 Suppl 5, no. Suppl 5, pp. S581-613, Oct 6 2010, doi: 10.1098/rsif.2010.0156.focus.

Chapter 2 Literature Review

2.1. Orthopaedic Implant Materials

2.1.1. Metallic Materials for Orthopaedic Applications

2.1.1.1. Stainless Steels and Cobalt-Chromium Alloys

For biomedical implants, metallic materials remain the preferred choice because of their decent biocompatibility and capacity to withstand a wide range of mechanical loads that the implants will encounter during their lifetime[1-3]. AISI 316 and 316L stainless steel (SS) were often employed for biomedical applications because of their ductility, strength, corrosion resistance, simplicity of fabrication, and low cost[2, 4, 5]. SS was the first metallic material used therapeutically for total hip arthroplasty (THA). The ASTM advises using stainless steels from the 316 family for biomedical implant applications due to their reduced carbon content, which increases their resistance to corrosion in physiological fluid[6]. Even today, AISI 316 and 316L SS are often used for long-term orthopaedic applications like complete hip or knee replacements as well as short-term ones like surgical screws and bone plates[7]. When it comes to THA applications, the low wear resistance of SS alloys in comparison to other metals is crucial because it stops the production of harmful wear particles, which in turn prevents inflammation, osteolysis, and aseptic loosening[6]. Since 316L SS has been demonstrated to induce inflammation and allergy responses and is thought to be carcinogenic and genotoxic, the main worry related to its usage is the release of toxic nickel ions as a consequence of corrosion or wear particle production[4, 6]. In addition, chronic nickel exposure raises the risk of renal, cardiovascular, and cancer diseases[4]. Nitrogen was used to substitute nickel in the development of Ni-free stainless steel (ASTM F2229), allaying worries about the leakage of harmful nickel ions from 316L SS[5]. Ni-free stainless-steel alloys

show low corrosion resistance, decreased fatigue behaviour under physiological settings, and poor bioactivity compared to other metallic biomaterials, despite the fact that nitrogen addition prevented Ni ion release[5].

Cobalt-chromium alloys were offered as an alternative to 316 and 316L SS because to their high wear resistance and mechanical strength in an effort to decrease the formation of hazardous wear particles and perhaps increase the lifetime of orthopaedic implants[5, 6]. Specifically, cobalt nickel molybdenum chromium (CoNiMoCr) and cobalt molybdenum chromium (CoMoCr) alloys are the two kinds of cobalt-chromium alloys that are utilized clinically for orthopaedic implant purposes[6]. Because CoCr alloys create a protective oxide layer in physiological conditions, they are also more corrosion resistant than SS[6]. In comparison to medical-grade SS, they also show greater wear resistance, but their manufacturing costs are higher, and there are still worries about the leakage of dangerous metal ions, notably nickel[5].

2.1.1.2. Titanium and Ti Alloys

The most popular metallic biomaterial for orthopedic applications is titanium and its alloys, mainly because to its excellent osseointegration, low toxicity, and strong corrosion resistance[5]. The degree to which a material establishes a functional bond with hard tissue at the interface between the implant and the bone is known as osseointegration[5]. SS and CoCr alloys show no osseointegration, but titanium shows a significant degree of osseointegration[5]. Because a layer of fibrous tissue separates the implant surface from the newly produced bone when SS and CoCr alloys are inserted, they are both regarded as bio-tolerant biomaterials[4]. Ti's high osseointegration sets it apart from other metals and their alloys, since the quality of the connection at the implant/tissue interface plays a major role in the long-term success of orthopaedic implants. Ti does not contain any poisonous elements for humans, although reports of the emission of

harmful corrosion products, such aluminium and vanadium ions, are constant[8]. Over time, prolonged exposure to corrosion products may have detrimental consequences on health as they accumulate in the lymphatic system[5]. Specifically, diagnoses of peripheral neuropathy, osteomalacia, and Alzheimer's have been linked to the body's release of Al and V ions after the implantation of Ti alloy[6, 7]. It has been suggested that alternative Ti alloys be developed with strengthening components that are non-allergic; however, this would require sophisticated production procedures and raise the total cost[5]. Moreover, it should be mentioned that the stress-shielding effect—a localized atrophy of bone caused by an elastic modulus mismatch between the metallic implant and human bone—makes all metallic implant materials susceptible to failure [6, 7, 9].

2.1.1.3. Shape Memory Alloys

Shape memory alloys (SMAs) are a kind of shape memory materials (SMMs) that can maintain an initial form when exposed to certain stimuli, such as changes in temperature or magnetism[10]. Currently, SMA namely nickel-titanium alloys (NiTi), are widely used in biomedical applications[11-13]. The most appealing characteristics of this category of materials are the ability to: (1) regain their initial shape after experiencing significant deformations caused by mechanical stress (pseudoelasticity) and (2) retain a distorted shape until heat triggers the restoration of the original shape[11]. The unique characteristics of SMAs make them very desirable for use in a wide range of applications, including automotive and robotic actuators, connections, smart wings for aerospace shuttles, and smart medicinal devices[10].

At present, biocompatible SMAs may be categorized as follows: NiTi [47], Fe-[14], Mg-[15], and the newly patented Cu-based[14] SMAs. The NiTi-based SMAs are very advantageous for a wide range of applications due to their exceptional biocompatibility, stability, and thermo-

mechanical performance[10, 16]. NiTi-based alloys, which contain 48-52% Ni by weight, are a type of shape memory alloy. These alloys exhibit both shape-memory and pseudoelastic effects, which are characterized by large plateau and stress hysteresis. They also have good workability in the martensite phase and are resistant to corrosion and fatigue. Their suitability for biological applications is further shown by their good biocompatibility and exceptional compatibility with magnetic resonance and computer tomography. In addition, the mechanical properties of NiTi are more closely aligned with the reaction of human tissue, as opposed to other regularly used metallic materials in biomedical devices such as SS 316L and chromium-cobalt (Cr-Co) alloys[11]. NiTi biomedical alloys have been extensively used in many clinical applications, such as orthodontic treatment, prosthesis, catheters, tissue anchoring and connection, and cardiovascular stents[17].

Nevertheless, NiTi-based SMA biomedical devices are enduring. Permanent devices, such as those used in bone fracture healing and cardiovascular applications, are recognized to have long-term health hazards. These dangers include the stress shielding effect in bone fracture healing and restenosis in cardiovascular applications. Conversely, if permanent implants need to be taken out, it will need secondary surgeries, resulting in more waste and significantly increased health risks. These problems may be easily resolved by creating biodegradable or bioresorbable SMAs. Implants constructed from a biodegradable SMA are anticipated to slowly break down and be assimilated by the human body while consistently providing the necessary mechanical reinforcement for the specified temporary duration to aid in tissue regeneration and self-repair[10].

2.1.2. Bioceramics and Bioactive Glasses

2.1.2.1. Alumina and Zirconia-based Ceramics

In recent years, ceramics have attracted significant interest from orthopedic and dental scientists and professionals because of their exceptional biomechanical and biocompatibility

properties[18-21]. Bioceramics may be categorized into three basic types: bioinert, bioactive, and bioresorbable ceramics[22]. Bioinert ceramics, such as alumina and zirconia, possess excellent chemical stability and strong mechanical qualities. When these ceramics come into touch with bone tissue, they exhibit a pattern known as "contact osteogenesis"[23-25]

Alumina, commonly known as aluminium oxide, has been widely employed in orthopedic joint prosthesis owing to its exceptional compressive strength and chemically inert qualities[26, 27]. Al_2O_3 was proposed as a substitute for metallic acetabular liners and femoral heads, with the aim of extending the lifetime of orthopaedic implants by reducing the production of wear particles and osteolysis[28, 29]. Al_2O_3 is very suitable for skeletal tissue restoration because to its exceptional mechanical strength in compression, remarkable wear resistance, and hydrophilic nature[29]. Pure Al_2O_3 has been used in medical applications such as hip and knee prosthesis, dental implants, and as a protective layer for metallic dental implants and femoral stems[29]. Despite the reduction in the production of inflammatory wear particles and osteolysis, the bioinert nature of Al_2O_3 ceramics has hindered the achievement of effective osseointegration[29]. Al_2O_3 demonstrates inferior fracture toughness in comparison to other bioceramics, such as Yttria-Stabilized Zirconia (YSZ), and is prone to brittle fracture and eventual catastrophic failure.

Since ZrO_2 -based ceramics are bioinert and have comparable mechanical qualities to Al_2O_3 in terms of compressive strength and wear resistance, they were offered as an option for ceramic acetabular liners, femoral heads, and acetabular liners. Compared to Al_2O_3 ceramics, ZrO_2 has a higher fracture toughness due to a unique transition toughening process[30-32]. ZrO_2 is in a metastable tetragonal state at ambient temperature, but it changes into a monoclinic state when stress is applied[31, 32]. Medical-grade ZrO_2 ceramics are stabilized by the inclusion of Y_2O_3 , which inhibits the premature phase-transformation from the tetragonal to the monoclinic phase at

room temperature[33]. Under ambient settings, stabilization of the tetragonal phase inhibits the propagation of cracks at localized fracture points; nevertheless, after clinical usage, it was shown that exposure to bodily fluid in vivo caused premature aging and YSZ femoral head failure[31]. The phenomenon under observation is known as low temperature thermal deterioration, and it refers to the early transition under physiological circumstances from the tetragonal to the monoclinic phase[30]. Moreover, this action raises the possibility of an early implant failure during fabrication or after surface treatments intended to enhance osseointegration[34]. Because of the high rate of YSZ implant failure, Zirconia Toughened Alumina (ZTA) composites have become popular as an alternative to YSZ femoral heads[35]. Because of their higher fracture toughness than pure Al_2O_3 or YSZ, ZTA composites—which are used clinically under the brand name BioloX® delta—have higher success rates than pure Al_2O_3 femoral heads[35]. Alumina Toughened Zirconia (ATZ) composites are being investigated for femoral head applications because of the success of ZTA, despite reports that ZTA has better mechanical characteristics than ATZ[32].

2.1.2.2. Titania Ceramics

Titanium dioxide (TiO_2) nanostructures are numerous substances that have been widely used in many technological domains including medicine, energy, and biosensing. Titanium dioxide (TiO_2) is a white substance that has limited solubility and is often used in many biomedical applications, such as cosmetics, medications, and pharmaceutical items. The substance is crystallized in two distinct crystalline structures, rutile or anatase, which have significant industrial uses. Research has shown that the presence of mixed polymorphs of TiO_2 , such as anatase (80%) and rutile (20%), is more effective for biomedical applications compared to the presence of a single phase[36]. The anatase form of TiO_2 has more activity than the rutile form in terms of photocatalytic and cytotoxic characteristics. Nevertheless, the majority of metal-oxide

nanoparticles (NPs) are expensive when produced on a large scale for commercial purposes, and some types are also harmful to living organisms. Titanium dioxide (TiO_2) is not only cost-effective but also mostly non-toxic. It has received approval from the American Food and Drug Administration (FDA) for use in food and drug-related goods. Nanostructured TiO_2 has a wide range of possible applications because to its nanoscale characteristics, little toxicity, favourable biocompatibility, inherent qualities, and adaptable manufacturing methods[36]. Nanostructured materials based on functionalized TiO_2 have beneficial properties in several biomedical applications, including bone scaffolds, vascular stents, drug delivery systems[37], and biosensors[38].

There is a thin bioactive layer of naturally occurring TiO_2 oxide coated on titanium and its alloys. This layer is thought to be contributing to the success of titanium implants and their capacity to osseointegrate[39, 40]. It is important to remember that while this oxide layer helps with osseointegration, it is not a long-term corrosion barrier, it does not stop harmful Al and V ions from escaping, and it does not improve the lifespan of implants[41]. Applying a TiO_2 coating to the Ti alloy substrate is one way to improve osseointegration and corrosion protection while continuing to function as a physical barrier that releases toxic metal ions and protects against corrosion[41]. This also improves the bioactivity of the underlying titanium substrate. The ability to load TiO_2 nanotube coatings with functional molecules, such as anti-bacterial drugs for post-operative infection prevention[42], and the potential for increased osseointegration and osteogenesis through the introduction of nanoscale surface feature[3, 43, 44]s have generated particular interest in these coatings in recent years. Electrochemical anodization is a commonly used method to create TiO_2 -nanotube based coatings, which enables the coating of complex structures such as porous Ti scaffolds. [3]. Improved coatings for better osseointegration and

reduced risk of infection have been created by depositing HA on the surface of the nanotube[3], loading the nanotubes with antibiotics like vancomycin[42], or functionalizing the surface with Ag NPs[45]. Despite the development of functional orthopaedic coatings utilizing TiO₂ nanotubes, there are still issues with the effectiveness of coatings that are loaded with antibiotics because of antibiotic resistance[45]. Though coatings containing silver nanoparticles (Ag NPs) have been shown to be cytotoxic to osteoblast cells at concentrations of Ag NPs high enough to have an anti-bacterial impact, they may provide a viable solution to stop the development of bacterial biofilms[3].

2.1.2.3. Calcium Phosphate and Hydroxyapatite

Calcium phosphates are mineral compounds containing calcium and phosphate ions. They are recognized as the primary inorganic components in almost 60% of all natural human bones. The presence of calcium phosphates in bones was initially observed in 1769, and in the 1800s, these calcium phosphates found in bones were classified into several groups. Since the 1900s, researchers have extensively investigated the therapeutic use of synthetic calcium phosphates[46-48]. Subsequently, bone regenerating applications, such as bone cements, scaffolds, implants, and coating processes employing calcium phosphates, have been developed and a few have been made available for commercial use[49-51]. The features of calcium phosphates have been investigated for their potential use in bone regeneration, much as the ones mentioned above.

Because of their compositional similarities to the inorganic component of human bone, carbonate substituted HA ($\text{Ca}_{10}(\text{PO}_4)_{6-x}(\text{CO}_3)_x(\text{OH})_2$), CaP bioceramics were first used in clinical settings[52, 53]. Although the Ca/P stoichiometric ratio and crystallinity determine whether a CaP ceramic is resorbable, all CaP ceramics are considered to be bioactive[54]. Compared to HA with a lower degree of crystallinity, HA with a higher degree of crystallinity is less resorbable and more

stable[5]. Pure HA is non-resorbable and has a Ca/P stoichiometric ratio of 1.67[52]. Tricalcium phosphate (TCP) alpha- or beta-polymorphs may occur when the stoichiometric ratio is less than 1.67, whereas calcium oxide (CaO) arises as an impurity phase when it is larger than 1.67[52]. For applications like osseous defect repair, where simultaneous bone resorption and hard tissue regeneration are desired, HA containing CaO or polymorphs of TCP are both regarded as resorbable[52, 55]. It is important to remember that although a slight deviation from the ideal stoichiometric Ca/P ratio of 1.67 results in ceramics with acceptable qualities, CaP ceramics with a Ca/P ratio less than 1 are too resorbable and unsuitable for implantable uses[52]. Additionally, it has been shown that whereas CaP ceramics are typically thought of being osteoconductive in two-dimensional configurations, in certain three-dimensional configurations they have been shown to induce osteogenesis, making them osteoinductive[56]. For load-bearing applications, HA is not suitable because to its mechanical qualities. Its fracture toughness is much lower than cortical bone and other bioceramics (e.g., Al_2O_3 , YSZ)[5, 52]. To integrate the mechanical qualities of metallic implants with the bioactive surface qualities of hydroxyapatite, HA has been coated on metallic femoral stems[52, 57]. For more than 20 years, plasma-spraying has been utilized to coat femoral stems with HA; nevertheless, a comprehensive evaluation indicated no advantage when compared to uncoated femoral implant components[58]. It is suggested that the thickness of HA coatings, which results from the coating process, is the cause of their unremarkable performance in the early investigations. HA coatings (50-100 μm) produced by plasma spraying are relatively thick, leading to poor adhesion, low interfacial shear strength, fragmentation, and in-situ release[52, 59]. Low temperature processing techniques, such as sol-gel deposition, electrophoretic deposition, biomimetic deposition, and electrochemical deposition, are being researched as alternatives to the

formation of thin, adherent calcium phosphate ceramic films in order to address the processing issues related to plasma spraying[52, 59, 60].

2.1.2.4. Bioactive Glasses

Bioglass exhibits biocompatibility, non-toxicity, and chemical stability in a biological setting. It possesses antibacterial properties by increasing the pH and osmolarity in the nearby area, providing an unfavourable environment for bacterial development[61, 62]. Bioglass has significant differences in its dissolving compared to normal glass. Bioglass is activated by a specific dissolving process, achieved by adding network modifiers such as CaO or Na₂O. This activation enhances the reactivity of both the surface and silica of the Bioglass[61]. The combination of alkali-free Bioglass with zinc oxide and strontium oxide provides an antibacterial effect against *Staphylococcus aureus* and *Escherichia coli*. Bioglass is a highly effective bone substitute for treating osteomyelitis, peri-implant infection, sinus augmentation, and fixing orbital floor defects[62, 63]. Bioglass can be utilized as a covering for dental implants because to its ability to be integrated into both hydrophilic and hydrophobic environments. Particle size also affects the antibacterial capabilities. Smaller particles have a bigger surface area, which leads to increased antimicrobial effects[64].

Bioactive glasses are remarkable biomaterials because they are simultaneously osteoinductive, osteoconductive and resorbable[9, 65, 66]. Due to their ability to rapidly grow new bone while resorbing over time, these characteristics make them ideal for use as tissue scaffolds in regenerative medicine[66]. Larry Hench initially identified bioactive glass, or Bioglass® 45S5, in the late 1960s. It had 46.1 mol% SiO₂, 24.4% NaO, 26.9% CaO, and 2.6% P₂O₅ [38, 39]. Because it was the first substance capable of bonding with and promoting the development of new calcified tissue, Hench's initial bioactive glass was groundbreaking[5]. The following is the general bonding

process of bioactive glass: First, the glass will quickly corrode and dissolve the alkali ions when exposed to physiological fluids; these ions will then be replaced by H^+ or H_3O^+ ions[65, 66]. This causes the Si-O-Si bonds to break, a local pH rise, and the condensation polymerization of silicon ($Si(OH)_4$) gel on the glass surface[65, 66]. When CO_3^{2-} and OH^- anions from physiological fluid are included, the amorphous CaP layer that was formed by the diffusion of Ca ions and PO_4^{3-} groups towards the silanol eventually crystallizes and develops into carbonated HA[65, 66].

Hench and colleagues discovered in the 1990s that bioactive glass could be fabricated using the sol-gel method (named 58S Bioglass®), but these glasses were not suitable for use as tissue scaffolds because they were made using high temperature techniques, which prevented them from introducing porosity[67]. Prior to the development of the sol-gel approach for bioactive glass manufacturing, conventional melt-quench fabrication techniques were unable to create porous structures like tissue scaffolds[67]. By doping the glass with Ag ions, antibacterial bioactive glasses have also been created[68, 69]. Although bioactive glasses have been utilized in clinical settings since the 1980s, the FDA's limits on highly bioactive materials have resulted in fewer items being commercially accessible than HA[65]. Bioactive glasses' weak and brittle character has restricted their usage in load-bearing applications, but if combined with metals or polymers to increase their mechanical strength and ductility, they may find therapeutic value[67]. The comparatively quick resorption rate of bioactive glass—which has occasionally been shown to surpass spontaneous bone remodeling—is another barrier to the broad application of bioactive glass. This creates a space at the contact between the implant and the bone, which causes the implant to separate and fail. Lastly, the local pH rise brought on by the first dissolution of alkali ions raises concerns regarding cytotoxicity[66].

2.1.3. Polymers on Biomedical applications

2.1.3.1. PMMA and PEMA

PMMA, also known as polymethyl methacrylate, is a thermoplastic material that is highly transparent. PMMA is an amorphous polymer from the acrylate family. PMMA is a polymer that is resistant to ultraviolet (UV) radiation and has very little variation. [70]. It has excellent thermal stability and can tolerate temperatures up to 100°C and down to -70°C. It also has extremely good optical characteristics. PMMA has great mechanical strength with little elongation at breakage[70, 71]. PMMA is commonly utilized in solar cells[72], batteries[73], supercapacitors[74], and optical devices[70, 75, 76]. PMMA has been utilized in the field of biomedical applications, namely in the formulation of bone cements for the purpose of medication administration and release, as well as in cranioplasty procedures. The polymer possesses several desirable characteristics that make it suitable for various applications, such as non-toxicity, cost-effectiveness, ease of processing, compatibility, minimum inflammatory responses with tissues, and enhanced fracture resistance, particularly in cranioplasty procedures[70]. In addition to these, PMMA applications also include biosensors[77], orthopaedic devices[78], and dental implants[79].

PMMA has also been used to widen the applications of chitosan in various fields that include biomedical and pharmaceutical applications. Zuhair et al. reported the successful grafting of a PMMA/chitosan blend, which illustrate its potentials for drug release applications[70]. Zuber et al. reported the synthesis of composite materials based on a combination of polyurethane-poly(methyl methacrylate) (PU-PMMA) and titanium oxide (TiO₂). According to the findings of the research, the blend exhibited non-toxicity towards live cells, had excellent mechanical strength, and showed biocompatibility for use in dental implant applications[70]. Nein et al. have developed a bone cement that can release pharmaceuticals in a controlled manner. This cement not only

enhances the pace and amount of drug release, but also maintains its mechanical qualities[70]. Moreover, PMMA composites have been developed and successfully applied for controlled medication delivery[80], cranioplasty[81], biomedical implants[71], bone and dental cements[79, 82, 83],.

Poly ethyl methacrylate (PEMA) is a versatile polymer with diverse uses across several industries. PEMA is a specific polymer classified within the polymethyl methacrylate (PMMA) family. PMMA, sometimes referred to as acrylic or plexiglass, is a thermoplastic material notable for its transparency. PEMA is a modified form of PMMA in which a tiny fraction of the methyl methacrylate monomer is substituted with ethyl methacrylate monomer during the process of polymerization[84]. PEMA has some features that are similar to PMMA, including transparency, exceptional weather resistance, and a high level of impact resistance. It is frequently employed as a replacement for PMMA when desirable characteristics are required. PEMA demonstrates enhanced flexibility and a reduced glass transition temperature in comparison to PMMA by integrating ethyl methacrylate units into the polymer chain[84].

PEMA, like PMMA, has applications in areas such as automotive, construction, electronics, signs, and medical equipment. PEMA is present in many items such as light coverings, windows, lenses, displays, and protective coatings. It is crucial to acknowledge that PMMA and PEMA have many similarities. However, the inclusion of ethyl methacrylate in PEMA might somewhat modify its characteristics. Therefore, it is vital to carefully analyze the unique needs of a given application when deciding between PMMA and PEMA[84]. PEMA has also attracted a lot of interest for a variety of biomedical applications, including the repair of bone and cartilage[84, 85], polymer electrolytes and membranes for energy generation and storage devices[86], biodegradable

antimicrobial packaging materials[87, 88], optical[84, 89] and electronic components[90], and corrosion protection coatings[91, 92].

PEMA and its composites have favourable biocompatibility characteristics, giving them a viable option for biomedical applications. Biocompatibility is the capacity of a substance to interact with biological systems without inducing any detrimental consequences. Research has demonstrated that PEMA and its composites have a little harmful effect on cells and are highly compatible with human cells[84]. PEMA exhibits a minimal inflammatory reaction, making it very suitable for biological purposes. PEMA and its composites possess features that render them appropriate for utilization in diverse biomedical applications, including orthopedic implants, dental materials, and drug delivery systems[84]. In addition, PEMA composites may be customized to possess precise biocompatibility characteristics by the integration of bioactive substances, such as growth stimulants and antibiotics, into the material. This characteristic enhances its potential for utilization in biological applications[84].

However, it mostly demonstrates solubility in extremely harmful and carcinogenic solvents including benzene[93-95], toluene[94-96], and methyl ethyl ketone[97]. This is a significant barrier to PMMA/PEMA's use in the biomedical industry. This is because solvent molecules will still be present in the bulk or on the surface even after the solvent has mainly evaporated, leaving behind a solid polymer layer. In addition to the choice of the suitable solvent for PMMA/PEMA, making functional inorganic or organic components well disseminated in the PMMA/PEMA matrix is another challenge in the creation of PMMA/PEMA composites.

2.1.3.2. PVDF

PVDF is a thermoplastic that is highly non-reactive and belongs to the fluoropolymer family. The Curie brothers first introduced the piezoelectric characteristics of PVDF in 1880[98]. PVDF is a famous pure and highly non-reactive fluoropolymer with molecular formula $(\text{CH}_2\text{CF}_2)_n$. Polyvinylidene fluoride (PVDF) has remarkable resilience to both creep and fatigue. When PVDF is in thin parts, such films, filaments, and tubes, it exhibits a flexible nature and becomes translucent. Polyvinylidene fluoride (PVDF) possesses several outstanding features, such as a high dielectric constant, strong mechanical qualities, excellent thermal stability, resistance to chemicals, UV radiation, nuclear radiation, and weather conditions. PVDF has the ability to adopt various molecular crystal structures, which can undergo transformation depending on the procedure used for sample preparation. This characteristic enables the polymer to assume numerous shapes during its production [8]. PVDF is also a non-transparent polymer, which renowned for its exceptional mechanical robustness and electrical properties. The presence of piezoelectricity, pyroelectricity, and nonlinear optical characteristics distinguishes this organic molecule as unique[99].

Researchers have used PVDF, a piezoelectric material, to examine the piezoelectric characteristics of live tissue in tissue engineering research[100]. Piezoelectric characteristics may be detected in several organs of the human body, such as bone and ligaments[101-104]. The utilization of PVDF materials in tissue engineering demonstrates a favourable potential for enhancing human health and is an increasing area of focus in medical research. Recently, Atiye et al. published a study on a wound dressing material made of PVDF that includes ionic liquids[105]. This material is designed to regulate the administration of drugs and has the ability to provide dual therapeutic effects[105].

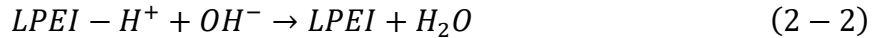
2.1.3.3. Polyethylenimine

Polyethylenimines, or PEIs, are cationic polymer [106] molecules made up of two aliphatic carbons and repeating units of amine groups. Linear polyethyleneimines (LPEIs) commonly synthesized through acid or amine hydrolysis in the polyoxazoline backbone and solely consist of secondary amino groups. On the other hand, branching polyethyleneimines (BPEIs) are generated through ring opening polymerization of aziridine and comprise all three types of amino groups.[107]. At room temperature, LPEI is solid (melting point: 73-75C), while BPEI is liquid (regardless of molecular weight). LPEI dissolves in ethanol, methanol, chloroform, and hot water with a low pH[107-109]. LPEI is generally less hazardous and has the potential for improved transfection efficiency, whereas BPEI has a higher chemical reactivity and can form smaller complexes with DNA in circumstances including salt[107, 110]. PEI has a wide range of applications because of its polycationic character[109]. In contrast to BPEIs, LPEIs are better able to adhere to a specific binding site and can easily change their geometry, as shown by the geographic characteristics of linear and branching PEIs. In general, PEIs' chemical properties are stable, and they are compatible with space. When compared to linear PEIs, branched PEIs typically have a negligible energy effect on the glucose oxidase enzyme (GO_x)[107, 109]. PEIs have a widespread application such as biomedical imaging[111-114], gene delivery[109, 115, 116], controlled drug delivery[107, 116-118], antimicrobial agents[119-123]. In previous study, it was investigated that the BPEI has been involved in the antibacterial applications which was co-synthesized to the hybrid hydrogels with polyvinyl alcohol and polydopamine[124]. Moreover, the BPEI was also considered to be modified with poly(L-lactic acid) to fabricate the biomedical scaffold[125]. As for the LPEI, it was used for the surface functionalization of hydroxyapatite and

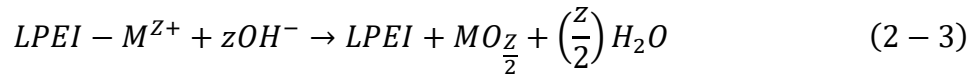
the preparation of biocomposites to fabricate the biomimetic scaffolds with controlled interconnected macroporosity, mechanical stability, and predictable degradation behavior[126]. LPEI can also be used for surface functionalization of gold nanoparticles for biomedical applications such as biosensors[127]. However, because BPEIs are liquids at all molecular weights and are highly soluble in water, the EPD of pure BPEI films for biomedical applications is challenging. On the other hand, only secondary amines make up the chemical structure of linear PEI (LPEI), which is a solid [128]. LPEI was dissolved in water after being protonated in acidic solutions:



The process of deposition involved the cataphoresis of protonated LPEI-H⁺ towards the cathode surface, where a local pH increase caused the production of LPEI films and deprotonation[128].



This approach made it possible to co-EPD proteins, medicines, and bioceramics with LPEI[128, 129]. LPEI can form soluble complexes with metal ions (M^{Z+}) by solubilizing it in solutions of metal salts. The cationic complexes LPEI-M^{Z+} undergo cataphoresis, which is the basis of the deposition process. The electrosynthesis of nanostructured metal hydroxides or oxides is paired with cathodic deposition of LPEI in this instance:



For thin film deposition in biosensor applications, the utilization of LPEI compounds shows promise[129].

2.2. Colloid Processing Techniques: Electrophoretic Deposition and Dip Coating

2.2.1. Fundamentals of Electrophoretic Deposition

Electrophoretic deposition (EPD) is a colloidal processing technique that utilizes the electrophoresis mechanism to move charged particles suspended in a solution under an electric field. This movement allows the particles to be deposited in an organized manner on a substrate, resulting in the formation of thin or thick films, coatings, and free-standing bodies. The utilization of EPD to arrange spherical colloids into meticulously structured colloidal crystals is widely recognized. EPD is attracting growing interest from the materials research community, and there is a growing number of new applications for this technique in the processing of both traditional and advanced materials. The interest in EPD stems from its exceptional versatility in working with various materials and combinations thereof. Additionally, EPD is highly cost-effective, typically necessitating only basic processing equipment and infrastructure. Additionally, EPD exhibits significant scalability, allowing for the production of products of various sizes, ranging from micrometres to meters. Furthermore, it can be easily customized to accommodate different shapes of devices and components. EPD is typically performed in a two-electrode cell, as illustrated in Figure 2-1. Electrophoresis is used to move charged particles in a liquid towards the working electrode. The formation and growth of solid deposits on the electrode mainly occur through particle coagulation. EPD can be utilized on a wide range of materials that are present as fine particles in colloidal suspensions. Metals, polymers, ceramics, glasses, and their composites can be deposited using the technique of EPD[130].

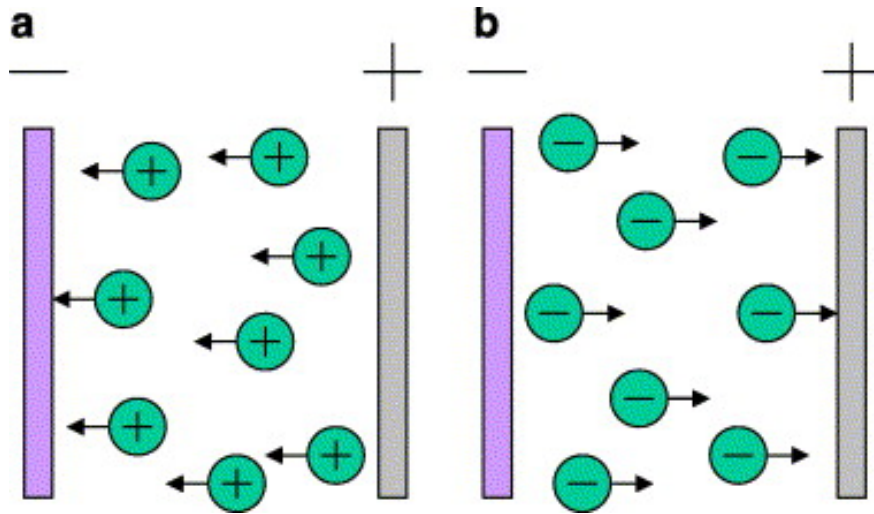


Figure 2-1 Schematic illustration of electrophoretic deposition process. (a) Cathodic EPD and (b) anodic EPD[131] with permission from Elsevier

EPD is particularly important for biomedical applications because of the remarkable purity of the deposits and the ability to uniformly deposit them on surfaces with complex forms. EPD of multilayer films, which consist of individual layers with precisely regulated thickness and content, is especially significant for biomedical applications. Furthermore, EPD enables the production of films with varying composition and precise morphological control. Another advantage of electrophoretic deposition (EPD) for biomedical applications is the ability to deposit diverse organic and inorganic composites at ambient temperature[132].

2.2.1.1. Particles interactions: The DLVO theory and other interparticle forces

The colloidal stability of suspensions for EPD can be analyzed by the application of Derjaguin-Landau-Verwey-Overbeek (DLVO) theory of colloidal stability. This theory states that the overall interaction between colloidal particles is comprised of two components: the Coulombic double-layer repulsion and the Van der Waals' attraction[133].

The total energy V_T of interaction of two isolated, identically charged particles can be calculated as:

$$V_T = V_A + V_R \quad (2 - 5)$$

Where V_A is the attractive energy of the London-van der Waals' interaction between two spherical particles and can be defined by:

$$V_A = -\frac{A}{6} \left(\frac{2}{s^2 - 4} + \frac{2}{s^2} + \ln \frac{s^2 - 4}{s^2} \right) \quad (2 - 6)$$

Where A is the Hamaker constant, and s can be defined as:

$$s = 2 + \frac{H}{a} \quad (2 - 7)$$

H is the shortest distance between the two particles and a is the radius of the spherical particles. In the case $H \ll a$, Eq.6 can be modified to:

$$V_A = -A \frac{a}{12H} \quad (2 - 8)$$

V_R is the repulsive energy and can be defined as:

$$V_R = 2\pi\epsilon\epsilon_0 a \psi^2 \ln[1 + e^{-kH}] \quad (2 - 9)$$

Where ϵ is the dielectric constant of the solvent, ϵ_0 is the vacuum dielectric permittivity, ψ is the surface potential, $1/\kappa$ is the Debye length using:

$$\kappa = \left(\frac{e_0^2 \sum n_i z_i^2}{\epsilon\epsilon_0 kT} \right)^{\frac{1}{2}} \quad (2 - 10)$$

The parameters in the equation are defined as follows: e_0 represents the charge of an electron, k represents the Boltzmann constant, T represents the temperature, and n_i represents the concentration of ions with a valence of z_i . The repulsion between two colloidal particles is proportional to the charge of the diffuse layer on the particles.

Figure 2-2A illustrates the correlation between the force profiles of particle interactions and the distance between particles. The Van der Waals forces controlled the profiles at both long and short distances, whereas the double layer contribution determined the forces at the middle distances. Figure 2-2B demonstrates that the overall interaction energy reached a peak, known as an energy barrier, which hinders the aggregation of particles. The maximum point on the total energy curve is reached when the repulsive force between the double layers is considerably greater than the attractive force of Van der Waals.

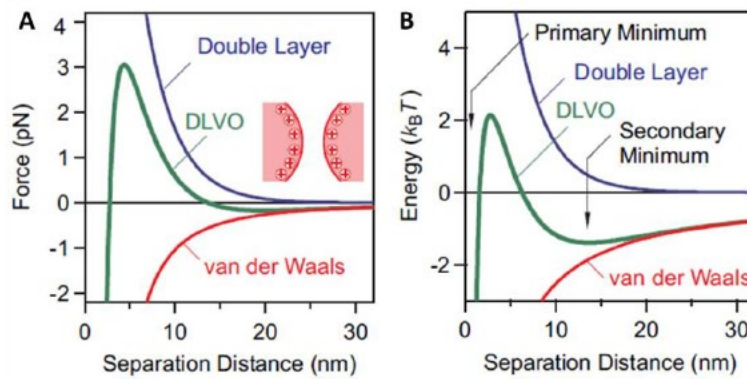


Figure 2-2 The force profiles (A) and the potential energy profiles (B) as functions of the separation distance between two particles, according to the DLVO theory[134], used with permission.

The DLVO theory takes into account the influence of electrolyte ions' concentration and valence, as seen in the equations above. This enables precise prediction of the stability of a colloidal solution. The thickness of electrical double layers, as determined by the Debye length ($1/\kappa$), is influenced by the concentration of the electrolyte[133]. The DLVO theory describes that there is a critical electrolyte concentration at which particles aggregate. The threshold diminishes as the valence of the electrolyte ions with an opposing charge to that of the particles increases[133]. The double layer force dominates in the interaction between particles when the electrolyte concentrations are low, or the surface charge densities are large. Conversely, the Van der Waals'

force governs the contact in situations when there are high concentrations of electrolytes or low surface charge densities. The energy profile demonstrates a peak at moderate concentrations or charge densities, with the highest value occurring at a separation distance around the Debye length[133, 134]. The energy profile peak diminishes as the electrolyte content increases. Coagulation is the process in which the energy barrier is eliminated[133].

The validity of the DLVO theory has been examined in prior scholarly works. Nevertheless, there are still constraints when examining the interaction between two particles. The DLVO hypothesis is only applicable to systems that are highly dilute. The theory relies on the Poisson-Boltzmann (PB) approximation, which, however, neglects the attractive ion correlation forces within the ion cloud. Thus, the theory is applicable solely for the examination of interactions among individual particles that are not connected or influenced by other factors. The phenomenon known as the volume exclusion effect[135, 136] results in a force of attraction between particles. This force of attraction results in the aggregation and flocculation of particles[137].

Furthermore, the DLVO theory fails to account for the impact of polymer bonding or adsorption on the particle surface, as it can give rise to both attractive and repulsive forces[138]. Upon introducing a polymer into the solution, one of two outcomes may arise: the particles either form a stable suspension or aggregate together[138, 139]. Steric stabilization refers to the repulsion force between particles induced by long-chain polymers fixed onto the particle surface, as depicted in Figure2-3. This repulsion force is a result of steric hindrance. The adsorption of polyelectrolytes enables dispersion through the combined effects of electrostatic and steric repulsion. At low concentrations of polymer, a single polymer chain can attach itself to many particle surfaces, causing a phenomenon known as "bridging flocculation" as shown Fig.2-3. In the colloidal system, non-adsorbing polymers may also cause depletion stabilization or depletion flocculation of the

particles (see Fig. 2-3)[140-142]. Prior research[139, 142, 143]indicates that dipole-dipole, hydrophobic, and electrostatic interactions occur between the particles and polyelectrolytes.

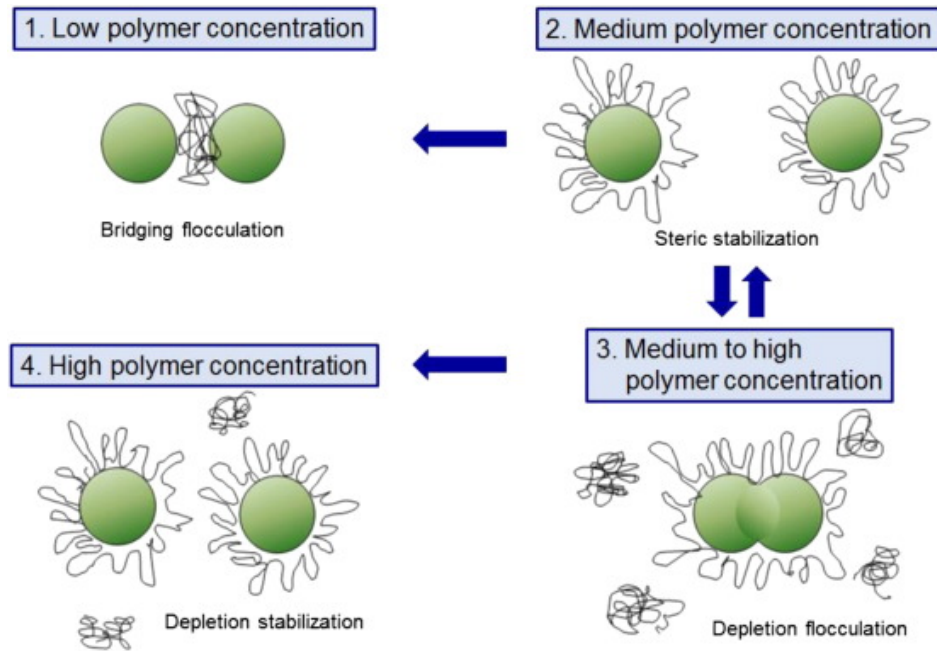


Figure 2-3 A simplified representation of the possible effects of polymer addition on the stability of colloidal system[142], used with permission.

Hence, the DLVO theory offers a means to regulate the stability of the colloidal system by manipulating factors such as electrolyte concentration and surface charge. Nevertheless, considering the mentioned constraints of the DLVO theory, the use of dispersing agents is a viable approach to enhance the stability of the colloidal system.

2.2.1.2. Suspension stability and particle charging

In order to sustain the suspension, a repulsion force must be generated between the particles that is strong enough to oppose their attraction. Three of the most common methods are electrostatic, steric, and electrosteric stabilization.

Electrostatic stability

When the particles experience repulsion from one another due to electrostatic charges, electrostatic stabilization takes place. The interaction of the electrical double layers of charge generated surrounding each particle is what causes the repulsion. There are two different situations that how particles get the electrostatic charges in both non-aqueous and aqueous solutions.

For aqueous solution: There are various ways for dispersed particles to acquire a charge on the surface in an aqueous liquid. They are as follows: (1) preferential ion adsorption; (2) surface group dissociation; (3) isomorphic substitution; and (4) polyelectrolyte adsorption. The preferential adsorption of ions in liquid is frequently observed for oxide particles, whereas clays frequently exhibit the isomorphic substitution process. It has been covered in Healy et al.'s research[144] that describes how common surface groups, such as sulphate, carboxyl, and sulfonate groups, dissociate. The charge on the particle surface and the opposing and equal countercharge are the two parts of charges in the electrostatically stabilized suspension. On the particle surface, it is presumed that the positive ions have been preferentially adsorbed. Positive ions on the particle surface will be neutralized by an equal amount of counterions in the absence of thermal motion. Nonetheless, there is enough thermal mobility to prevent the formation of a dense double layer. Conversely, the counterions are not permanently attached on the surface of the particle; rather, they move inside the media. They comprise the diffuse layer and are haphazardly arranged, as shown in Figure 2-4.

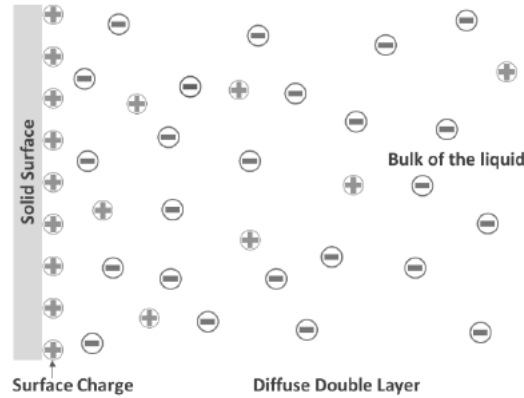


Figure 2-4 The schematic diagram of the electrical double layer associated with a positively charged surface in a liquid[141]

In Figure 2-5, when one moves farther away from the surface, the ion concentration rapidly changes and the electrical potential decreases correspondingly. At a distance of $1/\kappa$, the potential reduced to $1/e$ of the potential at the particle surface; beyond this, the potential changed very little as the distance increased[141]. As a result, the double layer thickness can be defined as $1/\kappa$, also known as the Debye length. For the examination of the electrical double layer, $1/\kappa$ frequently used Eq. (2-10) in section 2.2.1 states that a number of experimental parameters determine the size of the double layer. Modifying these values can affect the strength of the double layer repulsion and, consequently, the stability of the suspension[141].

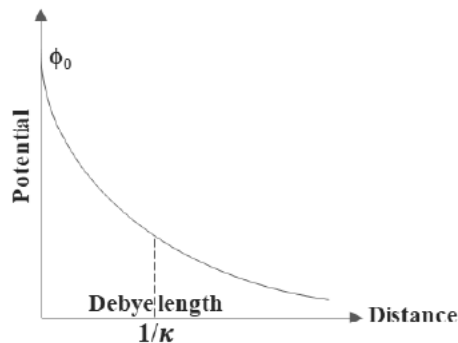


Figure 2-5 The electrical potential as a function of distance from the surface[141]

When two particles in the solution come into touch, the diffuse double layers will start to overlap. The contact between the double layers causes a repulsion between these two particles as a result. If the repulsion is strong enough to oppose the Van der Waals force that is attracting, a stable suspension will form.

For non-aqueous solution: Theoretically, the dielectric constant (ϵ) of the medium, which specifically affects stability via the stabilizing electrolyte's degree of dissociation, has a significant impact on the amount of electrostatic stabilization in non-aqueous liquid. A precise number of ions in the liquids similarly generate a sufficient repulsion force, except for the charge of the particles. The ionic strengths in non-aqueous media are frequently much lower than 10^{-6} M, their dielectric constant is comparatively low, and the electrolytes in those liquids cannot completely dissociate. In the non-aqueous media, there are very few charges present. Thus, in such a non-aqueous liquid, the charged and scattered particles are surrounded by the extended ionic layers and sit on the double layers of each other, unless the particle concentration is very low[145-148]. The interaction of multiple layers of particles in non-watery liquids is comparable to electrostatic repulsion in aqueous media. Because it influences the interaction in two ways—indirectly affecting the dissociation of electrolytes and directly measuring the solvent's screening of charges—the dielectric constant is a crucial metric in this situation. It is believed that in a liquid with a low dielectric constant, electrostatic repulsion is insufficient to produce suspension stability[149]. Three conditions need to be satisfied for the colloidal particles to stop coagulating irreversibly. (1) Enough charge must be applied to the particles. (2) There need to be a moderate amount of ions. If there are more ions than are needed, the double layer will be completely squeezed, but the potential decay surrounding the particles can be steepened. (3) A position must be determined where the electrostatic repulsion surpasses the attractive van der Waals' force. The Lifshitz theory

can be used to calculate the van der Waals attraction between particles in a medium with a low dielectric constant [150]. The van der Waals attraction between particles in mediums with a low dielectric constant is comparatively minimal when compared to water. Consequently, in the non-aqueous medium with low dielectric constant, repulsive pair interaction can be achieved with a reduced energy barrier.

Steric Stability

Steric stabilization, as illustrated in Figure 2-6, is a representation of colloidal stabilization, which is accomplished by the interaction between uncharged polymer chains adsorbed onto particle surfaces[151].

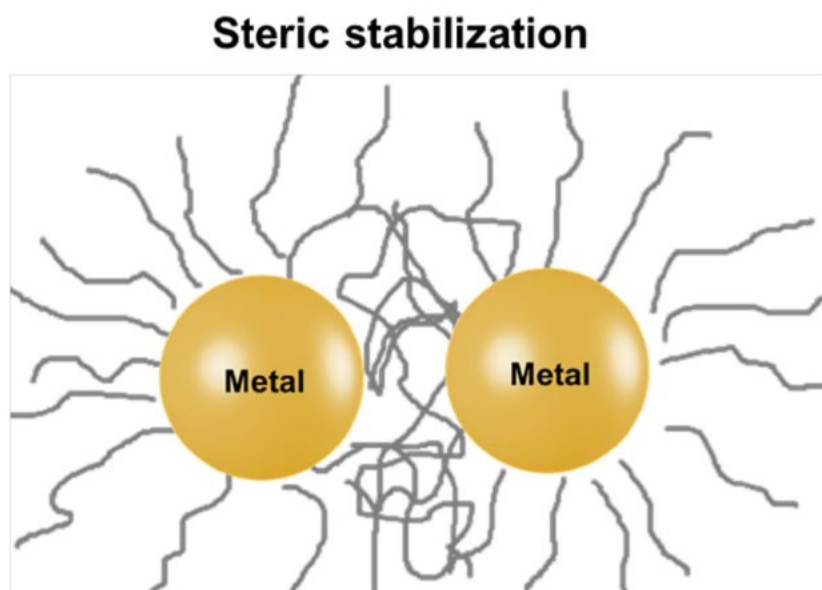


Figure 2-6 Schematic representation of steric stabilization of metal colloid particles[152], used with permission

In contrast to electrostatic stabilization, which is achieved by the interaction of charged particles, steric stabilization is facilitated by interactions among polymer chains, the nature of which is dictated by the chains' configurational entropy. Although steric stabilization is frequently

linked to particles in organic solvents, it can still work effectively in aqueous solutions. Nowadays, steric stabilization is used in the manufacturing of many different items, such as paints, inks, coatings, and medications. It is frequently used in ceramics processing to create stable suspensions during the consolidation of ceramic powders using casting techniques like tape casting and slip casting. In order to minimize the risk of desorption, the polymer chains must be well adsorbed onto the particle surface. Secondly, the adsorbed layer must be thick enough to provide enough repulsion force when the particles approach one another in order to achieve effective steric stabilization[141].

Electrosteric stabilization

Electrostatic and steric repulsion are combined in electrosteric stabilization (Figure 2-7). Adsorbed polymers must exist, and there must be a significant double layer repulsion[152].

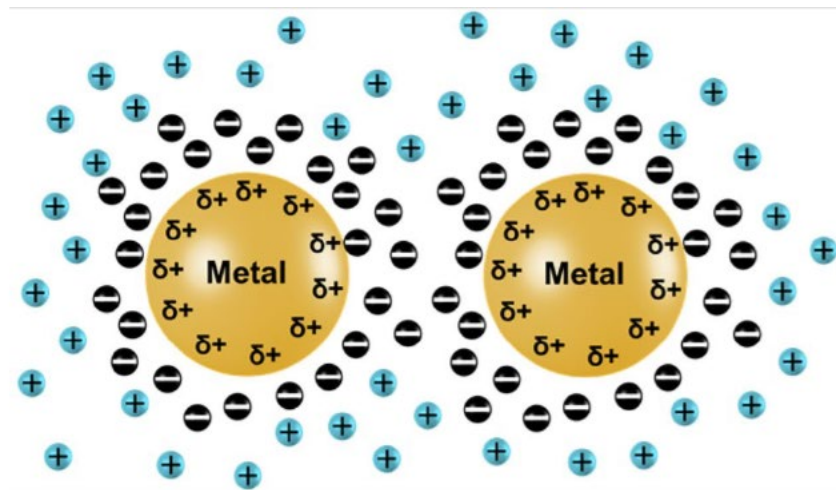
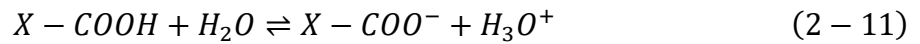


Figure 2-7 Schematic representation of electrosteric stabilization of metal colloid particles[152], used with permission

In most cases, electrosteric stabilization is connected to suspensions in aqueous media. Nevertheless, several studies have indicated that it is also possible to accomplish electrosteric stabilization in certain non-aqueous liquids[153]. Using polyelectrolytes with at least one ionizable

group—such as a carboxylic or sulfonic acid group—that can dissociate to produce charged polymers is a popular technique for electrosteric stabilization in aqueous media.

The dissociation and adsorption of polymers are greatly influenced by the characteristics of the solvent as well as the surface of the particle. The structures of two popular polymers—poly(methacrylic acid) (PMAA) and poly(acrylic acid) (PAA)—for electrosteric stabilization are shown in Figure 2-8. The following equation,



where X denotes PMAA or PAA's primary structure without the carboxylic group chain, describes the dissociation reaction. The pH and ionic concentration of the solution determine how much of the functional groups are dissociated and non-dissociated.

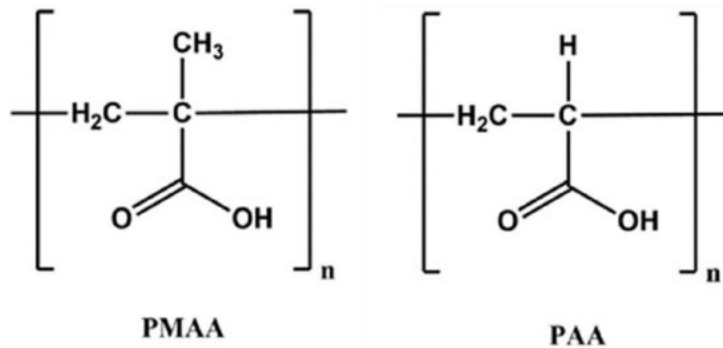


Figure 2-8 Schematic diagram showing the polymer segments of poly(methacrylic acid) (PMAA) and poly(acrylic acid) (PAA)[154], used with permission

Block copolymers, graft copolymers, and homopolymers like poly(acrylic acid) can all be used for electrosteric stabilization. In the business, polyelectrolytes are frequently used to create extremely concentrated ceramic suspensions (more than 50% particles by volume), which are then burned and condensed to create dense products.

2.2.1.3. Biomimetic Dispersing Agents

Charged or uncharged organic molecules or polymers are employed as dispersing agents to boost a colloid's overall stability[155]. They are extensively utilized in numerous industries, such as paint, personal cosmetics, and home cleansers, for a wide range of purposes. Dispersing agents have played an essential part in the progress of EPD processing in the past ten years. However, there has been a growing pursuit of novel organic molecules that possess the ability to both charge and disperse a wide range of inorganic particles or functional organic materials [156]. It can be difficult to develop new dispersants for biomedical applications because there are a lot more factors, such as toxicity and biocompatibility, to take into account than in ordinary uses. One method uses natural or biomimetic surfactants and draws inspiration from mother nature. Bile acids and their salts, as well as compounds from the catechol family, are two examples of biomimetic dispersion agents. When creating novel biomaterials, it is helpful to use a biomimetic approach because biomimetic molecules frequently overcome the limitations imposed during material selection and possess intriguing characteristics like ultra-high adhesion or the capacity to self-assemble into complex structures only seen in nature.

Catechol-based dispersants for metal oxides particles

The investigation of the process of mussel adhesion to various surfaces provided a new avenue for research on sophisticated dispersing agents that could be firmly fixed onto the particle surface[157, 158]. According to earlier research, protein macromolecules containing the catecholic amino acid L-3,4-dihydroxyphenylalanine (DOPA) are involved in the strong mussel adhesion. The main advantages of catechol chemistry are its good binding strength in wet environments and wide range of substrates[159]. The OH group of the catechol ligands complexes with metal atoms on material surfaces, which is the mechanism responsible for mussels' adherence (Figure 2-9).

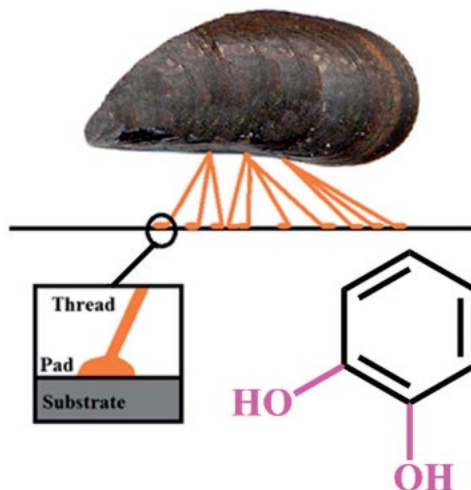


Figure 2-9 Schematic of mussel adsorption and chemical structure of catechol[156], used with permission.

Here, the catechol-based compounds' structures and adsorption processes are explained (Figure 2-10). A catechol is a phenolic group, an unsaturated six-carbon ring with two OH groups attached to neighbouring carbon atoms. DOPA is a member of the catechol group. A catechol ligand as well as extra carboxylic and amino groups are present in the chemical structure of DOPA (Figure 2-10). This molecule exhibits bidentate interfacial interactions with metal ions on various surfaces and zwitterionic characteristics. The zwitterionic characteristics of DOPA make it challenging to apply as charging agents for EPD, however research on other catechol-based compounds has been prompted by the study of DOPA adsorption.

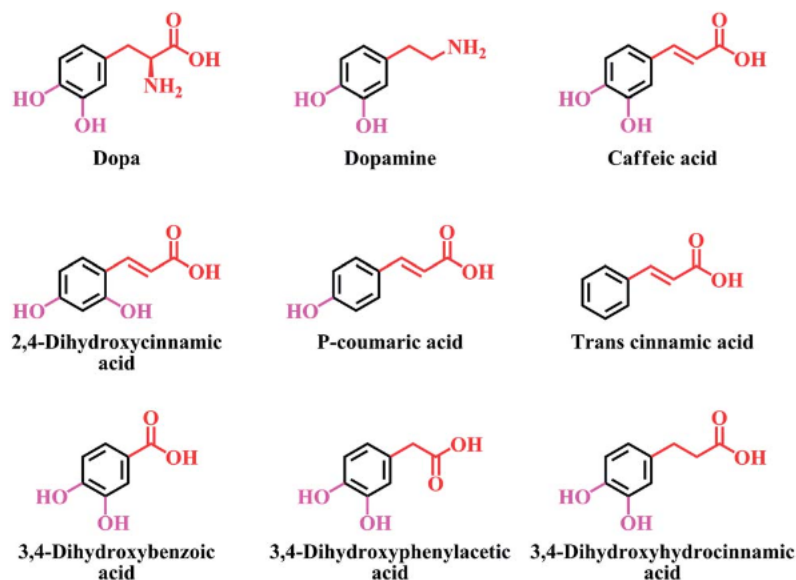


Figure 2-10 Structure of molecules from catechol family[156], used with permission

The two OH groups of the catechol ligand, whose adsorption is dependent on the chelating process, are present in the dopamine structure (Figure 2-10). In inorganic acids, the amino group is protonated. Dopamine exhibits cationic characteristics in acid as a result. In simple liquids, dopamine self-polymerizes, a process that was utilized to create polydopamine coatings. Strong adherence is exhibited by polydopamine to a variety of substrates, including Pt, TiO₂, stainless steel, and other materials[156]. When it comes to the EPD of ceramic particles, dopamine can be employed as a dispersing and charging agent. It can also be used with the EPD of cationic polyelectrolytes to create organic-inorganic composites[160].

For stainless steel, caffeic acid (CFA) can function as a highly effective green corrosion inhibitor. The molecular structures of CFA and DOPA are comparable (Figure 2-10). The anionic characteristics of CFA are linked to the carboxylic group's dissociation. In a variety of liquids, the robust adsorption of CFA has been observed on inorganic surfaces such as stainless steel, TiO₂, MnO₂[161, 162]. The adsorption of CFA involves both carboxylic (Figure 2-11) and phenolic bonding sites.[163] Mechanisms for bidentate bridging bonding (Figure 2-11b) and bidentate

chelating bonding (Figure 2-11a) were proposed[164, 165]. Depending on the makeup of the adsorbent materials, the adsorption may entail either outer sphere bonding (Figure 2-11b) or inner sphere bonding (Figure 2-11b). It was discovered that CA can be utilized in the anodic deposition of composite films as a co-dispersant.

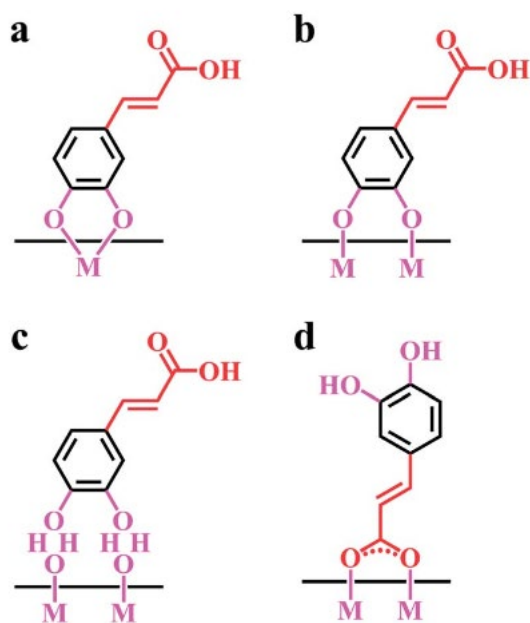


Figure 2-11 Suggested adsorption mechanisms of caffeic acid: (a) bidentate chelating bonding, (b) bidentate bridging bonding (inner sphere), (c) bidentate bridging bonding (outer sphere) of catechol group, (d) adsorption, involving a carboxylic group[156], used with permission

The chemical structures of the catechol family members 3,4-dihydroxybenzoic acid (DHB), 3,4-dihydroxyphenylacetic acid (DHP), and 3,4-dihydroxyhydrocinnamic acid (DHC) are shown in Figure 2-10. These compounds' anionic properties are partly due to the carboxylic groups. On metal salts, they exhibit high adsorption as well. These three compounds show promise as dispersing and charging agents for electrophoretic deposition (EPD) of various oxide materials from suspensions in ethanol, according to recent investigations[166, 167]. In particular, the studies showed that DHB and DHP strongly adsorbed to TiO₂ nanoparticles. Research also showed that

additional compounds with a similar structure, including gallic acid, can be employed for material EPD[168].

Bile Acids and Bile Acid Salts

Anionic biosurfactants with physiological significance, bile acid salts (BAS) are involved in numerous metabolic processes. Lipids, vitamins, cholesterol, and other useful biomolecules are all solubilized by BAS. BAS are hydrophobic and hydrophilic steroid compounds having SO_3^- or COO^- anionic groups on the hydrophilic side. Commercial BAS synthesis and its applications in the engineering and biomedical industries have attracted a lot of attention lately. There is growing interest in BAS's interactions with other materials and the creation of mixed micelles. Different materials become more soluble and dispersed as a result of these interactions. Experiments on the solubilization of medicines in water are particularly interesting because they offer a platform for the creation of novel drug delivery systems. Excellent dispersion of hydrophobic materials, including graphene, carbon nanotubes, diamonds, and polymers, was made possible by BAS, for use in biosensors and biomedical implants. By preventing defect development in the conductive carbon network, the surface modification and dispersion of carbon nanotubes using adsorbed BAS provides advantages over chemical functionalization approaches for biosensor applications. The amphiphilic structure of BAS governs its gel-forming capabilities and aids in the production of composite gels. Drug delivery is one area in which BAS gels have numerous significant uses[169].

In particular, BAS are crucial for electrophoretic deposition (EPD). Many articles in the past have demonstrated the success of bile acids and bile acids salts as dispersing agents. It has been proved that the composite films could be obtained by using tetracycline and ibuprofen as model drugs with commercial BAS[170]. Polymers such as PVDF also can be solubilized by BAS[171] and inorganic materials like multiwalled carbon nanotubes (MWCNT) [172] can be

dispersed by BAS as well. BAS show great promise in material surface modification and composite film manufacturing for biological applications.

2.2.2. Dip coating

Dip coating is an incredibly easy, affordable, and repeatable method. Figure 2-12 is an illustration of the dip coating procedure[173]. The substrate must first be submerged in a solution containing coating component particles in order to begin the dip coating process. The next step is to retreat into an environment that contains water vapour at a steady speed. Afterwards, the substrate's surface is covered uniformly with a liquid coating. After drying at room temperature, the volatile solvents can be eliminated and some chemical processes that could result in the creation of films [173]. Following that, the coating typically requires heat treatment to harden it or change its chemical composition[173].

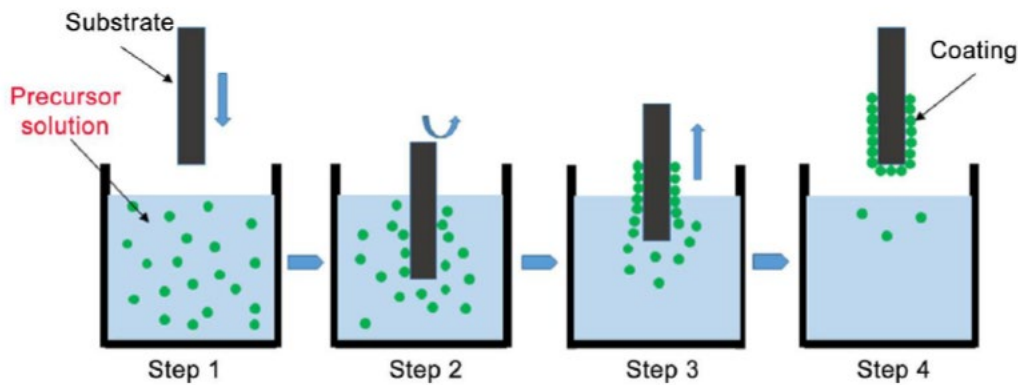


Figure 2-12 Graphical representation of dip coating technique[173], used with permission

The liquid characteristics in the dip coating process determine the quality and functionality of the deposited coatings. Thus, it is crucial to choose solvents and solutes carefully. First, one crucial element that must be taken into account is solvent volatility. In addition to allowing the liquid film to appropriately level off, moderate volatility can minimize the drying time. Secondly, the liquid should flow uniformly and the substrate should be fully wetted when the surface tension

is low enough. Short-chain aliphatic alcohols, like ethanol, isopropanol, and n-propanol, are frequently chosen as solvents for dip coating based on the criterion[174]. Beyond that, the performance of the deposition is frequently customized by combining different solvents[174, 175]. The choice of solute is far more complicated. The solute needs to be able to dissolve at the right concentration first. For instance, it is challenging to provide adequate substrate coverage while utilizing diluted polymer solutions. Second, as the solvent evaporates, the solute tends to hydrolyze into an amorphous gel film rather than crystallize or precipitate[174]. More than that, because of their potent film-forming and binding qualities, high molecular weight polymers are recommended.

The coating thickness can be predicted using the below Landau-Levich equation:

$$h = 0.94(\eta U)^{\frac{2}{3}}/\gamma_{LV}^{\frac{1}{6}}(\rho g)^{1/2} \quad (2 - 12)$$

where g stands for gravity, h for coating thickness, η for liquid viscosity, U for withdrawal speed, γ_{LV} for liquid-vapor surface tension, and ρ for sol-specific gravity. This equation states that thicker films are produced by increasing viscosity and withdrawal speed, however coating thickness is reduced by the subsequent drying and sintering processes. Hijon[176] and Mohseni[177] assert that another significant element affecting the thickness and homogeneity of the as-deposited thin coating is the suspension's concentration. The layer that forms is thinner and the adhesion between the coating and substrate is higher at lower concentrations. As a result, in a particular system, the coating liquid concentration and withdrawal speed can both regulate the thickness of formed films. In a colloidal system, films as thin as 1 nm can be created, and the coating of an organic-inorganic composite can attain a thickness of multiple microns due to the network's increased flexibility and decreased shrinkage[174]. Thick films can also be obtained via

the dip coating procedure through multiple depositions. Furthermore, a laminate including various coating materials can be constructed using this technology.

Consequently, for a high-quality film to be produced during the polymer coating process, a high molecular weight polymer that is highly soluble as the solute and a blend of several solvents as the solvent are required. Furthermore, the multiple deposition approach makes it possible to create laminates with several functional layers made of various materials.

2.3.Objectives

The main goal of my research is to develop new colloidal and electrochemical techniques to create advanced nanocomposite coatings for biomedical applications. These coatings will have multiple functions, such as preventing infections and enhancing the compatibility and performance of medical devices. The research will focus on three key areas to achieve this goal:

1. Design of advanced synthesis methods that prevent agglomeration and control the size of inorganic nanoparticles.
2. Development of advanced solubilization and deposition methods for commercially available water-insoluble drugs and polymers for the fabrication of drug-containing coatings to prevent surgical infection.
3. Develop biopolymers and polymeric hydrogels for the fabrication of novel biomaterials for biomedical applications.

2.4.References

- [1] M. Aslam, F. Ahmad, P. S. M. B. M. Yusoff, K. Altaf, M. A. Omar, and R. M. German, "Powder injection molding of biocompatible stainless steel biodevices," *Powder Technology*, vol. 295, pp. 84-95, 2016, doi: 10.1016/j.powtec.2016.03.039.

- [2] M. Talha *et al.*, "Corrosion performance of cold deformed austenitic stainless steels for biomedical applications," *Corrosion Reviews*, vol. 37, no. 4, pp. 283-306, 2019.
- [3] N. K. Awad, S. L. Edwards, and Y. S. Morsi, "A review of TiO₂ NTs on Ti metal: Electrochemical synthesis, functionalization and potential use as bone implants," *Materials Science and Engineering: C*, vol. 76, pp. 1401-1412, 2017.
- [4] M. Talha, C. Behera, and O. Sinha, "A review on nickel-free nitrogen containing austenitic stainless steels for biomedical applications," *Materials Science and Engineering: C*, vol. 33, no. 7, pp. 3563-3575, 2013.
- [5] M. Z. Ibrahim, A. A. Sarhan, F. Yusuf, and M. Hamdi, "Biomedical materials and techniques to improve the tribological, mechanical and biomedical properties of orthopedic implants—A review article," *Journal of Alloys and Compounds*, vol. 714, pp. 636-667, 2017.
- [6] N. Manam *et al.*, "Study of corrosion in biocompatible metals for implants: A review," *Journal of alloys and compounds*, vol. 701, pp. 698-715, 2017.
- [7] Q. Chen and G. A. Thouas, "Metallic implant biomaterials," *Materials Science and Engineering: R: Reports*, vol. 87, pp. 1-57, 2015.
- [8] S. Wu *et al.*, "Microstructure and properties of TiO₂ nanotube coatings on bone plate surface fabrication by anodic oxidation," *Surface and Coatings Technology*, vol. 374, pp. 362-373, 2019.
- [9] X. Fan *et al.*, "Fabrication of TiO₂ nanotubes on porous titanium scaffold and biocompatibility evaluation in vitro and in vivo," *Journal of biomedical materials research Part A*, vol. 100, no. 12, pp. 3422-3427, 2012.

- [10] Y. Wang, J. Venezuela, and M. Dargusch, "Biodegradable shape memory alloys: Progress and prospects," *Biomaterials*, vol. 279, p. 121215, Dec 2021, doi: 10.1016/j.biomaterials.2021.121215.
- [11] L. Petrini and F. Migliavacca, "Biomedical Applications of Shape Memory Alloys," *Journal of Metallurgy*, vol. 2011, pp. 1-15, 2011, doi: 10.1155/2011/501483.
- [12] A. Biesiekierski, J. Wang, M. A. Gepreel, and C. Wen, "A new look at biomedical Ti-based shape memory alloys," *Acta Biomater*, vol. 8, no. 5, pp. 1661-9, May 2012, doi: 10.1016/j.actbio.2012.01.018.
- [13] M. Zainal, S. Sahlan, and M. Ali, "Micromachined Shape-Memory-Alloy Microactuators and Their Application in Biomedical Devices," *Micromachines*, vol. 6, no. 7, pp. 879-901, 2015, doi: 10.3390/mi6070879.
- [14] N. Sabahi, W. Chen, C.-H. Wang, J. J. Kruzic, and X. Li, "A Review on Additive Manufacturing of Shape-Memory Materials for Biomedical Applications," *Jom*, vol. 72, no. 3, pp. 1229-1253, 2020, doi: 10.1007/s11837-020-04013-x.
- [15] Y. Ogawa, D. Ando, Y. Sutou, and J. Koike, "A lightweight shape-memory magnesium alloy," *Science*, vol. 353, no. 6297, pp. 368-370, 2016.
- [16] M. Balasubramanian, R. Srimath, L. Vignesh, and S. Rajesh, "Application of shape memory alloys in engineering—A review," in *Journal of Physics: Conference Series*, 2021, vol. 2054, no. 1: IOP Publishing, p. 012078.
- [17] H. F. Li, K. J. Qiu, F. Y. Zhou, L. Li, and Y. F. Zheng, "Design and development of novel antibacterial Ti-Ni-Cu shape memory alloys for biomedical application," *Sci Rep*, vol. 6, p. 37475, Nov 29 2016, doi: 10.1038/srep37475.

- [18] M. Montazerian and E. Dutra Zanotto, "History and trends of bioactive glass-ceramics," *Journal of Biomedical Materials Research Part A*, vol. 104, no. 5, pp. 1231-1249, 2016.
- [19] N. Nezafati, F. Moztarzadeh, S. Hesaraki, and M. Mozafari, "Synergistically reinforcement of a self-setting calcium phosphate cement with bioactive glass fibers," *Ceramics International*, vol. 37, no. 3, pp. 927-934, 2011.
- [20] A. Yazdanpanah, R. Kamalian, F. Moztarzadeh, M. Mozafari, R. Ravarian, and L. Tayebi, "Enhancement of fracture toughness in bioactive glass-based nanocomposites with nanocrystalline forsterite as advanced biomaterials for bone tissue engineering applications," *Ceramics International*, vol. 38, no. 6, pp. 5007-5014, 2012.
- [21] M. Rahmati and M. Mozafari, "Biocompatibility of alumina-based biomaterials-A review," *J Cell Physiol*, vol. 234, no. 4, pp. 3321-3335, Apr 2019, doi: 10.1002/jcp.27292.
- [22] S. Anu and S. Gayatri, "Clinical application of bio ceramics," in *AIP Conference Proceedings*, 2016, vol. 1728, no. 1: AIP Publishing.
- [23] S. Banijamali, B. E. Yekta, and A. Aghaei, "Self-patterning of porosities in the CaO–Al₂O₃–TiO₂–P₂O₅ glass–ceramics via ion exchange and acid leaching process," *Journal of non-crystalline solids*, vol. 380, pp. 114-122, 2013.
- [24] A. G. Nazari and M. Mozafari, "Simulation of structural features on mechanochemical synthesis of Al₂O₃–TiB₂ nanocomposite by optimized artificial neural network," *Advanced Powder Technology*, vol. 23, no. 2, pp. 220-227, 2012.
- [25] C. Piconi, S. G. Condo, and T. Kosmač, "Alumina-and zirconia-based ceramics for load-bearing applications," *Advanced ceramics for dentistry*, pp. 219-253, 2014.
- [26] M. S. Aw and D. Losic, "Nanoporous alumina as an intelligent nanomaterial for biomedical applications," *Intelligent Nanomaterials*, vol. 2, pp. 127-159, 2016.

- [27] T. J. Webster, R. W. Siegel, and R. Bizios, "Design and evaluation of nanophase alumina for orthopaedic/dental applications," *Nanostructured materials*, vol. 12, no. 5-8, pp. 983-986, 1999.
- [28] L. Rony, P. de Sainte Hermine, V. Steiger, R. Mallet, L. Hubert, and D. Chappard, "Characterization of wear debris released from alumina-on-alumina hip prostheses: Analysis of retrieved femoral heads and peri-prosthetic tissues," *Micron*, vol. 104, pp. 89-94, 2018.
- [29] B. Ben-Nissan, A. Choi, and R. Cordingley, "Alumina ceramics," in *Bioceramics and their clinical applications*: Elsevier, 2008, pp. 223-242.
- [30] B. McEntire, B. S. Bal, M. Rahaman, J. Chevalier, and G. Pezzotti, "Ceramics and ceramic coatings in orthopaedics," *Journal of the European Ceramic Society*, vol. 35, no. 16, pp. 4327-4369, 2015.
- [31] J. Chevalier and L. Gremillard, "Zirconia ceramics," in *Bioceramics and their clinical applications*: Elsevier, 2008, pp. 243-265.
- [32] M. Aragón-Duarte *et al.*, "Nanomechanical properties of zirconia-yttria and alumina zirconia-yttria biomedical ceramics, subjected to low temperature aging," *Ceramics International*, vol. 43, no. 5, pp. 3931-3939, 2017.
- [33] M. Swain and L. He, "Mechanical properties of bioceramics," in *Bioceramics and their Clinical Applications*: Elsevier, 2008, pp. 78-105.
- [34] J. Moritz *et al.*, "Nanoroughening of sandblasted 3Y-TZP surface by alumina coating deposition for improved osseointegration and bacteria reduction," *Journal of the European Ceramic Society*, vol. 39, no. 14, pp. 4347-4357, 2019.

- [35] G.-C. Lee and R. H. Kim, "Incidence of modern alumina ceramic and alumina matrix composite femoral head failures in nearly 6 million hip implants," *The Journal of arthroplasty*, vol. 32, no. 2, pp. 546-551, 2017.
- [36] S. Jafari, B. Mahyad, H. Hashemzadeh, S. Janfaza, T. Gholikhani, and L. Tayebi, "Biomedical Applications of TiO₂ Nanostructures: Recent Advances," *Int J Nanomedicine*, vol. 15, pp. 3447-3470, 2020, doi: 10.2147/IJN.S249441.
- [37] M. F. Kunrath, R. Hubler, R. S. A. Shinkai, and E. R. Teixeira, "Application of TiO₂ Nanotubes as a Drug Delivery System for Biomedical Implants: A Critical Overview," *ChemistrySelect*, vol. 3, no. 40, pp. 11180-11189, 2018, doi: 10.1002/slct.201801459.
- [38] S. Wu, Z. Weng, X. Liu, K. W. K. Yeung, and P. K. Chu, "Functionalized TiO₂ Based Nanomaterials for Biomedical Applications," *Advanced Functional Materials*, vol. 24, no. 35, pp. 5464-5481, 2014, doi: 10.1002/adfm.201400706.
- [39] K. Almas, S. Smith, and A. Kutkut, "What is the best micro and macro dental implant topography?," *Dental Clinics*, vol. 63, no. 3, pp. 447-460, 2019.
- [40] C. N. Elias, Y. Oshida, J. H. C. Lima, and C. A. Muller, "Relationship between surface properties (roughness, wettability and morphology) of titanium and dental implant removal torque," *Journal of the mechanical behavior of biomedical materials*, vol. 1, no. 3, pp. 234-242, 2008.
- [41] N. Drnovšek, K. Rade, R. Milačič, J. Štrancar, and S. Novak, "The properties of bioactive TiO₂ coatings on Ti-based implants," *Surface and Coatings Technology*, vol. 209, pp. 177-183, 2012.

- [42] H. Zhang *et al.*, "Improved antibacterial activity and biocompatibility on vancomycin-loaded TiO₂ nanotubes: in vivo and in vitro studies," *International Journal of Nanomedicine*, pp. 4379-4389, 2013.
- [43] B. E. Lee, H. Exir, A. Weck, and K. Grandfield, "Characterization and evaluation of femtosecond laser-induced sub-micron periodic structures generated on titanium to improve osseointegration of implants," *Applied Surface Science*, vol. 441, pp. 1034-1042, 2018.
- [44] K. Gulati *et al.*, "Anodized 3D-printed titanium implants with dual micro- and nano-scale topography promote interaction with human osteoblasts and osteocyte-like cells," *Journal of tissue engineering and regenerative medicine*, vol. 11, no. 12, pp. 3313-3325, 2017.
- [45] U. F. Gunpath, H. Le, R. D. Handy, and C. Tredwin, "Anodised TiO₂ nanotubes as a scaffold for antibacterial silver nanoparticles on titanium implants," *Materials Science and Engineering: C*, vol. 91, pp. 638-644, 2018.
- [46] H. G. Wells, "Pathological calcification," *The Journal of medical research*, vol. 14, no. 3, p. 491, 1906.
- [47] F. H. Albee, "Studies in bone growth: triple calcium phosphate as a stimulus to osteogenesis," *Annals of surgery*, vol. 71, no. 1, p. 32, 1920.
- [48] W. Schram and L. Fosdick, "Stimulation of healing in long bones by use of artificial material," *Journal of oral surgery*, vol. 6, no. 3, pp. 209-217, 1948.
- [49] M. E. Norman, H. M. Elgendy, E. C. Shors, S. F. El-Amin, and C. T. Laurencin, "An in vitro evaluation of coralline porous hydroxyapatite as a scaffold for osteoblast growth," *Clinical materials*, vol. 17, no. 2, pp. 85-91, 1994.

- [50] R. Dekker, J. De Bruijn, I. Van Den Brink, Y. Bovell, P. Layrolle, and C. Van Blitterswijk, "Bone tissue engineering on calcium phosphate-coated titanium plates utilizing cultured rat bone marrow cells: a preliminary study," *Journal of Materials Science: Materials in Medicine*, vol. 9, pp. 859-863, 1998.
- [51] C. D. Friedman, P. D. Costantino, S. Takagi, and L. C. Chow, "BoneSource™ hydroxyapatite cement: a novel biomaterial for craniofacial skeletal tissue engineering and reconstruction," *Journal of biomedical materials research*, vol. 43, no. 4, pp. 428-432, 1998.
- [52] S. Best, A. Porter, E. Thian, and J. Huang, "Bioceramics: Past, present and for the future," *Journal of the European Ceramic Society*, vol. 28, no. 7, pp. 1319-1327, 2008.
- [53] Y. Tanaka and K. Yamashita, "Bioceramics and their clinical applications, Fabrication processes for bioceramics," ed: Cambridge: Woodhead Publishing Limited, England, 2008.
- [54] V. Ingole, B. Sathe, and A. Ghule, "Bioactive ceramic composite material stability, characterization," *Fundamental biomaterials: ceramics*, pp. 273-96, 2018.
- [55] R. G. Carrodeguas and S. De Aza, " α -Tricalcium phosphate: Synthesis, properties and biomedical applications," *Acta Biomaterialia*, vol. 7, no. 10, pp. 3536-3546, 2011.
- [56] X. Hou *et al.*, "Calcium phosphate-based biomaterials for bone repair," *Journal of functional biomaterials*, vol. 13, no. 4, p. 187, 2022.
- [57] E. Rigo, A. Boschi, M. Yoshimoto, S. Allegrini Jr, B. Konig Jr, and M. Carbonari, "Evaluation in vitro and in vivo of biomimetic hydroxyapatite coated on titanium dental implants," *Materials Science and Engineering: C*, vol. 24, no. 5, pp. 647-651, 2004.
- [58] J. Goosen, A. Kums, B. Kollen, and C. Verheyen, "Porous-coated femoral components with or without hydroxyapatite in primary uncemented total hip arthroplasty: a systematic

- review of randomized controlled trials," *Archives of orthopaedic and trauma surgery*, vol. 129, pp. 1165-1169, 2009.
- [59] S. Leeuwenburgh, J. Wolke, J. Jansen, and K. De Groot, "Calcium phosphate coatings," in *Bioceramics and their clinical applications*: Elsevier, 2008, pp. 464-484.
- [60] S. B. Goodman, Z. Yao, M. Keeney, and F. Yang, "The future of biologic coatings for orthopaedic implants," *Biomaterials*, vol. 34, no. 13, pp. 3174-3183, 2013.
- [61] R. G. Hill and D. S. Brauer, "Predicting the bioactivity of glasses using the network connectivity or split network models," *Journal of Non-Crystalline Solids*, vol. 357, no. 24, pp. 3884-3887, 2011.
- [62] P. Stoor, E. Söderling, and J. I. Salonen, "Antibacterial effects of a bioactive glass paste on oral microorganisms," *Acta Odontologica Scandinavica*, vol. 56, no. 3, pp. 161-165, 1998.
- [63] N. Lindfors *et al.*, "Bioactive glass S53P4 as bone graft substitute in treatment of osteomyelitis," *Bone*, vol. 47, no. 2, pp. 212-218, 2010.
- [64] S. Singh, A. Patil, S. Mali, and H. Jaiswal, "Bioglass: A New Era in Modern Dentistry," *European Journal of General Dentistry*, vol. 11, no. 01, pp. 001-006, 2022, doi: 10.1055/s-0042-1742356.
- [65] J. Jones, "Bioactive glass," in *Bioceramics and their clinical applications*: Elsevier, 2008, pp. 266-283.
- [66] H. R. Fernandes, A. Gaddam, A. Rebelo, D. Brazete, G. E. Stan, and J. M. Ferreira, "Bioactive glasses and glass-ceramics for healthcare applications in bone regeneration and tissue engineering," *Materials*, vol. 11, no. 12, p. 2530, 2018.
- [67] L. L. Hench, "The story of Bioglass®," *Journal of Materials Science: Materials in Medicine*, vol. 17, no. 11, pp. 967-978, 2006.

- [68] D. Clupper and L. Hench, "Bioactive response of Ag-doped tape cast Bioglass® 45S5 following heat treatment," *Journal of Materials Science: Materials in Medicine*, vol. 12, no. 10, pp. 917-921, 2001.
- [69] C. Mariappan and N. Ranga, "Influence of silver on the structure, dielectric and antibacterial effect of silver doped bioglass-ceramic nanoparticles," *Ceramics International*, vol. 43, no. 2, pp. 2196-2201, 2017.
- [70] U. Ali, K. J. B. A. Karim, and N. A. Buang, "A Review of the Properties and Applications of Poly (Methyl Methacrylate) (PMMA)," (in en), *Polymer Reviews*, vol. 55, no. 4, pp. 678-705, 2015/10/02/ 2015, doi: 10.1080/15583724.2015.1031377.
- [71] A. D'Elia, J. Deering, A. Clifford, B. E. J. Lee, K. Grandfield, and I. Zhitomirsky, "Electrophoretic deposition of polymethylmethacrylate and composites for biomedical applications," *Colloids Surf B Biointerfaces*, vol. 188, p. 110763, Apr 2020, doi: 10.1016/j.colsurfb.2019.110763.
- [72] Y. Beilei *et al.*, "PMMA passivated CsPbI₂Br perovskite film for highly efficient and stable solar cells," *Journal of Physics and Chemistry of Solids*, vol. 153, p. 110000, 2021, doi: <https://doi.org/10.1016/j.jpcs.2021.110000>.
- [73] N.-S. Choi and J.-K. Park, "New polymer electrolytes based on PVC/PMMA blend for plastic lithium-ion batteries," *Electrochimica Acta*, vol. 46, no. 10-11, pp. 1453-1459, 2001.
- [74] N. C. Abeykoon, J. S. Bonso, and J. P. Ferraris, "Supercapacitor performance of carbon nanofiber electrodes derived from immiscible PAN/PMMA polymer blends," *Rsc Advances*, vol. 5, no. 26, pp. 19865-19873, 2015.
- [75] X. Li and I. Zhitomirsky, "Deposition of poly(methyl methacrylate) and composites containing bioceramics and bioglass by dip coating using isopropanol-water co-solvent,"

- (in en), *Progress in Organic Coatings*, vol. 148, p. 105883, 2020/11// 2020, doi: 10.1016/j.porgcoat.2020.105883.
- [76] J. James *et al.*, "Optical and physical properties of zirconium dioxide reinforced poly(methyl methacrylate) nanocomposite films," *Journal of Applied Polymer Science*, vol. 141, no. 8, 2023, doi: 10.1002/app.54977.
- [77] S. R. Nugen, P. J. Asiello, J. T. Connelly, and A. J. Baeumner, "PMMA biosensor for nucleic acids with integrated mixer and electrochemical detection," *Biosensors and Bioelectronics*, vol. 24, no. 8, pp. 2428-2433, 2009.
- [78] T. Jaeblo, "Polymethylmethacrylate: properties and contemporary uses in orthopaedics," *JAAOS-Journal of the American Academy of Orthopaedic Surgeons*, vol. 18, no. 5, pp. 297-305, 2010.
- [79] M. S. Zafar, "Prosthodontic applications of polymethyl methacrylate (PMMA): An update," *Polymers*, vol. 12, no. 10, p. 2299, 2020.
- [80] M. Lin *et al.*, "Structure and release behavior of PMMA/silica composite drug delivery system," *Journal of pharmaceutical sciences*, vol. 96, no. 6, pp. 1518-1526, 2007.
- [81] S.-C. Lee, C.-T. Wu, S.-T. Lee, and P.-J. Chen, "Cranioplasty using polymethyl methacrylate prostheses," *Journal of clinical neuroscience*, vol. 16, no. 1, pp. 56-63, 2009.
- [82] J. Webb and R. Spencer, "The role of polymethylmethacrylate bone cement in modern orthopaedic surgery," *The Journal of Bone & Joint Surgery British Volume*, vol. 89, no. 7, pp. 851-857, 2007.
- [83] M. Hossain, J. H. Jeong, T. Sultana, J. H. Kim, J. E. Moon, and S. Im, "A composite of polymethylmethacrylate, hydroxyapatite, and beta-tricalcium phosphate for bone

- regeneration in an osteoporotic rat model," *J Biomed Mater Res B Appl Biomater*, vol. 111, no. 10, pp. 1813-1823, Oct 2023, doi: 10.1002/jbm.b.35287.
- [84] S. Rawal, "Poly (Ethyl Methacrylate) (PEMA) and its Composites for Various Applications: Background, Recent Progress, and Future challenges," *Macromolecular Symposia*, vol. 413, no. 1, 2024, doi: 10.1002/masy.202300096.
- [85] R. Wyre and S. Downes, "An in vitro investigation of the PEMA/THFMA polymer system as a biomaterial for cartilage repair," *Biomaterials*, vol. 21, no. 4, pp. 335-343, 2000.
- [86] S. Jayanthi, S. Shenbagavalli, M. Muthuvinayagam, and B. Sundaresan, "Effect of nano TiO₂ on the transport, structural and thermal properties of PEMA-NaI solid polymer electrolytes for energy storage devices," *Materials Science and Engineering: B*, vol. 285, p. 115942, 2022.
- [87] F. Mohanty and S. K. Swain, "Nano silver embedded starch hybrid graphene oxide sandwiched poly(ethylmethacrylate) for packaging application," *Nano-Structures & Nano-Objects*, vol. 18, 2019, doi: 10.1016/j.nanoso.2019.100300.
- [88] J. Behera *et al.*, "Nano boron nitride laminated poly(ethyl methacrylate)/poly(vinyl alcohol) composite films imprinted with silver nanoparticles as gas barrier and bacteria resistant packaging materials," *Journal of Applied Polymer Science*, 2024, doi: 10.1002/app.55246.
- [89] S. Fares, "Influence of gamma-ray irradiation on optical and thermal degradation of poly (ethyl-methacrylate)(PEMA) polymer," *Natural Science*, vol. 4, no. 7, pp. 499-507, 2012.
- [90] M. El-Sharnouby *et al.*, "Enhanced electrical conductivity and dielectric performance of ternary nanocomposite film of PEMA/PS/silver NPs synthesized by laser ablation," *Journal of Inorganic and Organometallic Polymers and Materials*, vol. 32, no. 6, pp. 2269-2278, 2022.

- [91] X. Liu, S. Veldhuis, R. Mathews, and I. Zhitomirsky, "Dip coating of poly(ethyl methacrylate) and composites from solutions in isopropanol-water co-solvent," (in en), *Colloids and Surfaces A: Physicochemical and Engineering Aspects*, vol. 631, p. 127703 %U <https://linkinghub.elsevier.com/retrieve/pii/S0927775721015727>, 2021.
- [92] J. Carneiro *et al.*, "Functionalized chitosan-based coatings for active corrosion protection," *Surface and Coatings Technology*, vol. 226, pp. 51-59, 2013.
- [93] E. Nieuwenhuis, C. Pathmamanoharan, and A. Vrij, "Liquid-like structures in concentrated latex dispersions. a light-scattering study of pmma particles in benzene," *Journal of Colloid and Interface Science*, vol. 81, no. 1, pp. 196-213, 1981.
- [94] D. Adapa, *Sorption of Benzene, Toluene and Ethylbenzene by Plasticized PEMA and PEMA/PMMA Sensing Films Using a Quartz Crystal Microbalance (QCM) at 298.15 K*. University of South Florida, 2019.
- [95] A. R. Iyer, V. B. Mitevska, J. J. Samuelson, S. W. Campbell, and V. R. Bhethanabotla, "Sorption of Benzene, Toluene, and Ethylbenzene at Low Concentrations by Plasticized Poly (ethyl methacrylate) and Polystyrene Polymers Using a Quartz Crystal Microbalance at 298.15 K," *Journal of Chemical & Engineering Data*, vol. 66, no. 8, pp. 3354-3359, 2021.
- [96] C. B. Walsh and E. I. Franses, "Ultrathin PMMA films spin-coated from toluene solutions," *Thin Solid Films*, vol. 429, no. 1-2, pp. 71-76, 2003.
- [97] K. Kaur, A. R. Iyer, S. W. Campbell, and V. R. Bhethanabotla, "Sorption of benzene, toluene, and ethylbenzene by poly (ethyl methacrylate) and plasticized poly (ethyl methacrylate) AT 298.15 k using a quartz CRYSTAL Microbalance," *Journal of Chemical & Engineering Data*, vol. 65, no. 10, pp. 5046-5054, 2020.

- [98] P. Curie and J. Curie, "Développement, par pression, de l'électricité polaire dans les cristaux hémihédres à faces inclinées," *C R Acad Sci*, vol. 91, pp. 294-295, 1880 1880.
- [99] P. Saxena and P. Shukla, "A comprehensive review on fundamental properties and applications of poly(vinylidene fluoride) (PVDF)," *Adv Compos Hybrid Mater*, vol. 4, pp. 8-26, 2021 2021, doi: 10.1007/s42114-021-00217-0.
- [100] J. J. Telega and R. Wojnar, "Piezoelectric effects in biological tissues," *J Theor Appl Mech*, vol. 40, pp. 723-759, 2002 2002.
- [101] H. Chang and Y. Wang, *Regenerative medicine and tissue engineering—cells and biomaterials*. Rijeka, Croatia: InTech, 2011, pp. 569–588.
- [102] L. Marques *et al.*, "Subcutaneous tissue reaction and cytotoxicity of polyvinylidene fluoride and polyvinylidene fluoride-trifluoroethylene blends associated with natural polymers," *J Biomed Mater Res Part B Appl Biomater*, vol. 101, pp. 1284-1293, 2013 2013.
- [103] C. Ribeiro, V. Sencadas, D. M. Correia, and S. Lanceros-Méndez, "Piezoelectric polymers as biomaterials for tissue engineering applications," *Colloids Surf B Biointerfaces*, vol. 136, pp. 46-55, 2015 2015.
- [104] Z. Ma, M. Kotaki, R. Inai, and S. Ramakrishna, "Potential of nanofiber matrix as tissue-engineering scaffolds," *Tissue Eng*, vol. 11, pp. 101-109, 2005 2005.
- [105] A. Abednejad *et al.*, "Polyvinylidene fluoride–Hyaluronic acid wound dressing comprised of ionic liquids for controlled drug delivery and dual therapeutic behavior," *Acta Biomater*, vol. 100, pp. 142-157, 2019 2019, doi: 10.1016/j.actbio.2019.10.007.
- [106] I. Richard, M. Thibault, G. De Crescenzo, M. D. Buschmann, and M. Lavertu, "Ionization Behavior of Chitosan and Chitosan–DNA Polyplexes Indicate That Chitosan Has a Similar

- Capability to Induce a Proton-Sponge Effect as PEI," (in en), *Biomacromolecules*, vol. 14, no. 6, pp. 1732-1740, 2013/06/10/ 2013, doi: 10.1021/bm4000713.
- [107] A. Zakeri *et al.*, "Polyethylenimine-based nanocarriers in co-delivery of drug and gene: a developing horizon," *Nano Reviews & Experiments*, vol. 9, no. 1, p. 1488497, 2018/01/01 2018, doi: 10.1080/20022727.2018.1488497.
- [108] S. Shi *et al.*, "The use of cationic MPEG-PCL-g-PEI micelles for co-delivery of Msurvivin T34A gene and doxorubicin," *Biomaterials*, vol. 35, no. 15, pp. 4536-4547, 2014/05/01/ 2014, doi: <https://doi.org/10.1016/j.biomaterials.2014.02.010>.
- [109] C. N. Lungu, M. V. Diudea, M. V. Putz, and I. P. Grudzinski, "Linear and Branched PEIs (Polyethylenimines) and Their Property Space," *Int J Mol Sci*, vol. 17, no. 4, p. 555, Apr 13 2016, doi: 10.3390/ijms17040555.
- [110] W.-F. Lai, D. W Green, and H.-S. Jung, "Linear poly (ethylenimine) cross-linked by methyl- β -cyclodextrin for gene delivery," *Current Gene Therapy*, vol. 14, no. 4, pp. 258-268, 2014.
- [111] X. Sun *et al.*, "A polyethylenimine functionalized porous/hollow nanoworm as a drug delivery system and a bioimaging agent," *Physical Chemistry Chemical Physics*, vol. 18, no. 11, pp. 7820-7828, 2016.
- [112] L. Shen, L. Zhang, M. Chen, X. Chen, and J. Wang, "The production of pH-sensitive photoluminescent carbon nanoparticles by the carbonization of polyethylenimine and their use for bioimaging," *Carbon*, vol. 55, pp. 343-349, 2013.
- [113] L. Shao *et al.*, "A non-conjugated polyethylenimine copolymer-based unorthodox nanoprobe for bioimaging and related mechanism exploration," *Biomaterials science*, vol. 7, no. 7, pp. 3016-3024, 2019.

- [114] H. Kim, R. Namgung, K. Singha, I.-K. Oh, and W. J. Kim, "Graphene oxide–polyethylenimine nanoconstruct as a gene delivery vector and bioimaging tool," *Bioconjugate chemistry*, vol. 22, no. 12, pp. 2558-2567, 2011.
- [115] L. Zou *et al.*, "Facile Gene Delivery Derived from Branched Low Molecular Weight Polyethylenimine by High Efficient Chemistry," (in en), *j biomed nanotechnol*, vol. 14, no. 10, pp. 1785-1795, 2018/10/01/ 2018, doi: 10.1166/jbn.2018.2620.
- [116] U. Lungwitz, M. Breunig, T. Blunk, and A. Göpferich, "Polyethylenimine-based non-viral gene delivery systems," *European Journal of Pharmaceutics and Biopharmaceutics*, vol. 60, no. 2, pp. 247-266, 2005/07/01/ 2005, doi: <https://doi.org/10.1016/j.ejpb.2004.11.011>.
- [117] S. Taghavi, A. H. Nia, K. Abnous, and M. Ramezani, "Polyethylenimine-functionalized carbon nanotubes tagged with AS1411 aptamer for combination gene and drug delivery into human gastric cancer cells," *International journal of pharmaceutics*, vol. 516, no. 1-2, pp. 301-312, 2017.
- [118] J. Zhao, C. Lu, X. He, X. Zhang, W. Zhang, and X. Zhang, "Polyethylenimine-grafted cellulose nanofibril aerogels as versatile vehicles for drug delivery," *ACS Appl. Mater. Interfaces*, vol. 7, no. 4, pp. 2607-2615, 2015.
- [119] Y. Zou, D. Li, M. Shen, and X. Shi, "Polyethylenimine-Based Nanogels for Biomedical Applications," (in en), *Macromolecular Bioscience*, vol. 19, no. 11, p. 1900272, 2019/11// 2019, doi: 10.1002/mabi.201900272.
- [120] H. Khalil, T. Chen, R. Riffon, R. Wang, and Z. Wang, "Synergy between polyethylenimine and different families of antibiotics against a resistant clinical isolate of *Pseudomonas aeruginosa*," *Antimicrobial agents and chemotherapy*, vol. 52, no. 5, pp. 1635-1641, 2008.

- [121] A. K. Tiwari, M. K. Gupta, G. Pandey, R. J. Narayan, and P. C. Pandey, "Molecular weight of polyethylenimine-dependent transfection and selective antimicrobial activity of functional silver nanoparticles," *Journal of Materials Research*, vol. 35, no. 18, pp. 2405-2415, 2020.
- [122] M. Liu, J. Li, and B. Li, "Mannose-modified polyethylenimine: a specific and effective antibacterial agent against *Escherichia coli*," *Langmuir*, vol. 34, no. 4, pp. 1574-1580, 2018.
- [123] N. Beyth, Y. Hourri-Haddad, L. Baraness-Hadar, I. Yudovin-Farber, A. J. Domb, and E. I. Weiss, "Surface antimicrobial activity and biocompatibility of incorporated polyethylenimine nanoparticles," *Biomaterials*, vol. 29, no. 31, pp. 4157-4163, 2008.
- [124] Q. Li, C. Wu, and B. Zhang, "Hybrid hydrogels based on polyvinyl alcohol, branched polyethylenimine, polydopamine, and phosphonium-based ionic liquid for effective synergetic antibacterial applications," (in en), *Colloids and Surfaces A: Physicochemical and Engineering Aspects*, vol. 648, p. 129277, 2022/09// 2022, doi: 10.1016/j.colsurfa.2022.129277.
- [125] M. Delyanee, A. Solouk, S. Akbari, and E. Seyedjafari, "Modification of electrospun poly(ϵ -lactic acid)/polyethylenimine nanofibrous scaffolds for biomedical application," (in en), *International Journal of Polymeric Materials and Polymeric Biomaterials*, vol. 67, no. 4, pp. 247-257, 2018/03/04/ 2018, doi: 10.1080/00914037.2017.1320661.
- [126] B. C. Simionescu *et al.*, "Biopolymers/poly(ϵ -caprolactone)/polyethylenimine functionalized nano-hydroxyapatite hybrid cryogel: Synthesis, characterization and application in gene delivery," (in en), *Materials Science and Engineering: C*, vol. 81, pp. 167-176, 2017/12// 2017, doi: 10.1016/j.msec.2017.07.031.

- [127] P. Pandey, G. Pandey, and R. Narayan, "Polyethylenimine-mediated controlled synthesis of Prussian blue-gold nanohybrids for biomedical applications," (in en), *J Biomater Appl*, vol. 36, no. 1, pp. 26-35, 2021/07// 2021, doi: 10.1177/0885328220975575.
- [128] Y. Sun, M. S. Ata, I. Zhitomirsky, and M. S. A. Y Sun, I Zhitomirsky, "Electrophoretic deposition of linear polyethylenimine and composite films," *Surface Engineering*, vol. 29, no. 7, 2013-08-01, doi: 10.1179/1743294413Y.0000000156.
- [129] Z. Z. Wang, A. Clifford, J. Milne, R. Mathews, and I. Zhitomirsky, "Colloidal-electrochemical fabrication strategies for functional composites of linear polyethylenimine," *Journal of colloid and interface science*, vol. 552, pp. 1-8, 2019 2019.
- [130] A. R. Boccaccini, S. Keim, R. Ma, Y. Li, and I. Zhitomirsky, "Electrophoretic deposition of biomaterials," *J R Soc Interface*, vol. 7 Suppl 5, no. Suppl 5, pp. S581-613, Oct 6 2010, doi: 10.1098/rsif.2010.0156.focus.
- [131] L. Besra and M. Liu, "A review on fundamentals and applications of electrophoretic deposition (EPD)," *Progress in materials science*, vol. 52, no. 1, pp. 1-61, 2007.
- [132] R. Sikkema, K. Baker, and I. Zhitomirsky, "Electrophoretic deposition of polymers and proteins for biomedical applications," *Adv Colloid Interface Sci*, vol. 284, p. 102272, Oct 2020, doi: 10.1016/j.cis.2020.102272.
- [133] I. Zhitomirsky, "Cathodic electrodeposition of ceramic and organoceramic materials. Fundamental aspects," *Advances in Colloid and Interface Science*, vol. 97, no. 1, pp. 279-317, 2002/03/29/ 2002, doi: [https://doi.org/10.1016/S0001-8686\(01\)00068-9](https://doi.org/10.1016/S0001-8686(01)00068-9).
- [134] G. Trefalt and M. Borkovec, "Overview of DLVO theory," *Laboratory of Colloid and Surface Chemistry, University of Geneva, Switzerland*, vol. 304, 2014.

- [135] R. Kjellander, S. Marcelja, R. Pashley, and J. Quirk, "Double-layer ion correlation forces restrict calcium-clay swelling," *The Journal of Physical Chemistry*, vol. 92, no. 23, pp. 6489-6492, 1988.
- [136] X. Chu and D. T. Wasan, "Attractive interaction between similarly charged colloidal particles," *Journal of colloid and interface science*, vol. 184, no. 1, pp. 268-278, 1996.
- [137] J. Y. Walz and A. Sharma, "Effect of long range interactions on the depletion force between colloidal particles," *Journal of colloid and interface science*, vol. 168, no. 2, pp. 485-496, 1994.
- [138] J. Ennis, L. Sjöström, T. Åkesson, and B. Jönsson, "Surface interactions in the presence of polyelectrolytes. A simple theory," *Langmuir*, vol. 16, no. 18, pp. 7116-7125, 2000.
- [139] N. G. Hoogeveen, M. A. C. Stuart, and G. J. Fleer, "Polyelectrolyte adsorption on oxides: II. Reversibility and exchange," *Journal of colloid and interface science*, vol. 182, no. 1, pp. 146-157, 1996.
- [140] E. Dickinson and L. Eriksson, "Particle flocculation by adsorbing polymers," *Advances in Colloid and Interface Science*, vol. 34, pp. 1-29, 1991.
- [141] M. N. Rahaman, *Ceramic processing*. CRC press, 2017.
- [142] T. Kuroiwa, I. Kobayashi, A. M. Chuah, M. Nakajima, and S. Ichikawa, "Formulation and stabilization of nano-/microdispersion systems using naturally occurring edible polyelectrolytes by electrostatic deposition and complexation," *Advances in Colloid and Interface Science*, vol. 226, pp. 86-100, 2015.
- [143] T. Okubo and M. Suda, "Absorption of polyelectrolytes on colloidal surfaces as studied by electrophoretic and dynamic light-scattering techniques," *Journal of colloid and interface science*, vol. 213, no. 2, pp. 565-571, 1999.

- [144] T. W. Healy and L. R. White, "Ionizable surface group models of aqueous interfaces," *Advances in Colloid and Interface Science*, vol. 9, no. 4, pp. 303-345, 1978.
- [145] H. Koelmans and J. T. G. Overbeek, "Stability and electrophoretic deposition of suspensions in non-aqueous media," *Discussions of the Faraday Society*, vol. 18, pp. 52-63, 1954.
- [146] A. Kitahara, S. Karasawa, and H. Yamada, "The effect of water on electrokinetic potential and stability of suspensions in nonpolar media," *Journal of Colloid and Interface Science*, vol. 25, no. 4, pp. 490-495, 1967.
- [147] J. Lyklema, "Principles of the stability of lyophobic colloidal dispersions in non-aqueous media," *Advances in Colloid and Interface Science*, vol. 2, no. 2, pp. 67-114, 1968.
- [148] C. Chen and S. Levine, "The double-layer interaction of two charged colloidal spherical particles of a concentrated dispersion in a medium of low dielectric constant: I. Force calculations," *Journal of Colloid and Interface Science*, vol. 43, no. 3, pp. 599-615, 1973.
- [149] G. Feat and S. Levine, "The double-layer interaction of two charged colloidal spherical particles of a concentrated dispersion in a medium of low dielectric constant: III. Approximation of perfectly conducting particles," *Journal of Colloid and Interface Science*, vol. 54, no. 1, pp. 34-44, 1976.
- [150] D. B. Hough and L. R. White, "The calculation of Hamaker constants from Lifshitz theory with applications to wetting phenomena," *Advances in Colloid and Interface Science*, vol. 14, no. 1, pp. 3-41, 1980.
- [151] D. H. Napper, "Polymeric stabilization of colloidal dispersions," (*No Title*), 1983.

- [152] M. Navlani-García, D. Salinas-Torres, K. Mori, Y. Kuwahara, and H. Yamashita, "Tailoring the size and shape of colloidal noble metal nanocrystals as a valuable tool in catalysis," *Catalysis Surveys from Asia*, vol. 23, pp. 127-148, 2019.
- [153] P. M. Raj and W. R. Cannon, "Electrosteric stabilization mechanisms in nonaqueous high solids loading dispersions," *Surfactant Science Series*, vol. 104, pp. 27-61, 2001.
- [154] A. Pettersson, G. Marino, A. Pursiheimo, and J. B. Rosenholm, "Electrosteric stabilization of Al₂O₃, ZrO₂, and 3Y–ZrO₂ suspensions: effect of dissociation and type of polyelectrolyte," *Journal of colloid and interface science*, vol. 228, no. 1, pp. 73-81, 2000.
- [155] F. O. Pirrung, P. H. Quednau, and C. Auschra, "Wetting and dispersing agents," *Chimia*, vol. 56, no. 5, pp. 170-170, 2002.
- [156] M. S. Ata, Y. Liu, and I. Zhitomirsky, "A review of new methods of surface chemical modification, dispersion and electrophoretic deposition of metal oxide particles," *RSC Advances*, 10.1039/C4RA02218A vol. 4, no. 43, pp. 22716-22732, 2014, doi: 10.1039/C4RA02218A.
- [157] B. P. Lee, P. B. Messersmith, J. N. Israelachvili, and J. H. Waite, "Mussel-inspired adhesives and coatings," *Annual review of materials research*, vol. 41, pp. 99-132, 2011.
- [158] H. Lee, S. M. Dellatore, W. M. Miller, and P. B. Messersmith, "Mussel-inspired surface chemistry for multifunctional coatings," *science*, vol. 318, no. 5849, pp. 426-430, 2007.
- [159] L. Petrone, "Molecular surface chemistry in marine bioadhesion," *Advances in colloid and interface science*, vol. 195, pp. 1-18, 2013.
- [160] K. Wu, P. Imin, A. Adronov, and I. Zhitomirsky, "Electrophoretic deposition of poly [3-(3-N, N-diethylaminopropoxy) thiophene] and composite films," *Materials Chemistry and Physics*, vol. 125, no. 1-2, pp. 210-218, 2011.

- [161] F. S. de Souza and A. Spinelli, "Caffeic acid as a green corrosion inhibitor for mild steel," *Corrosion science*, vol. 51, no. 3, pp. 642-649, 2009.
- [162] Y. Sun and I. Zhitomirsky, "Electrophoretic deposition of titanium dioxide using organic acids as charging additives," *Materials letters*, vol. 73, pp. 190-193, 2012.
- [163] Y. Wang and I. Zhitomirsky, "Bio-inspired catechol chemistry for electrophoretic nanotechnology of oxide films," *Journal of colloid and interface science*, vol. 380, no. 1, pp. 8-15, 2012.
- [164] Q. Ye, F. Zhou, and W. Liu, "Bioinspired catecholic chemistry for surface modification," *Chemical Society Reviews*, vol. 40, no. 7, pp. 4244-4258, 2011.
- [165] Q. Chen, Y. Jia, S. Liu, G. Mogilevsky, A. Kleinhammes, and Y. Wu, "Molecules immobilization in titania nanotubes: a solid-state NMR and computational chemistry study," *The Journal of Physical Chemistry C*, vol. 112, no. 44, pp. 17331-17335, 2008.
- [166] I. A. Jankovic, Z. V. Saponjic, M. I. Comor, and J. M. Nedeljkovic, "Surface modification of colloidal TiO₂ nanoparticles with bidentate benzene derivatives," *The Journal of Physical Chemistry C*, vol. 113, no. 29, pp. 12645-12652, 2009.
- [167] J. Peyre, V. Humblot, C. Méthivier, J.-M. Berjeaud, and C.-M. Pradier, "Co-grafting of amino-poly (ethylene glycol) and magainin I on a TiO₂ surface: tests of antifouling and antibacterial activities," *The Journal of Physical Chemistry B*, vol. 116, no. 47, pp. 13839-13847, 2012.
- [168] K. Wu, Y. Wang, and I. Zhitomirsky, "Electrophoretic deposition of TiO₂ and composite TiO₂-MnO₂ films using benzoic acid and phenolic molecules as charging additives," *Journal of colloid and interface science*, vol. 352, no. 2, pp. 371-378, 2010.

- [169] Z. Wang and I. Zhitomirsky, "Bile Acid Salt as a Vehicle for Solubilization and Electrodeposition of Drugs and Functional Biomolecules for Surface Modification of Materials," *Biomedical Materials & Devices*, vol. 2, no. 1, pp. 397-406, 2024.
- [170] A. Clifford and I. Zhitomirsky, "Aqueous electrophoretic deposition of drugs using bile acids as solubilizing, charging and film-forming agents," *Materials Letters*, vol. 227, pp. 1-4, 2018.
- [171] Q. Zhao, S. Veldhuis, R. Mathews, and I. Zhitomirsky, "Influence of chemical structure of bile acid dispersants on electrophoretic deposition of poly (vinylidene fluoride) and composites," *Colloids and Surfaces A: Physicochemical and Engineering Aspects*, vol. 627, p. 127181, 2021.
- [172] M. Ata and I. Zhitomirsky, "Colloidal methods for the fabrication of carbon nanotube–manganese dioxide and carbon nanotube–polypyrrole composites using bile acids," *Journal of colloid and interface science*, vol. 454, pp. 27-34, 2015.
- [173] I. Neacșu, A. Nicoară, O. R. Vasile, and B. Vasile, "Inorganic micro-and nanostructured implants for tissue engineering, Nanobiomaterials in Hard Tissue Engineering," 2016.
- [174] M. A. Aegerter and M. Mennig, *Sol-gel technologies for glass producers and users*. Springer Science & Business Media, 2013.
- [175] P. Löbmann, "Soluble powders as precursors for TiO₂ thin films," *Journal of sol-gel science and technology*, vol. 33, pp. 275-282, 2005.
- [176] N. Hijón, M. V. Cabanas, J. Pena, and M. Vallet-Regí, "Dip coated silicon-substituted hydroxyapatite films," *Acta Biomaterialia*, vol. 2, no. 5, pp. 567-574, 2006.

- [177] E. Mohseni, E. Zalnezhad, and A. R. Bushroa, "Comparative investigation on the adhesion of hydroxyapatite coating on Ti-6Al-4V implant: A review paper," *International Journal of Adhesion and Adhesives*, vol. 48, pp. 238-257, 2014.

Chapter 3 Deposition of Organic-Inorganic Nanocomposite

Coatings for Biomedical Applications

3.1. Abstract

Polymethylmethacrylate (PMMA) is a material of choice for many biomedical coating applications. However, such applications are limited due to the toxicity of the traditional solvents used for the solution processing of PMMA coatings and composites. This problem is addressed using an isopropanol-water co-solvent, which allows for the dissolution of high molecular mass PMMA and the fabrication of coatings by a dip-coating method from concentrated PMMA solutions. The use of the co-solvent offers a versatile strategy for PMMA solubilization and coating deposition, despite the insolubility of PMMA in water and isopropanol. Composite coatings are obtained, containing hydroxyapatite, silver oxide, zinc oxide, micron size silica and nanosilica. Such coatings are promising for the manufacturing of implants with enhanced biocompatibility, bioactivity and antimicrobial properties and the fabrication of biosensors. Ibuprofen, tetracycline and amoxicillin are used as model drugs for the fabrication of PMMA-drug composite coatings for drug delivery. The microstructure and composition of the coatings are analyzed. The versatile dip-coating method of this investigation provides a platform for various biomedical applications.

3.2. Introduction

Polymethylmethacrylate (PMMA) is widely used for various applications in optical devices, solar cells, batteries and supercapacitors [1–4]. PMMA is a material of choice for various biomedical applications in dental implants, orthopedic devices and biosensors [1,5–7]. The interest in PMMA for biomedical applications is attributed to its biocompatibility, chemical stability and good mechanical properties [1]. Many investigations reported the development and successful

applications of PMMA composites for the controlled delivery of drugs [1,8], cranioplasty [9], biomedical implants [10] and bone and dental cements [1,11,12]. Composite materials containing TiO₂ [13], Al₂O₃ [14], hydroxyapatite [15,16] and bioglass [17] were developed. Such composites showed enhanced biocompatibility, bioactivity and enhanced mechanical and other functional properties. PMMA composite films and coatings have generated significant interest, which was fueled by various applications. PMMA composite coatings containing bioactive ceramics were developed [18]. PMMA coatings and films provided a platform for advanced drug delivery applications [19,20]. PMMA exhibits remarkable properties for thin film applications in eye lenses [21,22] and thin film biosensors [23,24]. PMMA films and coatings were deposited by plasma polymerization [25] and laser evaporation [18]. Many investigations focused on the development of solution deposition techniques, such as solution polymerization [26], electrophoretic deposition [27], sol-gel deposition [28], spin coating [29] and dip coating [30–32]. Various solvents were used for PMMA, such as toluene, benzene, methyl ethyl ketone and other organic solvents, which are carcinogenic and toxic. The application of such solvents for biomedical applications presents difficulties, because solvent molecules can remain adsorbed on the surface or in the bulk of the PMMA coatings.

Recent studies showed that dip coating of PMMA can be performed using a mixed isopropanol-water co-solvent [33]. Despite the PMMA insolubility in individual solvents, such as water and isopropanol, solutions of high molecular mass PMMA with high concentration were prepared. The use of such solutions was a key factor for successful film deposition by a dip coating method [33]. It should be noted that isopropanol offers benefits for film deposition for biomedical applications due to low evaporation temperature and miscibility with water. Isopropanol has been utilized in many studies focused on the manufacturing of coatings and thin films for biomedical

applications and offered the advantage of low cytotoxicity compared to other organic solvents [34–38]. Good cell proliferation and attachment were observed on the surfaces of the coatings prepared using isopropanol [39–41]. The investigations focused on applications of isopropanol for protein purification and extraction [42], the fabrication of fibrous implant materials for tissue engineering [43], the manufacturing of scaffolds for wound healing [44] and the development of thin films for controlled drug delivery [45]. Therefore, the further development of dip coating from a mixed water-isopropanol solvent is a promising strategy for the fabrication of composites containing different functional materials for biomedical applications. The goal of this investigation was the fabrication of composite coatings containing different functional biomaterials in the PMMA matrix using a water-isopropanol co-solvent. We targeted the fabrication of organic–inorganic composites containing bioactive ceramics, such as hydroxyapatite, silica and materials with antimicrobial properties, such as Ag₂O and ZnO. Moreover, the fabrication of PMMA-ZnO composite coatings paves the way for the development of biosensors. Ibuprofen, tetracycline and amoxicillin were used as model drugs for the fabrication of coatings for drug delivery. The results presented below showed that the dip coating method is a versatile strategy for the development of composite coatings.

3.3. Experimental

Poly(methyl methacrylate) (PMMA, $M_w = 350,000$, Aldrich, Oakville, ON, Canada), ZnO, Ag₂O, nanosilica, isopropanol, ibuprofen, tetracycline and amoxicillin were received from the MilliporeSigma company. Micron size silica was obtained from PCR Inc. Hydroxyapatite (HA) nanoparticles were prepared by a chemical precipitation method, as described in previous investigations [46,47]. PMMA was dissolved in a mixture of water and isopropanol (20% water) at 50 °C, and the obtained solution was cooled to room temperature. The substrates for coating

deposition were stainless steel foils (304 type, area 30×50 mm, thickness 0.1 mm). It should be noted that PMMA can also be dissolved in ethanol-water mixtures. However, the isopropanol-water solvent allowed for better PMMA solubility. Dip coating was performed at a substrate withdrawal speed of 10 mm min^{-1} from 10 g L^{-1} PMMA solutions without and with other functional materials for biomedical applications. The concentrations of such materials in the 10 g L^{-1} PMMA solutions were 5 g L^{-1} ZnO, HA, micron size silica and nanosilica, ibuprofen, tetracycline, amoxicillin and 0.5 g L^{-1} Ag₂O. The thickness of the as-deposited and room-temperature-dried monolayer coatings was 2–3 μm . Coating annealing was performed at $200 \text{ }^\circ\text{C}$ for 1 h. The coating microstructure was examined using a JEOL SEM (scanning electron microscope, JSM-7000F). The coating composition was examined using a Bruker Smart 6000 X-ray diffractometer (XRD, CuK radiation). Thermogravimetric analysis (TGA, thermoanalyzer Netzsch STA-409) was carried out in air at a heating rate of $5 \text{ }^\circ\text{C}/\text{min}$. For the TGA investigations, the deposits were removed from the substrates. A Bruker Vertex 70 spectrometer was used for the Fourier Transform Infrared Spectroscopy (FTIR) experiments.

3.4. Results and Discussion

Figure 3-1 shows SEM images of PMMA coating prepared from 10 g L^{-1} PMMA solution. The microstructure of the as-deposited coating contained porous surface island networks formed on a relatively dense layer (Figure 3-1A). Such microstructure can result from the Stranski–Krastanov mode of film growth [48]. It should be also noted that PMMA is soluble in the isopropanol-water mixture in a narrow water concentration range. Therefore, a faster isopropanol evaporation rate during drying can result in a change in the solvent composition and precipitation of PMMA particles in the surface layer to form a porous network. Annealing resulted in the film melting and formation of dense coatings.

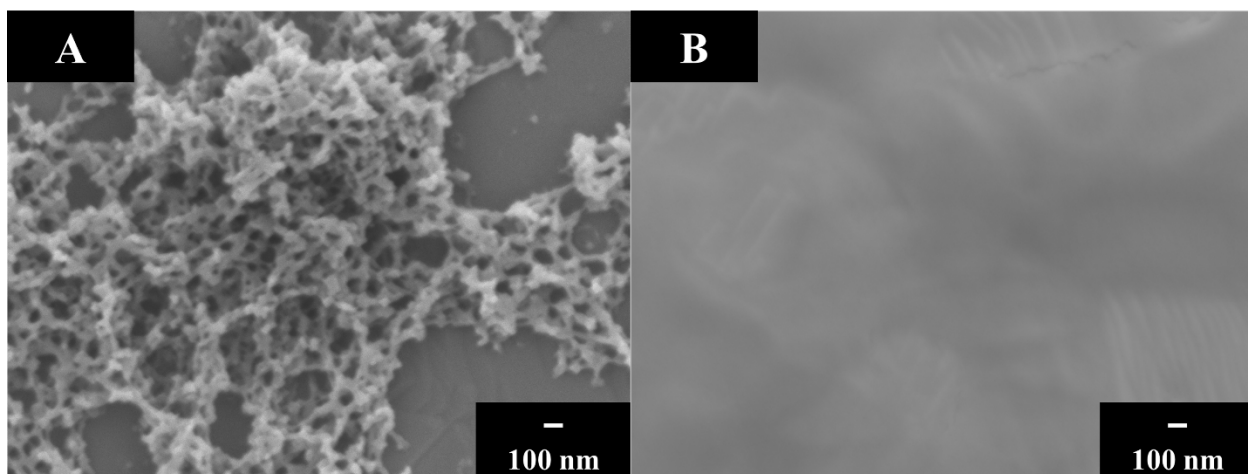


Figure 3-1 SEM images of PMMA coating: (A) as-deposited and room-temperature-dried, (B) annealed at 200 °C.

PMMA was successfully co-deposited with inorganic materials. Figure 3-2 shows SEM images of as-deposited and annealed coating prepared from 10 g L⁻¹ PMMA solutions containing 0.5 g L⁻¹ Ag₂O, 5 g L⁻¹ HA and 5 g L⁻¹ ZnO. The interest in polymer coatings containing Ag₂O is attributed to the antimicrobial properties of Ag₂O [49,50]. Therefore, small additives of Ag₂O can be beneficial for biomedical applications of PMMA coatings. ZnO is widely used for the fabrication of biosensors. This strategy is based on the relatively high isoelectric point of ZnO, which was reported to be about pH = 9 [51]. Electrostatic interactions of ZnO with various biosensing molecules, which have a low isoelectric point and negative charge at pH = 7, facilitated the immobilization of such molecules on the positively charged ZnO particles [51]. The antimicrobial properties of ZnO particles are important for biomedical applications [52,53]. HAP is widely used for implant applications because its chemical composition is similar to that of the mineral part of natural bone [54–56]. The concentration of ZnO and HA in the suspensions was larger than the Ag₂O concentration in order to achieve a larger content of ZnO and HA in the coatings. A larger HA and ZnO content is necessary for the fabrication of bioactive coatings based on HA [57] and the immobilization of biosensing molecules in coatings based on ZnO particles

[51]. The as-deposited PMMA-Ag₂O, PMMA-ZnO and PMMA-HA coatings were porous (Figure 2). Annealing resulted in reduced coating porosity. The relatively high porosity of as-deposited PMMA-ZnO and PMMA-HA coatings resulted from the packing of ZnO and HA particles. The HA particles had a needle shape. The SEM images of annealed PMMA-ZnO and PMMA-HA coatings showed ZnO and HA particles on the coating surface. The annealed films were crack free and relatively dense. The polymer acted as a binding and film-forming agent. The fabrication of PMMA-silica coatings was motivated by their applications for the corrosion protection of biomedical implants with enhanced biocompatibility [58]. Figure 3-3 shows SEM images of as-deposited and annealed PMMA-silica coatings. The SEM images of as-deposited coatings showed particles of micron size silica and nanosilica. Annealing resulted in the formation of relatively dense coatings containing silica particles in the PMMA matrix. The nanosilica nanoparticles were incorporated into the PMMA matrix as individual particles or agglomerates.

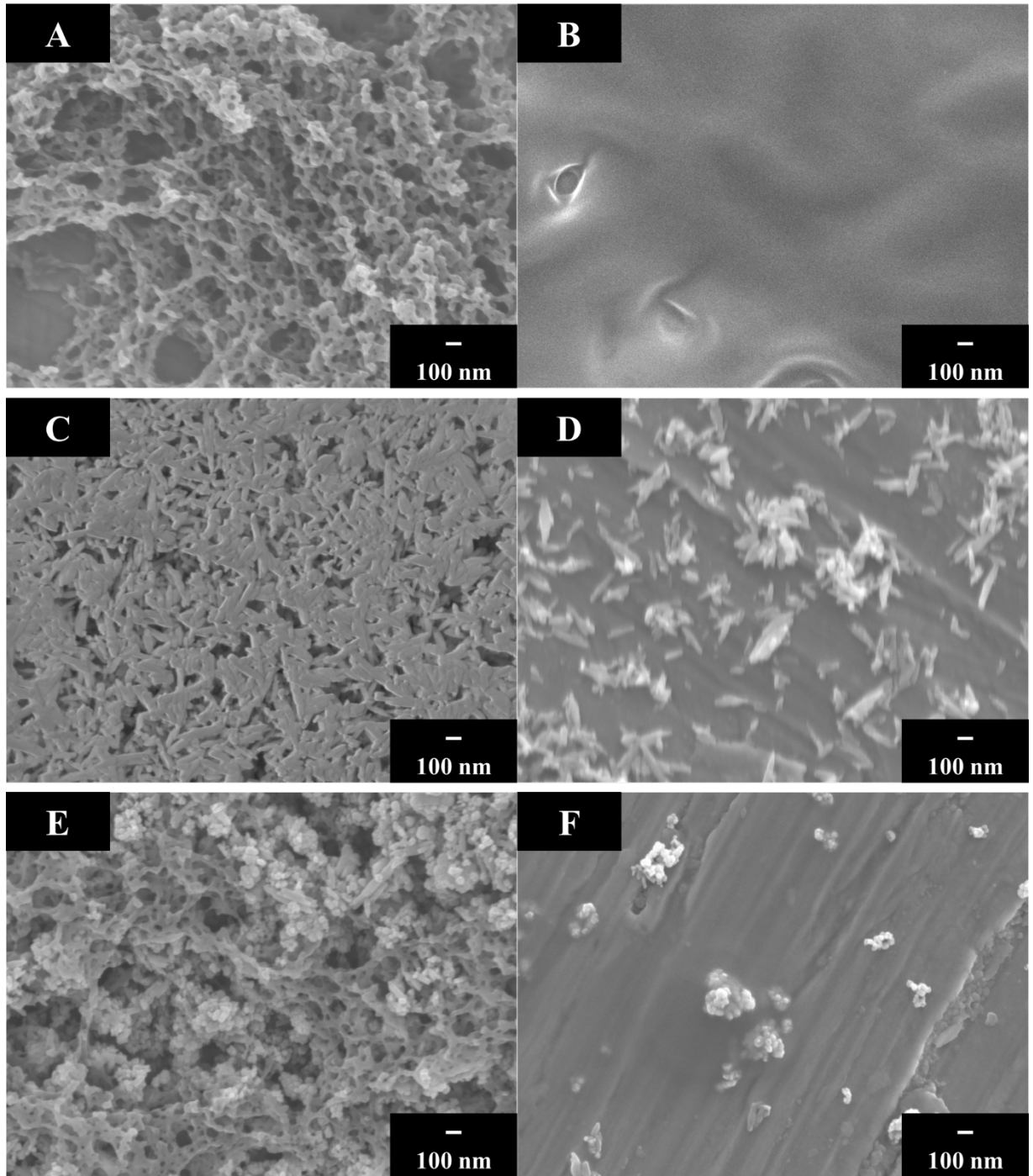


Figure 3-2 SEM images of (A,B) PMMA-Ag₂O, (C,D) PMMA-HA and PMMA-ZnO coatings, (A,C,E) as-deposited and room-temperature-dried, (B,D,F) annealed at 200 °C.

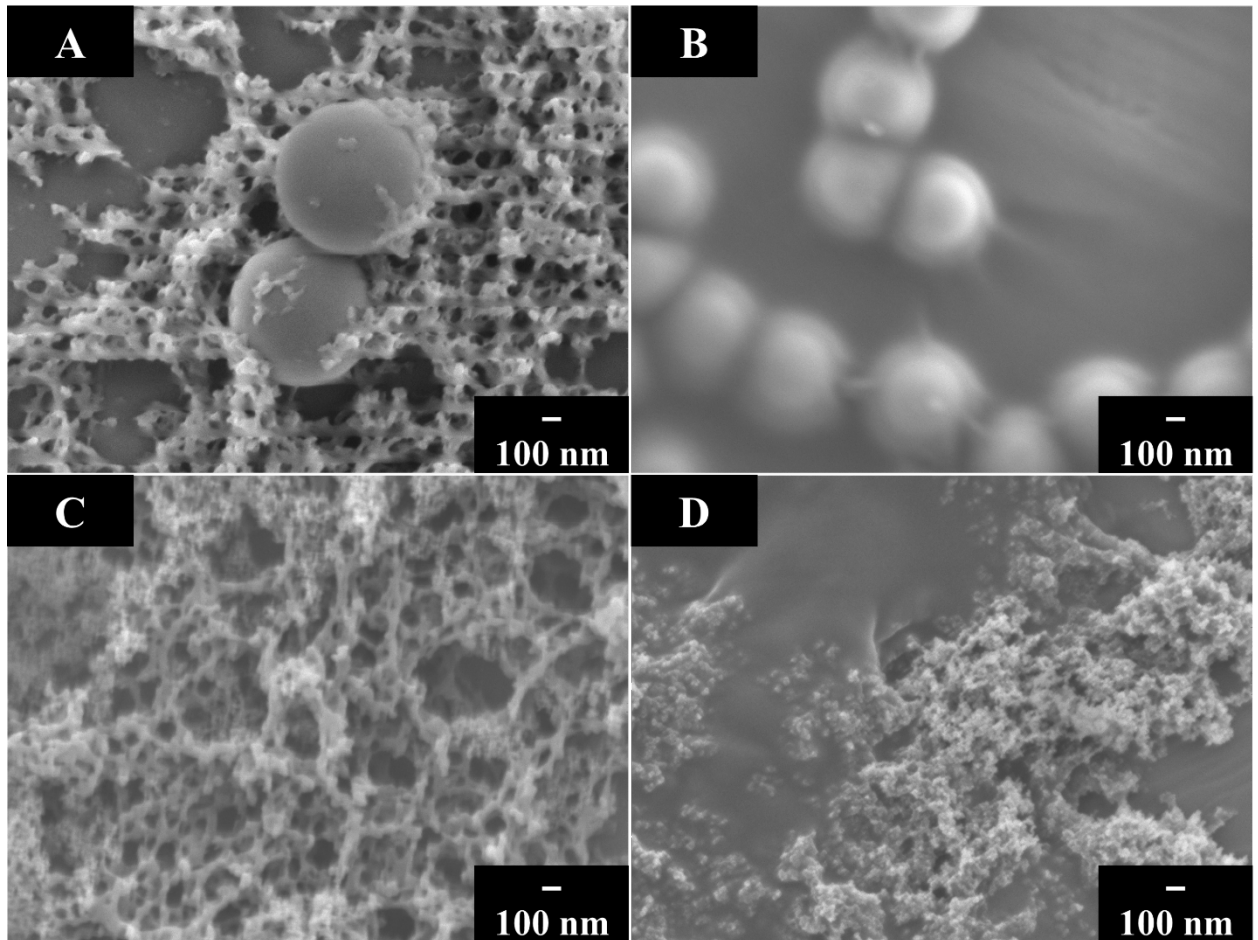


Figure 3-3 SEM images of (A,B) PMMA-micron size composites and (C,D) PMMA-nanosilica composites, (A,C) as-deposited and room-temperature-dried, (B,D) annealed at 200 °C.

The XRD and TGA methods were used for the analysis of the composite coatings. Figure 3-4a shows relatively broad peaks of pure PMMA.

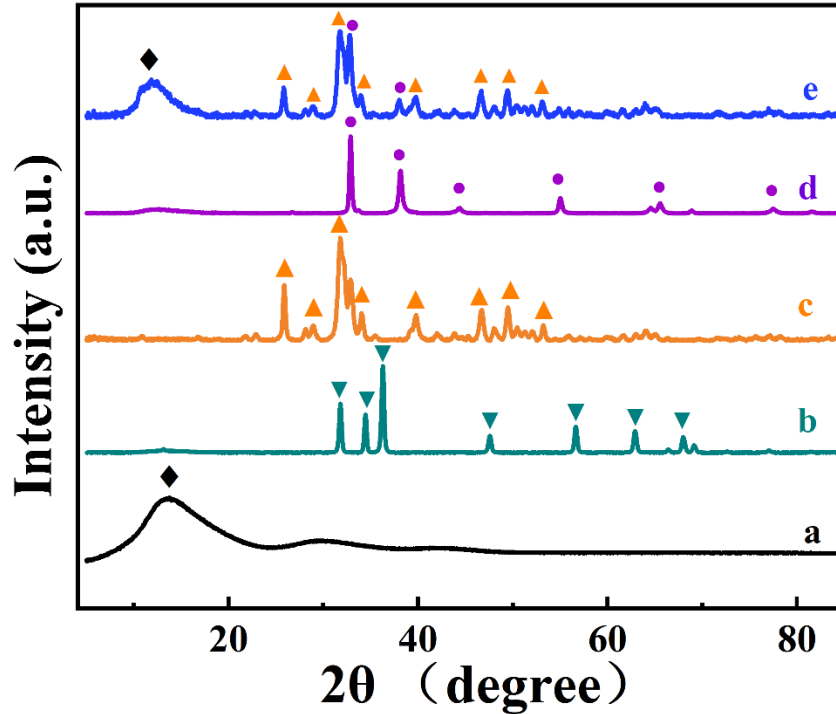


Figure 3-4 X-ray diffraction patterns of (a) as-received PMMA, and composites (b) PMMA-ZnO, (c) PMMA-HA, (d) PMMA-Ag₂O and (e) PMMA-HAP-Ag₂O, ▼—JCPDS file 04-020-9583, ▲—JCPDS file 04-008-4759, ●—JCPDS file 00-041-1104, ◆—PMMA.

XRD studies showed that the composite PMMA-ZnO, PMMA-HAP and PMMA-Ag₂O coatings exhibited peaks of ZnO (Figure 3-4b), HA (Figure 3-4c) and Ag₂O (Figure 3-4d), respectively. Moreover, X-ray diffraction studies (Figure 3-4e) showed that the deposition from 10 g L⁻¹ PMMA solutions containing 5 g L⁻¹ HA and 0.5 g L⁻¹ Ag₂O resulted in the fabrication of composite coatings containing HA and Ag₂O. Such coatings can potentially be used for the fabrication of biomedical implants with enhanced bioactivity and antimicrobial properties. The XRD studies also confirmed the fabrication of composite PMMA-silica coatings. Figure 3-5 compares the X-ray diffraction patterns of nanosilica, micron size silica and PMMA with the X-ray diffraction patterns of PMMA composites containing nanosilica and micron size silica. The X-

ray diffraction patterns of individual materials showed broad peaks, and the composite materials showed peaks of both PMMA and silica, confirming the fabrication of composites.

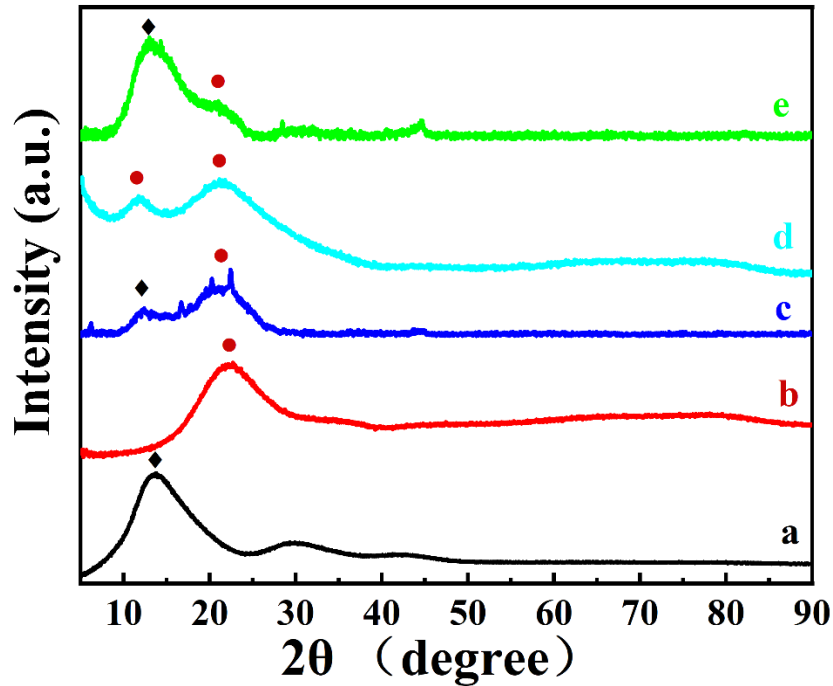


Figure 3-5 X-ray diffraction patterns of (a) PMMA, (b) micron size silica, (c) PMMA-micron size silica, (d) nanosilica and (e) PMMA-nanosilica (●—silica, ◆—PMMA).

The results of TGA studies of the composite coatings are presented in Figure 3-6. It is known [59] that the decomposition of PMMA in air occurs in the temperature range of 250–400 °C.

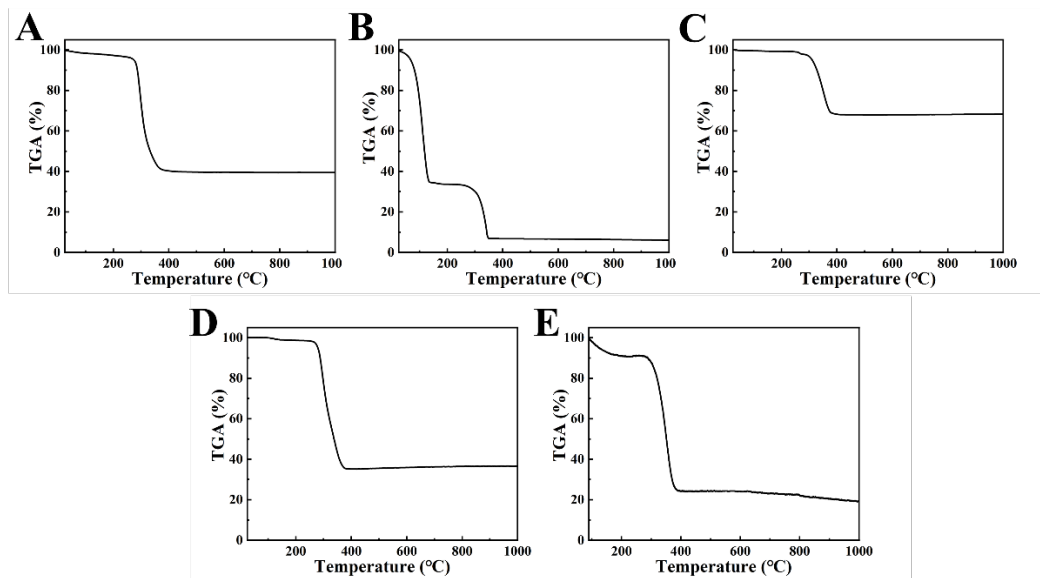


Figure 3-6 TGA data for (A) PMMA-HA, (B) PMMA-Ag₂O, (C) PMMA-ZnO, (D) PMMA-micron size silica and (E) PMMA-nanosilica composites.

The TGA data for PMMA-HA showed a small variation the sample mass below 300 °C and sharp reduction in the sample mass at higher temperatures due to the burning out of PMMA. The total mass loss at 1000 °C was found to be 61%, which indicated that the HA content in the composite was 39%. The TGA data for PMMA-Ag₂O showed weight losses at lower temperatures, which included two steps. A weight loss can result from dehydration, the decomposition of Ag₂O [60] and the burning out of PMMA. The total mass loss at 1000 °C was found to be 94%. The decomposition of PMMA and Ag₂O was observed [59,61] at temperatures above 200 °C. Therefore, weight loss in the range of 80–120 °C for PMMA-Ag₂O can be attributed to dehydration. It is in this regard that porous and composite materials can accumulate a significant amount of water during synthesis [62–65]. Therefore, the drying of PMMA-Ag₂O coatings at temperatures of 60–100 °C can be beneficial for antimicrobial applications. The TGA studies of the PMMA-ZnO, PMMA-micron size silica and PMMA-nanosilica showed a sharp reduction in mass loss at temperatures above 250–300 °C, and total mass loss was 32, 64 and 81%, respectively. The content

of ZnO, micron size silica and nanosilica in the composite coatings was found to be 68, 36 and 19%, respectively. Therefore, the results of the XRD and TGA studies confirmed the formation of composite coating by a dip-coating method. The difference in the thermal behavior of the composites can result from different factors, such as different concentrations of inorganic components, silver reduction, different amounts of adsorbed water, the influence of the inorganic phase on the burning out of polymer and other factors. The dip coating methods allowed for the fabrication of composite coatings containing drugs of different types. Ibuprofen, tetracycline and amoxicillin were used as model drugs of different types for the development of the dip coating method. Figure 3-7 shows SEM images of the composite coatings. The coatings show porous microstructures, which are beneficial for the drug release. Moreover, the biodegradability of PMMA is another beneficial factor for drug delivery [66].

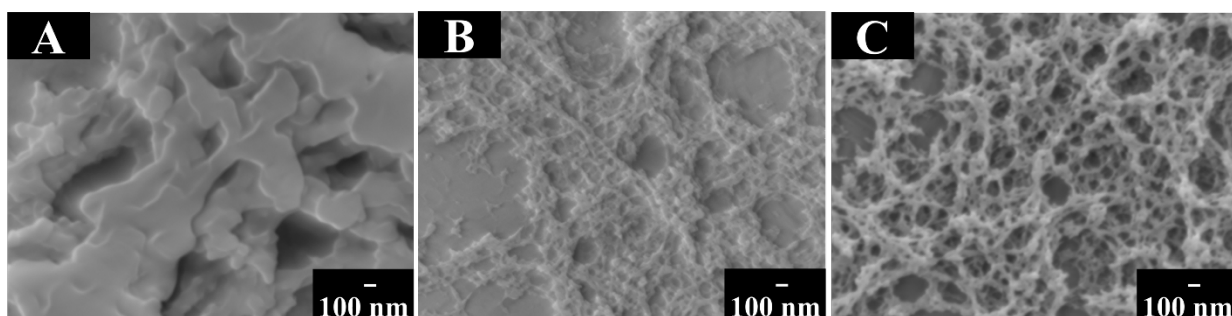


Figure 3-7 SEM images of as-deposited and room-temperature-dried coatings: (A) PMMA- ibuprofen, (B) PMMA-tetracycline and (C) PMMA-amoxicillin coatings.

The co-deposition of PMMA with drugs was confirmed by the XRD data presented in Figure 3-8. The X-ray diffraction patterns showed peaks of the drug materials.

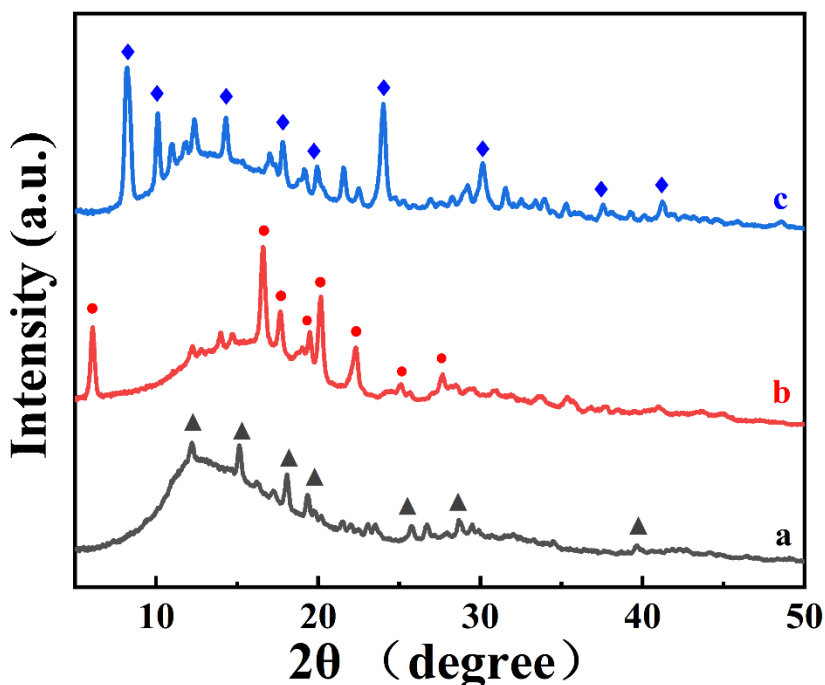


Figure 3-8 X-ray diffraction patterns of (a) PMMA-amoxicillin, (b) PMMA-ibuprofen and (c) PMMA-tetracycline; major XRD peaks are labeled: \blacktriangle —peaks corresponding to JCPDS file 00-039-1832 of amoxicillin, \bullet —peaks corresponding to JCPDS file 00-032-1723 of ibuprofen, \blacklozenge —peaks corresponding to JCPDS file 00-039-1985 of tetracycline.

The fabrication of the composite coatings was also confirmed by the results of FTIR spectroscopy. Figure 3-9 compares the FTIR spectra of as-received PMMA and drugs with the FTIR data for PMMA coatings containing drugs. The most intense bands in the spectrum of PMMA at 1703 , 1230 and 1068 cm^{-1} are attributed to the carbonyl $\text{C}=\text{O}$ stretching, $\text{C}-\text{C}-\text{C}$ stretching and skeletal rocking vibration of the polymer backbone, respectively [67]. The absorptions in the range of $1500\text{--}1400\text{ cm}^{-1}$ are related to the bending of the CH_2 , CH_3 and OCH_3 groups [67]. Similar absorptions were observed in the spectra of PMMA-ibuprofen, PMMA-tetracycline and PMMA-amoxicillin coatings. The FTIR spectra of ibuprofen [68] showed vibrational peaks at 935 cm^{-1} , which resulted from the $\text{O}-\text{H}$ bending group of ibuprofen. Carbonyl stretching vibration ($\text{C}=\text{O}$) is observed at 1718 cm^{-1} , which corresponds to the carboxyl group (COOH) of ibuprofen.

C–O stretching vibration is seen at 1230 cm^{-1} . Such absorptions were observed in the spectrum of PMMA-ibuprofen. The main characteristic peaks of tetracycline [69] are located in the range of $1200\text{--}1700\text{ cm}^{-1}$. The peak at 1575 cm^{-1} is attributed to the vibration of NH_2 amide [69]. The peak at 1446 cm^{-1} can be assigned to the C-ring-C stretching vibration [69]. Such peaks were observed in the spectrum of PMMA-tetracycline. The FTIR spectrum of amoxicillin [70] showed a C=O stretching band at 1772 cm^{-1} , a C=O stretching band of amide at 1683 cm^{-1} and absorption due to the asymmetric stretching of carboxylate at 1573 cm^{-1} . Additionally, the C-O bending vibration peak was observed at 1076 cm^{-1} . Similar peaks were observed in the spectrum of PMMA-amoxicillin.

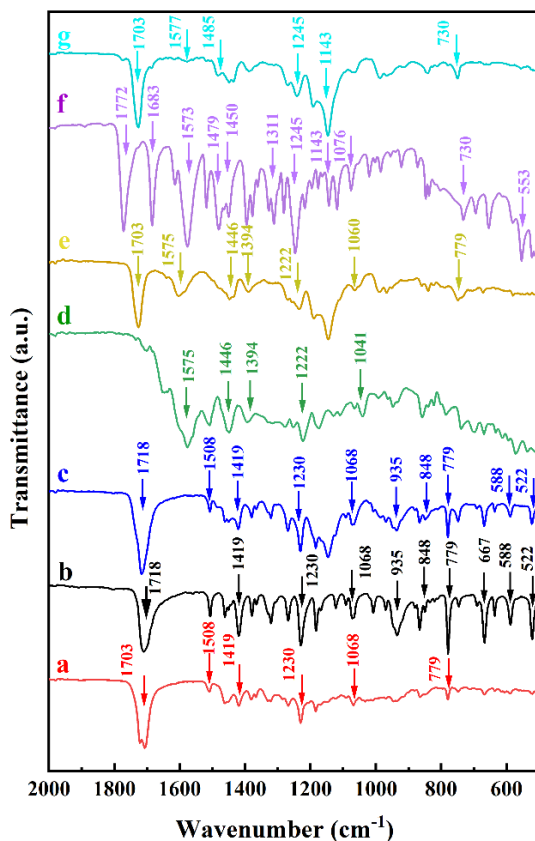


Figure 3-9 FTIR spectra of (a) as-received PMMA (b) as-received ibuprofen, (c) PMMA-ibuprofen, (d) asreceived tetracycline, (e) PMMA-tetracycline, (f) as-received amoxicillin and (g) PMMA-amoxicillin.

The experimental results described above confirmed the fabrication of composite coatings. The dip coating method developed in this investigation is a versatile strategy for the fabrication of composite coatings containing functional biomaterials of different types. Compared to other coating techniques, such as knife-coating or bar coating, dip coating involved the use of low-cost equipment. The isopropanol-water solvent offers benefits because the use of traditional toxic solvents for PMMA dissolution was avoided. The coatings obtained in this investigation provide a platform for the fabrication of implants with enhanced biocompatibility and antimicrobial properties, coatings for drug delivery and biosensors.

3.5. Conclusions

The ability to eliminate the use of traditional toxic solvents for PMMA offers benefits for the fabrication of composite coatings for biomedical applications. PMMA and composite coatings were obtained using a water-isopropanol solvent, avoiding the use of traditional toxic solvents. The dip coating method is a versatile strategy for the fabrication of composite coatings containing various functional materials, such as bioceramics, antimicrobial agents and drugs. PMMA coatings containing hydroxyapatite and silica are promising for the fabrication of biomedical implants with enhanced bioactivity and biocompatibility. The incorporation of materials with antimicrobial properties, such as Ag₂O and ZnO, into the PMMA matrix can potentially impart antimicrobial properties to the composite coatings. PMMA-ZnO coating can provide a platform for the immobilization of biosensing molecules and the fabrication of biosensors. PMMA-drug composite coatings offer potential for drug delivery. The dip coating method is a simple, low-cost technique, ideally suitable for multilayer processing. Therefore, further development of this method can result in advanced microstructures containing layers of different functional materials. It is expected that

future progress in this method will result in the deposition of new coatings containing other functional biomaterials for various applications.

3.6. Acknowledgements

The authors acknowledge the support of the Natural Sciences and Engineering Research Council (NSERC) of Canada, the CRC program and the Canadian Centre for Electron Microscopy.

3.7. References

1. Ali, U.; Karim, K.J.B.A.; Buang, N.A. A review of the properties and applications of poly (methyl methacrylate)(PMMA). *Polym. Rev.* 2015, 55, 678–705.
2. Wang, H.; Wang, L.; Meng, S.; Lin, H.; Correll, M.; Tong, Z. Nanocomposite of Graphene Oxide Encapsulated in Polymethylmethacrylate (PMMA): Pre-Modification, Synthesis, and Latex Stability. *J. Compos. Sci.* 2020, 4, 118
3. Saha, D.; Majumdar, M.K.; Das, A.K.; Chowdhury, A.M.S.; Ashaduzzaman, M. Structural Nanocomposite Fabrication from Self-Assembled Choline Chloride Modified Kaolinite into Poly(Methylmethacrylate). *J. Compos. Sci.* 2019, 3, 83
4. Poon, R.; Zhitomirsky, I. Application of Cyrene as a solvent and dispersing agent for fabrication of Mn₃O₄-carbon nanotube supercapacitor electrodes. *Colloid Interface Sci. Commun.* 2020, 34, 100226
5. Dimitrova, M.; Corsalini, M.; Kazakova, R.; Vlahova, A.; Chuchulska, B.; Barile, G.; Capodiferro, S.; Kazakov, S. Comparison between Conventional PMMA and 3D Printed Resins for Denture Bases: A Narrative Review. *J. Compos. Sci.* 2022, 6, 87
6. Sikkema, R.; Baker, K.; Zhitomirsky, I. Electrophoretic deposition of polymers and proteins for biomedical applications. *Adv. Colloid Interface Sci.* 2020, 284, 102272

7. Baker, K.; Sikkema, R.; Liang, W.; Zhitomirsky, I. Multifunctional Properties of Commercial Bile Salts for Advanced Materials Engineering. *Adv. Eng. Mater.* 2021, 23, 2001261
8. Inzana, J.A.; Schwarz, E.M.; Kates, S.L.; Awad, H.A. Biomaterials approaches to treating implant-associated osteomyelitis. *Biomaterials* 2016, 81, 58–71.
9. Leão, R.D.S.; Maior, J.R.S.; Lemos, C.A.D.A.; Vasconcelos, B.C.D.E.; Montes, M.A.J.R.; Pellizzer, E.P.; Moraes, S.L.D. Complications with PMMA compared with other materials used in cranioplasty: A systematic review and meta-analysis. *Braz. Oral Res.* 2018, 32, e31.
10. Jaebon, T. Polymethylmethacrylate: Properties and contemporary uses in orthopaedics. *JAAOS-J. Am. Acad. Orthop. Surg.* 2010, 18, 297–305.
11. Bistolfi, A.; Ferracini, R.; Albanese, C.; Vernè, E.; Miola, M. PMMA-Based Bone Cements and the Problem of Joint Arthroplasty Infections: Status and New Perspectives. *Materials* 2019, 12, 4002.
12. Lewis, G. Properties of nanofiller-loaded poly (methyl methacrylate) bone cement composites for orthopedic applications: A review. *J. Biomed. Mater. Res. Part B Appl. Biomater.* 2017, 105, 1260–1284.
13. Chatterjee, A. Properties improvement of PMMA using nano TiO₂. *J. Appl. Polym. Sci.* 2010, 118, 2890–2897.
14. Hazim, A.; Abduljalil, H.M.; Hashim, A. Analysis of Structural and Electronic Properties of Novel (PMMA/Al₂O₃, PMMA/Al₂O₃Ag, PMMA/ZrO₂, PMMA/ZrO₂-Ag, PMMA-Ag) Nanocomposites for Low Cost Electronics and Optics Applications. *Trans. Electr. Electron. Mater.* 2020, 21, 48–67

15. Bai, H.; Walsh, F.; Gludovatz, B.; Delattre, B.; Huang, C.; Chen, Y.; Tomsia, A.P.; Ritchie, R.O. Bioinspired hydroxyapatite/poly (methyl methacrylate) composite with a nacre-mimetic architecture by a bidirectional freezing method. *Adv. Mater.* 2016, 28, 50–56.
16. Carranza, A.; Romero-Perez, D.; Almanza-Reyes, H.; Bogdanchikova, N.; Juarez-Moreno, K.; Pojman, J.A.; Velasquillo, C.; Mota-Morales, J.D. Nonaqueous Synthesis of Macroporous Nanocomposites Using High Internal Phase Emulsion Stabilized by Nanohydroxyapatite. *Adv. Mater. Interfaces* 2017, 4, 1700094.
17. Haach, L.C.D.A.; Purquerio, B.D.M.; Silva Junior, N.F.D.; Gaspar, A.M.M.; Fortulan, C.A. Comparison of two composites developed to be used as bone replacement-PMMA/Bioglass 45S5® microfiber and PMMA/Hydroxyapatite. *Bioceram. Dev. Appl.* 2014, 4, 1000071.
18. Floroian, L.; Samoila, C.; Badea, M.; Munteanu, D.; Ristoscu, C.; Sima, F.; Negut, I.; Chifiriuc, M.; Mihailescu, I. Stainless steel surface biofunctionalization with PMMA-bioglass coatings: Compositional, electrochemical corrosion studies and microbiological assay. *J. Mater. Sci. Mater. Med.* 2015, 26, 195.
19. Kettel, M.J.; Heine, E.; Schaefer, K.; Moeller, M. Chlorhexidine Loaded Cyclodextrin Containing PMMA Nanogels as Antimicrobial Coating and Delivery Systems. *Macromol. Biosci.* 2017, 17, 1600230.
20. Neumann, S.E.; Chamberlayne, C.F.; Zare, R.N. Electrically controlled drug release using pH-sensitive polymer films. *Nanoscale* 2018, 10, 10087–10093.

21. Rezaei, F.; Abbasi-Firouzjah, M.; Shokri, B. Investigation of antibacterial and wettability behaviours of plasma-modified PMMA films for application in ophthalmology. *J. Phys. D Appl. Phys.* 2014, 47, 085401.
22. Shanzuo, J.; Ponting, M.; Lepkowicz, R.S.; Rosenberg, A.; Flynn, R.; Beadie, G.; Baer, E. A bio-inspired polymeric gradient refractive index (GRIN) human eye lens. *Opt. Express* 2012, 20, 26746–26754.
23. Nugen, S.R.; Asiello, P.J.; Connelly, J.T.; Baeumner, A.J. PMMA biosensor for nucleic acids with integrated mixer and electrochemical detection. *Biosens. Bioelectron.* 2009, 24, 2428–2433.
24. Irawati, N.; Harun, S.W.; Adwan, S.; Alnowami, M.; Ahmad, H. PMMA microfiber coated with Al-doped ZnO nanostructures for detecting uric acid. *Microw. Opt. Technol. Lett.* 2015, 57, 2455–2457.
25. Cools, P.; De Geyter, N.; Vanderleyden, E.; Barberis, F.; Dubruel, P.; Morent, R. Adhesion improvement at the PMMA bone cement-titanium implant interface using methyl methacrylate atmospheric pressure plasma polymerization. *Surf. Coat. Technol.* 2016, 294, 201–209.
26. Coan, T.; Barroso, G.; Machado, R.; De Souza, F.; Spinelli, A.; Motz, G. A novel organic-inorganic PMMA/polysilazane hybrid polymer for corrosion protection. *Prog. Org. Coat.* 2015, 89, 220–230.
27. D’Elia, A.; Deering, J.; Clifford, A.; Lee, B.; Grandfield, K.; Zhitomirsky, I. Electrophoretic deposition of polymethylmethacrylate and composites for biomedical applications. *Colloids Surf. B Biointerfaces* 2020, 188, 110763.

28. Norouzi, M.; Garekani, A.A. Corrosion protection by zirconia-based thin films deposited by a sol–gel spin coating method. *Ceram. Int.* 2014, 40, 2857–2861.
29. Jin, W.; Hao, Q.; Peng, X.; Chu, P.K. Enhanced corrosion resistance and biocompatibility of PMMA-coated ZK60 magnesium alloy. *Mater. Lett.* 2016, 173, 178–181.
30. Coan, T.; Barroso, G.S.; Motz, G.; Bolzán, A.; Machado, R.A.F. Preparation of PMMA/hBN composite coatings for metal surface protection. *Mater. Res.* 2013, 16, 1366–1372.
31. Negi, Y.; Adhyapak, P.; Damkale, S.; Goyal, R.; Islam, M.; Aiyer, R. Preparation of novel optical-grade metanitroaniline and polymethylmethacrylate-coated single crystals and their optical properties. *Mater. Lett.* 2004, 58, 3929–3932.
32. Sathish, S.; Shekar, B.C. Dip and spin coated nanoscale transparent PMMA thin films for field effect thin film transistors and optoelectronic devices. *J. Optoelectron. Adv. Mater* 2013, 15, 139–144.
33. Li, X.; Zhitomirsky, I. Deposition of poly (methyl methacrylate) and composites containing bioceramics and bioglass by dip coating using isopropanol-water co-solvent. *Prog. Org. Coat.* 2020, 148, 105883.
34. Sreekantan, S.; Hassan, M.; Sundera Murthe, S.; Seenii, A. Biocompatibility and Cytotoxicity Study of Polydimethylsiloxane (PDMS) and Palm Oil Fuel Ash (POFA) Sustainable Super-Hydrophobic Coating for Biomedical Applications. *Polymers* 2020, 12, 3034.

35. Cooperstein, M.A.; Canavan, H.E. Assessment of cytotoxicity of (N-isopropyl acrylamide) and poly (N-isopropyl acrylamide)coated surfaces. *Biointerphases* 2013, 8, 19.
36. Hadidi, M.; Bigham, A.; Saebnoori, E.; Hassanzadeh-Tabrizi, S.; Rahmati, S.; Alizadeh, Z.M.; Nasirian, V.; Rafienia, M. Electrophoretic-deposited hydroxyapatite-copper nanocomposite as an antibacterial coating for biomedical applications. *Surf. Coat. Technol.* 2017, 321, 171–179.
37. Farrokhi-Rad, M. Electrophoretic deposition of titania nanostructured coatings with different porous patterns. *Ceram. Int.* 2018, 44, 15346–15355.
38. Farrokhi-rad, M.; Emamalipour, S.; Mohammadzadeh, F.; Beygi-Khosrowshahi, Y.; Hassannejad, H.; Nouri, A. Electrophoretic deposition of alginate coatings from different alcohol-water mixtures. *Surf. Eng.* 2021, 37, 1176–1185.
39. Narkevica, I.; Stradina, L.; Stipniece, L.; Jakobsons, E.; Ozolins, J. Electrophoretic deposition of nanocrystalline TiO₂ particles on porous TiO₂-X ceramic scaffolds for biomedical applications. *J. Eur. Ceram. Soc.* 2017, 37, 3185–3193.
40. Bano, S.; Romero, A.R.; Grant, D.; Nommeots-Nomm, A.; Scotchford, C.; Ahmed, I.; Hussain, T. In-vitro cell interaction and apatite forming ability in simulated body fluid of ICIE16 and 13–93 bioactive glass coatings deposited by an emerging suspension high velocity oxy fuel (SHVOF) thermal spray. *Surf. Coat. Technol.* 2021, 407, 126764.
41. Grigaleviciute, G.; Baltriukiene, D.; Bukelskiene, V.; Malinauskas, M. Biocompatibility Evaluation and Enhancement of Elastomeric Coatings Made Using Table-Top Optical 3D Printer. *Coatings* 2020, 10, 254.

42. Zhang, M.; Weng, Y.J.; Zhang, Y.Q. Accelerated desalting and purification of silk fibroin in a CaCl₂-EtOH-H₂O ternary system by excess isopropanol extraction. *J. Chem. Technol. Biotechnol.* 2021, 96, 1176–1186.
43. Silva, S.S.; Oliveira, N.M.; Oliveira, M.B.; Da Costa, D.P.S.; Naskar, D.; Mano, J.F.; Kundu, S.C.; Reis, R.L. Fabrication and characterization of Eri silk fibers-based sponges for biomedical application. *Acta Biomater.* 2016, 32, 178–189.
44. Pruetz, L.J.; Jenkins, C.H.; Singh, N.S.; Catallo, K.J.; Griffin, D.R. Heparin Microislands in Microporous Annealed Particle Scaffolds for Accelerated Diabetic Wound Healing. *Adv. Funct. Mater.* 2021, 31, 2104337.
45. Yu, Q.; Roberts, M.G.; Pearce, S.; Oliver, A.M.; Zhou, H.; Allen, C.; Manners, I.; Winnik, M.A. Rodlike block copolymer micelles of controlled length in water designed for biomedical applications. *Macromolecules* 2019, 52, 5231–5244.
46. Grandfield, K.; Zhitomirsky, I. Electrophoretic deposition of composite hydroxyapatite–silica–chitosan coatings. *Mater. Charact.* 2008, 59, 61–67.
47. Grandfield, K.; Sun, F.; FitzPatrick, M.; Cheong, M.; Zhitomirsky, I. Electrophoretic deposition of polymer-carbon nanotube hydroxyapatite composites. *Surf. Coat. Technol.* 2009, 203, 1481–1487.
48. Baskaran, A.; Smereka, P. Mechanisms of stranski-krastanov growth. *J. Appl. Phys.* 2012, 111, 044321.
49. Vithiya, K.; Kumar, R.; Sen, S. Antimicrobial activity of biosynthesized silver oxide nanoparticles. *J. Pure Appl. Microbiol* 2014, 4, 3263–3268.

50. D’Lima, L.; Phadke, M.; Ashok, V.D. Biogenic silver and silver oxide hybrid nanoparticles: A potential antimicrobial against multi drug-resistant *Pseudomonas aeruginosa*. *New J. Chem.* 2020, 44, 4935–4941.
51. Arya, S.K.; Saha, S.; Ramirez-Vick, J.E.; Gupta, V.; Bhansali, S.; Singh, S.P. Recent advances in ZnO nanostructures and thin films for biosensor applications. *Anal. Chim. Acta* 2012, 737, 1–21.
52. Janaki, A.C.; Sailatha, E.; Gunasekaran, S. Synthesis, characteristics and antimicrobial activity of ZnO nanoparticles. *Spectrochim. Acta Part A Mol. Biomol. Spectrosc.* 2015, 144, 17–22.
53. Shinde, S.S. Antimicrobial activity of ZnO nanoparticles against pathogenic bacteria and fungi. *Sci. Med. Cent.* 2015, 3, 1033.
54. Casas-Luna, M.; Horynová, M.; Tkachenko, S.; Klakurková, L.; Celko, L.; Diaz-de-la-Torre, S.; Montufar, E.B. Chemical Stability of Tricalcium Phosphate–Iron Composite during Spark Plasma Sintering. *J. Compos. Sci.* 2018, 2, 51.
55. Wang, K.; Pasbakhsh, P.; De Silva, R.T.; Goh, K.L. A Comparative Analysis of the Reinforcing Efficiency of Silsesquioxane Nanoparticles versus Apatite Nanoparticles in Chitosan Biocomposite Fibres. *J. Compos. Sci.* 2017, 1, 9.
56. Moura, N.K.D.; Siqueira, I.A.W.B.; Machado, J.P.D.B.; Kido, H.W.; Avanzi, I.R.; Rennó, A.C.M.; Trichês, E.D.S.; Passador, F.R. Production and Characterization of Porous Polymeric Membranes of PLA/PCL Blends with the Addition of Hydroxyapatite. *J. Compos. Sci.* 2019, 3, 45.
57. Pang, X.; Zhitomirsky, I. Electrophoretic deposition of composite hydroxyapatite-chitosan coatings. *Mater. Charact.* 2007, 58, 339–348.

58. Harb, S.V.; Uvida, M.C.; Trentin, A.; Lobo, A.O.; Webster, T.J.; Pulcinelli, S.H.; Santilli, C.V.; Hammer, P. PMMA-silica nanocomposite coating: Effective corrosion protection and biocompatibility for a Ti6Al4V alloy. *Mater. Sci. Eng. C* 2020, 110, 110713.
59. Fateh, T.; Richard, F.; Rogaume, T.; Joseph, P. Experimental and modelling studies on the kinetics and mechanisms of thermal degradation of polymethyl methacrylate in nitrogen and air. *J. Anal. Appl. Pyrolysis* 2016, 120, 423–433.
60. Mu, F.; Zhao, Z.; Zou, G.; Bai, H.; Wu, A.; Liu, L.; Zhang, D.; Norman Zhou, Y. Mechanism of Low Temperature Sintering-Bonding through In-Situ Formation of Silver Nanoparticles Using Silver Oxide Microparticles. *Mater. Trans.* 2013, 54, 872.
61. Ananth, A.; Mok, Y.S. Dielectric barrier discharge (DBD) plasma assisted synthesis of Ag₂O nanomaterials and Ag₂O/RuO₂ nanocomposites. *Nanomaterials* 2016, 6, 42.
62. Zhang, H.; Li, G.; An, L.; Yan, T.; Gao, X.; Zhu, H. Electrochemical lithium storage of titanate and titania nanotubes and nanorods. *J. Phys. Chem. C* 2007, 111, 6143–6148.
63. Porramezan, M.; Eisazadeh, H. Fabrication and characterization of polyaniline nanocomposite modified with Ag₂O nanoparticles. *Compos. Part B Eng.* 2011, 42, 1980–1986.
64. Pang, X.; Zhitomirsky, I.; Niewczas, M. Cathodic electrolytic deposition of zirconia films. *Surf. Coat. Technol.* 2005, 195, 138–146.
65. Zhitomirsky, I.; Petric, A. Electrochemical deposition of yttrium oxide. *J. Mater. Chem.* 2000, 10, 1215–1218.
66. Wentao, Z.; Lei, G.; Liu, Y.; Wang, W.; Song, T.; Fan, J. Approach to osteomyelitis treatment with antibiotic loaded PMMA. *Microb. Pathog.* 2017, 102, 42–44.

67. Huszánk, R.; Szilágyi, E.; Szoboszlai, Z.; Szikszai, Z. Investigation of chemical changes in PMMA induced by 1.6 MeV He⁺ irradiation by ion beam analytical methods (RBS-ERDA) and infrared spectroscopy (ATR-FTIR). *Nucl. Instrum. Methods Phys. Res. B* 2019, 450, 364–368.
68. Carvalho, R.B.; Joshi, S.V. Ibuprofen isobutanolammonium salt. *J. Therm. Anal. Calorim.* 2020, 139, 1971–1976.
69. Zhang, Z.; Liu, H.; Wu, L.; Lan, H.; Qu, J. Preparation of amino-Fe (III) functionalized mesoporous silica for synergistic adsorption of tetracycline and copper. *Chemosphere* 2015, 138, 625–632.
70. Iqbal, D.N.; Ehtisham-ul-Haque, S.; Ahmad, S.; Arif, K.; Hussain, E.A.; Iqbal, M.; Alshawwa, S.Z.; Abbas, M.; Amjed, N.; Nazir, A. Enhanced antibacterial activity of chitosan, guar gum and polyvinyl alcohol blend matrix loaded with amoxicillin and doxycycline hyclate drugs. *Arab. J. Chem.* 2021, 14, 103156.

Chapter 4 Surfactants for Electrophoretic Deposition of Polyvinylidene Fluoride–Silica Composites

4.1. Abstract

This investigation is motivated by the numerous advantages of electrophoretic deposition (EPD) for the fabrication of polyvinylidene fluoride (PVDF) and composite coatings and the various applications of such coatings. It is demonstrated that gallic acid (GA), caffeic acid (CFA), cholic acid (CA) and 2,3,4 trihydroxybenzoic acid (THB) can be used as charging and dispersing agents for the EPD of PVDF. The deposition yield of PVDF increases in the following order: THB < CFA < CA < GA. Test results indicate that the chemical structure of the dispersants exerts influence on the deposition efficiency. Potentiodynamic and impedance spectroscopy studies show the corrosion protection properties of PVDF coatings. GA is used for the co-EPD of PVDF with nanosilica and micron-size silica. The silica content in the composite coatings is varied by the variation of silica content in the suspensions. The ability to use GA as a charging and dispersing agent for the co-EPD of materials of different types paves the way for the fabrication of advanced organic–inorganic composites using EPD.

4.2. Introduction

Electrophoretic deposition (EPD) is an important technique for the surface modification of materials [1–3]. This technique is of particular interest for biomedical applications [4–7] due to the high purity of the deposited materials and the possibility of uniform deposition on complex shape substrates. Investigations focused on the development of advanced EPD bath formulations [8–10], particle charging additives [11], deposition kinetics and mechanisms [12–14]. Many investigations were performed on the EPD of organic–inorganic composites containing inorganic

particles in a polymer matrix [4–6,15,16]. Significant interest has been generated in the use of biosurfactants for the fabrication of colloidal suspensions and the EPD of different materials [17–20]. The chemical structure of surfactants is an important factor controlling their adsorption on particles and the efficiency of particle dispersion [21–23]. A dispersant adsorbed on a particle's surface imparts an electric charge to the particles and allows for their electrophoretic transport to the electrode [24]. One of the challenges in the EPD technology is the charging, dispersion and deposition of chemically inert polymers. Another challenge is related to the co-deposition of such polymers with inorganic materials. Difficulties are related to the poor adsorption of traditional surfactants on the surfaces of such polymers and the selection of charged co-dispersants for the co-deposition of polymers with inorganic nanoparticles. However, there is a need in the development of EPD for the fabrication of composites, based on chemically inert advanced functional polymers, such as polyvinylidene fluoride (PVDF). PVDF is a chemically inert polymer, which shows good resistance to inorganic and organic acids, various solvents and chemicals [25–27]. This polymer exhibits ferroelectric and piezoelectric properties, mechanical strength and low flammability [28–31]. Many PVDF applications involved the use of thin films and coatings [32–34]. Thin films were used for piezoelectric actuators and transducers, pyroelectric sensors, electrical insulators and capacitors [28,35,36]. Significant interest has been generated in PVDF films for water treatment and the removal of pollutants, gas separation membranes, polymer fuel cells and batteries [37–40]. Of particular interest are PVDF applications in different biosensors [41–43]. PVDF films are under investigation for application in implantable biomedical devices [44–46]. PVDF and PVDF–silica composites have generated significant interest for biomedical tissue engineering [47–49]. PVDF was used as a binder for [50–53] the EPD of different materials. In this strategy, a small amount of dissolved PVDF was co-deposited with particles of inorganic

or carbon materials. PVDF suspensions and solutions were used for EPD without charged dispersants [54–56]. However, the charging and deposition mechanisms were not understood. The EPD of PVDF films was achieved using bile acids as dispersing and charging agents [57]. This investigation was motivated by the need for the fabrication of PVDF and composite films and the numerous advantages of the EPD deposition method. The goal of this investigation was the EPD of pure PVDF and PVDF–silica films. The influence of different dispersants on the deposition yield was investigated. The highest deposition yield of PVDF was achieved using gallic acid (GA) as a dispersant. The PVDF films deposited using GA as a dispersant provided corrosion protection of stainless steel substrates. The use of GA facilitated the co-deposition of PVDF with micro- and nanosilica. The amount of silica co-deposited with PVDF could be varied. The results of this investigation indicated that catecholates and gallates can be used as efficient co-dispersants for the co-deposition of PVDF with inorganic particles.

4.3. Experimental

Poly (vinylidene fluoride) (PVDF, spherical particles, diameter 100 nm, Alfa Aesar, Tewksbury, MA, USA), gallic acid (GA), caffeic acid (CFA), cholic acid (CA), 2,3,4 trihydroxybenzoic acid (THB), NaCl, nanosilica (size 5–20 nm, MilliporeSigma, Oakville, ON, Canada) and micron-size silica (size $1\ \mu\text{m} \pm 10\%$, PCR Inc., Cumming, GA, USA) were used. PVDF films were prepared via EPD from $5\ \text{g L}^{-1}$ PVDF suspensions in ethanol, containing $1\ \text{g L}^{-1}$ dispersants, such as GA, CFA, CA and THB. The dispersants were dissolved in ethanol, and then, PVDF particles were added. Ultrasonication was performed for 30 min in order to obtain stable suspensions for EPD. The EPD of composite films was performed from $5\ \text{g L}^{-1}$ PVDF suspensions, containing $1\text{--}8\ \text{g L}^{-1}$ silica particles and $1\text{--}2\ \text{g L}^{-1}$ dispersants. Silica particles were added to the PVDF suspensions, containing dissolved dispersants. Ultrasonication was performed for 30 min

for the fabrication of stable suspensions for EPD. A type 304 stainless steel (dimensions $25 \times 30 \times 0.12$ mm) functioned as the working electrode, while a platinum sheet (dimensions $25 \times 30 \times 0.1$ mm) acted as the counter electrode, with a 17 mm spacing between them in the EPD cell. An Amersham Biosciences EPS 2A200 power supply was used for EPD. EPD was performed for 1–5 min at a deposition voltage of 100 V between two electrodes. Following deposition, the coatings were dried at room temperature before being thermally treated in a Carbolite ELF furnace at 200 °C for 1 h for further characterization. Deposition yield measurements were performed via measurement of substrate mass before and after deposition using precise Mettler Toledo XSR104 Analytical Balance. Zeta potential measurements were performed by a mass transfer method [58]. FTIR studies were performed using a Bruker Vertex 70 spectrometer (USA). A PARSTAT 2273 potentiostat from Ametek (USA) was used to conduct electrochemical characterization of coated and uncoated substrates in a 3.0 wt% aqueous NaCl solution with a 3-electrode cell that included an uncoated or coated stainless steel substrate as a working electrode, a saturated calomel reference electrode (SCE), and a Pt mesh counter electrode. The testing technique and data analysis were both controlled by PowerSuite software. To reduce the influence of oxygen, the aqueous NaCl solution was deoxygenated for at least 30 min using inert nitrogen gas before each test. Potentiodynamic polarization experiments were carried out at a 1.0 mV s^{-1} sweeping rate. Electrochemical impedance spectroscopy (EIS) experiments were carried out in the frequency range from 10 mHz to 10 kHz with a sinusoidal excitation voltage of 10 mV. Microstructure analysis was carried out using a JEOL JSM-7000F (Tokyo, Japan) scanning electron microscope (SEM) and a Talos 200X (ThermoFisher Scientific, Waltham, MA, USA) transmission electron microscope (TEM).

4.4. Results and Discussion

Figure 4-1 shows TEM images of PVDF particles used for EPD. The particles had a spherical shape with uniform diameters of ~200 nm. PVDF is an electrically neutral polymer. Therefore, PVDF particles must be charged and dispersed using additives for film formation via EPD. Figure 4-2 shows structures of GA, CFA, CA and THB used in this investigation as additives for PVDF deposition.

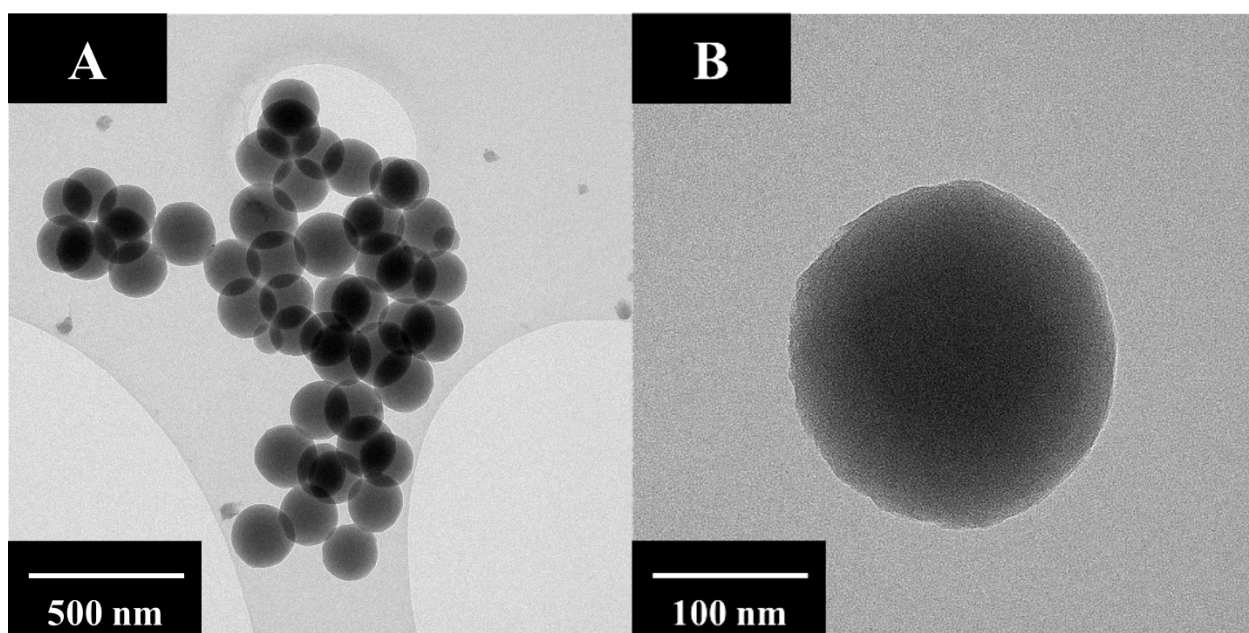


Figure 4-1 TEM images of PVDF particles at (A,B) different magnifications.

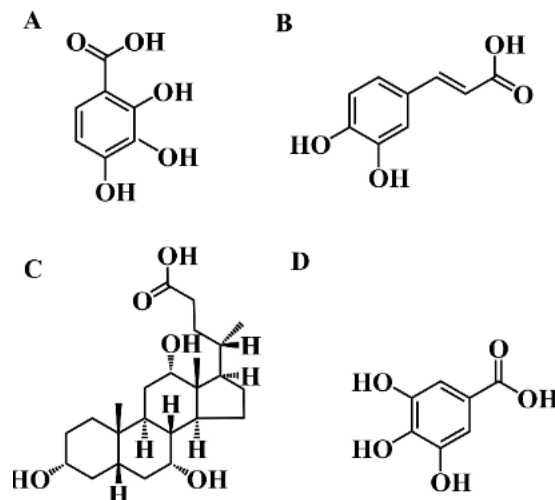


Figure 4-2 Chemical structures of (A) THB, (B) CFA, (C) CA and (D) GA.

The chemical structures of GA, CFA, CA and THB contain anionic COOH groups. The chemical structures of CA and aromatic GA, CFA and THB molecules are beneficial for their adsorption on organic materials [19]. THB, CA and GA are especially attractive for adsorption on inorganic materials, because such molecules can be adsorbed on particle surfaces via catecholate-type bonding (GA, CFA and THB) or salicylate-type bonding (THB) [18]. The interest in gallates and catecholates for the EPD of metal oxides resulted from the analysis of strong catecholate-type bonding of mussel proteins to inorganic surfaces [59–61]. In previous investigations, aromatic catecholate- and gallate-type molecules were used as charging and dispersing agents for the anodic EPD of different oxide particles in ethanol [62–66]. The adsorption of catecholate molecules containing COOH groups on positively charged MnO₂ particles resulted in a charge reversal and allowed for the anodic deposition of MnO₂ films from particle suspensions in ethanol [67]. The addition of GA, CFA, CA and THB to the PVDF suspensions in ethanol allowed for the fabrication of PVDF films via EPD. The suspensions of electrically neutral PVDF were unstable, and EPD was not achieved from such suspensions. It was hypothesized that added dispersants adsorbed on PVDF particles imparted an electric charge to the particles and allowed for the suspension

stabilization and deposition of PVDF from stable suspensions. Dispersant adsorption on particles can result from hydrophobic interactions. Figures 4-3B and 4-9 (Supplementary data) show the deposit masses of the films prepared with different dispersants at a PVDF concentration of 5 g L^{-1} . The EPD experiments indicated that selected anionic dispersants adsorbed on the PVDF imparted charge to the PVDF particles and allowed their EPD. The chemical structures of the aromatic dispersants THB, CFA and GA exerted influence on the deposition efficiency, with the highest deposition yield obtained using GA. The deposition yield obtained using CA was higher than that obtained using THB and CFA. The deposition yield increased in the following order: THB < CFA < CA < GA. The suspensions containing CA and GA were further investigated due to the larger deposition yields obtained using such dispersants. Moreover, CA and GA are promising for the dispersion and charging of inorganic particles because they allow for catecholate-type bonding to the particle surface [18]. The deposition yield increased with increasing PVDF concentration in suspensions with the highest deposition yield achieved using GA for all PVDF concentrations (Figures 4-3B and 4-10). The deposition yield of PVDF increased with increasing deposition voltage and time (Figures 4-11 and 4-12). Zeta potentials of PVDF particles obtained in the presence of THB, CFA, CA and GA were found to be -4.2 , -4.5 , -7.1 and -13.9 mV, respectively. The highest deposition yield and zeta potential of PVDF achieved using GA indicated stronger GA adsorption on PVDF and enhanced particle charging. The EPD of PVDF was optimized using GA dispersant at the deposition voltage of 100 V, deposition time of 5 min and PVDF concentration of 5 g L^{-1} . It should be noted that at higher voltages, deposition times and PVDF concentrations, the deposition process required the addition of a polymer binder due to increased deposit mass and risk of spalling of green deposits. A GA concentration of 1 g L^{-1} was the minimum concentration required for EPD from 5 g L^{-1} PVDF solutions and the co-EPD of PVDF with micron-size silica.

It is shown below that in the case of nanosilica with smaller particle sizes and large nanosilica concentrations, the GA content could be increased to 2 g L^{-1} in order to achieve the improved co-deposition of nanosilica with PVDF. The deposition of PVDF was also confirmed by results of Fourier Transform Infrared Spectroscopy (FTIR). The comparison of the FTIR spectrum of the as-received PVDF powder and spectra of deposits obtained using THB, CFA, CA and GA dispersants (Figure 4-13) indicated that PVDF coatings were deposited via EPD. The spectra of the deposits contained characteristic peaks of as-received PVDF (Figure 4-13). Figure 4-4A shows SEM images of the as-deposited PVDF film. The as-deposited film was porous. Annealing at $200 \text{ }^\circ\text{C}$ for 1 h resulted in the PVDF melting and the formation of a dense film (Figure 4-4B). The annealed PVDF films showed promising corrosion protection properties. Figure 5 presents potentiodynamic testing data for coated and uncoated substrates. Coated substrates showed a lower corrosion current of $0.27 \text{ } \mu\text{A cm}^{-2}$, compared to the corrosion current of $2.6 \text{ } \mu\text{A cm}^{-2}$ for uncoated steel. The Tafel plot for the coated sample showed reduced anodic current and increased corrosion potential. Moreover, the Bode plots of impedance data confirmed corrosion protection properties of the PVDF coatings (Figure 4-6). Coated samples showed larger impedance compared to uncoated substrate in 3% NaCl solutions. Therefore, deposited coating provided a barrier preventing electrolyte access to the substrate.

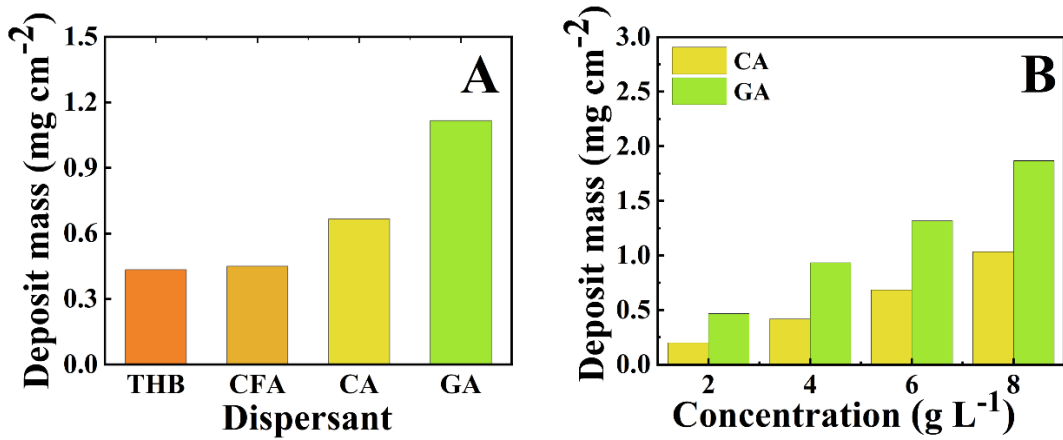


Figure 4-3 (A) Deposit mass achieved for different dispersants using 5 g L⁻¹ PVDF suspensions containing 1 g L⁻¹ dispersants, (B) deposit mass versus PVDF concentration in suspensions, containing 1 g L⁻¹ dispersants for deposition time of 5 min and deposition voltage of 100 V.

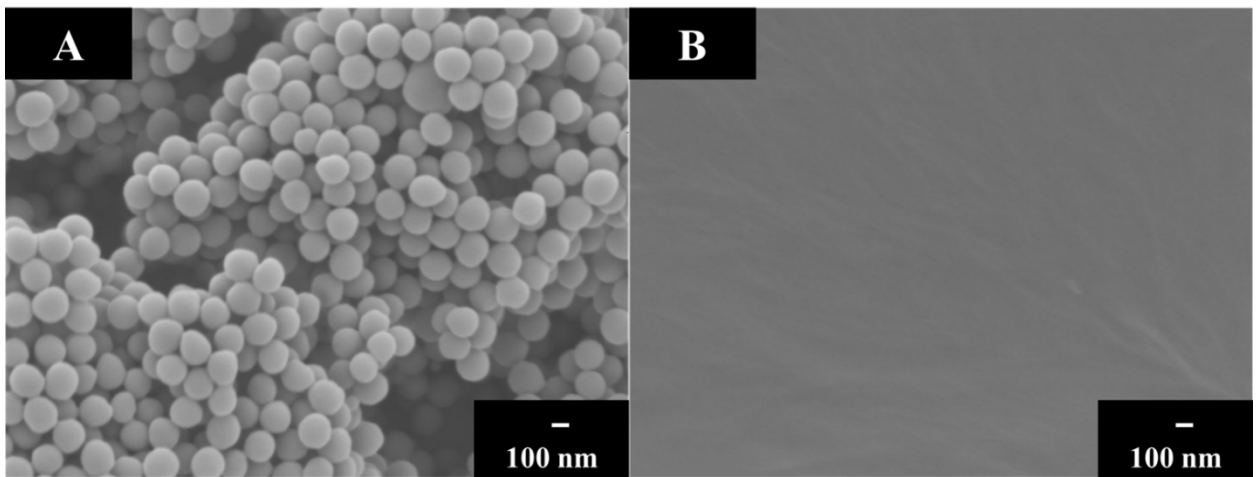


Figure 4-4 SEM images of (A) as-deposited and (B) annealed PVDF films fabricated via EPD from 5 g L⁻¹ PVDF suspension containing 1 g L⁻¹ GA as a dispersant. The films were obtained at deposition time of 5 min and deposition voltage of 100 V.

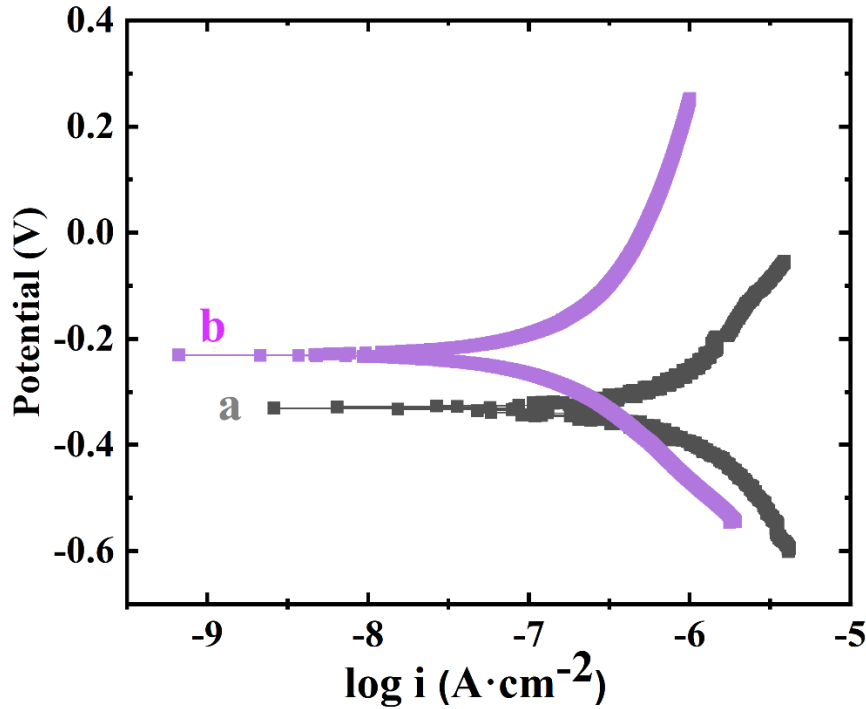


Figure 4-5 Tafel plots for (a) uncoated substrate and (b) coated from 5 g L⁻¹ PVDF suspensions containing 1 g L⁻¹ GA and annealed at 200 °C. PVDF films were obtained at deposition time of 5 min and deposition voltage of 100 V

As pointed out above, GA is an important dispersant for the EPD of oxide materials [18], which allows for catechol-type bonding to metal atoms on the particle surface. Therefore, it was hypothesized that GA can act as a co-dispersant for PVDF and silica particles. The co-EPD of PVDF and silica was performed using micron-size silica and nanosilica. Figure 4-7 shows SEM images of coatings prepared from PVDF and silica particles and dispersed using GA. The SEM images at different magnifications showed crack-free coatings containing nanosilica or micron-size silica particles. The particles were incorporated into the PVDF matrix as individual particles or agglomerates. The EPD of composite films was performed from suspensions with different concentrations of silica particles. Figure 4-8 shows films mass as a function of silica concentration in 5 g L⁻¹ PVDF suspensions, containing 1 g L⁻¹ GA. The deposition yield for suspensions,

containing micron-size silica particles increased with increasing concentrations of particles in suspension. The increase in the deposition yield indicated the increased deposition of silica and the possibility of variations in coating composition. The deposition yield for suspensions containing nanosilica increased in the concentration range of 0–4 g L⁻¹ and remained nearly constant at higher nanosilica concentrations. It is suggested that larger GA content is necessary for dispersion and deposition on nanosilica due to the larger surface area of this material. Indeed, a continuous increase in the deposition yield was observed with increasing nanosilica content in suspensions containing 5 g L⁻¹ PVDF and 2 g L⁻¹ GA (Figure 4-14). It is important to note that applications of many charging agents for EPD are limited to materials of specific types, such as metal oxides or carbon materials. The fabrication of composite coatings requires the use of advanced charging agents suitable for the charging of materials of different types. Therefore, GA is a promising charging agent for the fabrication of advanced organic–inorganic composites.

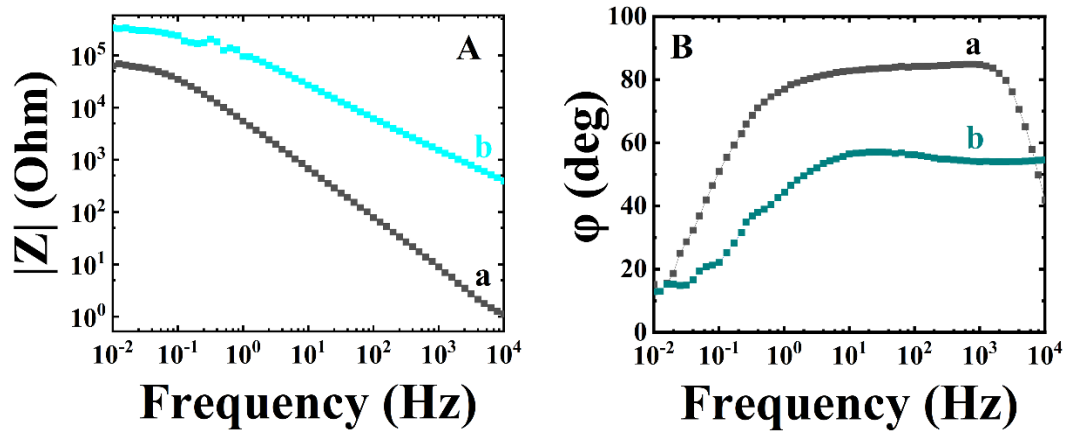


Figure 4-6 Bode plots for (a) uncoated substrate and (b) coated from 5 g L⁻¹ PVDF suspensions containing 1 g L⁻¹ GA and annealed at 200°C. PVDF films were obtained at deposition time of 5 min and deposition voltage of 100V

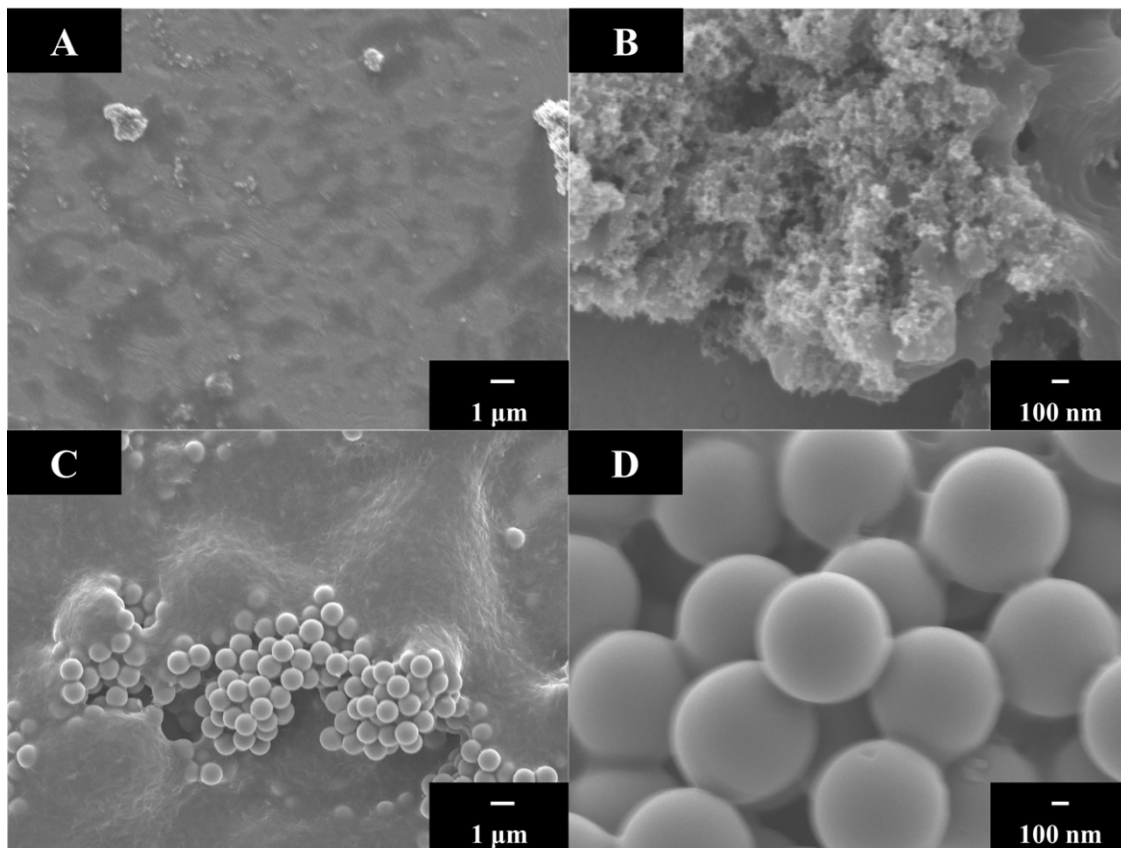


Figure 4-7 SEM images at different magnifications for coatings deposited from 5 g L^{-1} PVDF suspensions, containing 1 g L^{-1} GA and 1 g L^{-1} (A,B) nanosilica and (C,D) micron-size silica and annealed at $200 \text{ }^{\circ}\text{C}$. Deposition was performed during 5 min at a deposition voltage of 100 V.

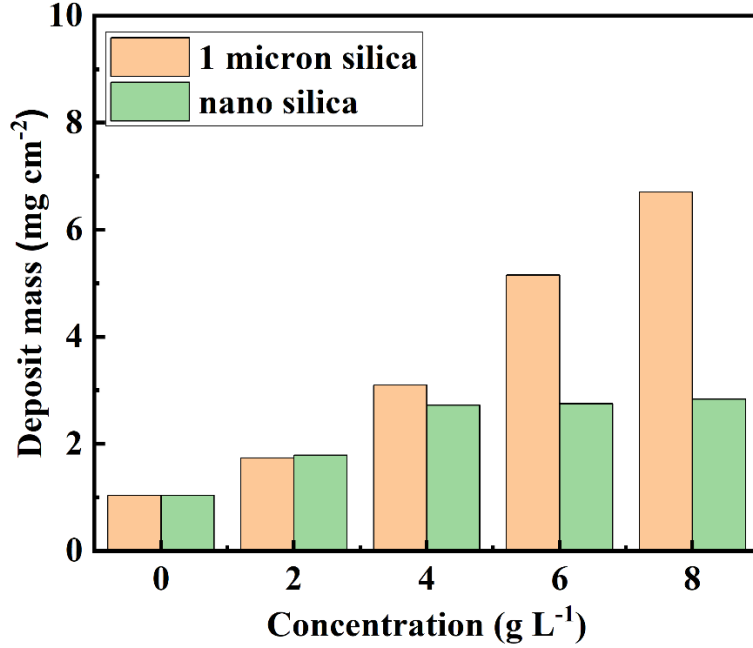


Figure 4-8 Deposit mass versus silica concentration in 5 g L⁻¹ PVDF suspension containing 1 g L⁻¹ GA. Deposition was performed during 5 min at a deposition voltage of 100 V

The co-deposition of PVDF with nanosilica and micron-size silica was also confirmed via the comparison of SEM images of annealed pure PVDF films without silica and with nanosilica or micron-size silica (Figure 4-15). EPD is a promising technique for the deposition of PVDF and composites based on the functional properties of PVDF and other functional materials. Such composites can potentially be used for applications in biomedical implants and devices. The results of this investigation pave the way for the deposition of PVDF films for applications based on the piezoelectric and ferroelectric properties of this polymer [68]. EPD is a versatile alternative for the fabrication of multifunctional composites, combining ferroelectric and magnetic properties of materials [69,70], thin film sensors [71], and energy storage devices [72].

4.5. Conclusions

GA, CFA, CA and THB showed adsorption on chemically inert, electrically neutral PVDF particles and were used as charging and dispersing agents for the EPD of PVDF coatings. The deposition yield of PVDF increased in the following order: THB < CFA < CA < GA. PVDF coatings exhibited corrosion protection properties. GA can be used as a charging dispersant for the co-deposition of PVDF with nanosilica or micron-size silica and the fabrication of composite films. The film composition can be varied by the variation of silica concentration in suspensions for EPD. The use of GA as a charging co-dispersant for materials of different types paves the way for the deposition of advanced organic–inorganic composites.

4.6. Acknowledgements

The authors acknowledge the support of the Natural Sciences and Engineering Research Council (NSERC) of Canada, the CRC program and the Canadian Centre for Electron Microscopy.

4.7. Supplementary data

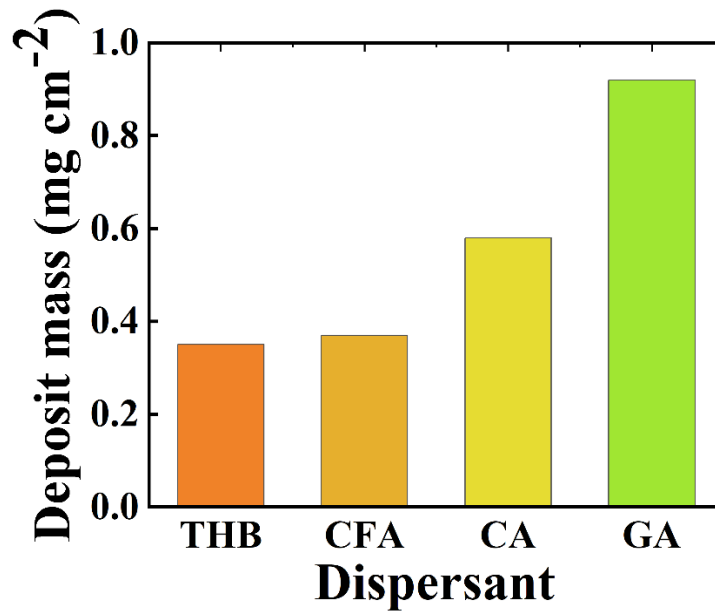


Figure 4-9 Deposit mass achieved for different dispersants using 5 g L⁻¹ PVDF suspensions containing 1 g L⁻¹ dispersants for deposition time of 5 min and deposition voltage of 50V.

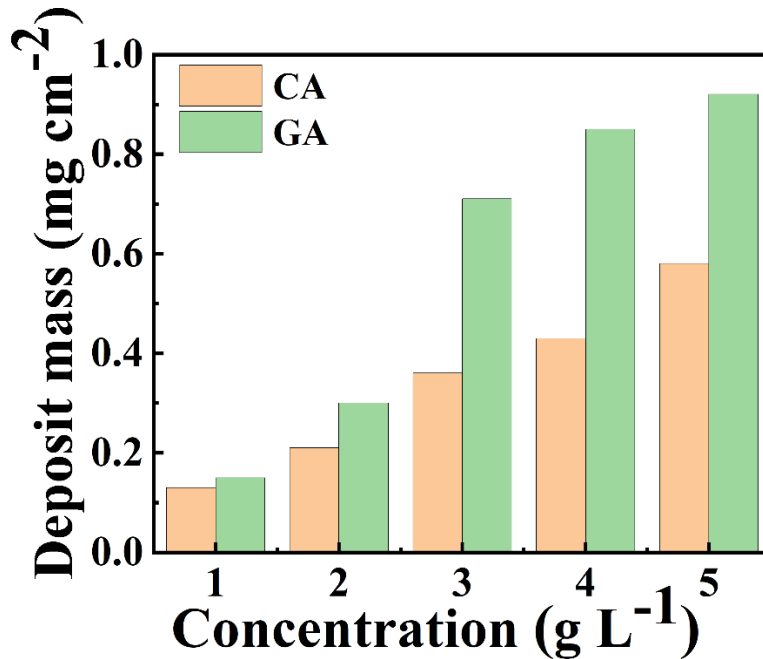


Figure 4-10 Deposit mass versus PVDF concentration in suspensions, containing 1 g L⁻¹ dispersants for deposition time of 5 min and deposition voltage of 50V.

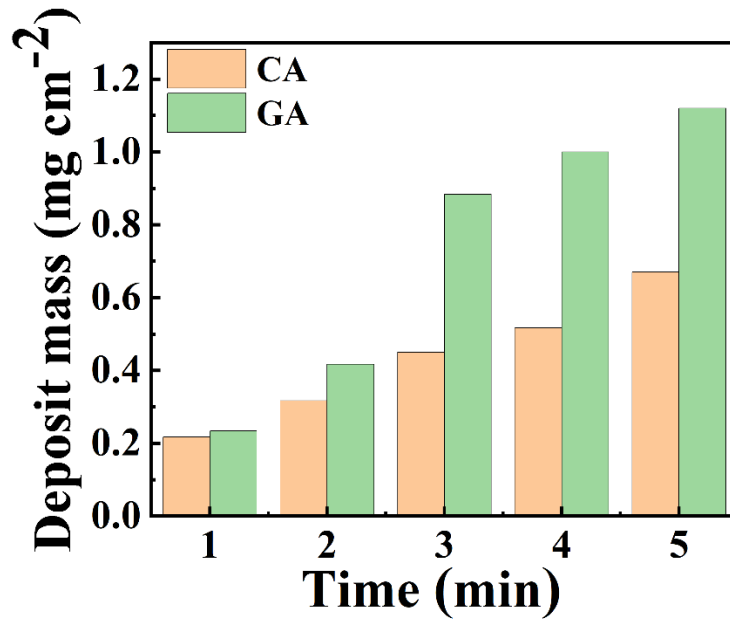


Figure 4-11 Deposit mass versus deposition time at a deposition voltage of 100 V for 5 g L⁻¹ PVDF suspensions.

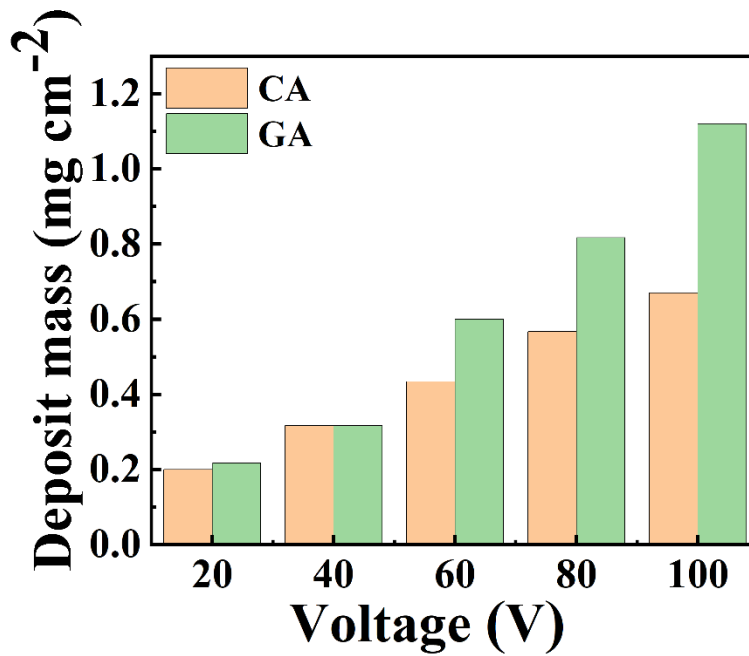


Figure 4-12 Deposit mass versus deposition voltage for 5 g L⁻¹ PVDF suspensions at deposition time of 5 min.

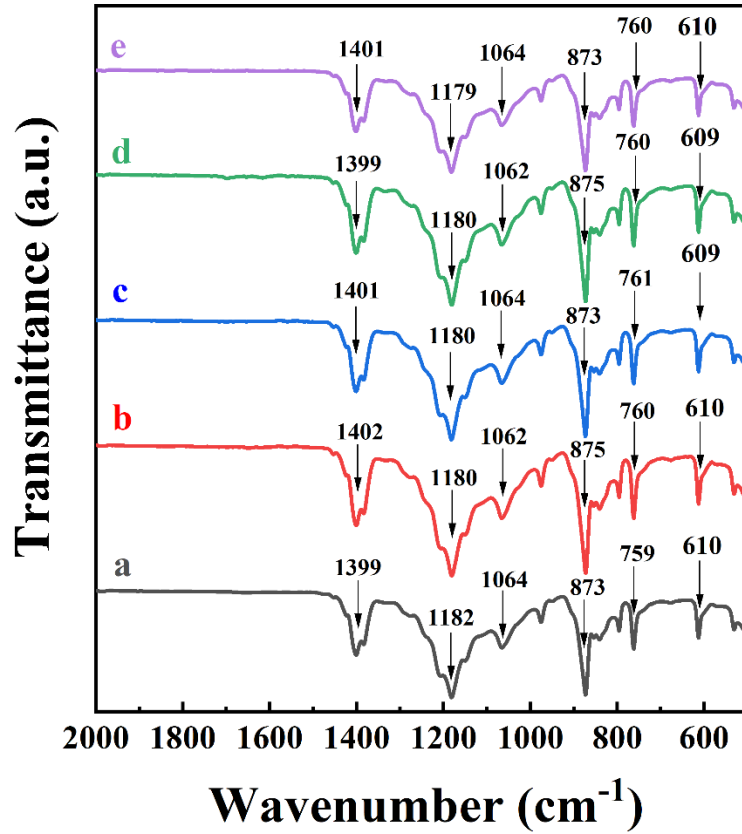


Figure 4-13 FTIR spectra of deposits, prepared from using 5 g L^{-1} PVDF suspensions containing 1 g L^{-1} dispersants: (a) THB, (b) CFA, (c) CA, (d) GA for deposition time of 5 min and deposition voltage of 100V and (e) as-received PVDF.

The spectra of deposited materials contains peaks similar to the peaks of as-received PVDF.

The strong broad absorption at 1401 cm^{-1} in the spectrum of as-received PVDF resulted from wagging of CH_2 and antisymmetric stretching of C-C bonds [1]. Other strong bands at 1179 and 873 cm^{-1} were associated with the stretching and rocking of CF_2 bonds [1, 2].

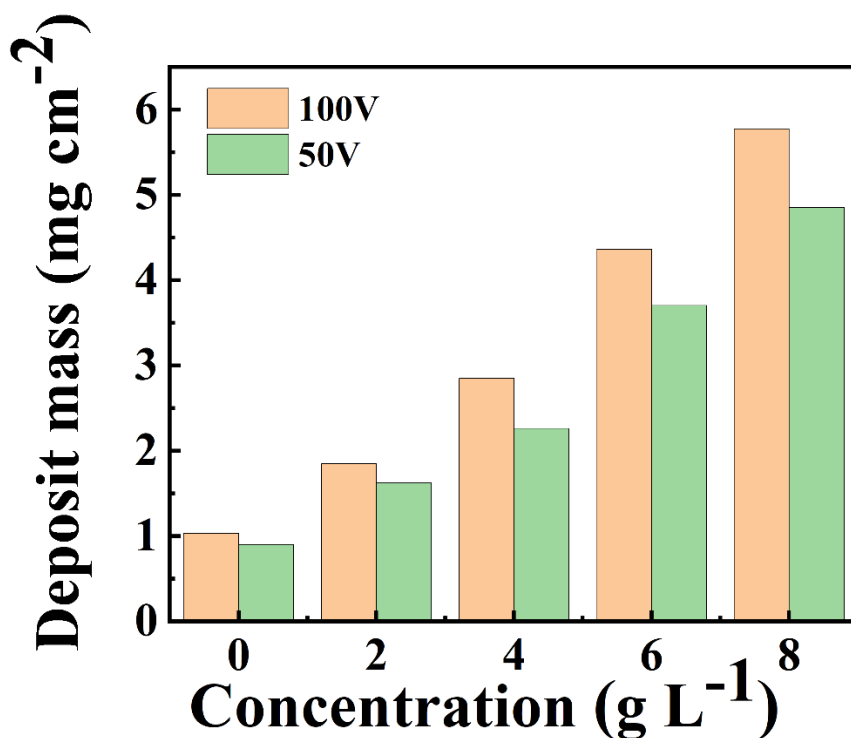


Figure 4-14 Deposit mass versus nanosilica concentration in 5 g L⁻¹ PVDF suspension containing 2 g L⁻¹ GA at deposition time of 5 min at voltages of 50 V and 100 V.

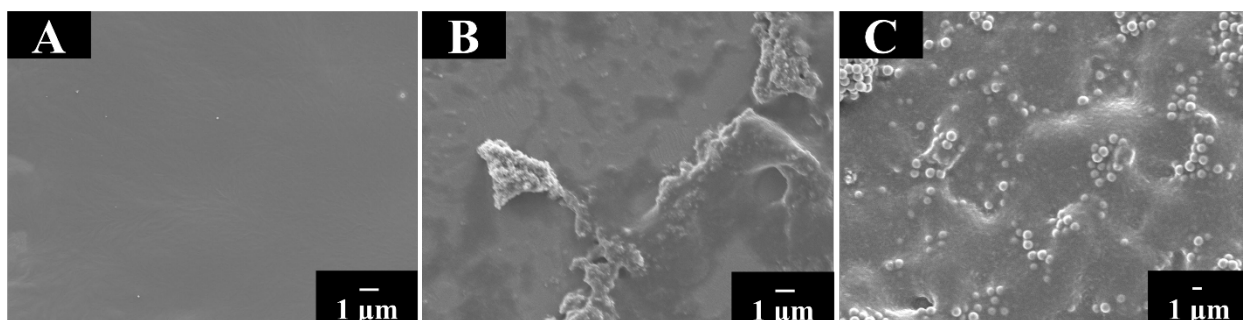


Figure 4-15 SEM images of coatings, prepared from 5 g L⁻¹ PVDF solution, containing 1 g L⁻¹ GA (A) without silica, (B) with 1 g L⁻¹ nanosilica and (C) with 1 g L⁻¹ micron size silica deposited at a deposition voltage of 100V and deposition time of 5 min and annealed at 200°C for 1 h.

1. Kobayashi, M.; Tashiro, K.; Tadokoro, H. Molecular vibrations of three crystal forms of poly (vinylidene fluoride). *Macromolecules* 1975, 8, 158-171.

2. Zeng, Z.; Yu, D.; He, Z.; Liu, J.; Xiao, F.-X.; Zhang, Y.; Wang, R.; Bhattacharyya, D.; Tan, T. T. Y. Graphene oxide quantum dots covalently functionalized PVDF membrane with significantly-enhanced bactericidal and antibiofouling performances. *Scientific reports* 2016, 6, 1-11.

4.8. References

1. Mishyn, V.; Aspermair, P.; Leroux, Y.; Happy, H.; Knoll, W.; Boukherroub, R.; Szunerits, S. “Click” Chemistry on Gold Electrodes Modified with Reduced Graphene Oxide by Electrophoretic Deposition. *Surfaces* 2019, 2, 193–204.
2. Besra, L.; Liu, M. A review on fundamentals and applications of electrophoretic deposition (EPD). *Prog. Mater. Sci.* 2007, 52, 1–61.
3. Van der Biest, O.O.; Vandeperre, L.J. Electrophoretic deposition of materials. *Annu. Rev. Mater. Sci.* 1999, 29, 327–352.
4. Batool, S.A.; Wadood, A.; Hussain, S.W.; Yasir, M.; Ur Rehman, M.A. A Brief Insight to the Electrophoretic Deposition of PEEK-, Chitosan-, Gelatin-, and Zein-Based Composite Coatings for Biomedical Applications: Recent Developments and Challenges. *Surfaces* 2021, 4, 205–239.
5. Ahmed, Y.; Yasir, M.; Ur Rehman, M.A. Fabrication and Characterization of Zein/Hydroxyapatite Composite Coatings for Biomedical Applications. *Surfaces* 2020, 3, 237–250.
6. Sorkhi, L.; Farrokhi-Rad, M.; Shahrabi, T. Electrophoretic Deposition of Hydroxyapatite–Chitosan–Titania on Stainless Steel 316 L. *Surfaces* 2019, 2, 458–467.

7. Sikkema, R.; Baker, K.; Zhitomirsky, I. Electrophoretic deposition of polymers and proteins for biomedical applications. *Adv. Colloid Interface Sci.* 2020, 284, 102272.
8. Chen, Y.; Ye, R.; Wang, J. Effect of voltage on the mechanical and water resistance properties of zein films by electrophoretic deposition. *Food Bioprocess Technol.* 2015, 8, 486–491.
9. Choudhary, B.; Anwar, S.; Besra, L.; Anwar, S. Electrophoretic deposition studies of Ba (Zr-Ce-Y) O₃ ceramic coating. *Int. J. Appl. Ceram. Technol.* 2019, 16, 1022–1031.
10. Dhand, C.; Singh, S.; Arya, S.K.; Datta, M.; Malhotra, B. Cholesterol biosensor based on electrophoretically deposited conducting polymer film derived from nanostructured polyaniline colloidal suspension. *Anal. Chim. Acta* 2007, 602, 244–251.
11. Dange-Delbaere, C.; Buron, C.; Euvrard, M.; Filiâtre, C. Stability and cathodic electrophoretic deposition of polystyrene particles pre-coated with chitosan–alginate multilayer. *Colloids Surf. A Physicochem. Eng. Asp.* 2016, 493, 1–8.
12. Biesheuvel, P.M.; Verweij, H. Theory of cast formation in electrophoretic deposition. *J. Am. Ceram. Soc.* 1999, 82, 1451–1455.
13. De Riccardis, M.F.; Martina, V.; Carbone, D. Study of polymer particles suspensions for electrophoretic deposition. *J. Phys. Chem. B* 2013, 117, 1592–1599.
14. Djošić, M.; Mišković-Stanković, V.B.; Kačarević-Popović, Z.M.; Jokić, B.M.; Bibić, N.; Mitrić, M.; Milonjić, S.K.; Jančić-Heinemann, R.; Stojanović, J. Electrochemical synthesis of nanosized monetite powder and its electrophoretic deposition on titanium. *Colloids Surf. A Physicochem. Eng. Asp.* 2009, 341, 110–117.

15. Zhitomirsky, I.; Petric, A. Electrochemical deposition of yttrium oxide. *J. Mater. Chem.* 2000, 10, 1215–1218.
16. Pang, X.; Zhitomirsky, I.; Niewczas, M. Cathodic electrolytic deposition of zirconia films. *Surf. Coat. Technol.* 2005, 195, 138–146.
17. Ruwoldt, J. A Critical Review of the Physicochemical Properties of Lignosulfonates: Chemical Structure and Behavior in Aqueous Solution, at Surfaces and Interfaces. *Surfaces* 2020, 3, 622–648.
18. Ata, M.; Liu, Y.; Zhitomirsky, I. A review of new methods of surface chemical modification, dispersion and electrophoretic deposition of metal oxide particles. *RSC Adv.* 2014, 4, 22716–22732.
19. Ata, M.S.; Poon, R.; Syed, A.M.; Milne, J.; Zhitomirsky, I. New developments in non-covalent surface modification, dispersion and electrophoretic deposition of carbon nanotubes. *Carbon* 2018, 130, 584–598.
20. Biswas, M.; Raichur, A.M. Electrokinetic and rheological properties of nano zirconia in the presence of rhamnolipid biosurfactant. *J. Am. Ceram. Soc.* 2008, 91, 3197–3201.
21. Alves, A.V.; Tsianou, M.; Alexandridis, P. Fluorinated Surfactant Adsorption on Mineral Surfaces: Implications for PFAS Fate and Transport in the Environment. *Surfaces* 2020, 3, 516–566.
22. Nawwar, M.; Poon, R.; Chen, R.; Sahu, R.P.; Puri, I.K.; Zhitomirsky, I. High areal capacitance of Fe₃O₄-decorated carbon nanotubes for supercapacitor electrodes. *Carbon Energy* 2019, 1, 124–133.

23. Su, Y.; Zhitomirsky, I. Electrophoretic deposition of graphene, carbon nanotubes and composite films using methyl violet dye as a dispersing agent. *Colloids Surf. A Physicochem. Eng. Asp.* 2013, 436, 97–103.
24. Li, J.; Zhitomirsky, I. Cathodic electrophoretic deposition of manganese dioxide films. *Colloids Surf. A Physicochem. Eng. Asp.* 2009, 348, 248–253.
25. Ghazali, N.; Basirun, W.J.; Mohammed Nor, A.; Johan, M.R. Super-amphiphobic coating system incorporating functionalized nano-Al₂O₃ in polyvinylidene fluoride (PVDF) with enhanced corrosion resistance. *Coatings* 2020, 10, 387.
26. Pornea, A.M.; Puguan, J.M.C.; Deonikar, V.G.; Kim, H. Fabrication of multifunctional wax infused porous PVDF film with switchable temperature response surface and anti corrosion property. *J. Ind. Eng. Chem.* 2020, 82, 211–219.
27. Kim, Y.H.; Kwon, Y.S.; Shon, M.Y.; Moon, M.J. Corrosion protection performance of PVDF/PMMA-blended coatings by electrochemical impedance method. *J. Electrochem. Sci. Technol.* 2018, 9, 1–8.
28. Ribeiro, C.; Costa, C.M.; Correia, D.M.; Nunes-Pereira, J.; Oliveira, J.; Martins, P.; Goncalves, R.; Cardoso, V.F.; Lanceros-Mendez, S. Electroactive poly (vinylidene fluoride)-based structures for advanced applications. *Nat. Protoc.* 2018, 13, 681.
29. Ji-Hun, B.; Seung-Hwan, C. PVDF-based ferroelectric polymers and dielectric elastomers for sensor and actuator applications: A review. *Funct. Compos. Struct.* 2019, 1, 012003.
30. Inderherbergh, J. Polyvinylidene fluoride (PVDF) appearance, general properties and processing. *Ferroelectrics* 1991, 115, 295–302.

31. Zhong, J.; Li, W.; Qian, J.; Fu, C.; Chu, H.; Xu, J.; Ran, X.; Nie, W. Modulation of the interfacial architecture enhancing the efficiency and energy density of ferroelectric nanocomposites via the irradiation method. *J. Colloid Interface Sci.* 2021, 586, 30–38.
32. Gupta, S.K.; Hernandez, C.; Zuniga, J.P.; Lozano, K.; Mao, Y. Luminescent PVDF nanocomposite films and fibers encapsulated with $\text{La}_2\text{Hf}_2\text{O}_7$: Eu^{3+} nanoparticles. *SN Appl. Sci.* 2020, 2, 1–11.
33. Wang, Y.; Zhu, X.; Zhang, T.; Bano, S.; Pan, H.; Qi, L.; Zhang, Z.; Yuan, Y. A renewable low-frequency acoustic energy harvesting noise barrier for high-speed railways using a Helmholtz resonator and a PVDF film. *Appl. Energy* 2018, 230, 52–61.
34. Hu, P.; Yan, L.; Zhao, C.; Zhang, Y.; Niu, J. Double-layer structured PVDF nanocomposite film designed for flexible nanogenerator exhibiting enhanced piezoelectric output and mechanical property. *Compos. Sci. Technol.* 2018, 168, 327–335.
35. Park, J.H.; Kurra, N.; AlMadhoun, M.; Odeh, I.N.; Alshareef, H.N. A two-step annealing process for enhancing the ferroelectric properties of poly (vinylidene fluoride)(PVDF) devices. *J. Mater. Chem. C* 2015, 3, 2366–2370.
36. Foster, F.S.; Harasiewicz, K.A.; Sherar, M.D. A history of medical and biological imaging with polyvinylidene fluoride (PVDF) transducers. *IEEE Trans. Ultrason. Ferroelectr. Freq. Control* 2000, 47, 1363–1371.
37. Kang, G.-d.; Cao, Y.-m. Application and modification of poly (vinylidene fluoride)(PVDF) membranes—A review. *J. Membr. Sci.* 2014, 463, 145–165.

38. Barbosa, J.C.; Correia, D.M.; Gonçalves, R.; de Zea Bermudez, V.; Silva, M.M.; Lanceros-Mendez, S.; Costa, C.M. Enhanced ionic conductivity in poly(vinylidene fluoride) electrospun separator membranes blended with different ionic liquids for lithium ion batteries. *J. Colloid Interface Sci.* 2021, 582, 376–386.
39. Cui, Y.; Yang, L.; Zheng, J.; Wang, Z.; Li, B.; Yan, Y.; Meng, M. Synergistic interaction of Z-scheme 2D/3D g-C₃N₄/BiOI heterojunction and porous PVDF membrane for greatly improving the photodegradation efficiency of tetracycline. *J. Colloid Interface Sci.* 2021, 586, 335–348.
40. Wei, N.; Li, Z.; Li, Q.; Yang, E.; Xu, R.; Song, X.; Sun, J.; Dou, C.; Tian, J.; Cui, H. Scalable and low-cost fabrication of hydrophobic PVDF/WS₂ porous membrane for highly efficient solar steam generation. *J. Colloid Interface Sci.* 2021, 588, 369–377.
41. Zhao, B.; Hu, J.; Ren, W.; Xu, F.; Wu, X.; Shi, P.; Ye, Z.-G. A new biosensor based on PVDF film for detection of nucleic acids. *Ceram. Int.* 2015, 41, S602–S606.
42. Song, Y.-S.; Yun, Y.; Lee, D.Y.; Kim, B.-Y. Effect of PVDF Concentration and Number of Fiber Lines on Piezoelectric Properties of Polymeric PVDF Biosensors. *Fibers Polym.* 2021, 22, 1200–1207.
43. Hartono, A.; Sanjaya, E.; Ramli, R. Glucose sensing using capacitive biosensor based on polyvinylidene fluoride thin film. *Biosensors* 2018, 8, 12.
44. Häslér, E.; Stein, L.; Harbauer, G. Implantable physiological power supply with PVDF film. *Ferroelectrics* 1984, 60, 277–282.

45. Yu, Y.; Sun, H.; Orbay, H.; Chen, F.; England, C.G.; Cai, W.; Wang, X. Biocompatibility and in vivo operation of implantable mesoporous PVDF-based nanogenerators. *Nano Energy* 2016, 27, 275–281.
46. Lu, L.; Ding, W.; Liu, J.; Yang, B. Flexible PVDF based piezoelectric nanogenerators. *Nano Energy* 2020, 78, 105251.
47. Houis, S.; Engelhardt, E.; Wurm, F.; Gries, T. Application of polyvinylidene fluoride (PVDF) as a biomaterial in medical textiles. In *Medical and Healthcare Textiles*; Elsevier: Amsterdam, The Netherlands, 2010; pp. 342–352.
48. Wang, H.; Klosterhalfen, B.; Müllen, A.; Otto, T.; Dievernich, A.; Jockenhövel, S. Degradation resistance of PVDF mesh in vivo in comparison to PP mesh. *J. Mech. Behav. Biomed. Mater.* 2021, 119, 104490.
49. Haddadi, S.A.; Ghaderi, S.; Amini, M.; Ramazani, S.A. Mechanical and piezoelectric characterizations of electrospun PVDF-nanosilica fibrous scaffolds for biomedical applications. *Mater. Today Proc.* 2018, 5, 15710–15716.
50. Kyeremateng, N.A.; Gukte, D.; Ferch, M.; Buk, J.; Hrebicek, T.; Hahn, R. Preparation of a Self-Supported SiO₂ Membrane as a Separator for Lithium-Ion Batteries. *Batter. Supercaps* 2020, 3, 456–462.
51. Prasanna, K.; Subburaj, T.; Jo, Y.N.; Lee, C.W. Optimization of electrophoretic suspension to fabricate Li[Ni_{1/3}Co_{1/3}Mn_{1/3}]O₂ based positive electrode for Li-ion batteries. *Electrochim. Acta* 2013, 95, 295–300.
52. Hagberg, J.; Maples, H.A.; Alvim, K.S.; Xu, J.; Johannisson, W.; Bismarck, A.; Zenkert, D.; Lindbergh, G. Lithium iron phosphate coated carbon fiber electrodes for structural lithium ion batteries. *Compos. Sci. Technol.* 2018, 162, 235–243.

53. Ui, K.; OKURA, K.; Koura, N.; Tsumeda, S.; Tamamitsu, K. Fabrication of the electrode for capacitor cell prepared by the electrophoretic deposition method. *Electrochemistry* 2007, 75, 604–606.
54. Lau, K.T.; Suan, M.S.M.; Zaimi, M.; Abd Razak, J.; Azam, M.; Mohamad, N. Microstructure and Phase of Poly (Vinylidene Fluoride) Films by Electrophoretic Deposition: Effect of Polymer Dispersion's Stirring Conditions. *J. Adv. Manuf. Technol. (JAMT)* 2016, 10, 57–66.
55. Lau, K.T.; Ab Razak, M.H.R.; Kok, S.L.; Zaimi, M.; Abd Rashid, M.W.; Mohamad, N.; Azam, M.A. Electrophoretic Deposition and Heat Treatment of Steel-Supported PVDF-Graphite Composite Film. In *Applied Mechanics and Materials*; Trans Tech Publications: Zurich, Switzerland, 2015; pp. 412–416.
56. Yin, J.; Fukui, T.; Murata, K.; Matsuda, M.; Miyake, M.; Hirabayashi, T.; Yamamuro, S. Fabrication of protective KB/PVdF composite films on stainless steel substrates for PEFCs through electrophoretic deposition. *J. Ceram. Soc. Jpn.* 2008, 116, 201–204.
57. Zhao, Q.; Veldhuis, S.; Mathews, R.; Zhitomirsky, I. Influence of chemical structure of bile acid dispersants on electrophoretic deposition of poly (vinylidene fluoride) and composites. *Colloids Surf. A Physicochem. Eng. Asp.* 2021, 627, 127181.
58. Hashiba, M.; Okamoto, H.; Nurishi, Y.; Hiramatsu, K. The zeta-potential measurement for concentrated aqueous suspension by improved electrophoretic mass transport apparatus—application to Al₂O₃, ZrO₃ and SiC suspensions. *J. Mater. Sci.* 1988, 23, 2893–2896.

59. Lee, B.P.; Messersmith, P.B.; Israelachvili, J.N.; Waite, J.H. Mussel-inspired adhesives and coatings. *Annu. Rev. Mater. Res.* 2011, 41, 99–132.
60. Lee, H.; Lee, B.P.; Messersmith, P.B. A reversible wet/dry adhesive inspired by mussels and geckos. *Nature* 2007, 448, 338–341
61. Xu, N.; Li, Y.; Zheng, T.; Xiao, L.; Liu, Y.; Chen, S.; Zhang, D. A mussel-inspired strategy for CNT/carbon fiber reinforced epoxy composite by hierarchical surface modification. *Colloids Surf. A Physicochem. Eng. Asp.* 2022, 635, 128085.
62. Sun, Y.; Ata, M.; Zhitomirsky, I. Electrophoretic deposition of TiO₂ nanoparticles using organic dyes. *J. Colloid Interface Sci.* 2012, 369, 395–401.
63. Sun, Y.; Zhitomirsky, I. Electrophoretic deposition of titanium dioxide using organic acids as charging additives. *Mater. Lett.* 2012, 73, 190–193.
64. Sun, Y.; Wang, Y.; Zhitomirsky, I. Dispersing agents for electrophoretic deposition of TiO₂ and TiO₂–carbon nanotube composites. *Colloids Surf. A Physicochem. Eng. Asp.* 2013, 418, 131–138.
65. Ata, M.; Zhitomirsky, I. Preparation of MnO₂ and composites for ultracapacitors. *Mater. Manuf. Processes* 2013, 28, 1014–1018
66. Wu, K.; Wang, Y.; Zhitomirsky, I. Electrophoretic deposition of TiO₂ and composite TiO₂–MnO₂ films using benzoic acid and phenolic molecules as charging additives. *J. Colloid Interface Sci.* 2010, 352, 371–378.
67. Wang, Y.; Zhitomirsky, I. Bio-inspired catechol chemistry for electrophoretic nanotechnology of oxide films. *J. Colloid Interface Sci.* 2012, 380, 8–15

68. Sharma, T.; Je, S.-S.; Gill, B.; Zhang, J.X. Patterning piezoelectric thin film PVDF–TrFE based pressure sensor for catheter application. *Sens. Actuators A Phys.* 2012, 177, 87–92.
69. Bhatt, A.S.; Bhat, D.K.; Santosh, M. Crystallinity, conductivity, and magnetic properties of PVDF-Fe₃O₄ composite films. *J. Appl. Polym. Sci.* 2011, 119, 968–972.
70. Venevtsev, Y.N.; Gagulin, V.V.; Zhitomirsky, I.D. Material science aspects of seignette-magnetism problem. *Ferroelectrics* 1987, 73, 221–248.
71. Luo, H.; Hanagud, S. PVDF film sensor and its applications in damage detection. *J. Aerosp. Eng.* 1999, 12, 23–30.
72. Li, W.; Song, Z.; Zhong, J.; Qian, J.; Tan, Z.; Wu, X.; Chu, H.; Nie, W.; Ran, X. Multilayer-structured transparent MXene/PVDF film with excellent dielectric and energy storage performance. *J. Mater. Chem. C* 2019, 7, 10371–10378.
73. Kobayashi, M.; Tashiro, K.; Tadokoro, H. Molecular vibrations of three crystal forms of poly (vinylidene fluoride). *Macromolecules* 1975, 8, 158–171.
74. Zeng, Z.; Yu, D.; He, Z.; Liu, J.; Xiao, F.-X.; Zhang, Y.; Wang, R.; Bhattacharyya, D.; Tan, T.T.Y. Graphene oxide quantum dots covalently functionalized PVDF membrane with significantly-enhanced bactericidal and antibiofouling performances. *Sci. Rep.* 2016, 6, 20142.

Chapter 5 Surfactant assisted dip-coating method for deposition of polyethylmethacrylate-diamond coatings

5.1. Abstract

This investigation is motivated by increasing interest in polymer-diamond coatings for biomedical applications in implants and sensors. A conceptually new strategy is based on the feasibility of solubilisation of polyethyl methacrylate (PEMA) in isopropanol using 18 β -glycyrrhetic acid (GRA) and rhamnolipids (RLP) as solubilising agents. This approach offers benefits for biomedical applications by avoiding the use of traditional toxic solvents for PEMA dissolution. The ability to obtain concentrated solutions of high molecular mass polymer is a crucial factor for the development of a dip coating method. Potentiodynamic and impedance spectroscopy studies indicate that PEMA films provide corrosion protection of stainless steel in 3% NaCl solutions. The use of GRA facilitates the fabrication of films with improved protective properties. PEMA films are obtained as monolayers or multilayers of controlled film mass. Another important finding is a good dispersion of chemically inert microdiamond and nanodiamond particles using GRA and RLP. For the first time composite PEMA-diamond films are obtained using GRA and RLP as solubilising agents for PEMA and dispersing agents for diamonds in isopropanol solvent. The detailed analysis of film microstructures provides an insight into the influence of chemical structure of GRA and RLP on their interactions with PEMA and diamonds. Moreover, microstructure analysis indicates that such interactions are important for preventing defects in the composite films. The benefits of steroid-like dispersants are discussed. Composite films are obtained as monolayers with different diamond content or PEMA-diamond multilayers of different composition and film mass. The method represents a versatile strategy for the

fabrication of alternating PEMA/PEMA-diamond multilayers. The benefits of the obtained microstructures for biomedical applications are discussed. The approach developed in this investigation opens an avenue for the fabrication of other polymer coatings containing various functional materials.

5.2.Introduction

Diamond has been widely used for advanced composite films and coatings because it possesses high hardness, low coefficient of friction, high wear resistance and biocompatibility [1]. Of particular interest are biomedical applications of polymer-diamond coatings. It has been stated that diamond-like carbon (DLC), coated with polymer can be used in biomedical devices for controlled drug release and enhanced of cell proliferation [2]. Nanostructured Nafion-coated boron-doped diamond coating reduced the biofouling effect and were used for the fabrication of dopamine sensors [3]. DLC thin film could improve the chemical resistance of polymer-based composites in alkaline environments [4]. Diamond and composite films are currently under intensive investigations for surface modification of biomedical implants. Significant interest has been generated in the development of coating techniques for the deposition of multilayer and functionally graded coatings with advanced functionality. Orthopaedic load-bearing surfaces covered with diamond-like carbon (DLC) were created and tested [5]. They were made up of three layers with different functionalities of the individual layers. Low-temperature magnetron sputtering on steel substrates was used for the manufacturing procedure [5]. A multilayer approach has been developed for enhancing the erosive wear resistance of diamond coatings [6]. It was found that multilayer strategies facilitated the fabrication of advanced diamond coatings on relatively soft substrates, such as steels [7]. Multilayer diamond coatings for biomedical applications were deposited on Ti6Al-4V alloy surfaces using microwave plasma chemical vapour

deposition [8] and such coatings showed enhanced adhesion and toughness. Many investigations focused on the development of deposition techniques for the fabrication of multilayer diamond polymer coatings with enhanced mechanical properties and improved adhesion [9–11]. Electrodeposition of DLC was performed on TiAlV alloy substrates at room temperature aiming to increase the wear resistance and corrosion resistance [12]. Advanced techniques are currently under development for deposition of DLC on implants [13]. New coating techniques are of particular interest for prevention of knee and hip implants failure due to mechanical stress and corrosion [14]. Diamond coatings allowed reduced levels of acute, chronic inflammatory, and foreign-body reactions, showing that diamonds are well tolerated in vivo [15]. Diamond is a promising inorganic material for the fabrication of biomedical implants and sensors, bioimaging, gene therapy and drug delivery applications [16,17]. Diamond-polymer coatings combined advanced properties of diamonds and polymers [3]. Polyethyl methacrylate (PEMA) is an advanced polymer that exhibits mechanical strength, thermal stability, biocompatibility, and chemical stability. PEMA has attracted interest for a variety of applications, including the repair of bone and cartilage, polymer electrolytes and membranes for energy generation and storage devices, biodegradable antimicrobial packaging materials, optical and electronic components, and corrosion protection coatings [18]. PEMA is a desirable material for bone cements since it has been demonstrated to improve osteoblast adhesion and proliferation while simultaneously offering excellent mechanical properties. In vivo bone healing and cell attachment are made easier by this polymer's water absorption characteristics. PEMA based shape memory materials show promise for use in medical equipment. Foamed PEMA and PEMA mixtures have a specific surface chemistry that supports cell adhesion, differentiation, and development, causing thick cartilaginous tissue to fill the pores. PEMA gels, cements, and films are suitable for dental applications,

craniofacial implants, and a range of other orthopaedic uses due to these characteristics [19]. However, PEMA is soluble in extremely harmful and carcinogenic solvents including benzene, toluene, and methyl ethyl ketone. This is a significant barrier to PEMA's use in the biomedical industry, because such solvent molecules remain in the bulk or on the surface of PEMA even after drying. Another challenge is related to dispersion of diamonds in solvents and in PEMA coatings. The goal of this investigation was the fabrication of PEMA-diamond coatings by a dip-coating method using isopropanol solvent. Isopropanol offers benefits of lower cytotoxicity compared to other organic solvents [20–24]. It is widely used for many biomedical fabrication applications, such as deposition of films for drug delivery [25], surface modification of implants with bioceramics, polymers and proteins [26,27], protein purification and extraction [28], manufacturing of fibrous implants [29], and biomedical scaffolds [30]. However, PEMA is insoluble in isopropanol. An important finding of this study was the solubilisation of PEMA in isopropanol in the presence of biosurfactants, such as 18β -glycyrrhetic acid (GRA) and rhamnolipids (RLP). The fabrication of concentrated high molecular mass PEMA solutions was one of the key factors for successful fabrication of PEMA coatings. Obtained coatings provided corrosion protection of stainless steel. Another important finding was the dispersibility of microdiamond and nanodiamond particles in isopropanol in the presence of GRA and RLP. It was found that the use of the biosurfactants as solubilising agents for PEMA and dispersing agents for diamond opened a versatile strategy for the fabrication of composite PEMA-diamond films. The analysis of coating microstructure provided an insight into the influence of the biosurfactants and diamond concentration on coating composition and morphology. This investigation opened a new avenue for the fabrication of composite coatings by a dip coating method.

5.3. Experimental

High molecular mass poly(ethyl methacrylate) (PEMA, $M_w = 515,000$), rhamnolipids (RLP), 18 β -glycyrrhetic acid (GRA), isopropanol, microdiamond (size < 1), nanodiamond (size < 10 nm) were received from the MilliporeSigma company. Stainless steel foils (304 type, 50 × 25 × 0.1 mm) were used as substrates for coating deposition. RLP and GRA were dissolved in isopropanol at a concentration of 2 g L⁻¹. Following this, PEMA was added at a concentration of 10 g L⁻¹ to both the RLP and GRA solutions. Upon heating to 55°C, the PEMA suspensions, containing dissolved RLP or GRA, turned from an opaque cloudy white to clear and transparent solutions which were cooled to room temperature and used for dip-coating. Microdiamond or nanodiamond particles were added at concentrations of 1–3 g L⁻¹ to the 10 g L⁻¹ PEMA solutions and obtained suspensions were ultrasonicated for 30 min prior to the deposition of composite films. The substrates were dipped in solutions or suspensions for 20 s. A JEOL SEM (scanning electron microscope, JSM7000F) was used for the analysis of coating microstructure. A Bruker Smart 6000 X-ray diffractometer (XRD, CuK α radiation) was utilised for the analysis of coating composition. Electrochemical characterisation was performed using a PARSTAT 2273 (Ametek) potentiostat-impedance analyzer. Testing was carried out in 30 g L⁻¹ NaCl solution in water using a corrosion cell, containing a working electrode (coated or uncoated stainless steel), counter-electrode (Pt mesh) and a reference electrode (SCE, saturated calomel electrode). The results of potentiodynamic studies (1 mV s⁻¹ rate) were presented in Tafel plots. Electrochemical impedance spectroscopy (EIS) data was obtained in the frequency range of 0.01 Hz–10 kHz and voltage amplitude of 5 mV.

5.4. Results and Discussion

Isopropanol is known as a non-solvent for PEMA. The problem of insolubility of PEMA in isopropanol is aggravated due to specific requirements for the dip coating method. The deposition of PEMA films by a dip coating method requires the use of high molecular mass PEMA in solutions of high concentrations. It is in this regard that low molecular mass polymers exhibit poor binding and film forming properties. The increase in the molecular mass of polymer molecules results in decreasing their solubility in solvents due to enhanced polymer-polymer interactions. In this investigation, a new approach has been developed, which allowed for the solubilisation of PEMA in isopropanol. This approach allowed the solubilisation of high molecular mass PEMA ($M_w = 515,000$) and formation of relatively concentrated stable solutions with concentration of 10 g L^{-1} . The use of such solutions was a key factor for successful deposition of PEMA on stainless steel (304 type) substrates. The approach developed in this investigation is based on the use of biosurfactants, such as RLP and GRA. Biosurfactants are especially important for colloidal processing of materials because they are biocompatible and safe to environment [31]. Figure 5-1A, B shows chemical structures of the biosurfactants. As-received RLP was a mixture of mono- and diRLP, which are amphiphilic glycolipids, produced by *Pseudomonas* [31]. The RLP structure contains fatty acid and rhamnose groups. The amphiphilic structure of RLP and their anionic carboxylic groups are important structure factors governing performance of RLP as biosurfactants. The strong dispersion and solubilisation power of RLP is related to their very low critical micelle concentration, which is 10–100 times lower than that of traditional chemical surfactants [31]. RLP can solubilise highly hydrophobic organic molecules in aqueous solutions [32]. RLP are very important biosurfactants for colloidal biotechnology due to their antimicrobial and anticancer properties [33,34]. GRA is another natural surfactant. It is produced from licorice,

which is the most common herb in Chinese medicine [35]. GRA structure contains five rings and an anionic carboxylic group. GRA and its derivatives show remarkable biological properties, including antitumour, antioxidant, antimicrobial, anti-inflammatory, antiviral, antiulcer, antidiabetic, and other valuable properties [35]. The chemical structure of GRA facilitates its binding to different organic molecules and adsorption on different surfaces [36]. The negative charge of the carboxylic acid group of adsorbed GRA is beneficial for dispersion of different materials. GRA and RLP interactions with PEMA in ethanol allowed solubilisation of PEMA in isopropanol and fabrication of PEMA films by a dip coating method. Moreover, using GRA and RLP we addressed challenges in dispersing of chemically inert diamond particles. The diamond suspensions in ethanol were unstable and showed rapid precipitation (Figure 5-1C). It was found that addition of GRA and RLP to diamond facilitated the formation stable suspensions (Figure 5-1C). The formation of stable suspensions is critically important for colloidal processing of materials [37–40]. The use of GRA and RLP for solubilisation of PEMA and diamond dispersion paved a way for the fabrication of composite films.

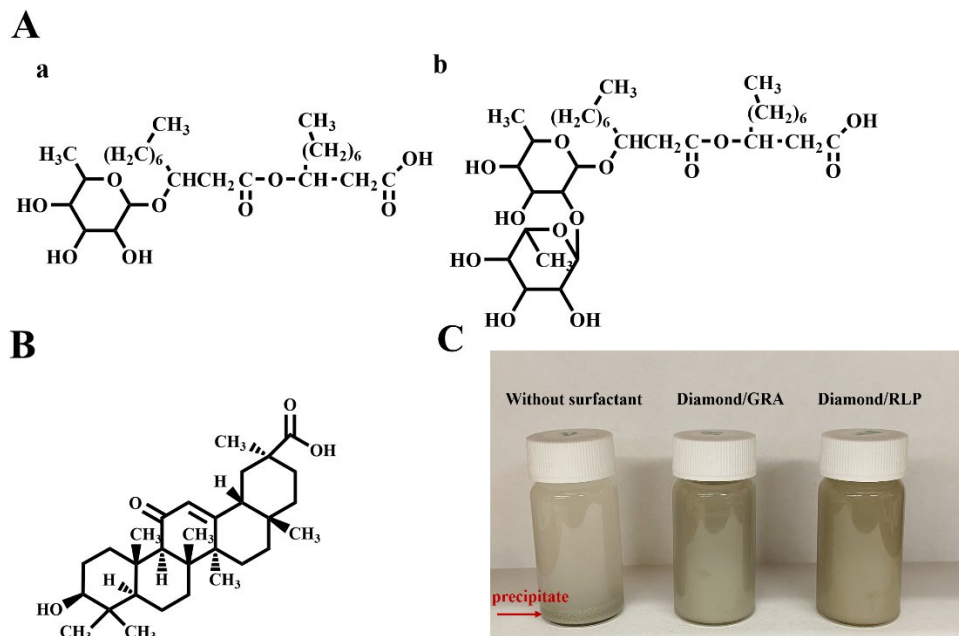


Figure 5-1 (A) Chemical structures of RLP: mono-RLP and di-RLP, (B) Chemical structure of GRA, (C) diamond suspensions in isopropanol without and with biosurfactants.

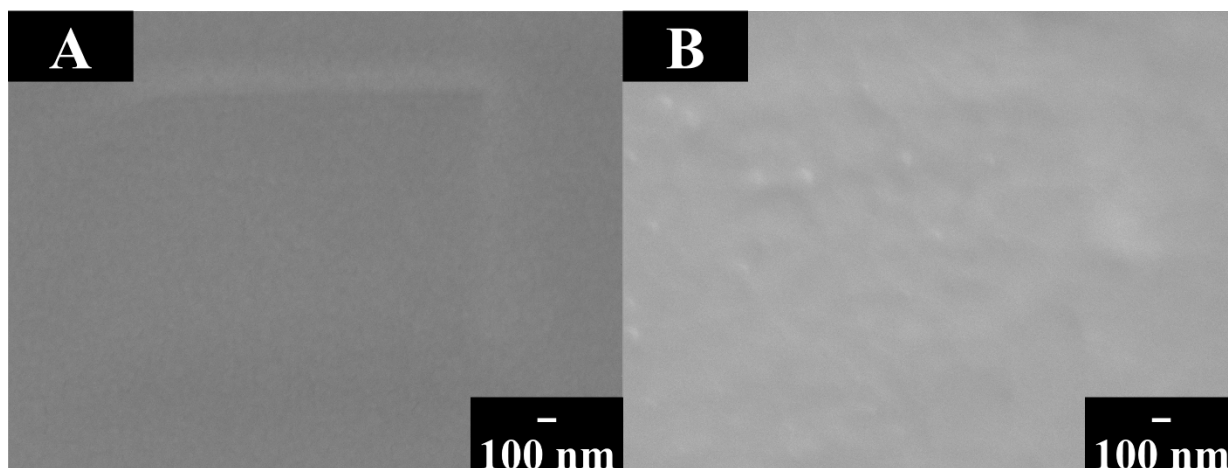


Figure 5-2 SEM images of PEMA films prepared from 10 g L^{-1} PEMA solutions, containing 2 g L^{-1} (A) GRA and (B) RLP.

Figure 5-2 shows SEM images of PEMA films prepared by a dip coating method. The films were smooth and crack-free. Motivated by the interest in PEMA films for corrosion protection, we investigated protective properties of the deposited films. Figure 5-3 compares results of

potentiodynamic studies of uncoated and coated stainless steels. The analysis of obtained Tafel plots indicated that film deposition resulted in increasing corrosion potential and reduction of corrosion currents. The corrosion currents were found to be 2.63, 1.44 and 0.64 μAcm^{-2} for uncoated stainless steel and PEMA coated using RLP and GRA, respectively. The lower corrosion current for PEMA films prepared using GRA indicates improved corrosion protection. The results of potentiodynamic studies are in agreement with electrochemical impedance spectroscopy data. Figure 5-4 shows EIS data presented in Bode plots. Relatively small increase in impedance values ($|Z|$) was observed for stainless steel coated with PEMA films prepared using RLP in comparison with uncoated steel. However, significant increase in impedance in a wide frequency range was observed for stainless steel samples coated with films prepared using GRA. The corresponding phase angle (φ) data showed significantly lower φ for such films at low frequencies. Therefore, such films acted as a barrier, which limited electrolyte access to the film surface. The simplicity of film preparation by a dip-coating method offers highly advantageous features, such as fabrication of multilayer films. The deposition of multilayer coatings was performed and the deposition yield was analysed. Figure 5-5 shows deposit mass versus number of the deposited layers. Nearly linear dependencies were obtained, which indicated good control of the deposition process. The deposition yield obtained using PLP was slightly higher than that obtained using GRA.

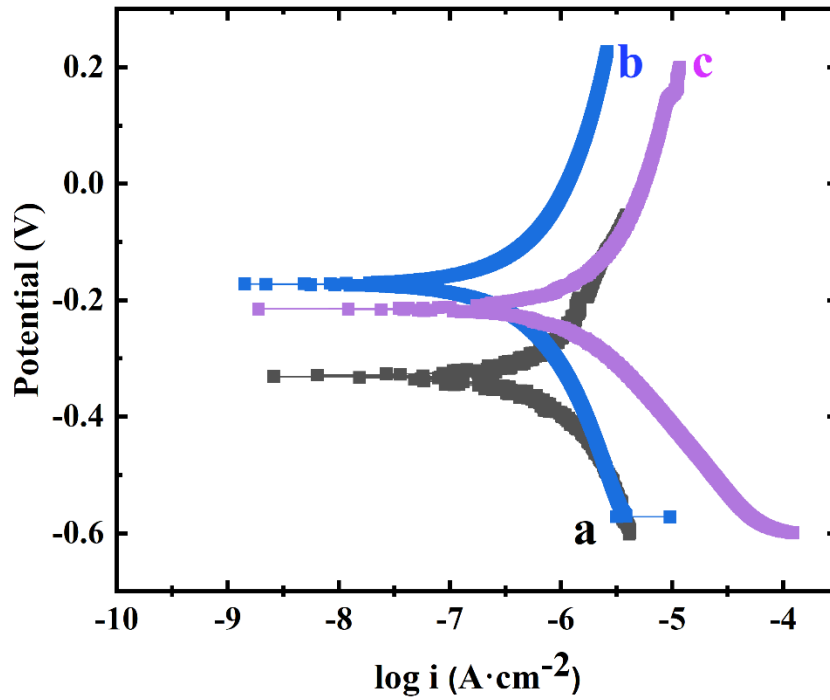


Figure 5-3 Tafel plots for (a) uncoated stainless steel and coated with PEMA films prepared using (b) GRA and (c) RLP. Coated samples contained one dip-coated layer.

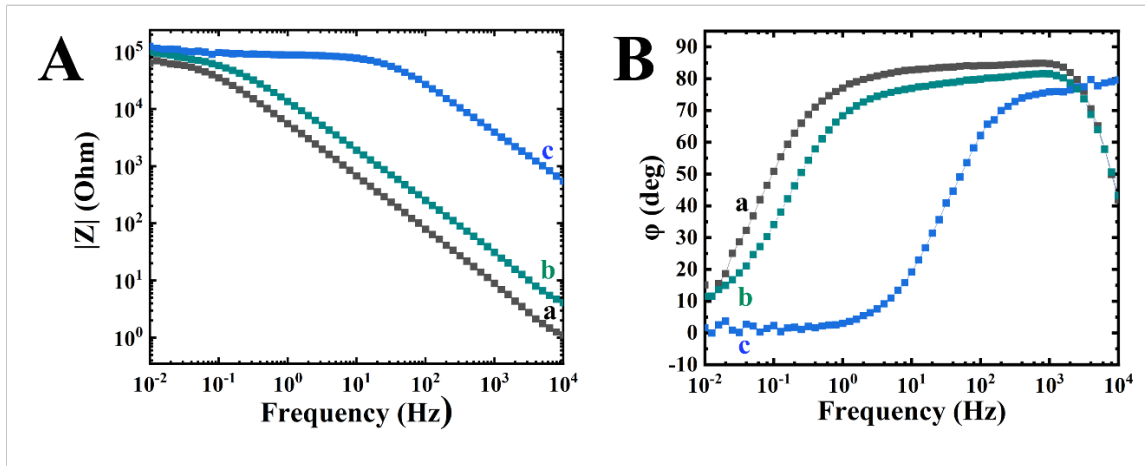


Figure 5-4 EIS data presented in Bode plots for (a) uncoated stainless steel and coated with PEMA films prepared using (b) RLP and (c) GRA

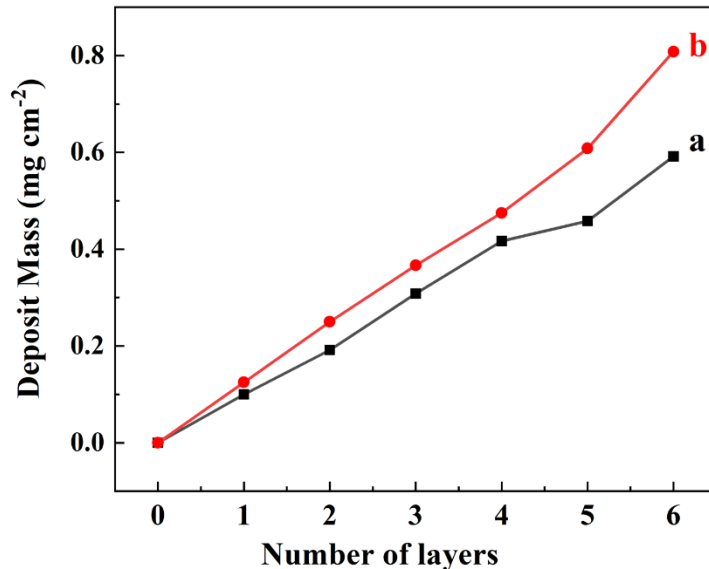


Figure 5-5 Deposit mass of PEMA films versus number of deposited layers prepared from 10 g L^{-1} PEMA solutions, containing 2 g L^{-1} (a) GRA and (b) RLP.

Following the goal of this investigation we performed co-deposition of PEMA and diamond particles. In this approach, GRA and RLP were used as solubilising agents for PEMA and dispersing agents for diamonds in isopropanol. Another important factor for coating fabrication is PEMA-dispersant-diamond interactions, which facilitate diamond particle incorporation into the PEMA matrix. Figure 5-6 shows SEM images of PEMA-microdiamond films prepared using RLP. The SEM images show diamond particles in PEMA film. The SEM images at low magnification showed that the increase in diamond concentration in suspension resulted in larger number of diamond particles in the deposited films. SEM studies showed that the increase in diamond concentration resulted in significant agglomeration of the diamond particles. Moreover, multiple defects were observed around the diamond particles. The SEM images at higher magnifications revealed areas of lower polymer thickness around the diamond particles and pores. Such images indicated poor integration of the diamond particles into the polymer matrix. The SEM images of

PEMA-nanodiamond films (Figure 5-7) prepared using RLP showed significant agglomeration of the nanoparticles, especially for films with larger nanodiamond concentration. The films showed defects, such as areas of lower thickness and pores. Similar defects were observed for films containing microdiamond prepared using RLP (Figure 5-6). The analysis of data obtained for PEMA-diamond films prepared using RLP showed that despite of good dispersion of diamonds in suspension, RLP provided poor dispersion of the chemically inert diamond particles in the PEMA matrix. Significant agglomeration of the diamond particles and formation of defects around the particles indicated that PEMA-diamond interactions in the films were weak. In contrast, the use of GRA allowed for improved film morphologies. Figure 5-8 shows SEM images of composite PEMA-microdiamond films. The diamond particles were well incorporated into the PEMA matrix and defects of the films around the particles were not observed. The diamond particles showed reduced agglomeration, compared to films prepared using RLP. The increase in particle concentration in suspensions resulted in increased particle concentration in the films. Similar morphologies were observed for PEMA-nanodiamond films prepared using GRA (Figure 5-9). The defects around the particles or small agglomerates were avoided. The nanodiamond particles showed reduced agglomeration, however the formation of agglomerates cannot be completely avoided. The ability to increase the diamond content in the coating by increasing the diamond concentration in suspension allows control of coating composition. It is suggested that enhanced diamond-GRA and PEMA-GRA interactions allowed for defects prevention and reduced agglomeration. Previous investigations [5–11], described in the Introduction section, highlighted benefits of multilayer diamond-polymer coatings and coatings of graded composition. These studies generated a need in the further development of deposition techniques. Motivated by the previous studies, we investigated the possibility of deposition of multilayer techniques for

deposition of layers of different composition. Figure 5-10 shows deposit mass versus number of the deposited layers for PEMA-microdiamond and PEMA-nanodiamond films, prepared using GRA or RLP. The deposition yield measurements show continuous increase in the deposit mass with increasing number of the deposited layers. Nearly linear dependences were obtained, which confirm continuous increase in the amount of the deposited material. The increase in diamond concentration in the suspension resulted in higher film mass. The dip-coating method developed in this investigation is promising for the fabrication of multilayer films, containing layers of different composition and functionally graded films. As a step in this direction, we investigated the possibility of deposition of multilayers, containing alternating PEMA and composite PEMA-diamond layers. The feasibility of deposition of such films was confirmed by the results of deposition yield measurements (Figure 5-11).

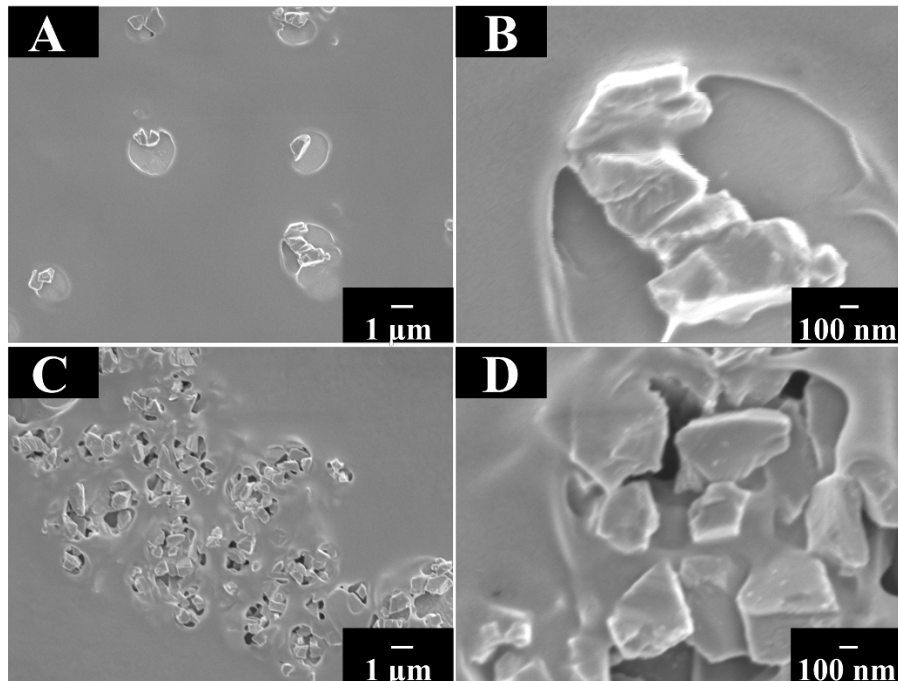


Figure 5-6 SEM images at different magnifications for films prepared from 10 g L^{-1} PEMA solutions, containing 2 g L^{-1} RLP and (A, B) 1 g L^{-1} and (C,D) 3 g L^{-1} microdiamond.

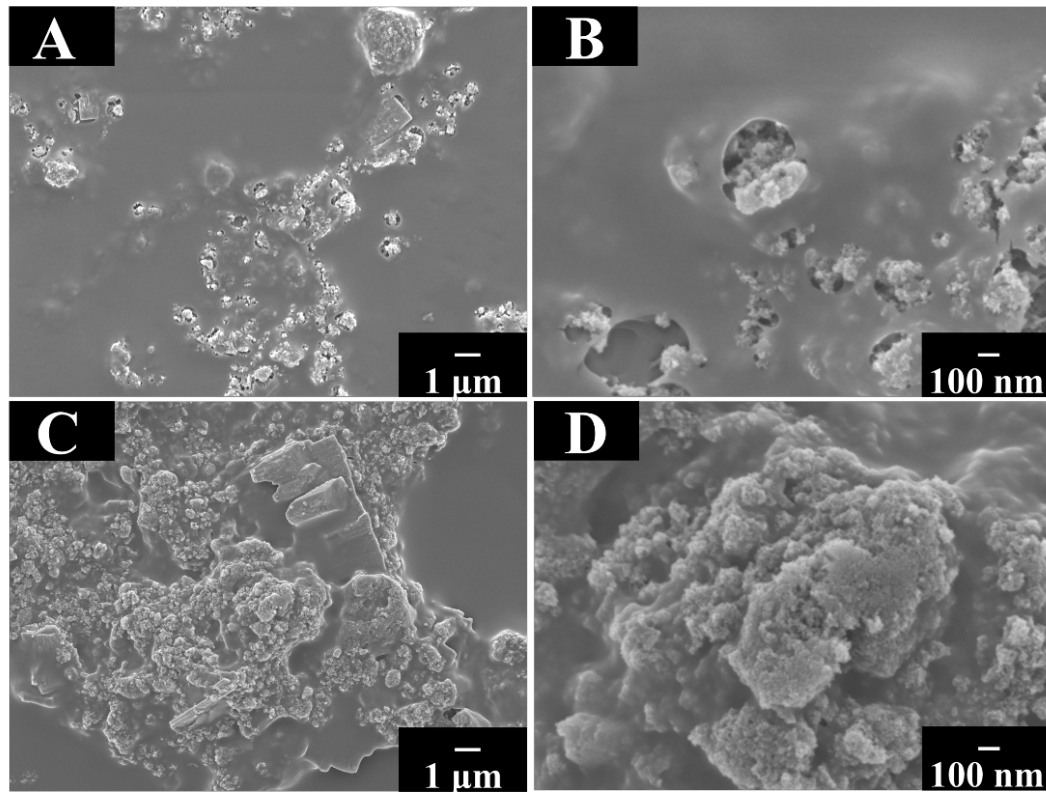


Figure 5-7 SEM images at different magnifications for films prepared from 10 g L⁻¹ PEMA solutions, containing 2 g L⁻¹ RLP and (A, B) 1 g L⁻¹ and (C,D) 3 g L⁻¹ nanodiamond.

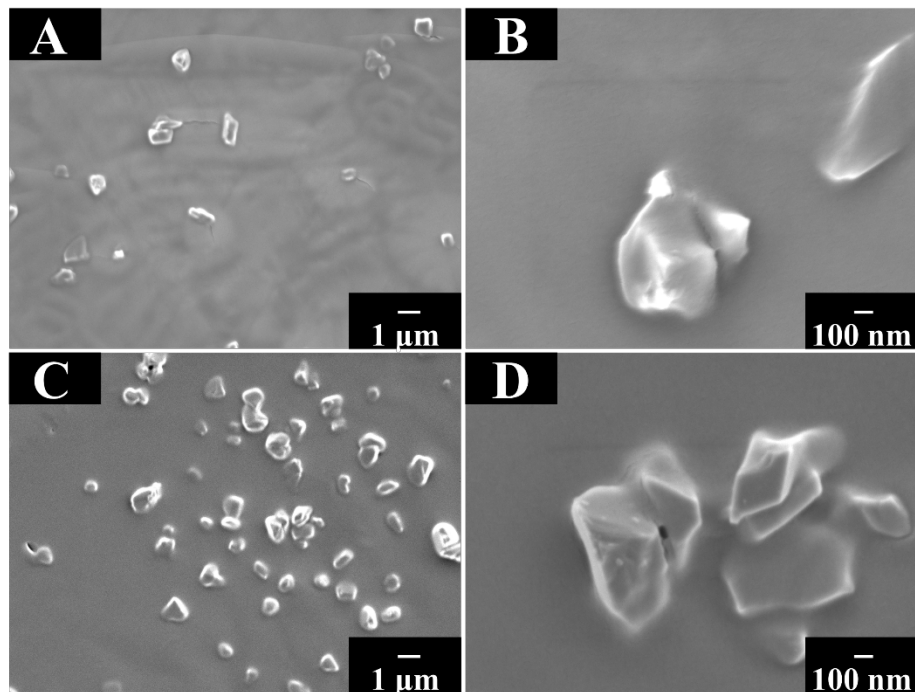


Figure 5-8 SEM images at different magnifications for films prepared from 10 g L^{-1} PEMA solutions, containing 2 g L^{-1} GRA and (A, B) 1 g L^{-1} and (C,D) 3 g L^{-1} microdiamond.

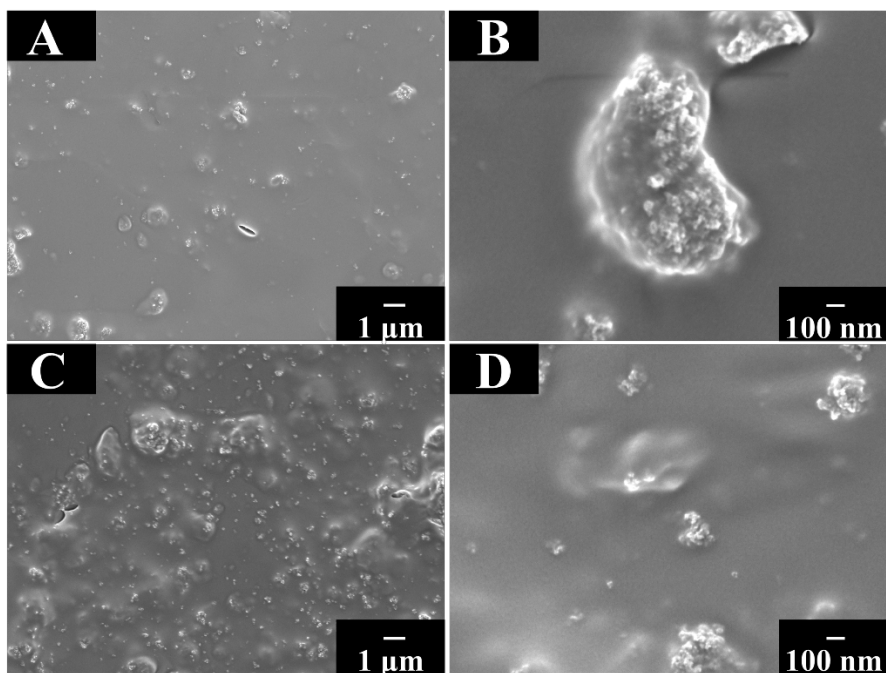


Figure 5-9 SEM images at different magnifications for films prepared from 10 g L^{-1} PEMA solutions, containing 2 g L^{-1} GRA and (A, B) 1 g L^{-1} and (C,D) 3 g L^{-1} nanodiamond.

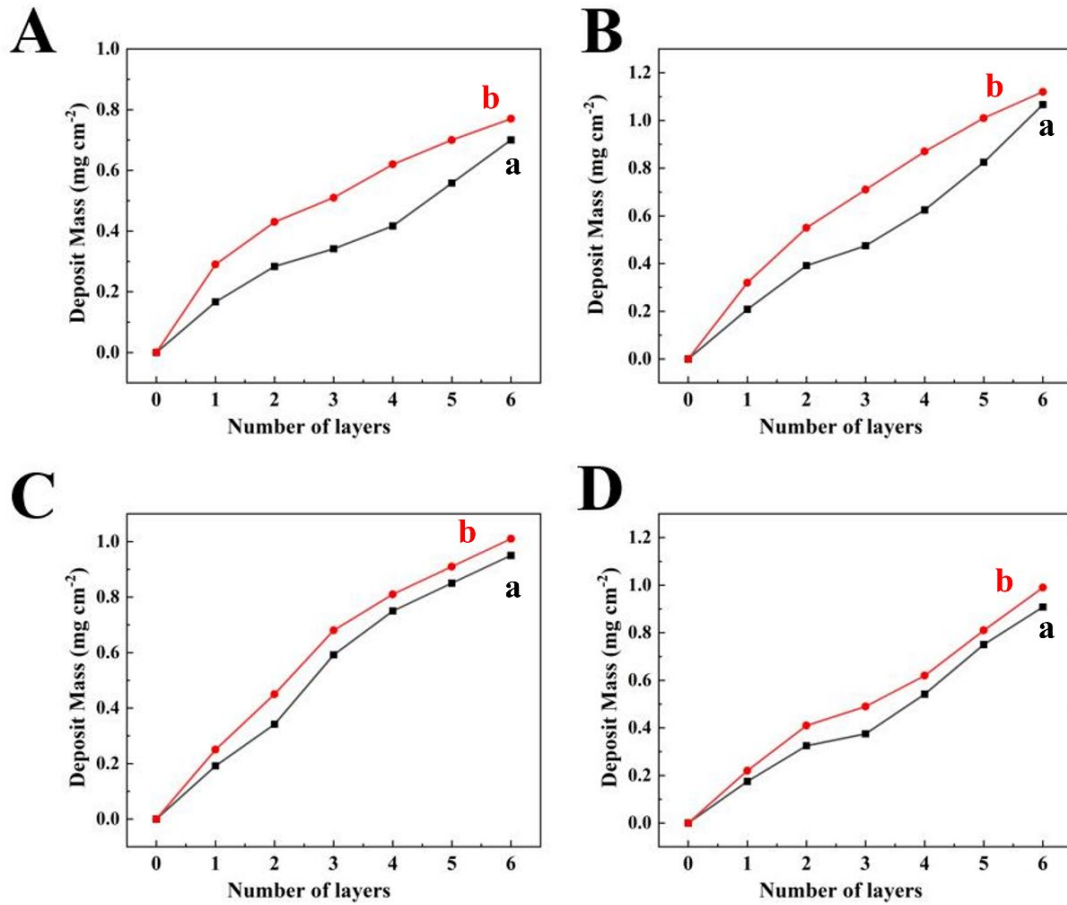


Figure 5-10 Film mass versus number of the deposited layers for films prepared from 10 g L^{-1} PEMA solutions containing (A,B) microdiamonds and (C,D) nanodiamonds, prepared using (A,C) 2 g L^{-1} GRA and (B,D) 2 g L^{-1} RLP and diamonds concentrations of (a) 1 g L^{-1} and (b) 3 g L^{-1}

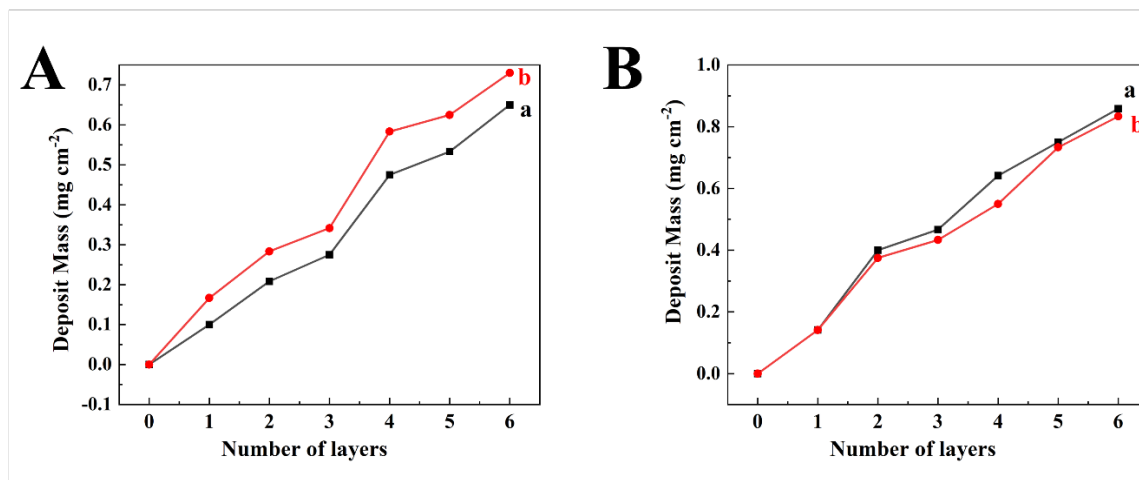


Figure 5-11 Film mass as a function of number of alternating (A) PEMA/PEMA-microdiamond and (B) PEMA/PEMA-nanodiamond layers, prepared from 10 g L⁻¹ PEMA/10 g L⁻¹ PEMA and 1 g L⁻¹ diamond media prepared using (a) 2 g L⁻¹ GRA and (b) 2 g L⁻¹ RLP.

The results presented demonstrate that GRA and RLP can be used as solubilising agents for PEMA and dispersing agents for micro- and nanodiamond particles. This observation is important given that the use of toxic solvents can be avoided, and the problems related to dispersion of chemically inert diamonds in solvents can be eliminated. This finding could also provide a novel strategy for solubilisation of other polymers and fabrication of composite coatings. The proposed approach creates a platform for deposition of coatings with different diamond content, which can be deposited as monolayers or multilayers of different composition. The results also stress importance of the dispersant structure on the fabrication of composite coatings. The chemical structure of GRA belongs to steroid derivatives of the sapogenins family. Steroid molecules, such as bile salts solubilise different biomolecules in a human body [41]. Bile acids and bile salts have generated significant interest in materials processing [41,42]. However, we were not able to dissolve PEMA in the presence of bile acids or bile salts. Therefore, further investigation of sapogenins and other steroid derivatives is promising for the development of composite coatings.

5.5. Conclusions

GRA and RLP can be used as solubilising agents for PEMA and the use of toxic solvents can be eliminated. We demonstrated the ability to dissolve high molecular mass PEMA and obtain concentrated solutions. These findings were crucial for the development of a dip coating method, which represents a versatile approach for the deposition of PEMA films. Obtained films provided corrosion protection of stainless steel. The films prepared using GRA provided improved corrosion protection, compared to the films prepared using RLP. The PEMA films can be deposited as monolayers or multilayers. Another important finding was the feasibility of dispersion of chemically inert diamond microparticles and nanoparticles. The ability to solubilise PEMA and disperse diamonds using GRA and RLP provided a platform for the fabrication of composite PEMA-diamond coatings. The composition of the films can be varied by variation of diamond concentration in suspensions. The analysis of film morphologies showed that chemical structures of GRA and RLP are important factors controlling their interactions with PEMA and diamonds. The films prepared using RLP showed defects at the diamond-PEMA interface, whereas such defects were avoided in the composite films prepared using GRA. Expansion of these studies can result in the development of other advanced steroid dispersants for solubilisation of polymers and dispersion of various materials. The dip coating method represents a simple strategy for the fabrication of multilayer PEMA/diamond films and films containing alternating PEMA/ PEMA-diamond layers. PEMA and composite coatings can be used for different biomedical applications in implants and sensors due to the use of biocompatible materials. The proposed approach opens an avenue for the fabrication of composite coatings containing other polymers and various functional nanoparticles.

5.6. Acknowledgements

This research was supported by the Natural Sciences and Engineering Research Council of Canada. Electron microscopy studies were performed at the Canadian Centre for Electron Microscopy.

5.7. References

1. Bociaga D, Sobczyk-Guzenda A, Szymanski W, et al. Mechanical properties, chemical analysis and evaluation of antimicrobial response of Si-DLC coatings fabricated on AISI 316 LVM substrate by a multi-target DC-RF magnetron sputtering method for potential biomedical applications. *Appl Surf Sci.* 2017;417:23–33.
2. Bito K, Hasebe T, Maegawa S, et al. In vitro basic fibroblast growth factor (bFGF) delivery using an antithrombogenic 2-methacryloyloxyethyl phosphorylcholine (MPC) polymer coated with a micropatterned diamond-like carbon (DLC) film. *J Biomed Mater Res A.* 2017;105:3384–3391.
3. Li H, Cao J, Wei Q, et al. Antifouling nanoporous diamond membrane for enhanced detection of dopamine in human serum. *J Mater Sci.* 2020;56:746–761.
4. Eshaghi A, Salehi M. Fabrication and characterization of optical: mechanical and chemical properties of diamond-like carbon thin film deposited on polymer substrate. *Opt Quantum Electron.* 2018;50.
5. Choudhury D, Morita T, Sawae Y, et al. A novel functional layered diamond like carbon coating for orthopedics applications. *Diamond Relat Mater.* 2016;61:56–69.

6. Salgueiredo E, Almeida F, Amaral M, et al. A multilayer approach for enhancing the erosive wear resistance of CVD diamond coatings. *Wear*. 2013;297:1064–1073.
7. Voevodin A, Walck S, Zabinski J. Architecture of multilayer nanocomposite coatings with super-hard diamond-like carbon layers for wear protection at high contact loads. *Wear*. 1997;203:516–527.
8. Booth L, Catledge SA, Nolen D, et al. Synthesis and characterization of multilayered diamond coatings for biomedical implants. *Materials (Basel)*. 2011;4:857–868.
9. Buchegger S, Schuster N, Stritzker B, et al. Multilayer diamond-like amorphous carbon coatings produced by ion irradiation of polymer films. *Surf Coat Technol*. 2017;327:42–47.
10. Roy RK, Lee KR. Biomedical applications of diamond-like carbon coatings: a review. *J Biomed Mater Res B: Appl Biomater: Off J Soc Biomater Jpn Soc Biomater Aust Soc Biomater Korean Soc Biomater*. 2007;83:72–84.
11. Huang H, Pierstorff E, Osawa E, et al. Protein-mediated assembly of nanodiamond hydrogels into a biocompatible and biofunctional multilayer nanofilm. *ACS Nano*. 2008;2:203–212.
12. Branzoi IV, Iordoc M, Branzoi F, et al. Synthesis and characterization of high-voltage electrodeposited diamond-like carbon protective coating on TiAlV biomedical substrates. *Surf Interface Anal*. 2012;44:1193–1197.
13. Lavrynenko SN, Mamalis AG, Starikova SL, et al. Diamond biocompatible coatings for medical implants. *J Biol Phys Chem*. 2016;16:70–74.

14. Gnanavel S, Ponnusamy S, Mohan L, et al. Electrochemical behavior of biomedical titanium alloys coated with diamond carbon in hanks' solution. *J Mater Eng Perform.* 2018;27:1635–1641.
15. Garrett DJ, Saunders AL, McGowan C, et al. In vivo biocompatibility of boron doped and nitrogen included conductive-diamond for use in medical implants. *J Biomed Mater Res B Appl Biomater.* 2016;104:19–26.
16. Pandey PC, Shukla S, Pandey G, et al. Nanostructured diamond for biomedical applications. *Nanotechnology.* 2021;32:132001.
17. Khalid A, Abraham A, Bai D, et al. Electrospun diamond-silk membranes for biosensing applications. *Biophotonics Australas.* 2019:2019.
18. Liu X, Veldhuis S, Mathews R, et al. Dip coating of poly(ethyl methacrylate) and composites from solutions in isopropanol-water co-solvent. *Colloids Surf, A.* 2021;631.
19. Baker K, Zhitomirsky I. Biomimetic approach to poly(ethyl methacrylate) solubilization, deposition, and coating loading with functional biomaterials. *Colloid Polym Sci.* 2022;300:599–607.
20. Sreekantan S, Hassan M, Sundera Murthe S, et al. Biocompatibility and cytotoxicity study of polydimethylsiloxane (PDMS) and palm Oil fuel Ash (POFA) sustainable super-hydrophobic coating for biomedical applications. *Polymers (Basel).* 2020;12:3034.
21. Cooperstein MA, Canavan HE. Assessment of cytotoxicity of (N-isopropyl acrylamide) and poly (N-isopropyl acrylamide)-coated surfaces. *Biointerphases.* 2013;8:19.

22. Hadidi M, Bigham A, Saebnoori E, et al. Electrophoretic-deposited hydroxyapatite-copper nanocomposite as an antibacterial coating for biomedical applications. *Surf Coat Technol.* 2017;321:171–179.
23. Farrokhi-Rad M. Electrophoretic deposition of titania nanostructured coatings with different porous patterns. *Ceram Int.* 2018;44:15346–15355.
24. Farrokhi-rad M, Emamalipour S, Mohammadzadeh F, et al. Electrophoretic deposition of alginate coatings from different alcohol-water mixtures. *Surf Eng.* 2021;37:1176–1185.
25. Yu Q, Roberts MG, Pearce S, et al. Rodlike block copolymer micelles of controlled length in water designed for biomedical applications. *Macromolecules.* 2019;52:5231–5244.
26. Cullis PS, Keene DJ, Zaman A, et al. Chemical stability of heparin, isopropanol, and ethanol line lock solutions. *J Pediatr Surg.* 2015;50:315–319.
27. Wang Z, Zhitomirsky I. Deposition of organic-inorganic nanocomposite coatings for biomedical applications. *Solids.* 2022;3:271–281.
28. Zhang M, Weng YJ, Zhang YQ. Accelerated desalting and purification of silk fibroin in a CaCl₂-EtOH-H₂O ternary system by excess isopropanol extraction. *J Chem Technol Biotechnol.* 2021;96:1176–1186.
29. Silva SS, Oliveira NM, Oliveira MB, et al. Fabrication and characterization of Eri silk fibers-based sponges for biomedical application. *Acta Biomater.* 2016;32:178–189.
30. Pruett LJ, Jenkins CH, Singh NS, et al. Heparin microislands in microporous annealed particle scaffolds for accelerated diabetic wound healing. *Adv Funct Mater.* 2021;31:2104337.

31. Marchant R, Banat IM. Microbial biosurfactants: challenges and opportunities for future exploitation. *Trends Biotechnol.* 2012;30:558–565.
32. Guo Y-P, Hu Y-Y. Solubilization of moderately hydrophobic 17 α -ethinylestradiol by mono- and di-rhamnolipid solutions. *Colloids Surf, A.* 2014;445:12–20.
33. Chen J, Wu Q, Hua Y, et al. Potential applications of biosurfactant rhamnolipids in agriculture and biomedicine. *Appl Microbiol Biotechnol.* 2017;101:8309–8319.
34. Vatsa P, Sanchez L, Clement C, et al. Rhamnolipid biosurfactants as new players in animal and plant defense against microbes. *Int J Mol Sci.* 2010;11:5095–5108.
35. Kowalska A, Kalinowska-Lis U. 18 β -Glycyrrhetic acid: its core biological properties and dermatological applications. *Int J Cosmet Sci.* 2019;41:325–331.
36. Bailly C, Vergoten G. Glycyrrhizin: an alternative drug for the treatment of COVID-19 infection and the associated respiratory syndrome? *Pharmacol Ther.* 2020;214:107618.
37. Pang X, Imin P, Zhitomirsky I, et al. Amperometric detection of glucose using a conjugated polyelectrolyte complex with single-walled carbon nanotubes. *Macromolecules.* 2010;43:10376–10381.
38. Li J, Zhitomirsky I. Cathodic electrophoretic deposition of manganese dioxide films. *Colloids Surf, A.* 2009;348:248–253.
39. Shojaeiarani J, Bajwa DS, Chanda S. Cellulose nanocrystal based composites: a review. *Composites Part C: Open Access.* 2021;5:100164.

40. Benega MAG, Silva WM, Schnitzler MC, et al. Improvements in thermal and mechanical properties of composites based on epoxy-carbon nanomaterials-a brief landscape. *Polym Test.* 2021;98:107180.

41. Baker K, Sikkema R, Liang W, et al. Multifunctional properties of commercial bile salts for advanced materials engineering. *Adv Eng Mater.* 2021;23:2001261.

42. Baker K, Sikkema R, Zhitomirsky I. Application of bile acids for biomedical devices and sensors. *Med Devices Sens.* 2020;3:e10119. Article first published online: May 1, 2023 Issue published: May 2023

Chapter 6 Bile Acid Salt as a Vehicle for Solubilization and Electrodeposition of Drugs and Functional Biomolecules for Surface Modification of Materials

6.1. Abstract

This investigation addresses the need in biocompatible biosurfactants for electrophoretic deposition (EPD) of biomaterials. It is motivated by unique multifunctional properties of bile acid salts. Sodium cholate CHOLNa is a primary bile acid salt, which can solubilize and disperse different functional biomaterials. The EPD mechanism of pure EPD involves electrophoresis (EP) of CHOL⁻ micelles, their discharge and gelation of cholic acid (CHOLH) to form anodic CHOLH films. The EPD strategy for immobilization of different functional biomolecules is based on the formation and EP of mixed micelles. Curcumin (CCM), hydrocortisone (HCS), and indomethacin (IDM) are used as model electrically neutral water insoluble drugs for EPD of composite films. CHOLNa acts as a solubilizing agent, which forms mixed micelles with the electrically neutral drugs for their EPD and formation of composite films. The pH-dependent charge of various functional biomolecules and charge reversal at isoelectric points prevents their deposition. This problem is addressed by the use CHOLH for codeposition with bovine serum albumin (BSA) and hemoglobin (Hb), which are used as model proteins for EPD of CHOLH-BSA and CHOLH-Hb films. Another challenge is related to EPD of functional biomolecules with pH-independent charge, such as heparin (HP). The feasibility of deposition of CHOLH-HP films is demonstrated. The deposition mechanisms, film composition, and films morphologies are discussed. The approach developed in this investigation offers advantages of the use of biosurfactants as charging and gel-

forming agents and mild EPD conditions for fabrication of films for drug delivery, biosensors, and surface modification of biomedical implants.

6.2. Introduction

Bile acid salts (BAS) are physiologically significant anionic biosurfactants[1], which have many metabolic functions. BAS solubilize lipids, vitamins, cholesterol, and other functional biomolecules. BAS are amphiphilic steroid molecules, containing a hydrophobic side and a hydrophilic side with anionic COO^- or SO_3^- groups. Recently, significant interest has been generated in commercial synthesis and applications of BAS in biomedical and engineering fields [1, 2]. It has been widely reported that self-aggregation properties of amphiphilic BAS promote the formation of micelles and gels [1–4]. The interactions of BAS with other materials and formation of mixed micelles are of increasing interest [1, 3, 5]. Such interactions promote solubilization and dispersion of different materials [1, 3]. Of particular interest are experiments on solubilization of drugs in water, which provide a platform for the development of new strategies for drug delivery [5–7]. BAS allowed excellent dispersion of various hydrophobic materials, such as diamonds, carbon nanotubes, graphene, and polymers [1, 8–10] for applications in biosensors and biomedical implants. The surface modification and dispersion of carbon nanotubes using adsorbed BAS [11] offers advantages for biosensor applications, compared to chemical functionalization techniques [12] by eliminating defect formation in the conductive carbon network. The gel-forming properties of BAS [13] are governed by their amphiphilic structure, which also facilitates the formation of composite gels. BAS gels have many important applications in the field of drug delivery [14].

BAS are very promising for surface modification of materials and fabrication of composite films for biomedical applications [15]. BAS are especially important for electrophoretic deposition

(EPD). Due to the excellent purity of the deposits, high deposition rate and the potential for uniform deposition of multilayer films on substrates of complex shapes, EPD is particularly valuable for biomedical applications and fabrication of composites [8, 16–22]. The feasibility of film deposition by this method is closely related to the use of efficient charging and film-forming agents [23]. However, many charging and film-forming agents are not biocompatible and cannot be used for EPD of biomaterials. Sodium cholate (CHOLNa) is a primary BAS (Fig. 6-1A), which has generated interest for EPD [24]. The electric charge of dissociated CHOLNa is related to anionic COO^- ligands. CHOLNa solutions were used for the fabrication of cholic acid (CHOLH) films [24].

The deposition mechanism involved dissociation of water-soluble CHOLNa and electrophoresis of CHOL^- anions, which resulted in the protonation and deposition of water-insoluble CHOLH gels on the conductive anodic substrates:



The current density was optimized to generate low pH close to the anode surface in a reaction:



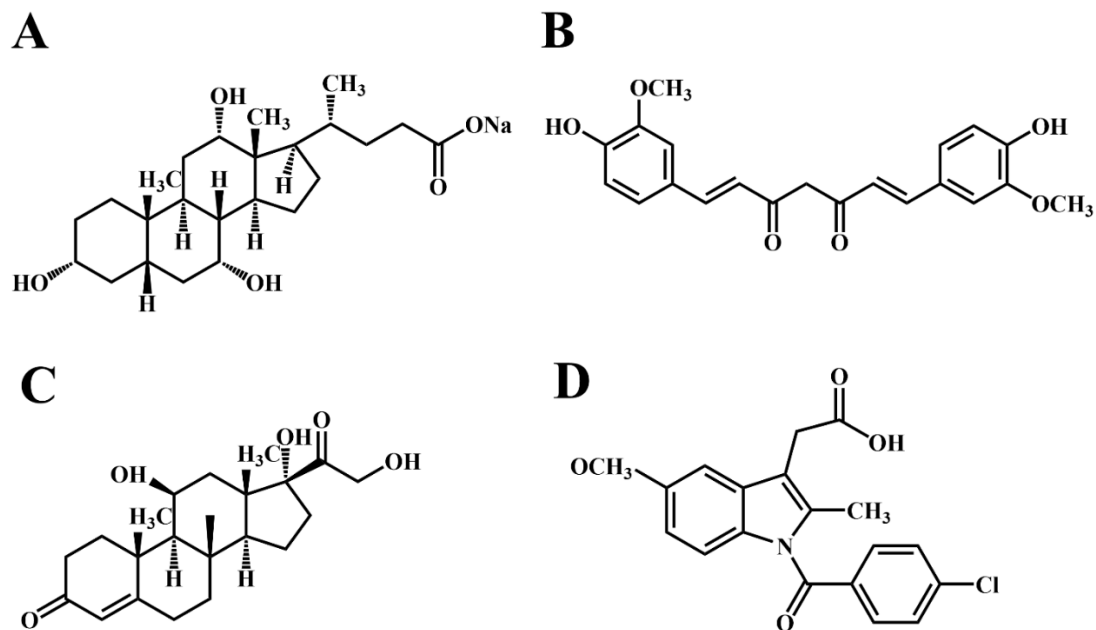


Figure 6-1 Chemical structures of (A) CHOLNa, (B) curcumin (C) hydrocortisone and (D) indomethacin

Drying of the CHOLH gels resulted in the formation of adherent films[24]. The approach developed in this investigation is based on interactions of CHOLNa with functional organic molecules and formation of mixed micelles in solutions, which opens an avenue for the EPD of composite films. Previous investigations showed that CHOLNa and other BAS can solubilize drugs, such as curcumin, hydrocortisone, and indomethacin [25]. This observation is important given that many failures in the development and applications of drugs are related to their poor water solubility [26]. It was demonstrated that CHOLNa and other BAS formed mixed micelles with drugs [25]. The formation of mixed micelles of BAS with curcumin, hydrocortisone, and indomethacin can involve hydrophobic interactions and hydrogen bond formation. Figure 6-1B–D shows chemical structures of curcumin, hydrocortisone, and indomethacin. We hypothesized that the formation of mixed micelles of CHOLNa with such water insoluble electrically neutral drugs can provide a strategy for the fabrication of composite films by EPD. In this approach,

CHOLNa can provide solubilization of the drug molecules and act as a charging and film forming agent for their deposition.

Electrodeposition of proteins and enzymes presents difficulties due to their charge reversal at isoelectric points. They are negatively charged at pH above the isoelectric points. However, such molecules acquire a positive charge at the electrode surface, where the pH is typically lower than their isoelectric point [27, 28]. In this case the mutual electrostatic repulsion between the molecules and electrostatic molecule-anode repulsion prevents deposition. Other difficulties are related to EPD of strong anionic polyelectrolytes with a pH-independent charge, such as heparin due to mutual electrostatic repulsion of anionic heparin molecules, containing multiple SO_3^- groups. Such problems can potentially be addressed by the use of gel-forming and film-forming properties of CHOLH.

The goal of this investigation was the development of EPD strategies for deposition of CHOLH films, containing drugs, such as curcumin, hydrocortisone, and indomethacin, proteins, such as albumin and hemoglobin, and other functional biomolecules, such as heparin. We developed deposition mechanisms and analyzed the mechanisms of charging, electrophoresis and films formation at the electrode surface. It was demonstrated for the first time that electrically neutral molecules, as well as molecules with charge reversal properties and strong anionic polyelectrolytes can be co-deposited with CHOLH. The findings of this work indicate that the use of CHOLNa for EPD method is a versatile strategy for deposition of various functional materials for biomedical applications.

6.3. Experimental

Sodium cholate (CHOLNa), curcumin (CCM), hydrocortisone (HCS), and indomethacin (IDM), bovine serum albumin (BSA), hemoglobin (Hb), and heparin (HP) were purchased from Aldrich. EPD of pure CHOLH films was performed from aqueous 3 g L^{-1} CHOLNa solutions. Composite films were deposited from aqueous 3 g L^{-1} CHOLNa solutions, containing 1 g L^{-1} CCM, HCS, IDM, BSA, Hb, and HP. EPD was performed at a constant deposition voltage of 10 V. The pH of the solutions was 7.2. The separation between stainless steel anodic substrates (304 type, $25 \times 50 \times 0.1 \text{ mm}$) and Pt ($25 \times 50 \times 0.1 \text{ mm}$) cathodes was 15 mm. The electrodes were ultrasonically cleaned in ethanol for 5 min. prior to deposition. The deposited films were dried in air at 20°C for 24 h. X-ray diffraction (XRD) studies were performed using a powder diffractometer (Nicolet I2, monochromatized CuK α radiation) at a scan rate of 0.5 deg s^{-1} . FTIR studies were performed using a Bruker Vertex 70 spectrometer (USA) in the range of $400\text{--}4000 \text{ cm}^{-1}$. Electron microscopy investigations were performed using a JEOL JSM-7000F scanning electron microscope (SEM) at a voltage of 3 kV and working distance of 10 mm. A conductive 4 nm Pt layer was deposited on the sample surface in order to improve electronic conductivity of the samples. FTIR and XRD studies were performed on powder samples, which were obtained by removing deposited materials from the substrates. Electrophoretic mobility measurements were performed by the mass transport method[29].

6.4. Results and discussion

The electrophoretic mobility of CHOLNa was found to be $3.4 \cdot 10^{-4} \text{ cm}^2 \text{ s}^{-1} \text{ V}^{-1}$. It is known that CHOLNa forms micelles in solutions[3, 30]. The critical micelle concentrations (CMCs) were obtained by different methods [3, 30] and it was shown that the stepwise micelle formation results in a CMC range, rather than a specific CMC value. The CMC for CHOLNa is in the range of 1.6–

17.4 mM[1]. The CHOLNa concentration in the solutions used in this study was about 7 mM. Therefore, the formation of micelles can be expected. Figure 6-2 shows basic deposition mechanisms. The deposition mechanism of pure CHOLH involves electrophoresis (EP) of CHOL^- micelles (Fig. 6-2A). A local pH decrease at the anode and protonation of CHOL^- species in reactions (6-1,6-2) resulted in formation of CHOLH gel. CHOLH films were formed after drying of the deposited gels.

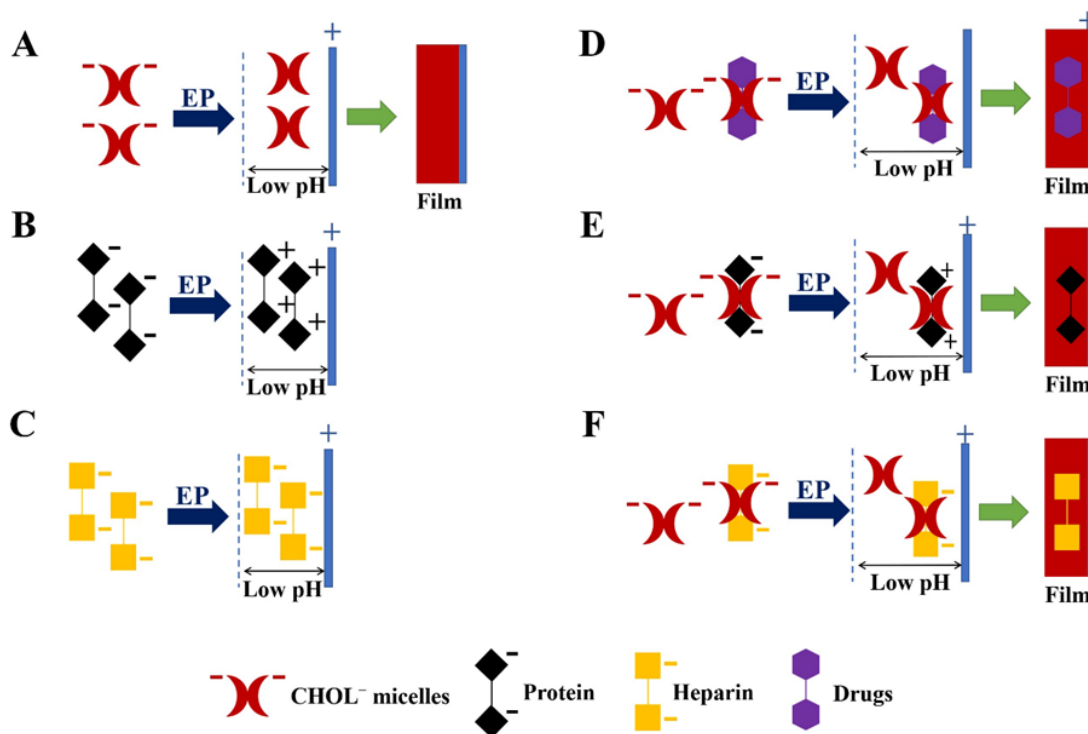


Figure 6-2 Schematics of electrophoresis (EP) and phenomena at the electrode surface for (A) CHOL^- micelles, (B) proteins or enzymes (C) heparin and (D-F) CHOL^- micelles with mixed micelles, containing CHOL^- and (D) drugs, (E) Hb or BSA, F (HP). Formation of (A) pure CHOLH films and (D-E) composite films by EPD.

The net charge of Hb and BSA is a sum of charges of anionic and cationic groups [27, 28], such as carboxylic and amino groups. The degree of ionization and charge of such groups depend on pH. As a result, Hb and BSA exhibit charge reversal at isoelectric points. The isoelectric points of BSA[27] and Hb [28] are located at $\text{pH} \sim 5$ and $\text{pH} \sim 7$, respectively. The mutual repulsion of

positively charged Hb or BSA molecules at the electrode surface prevents their deposition (Fig. 6-2B). Moreover, electric field promotes their electromigration away from the positively charged anode. HP is a highly charged molecule, which exhibits a pH-independent charge. The electric charge of HP is related to multiple SO_3^- groups. The mutual repulsion of HP molecules prevents deposition (Fig. 6-2C). As pointed out above, literature data present evidence of solubilization of CCM, HCS, and IDM in CHOLNa solutions and formation of mixed micelles[25]. Turning again to the chemical structures of CHOLH and drugs (Fig. 6-1) it can be suggested that micelle formation can result from hydrophilic interactions of OH groups and hydrophobic interactions of hydrocarbon groups of the molecules. It was hypothesized that mixed CHOL^- -drug micelles can be used for HP transport of the drug molecules toward the electrode surface. EP from solutions, containing the mixed micelles and CHOL^- micelles can result in gel formation. The films, containing drugs can be obtained after drying of the gel deposits (Fig. 6-2D). Similar deposition mechanism can be proposed for co-deposition of Hb or BSA with CHOLH (Fig. 6-2E) and co-deposition of HP with CHOLH (Fig. 6-2F). The experimental results presented below provide experimental evidence of the fabrication of composite films. Figure 6-3 shows microstructure of a pure CHOLH film at different magnifications. SEM studies showed the formation of a continuous crack-free film layer (Fig. 6-3A) and aggregates of spherical particles with a typical size of 50–150 nm (Fig. 6-3B) on the top of the continuous film layer. The SEM image also showed necks formation between the individual particles. Such film microstructure can result from Stranski–Krastanov layer-plus-island film growth mechanism[31, 32]

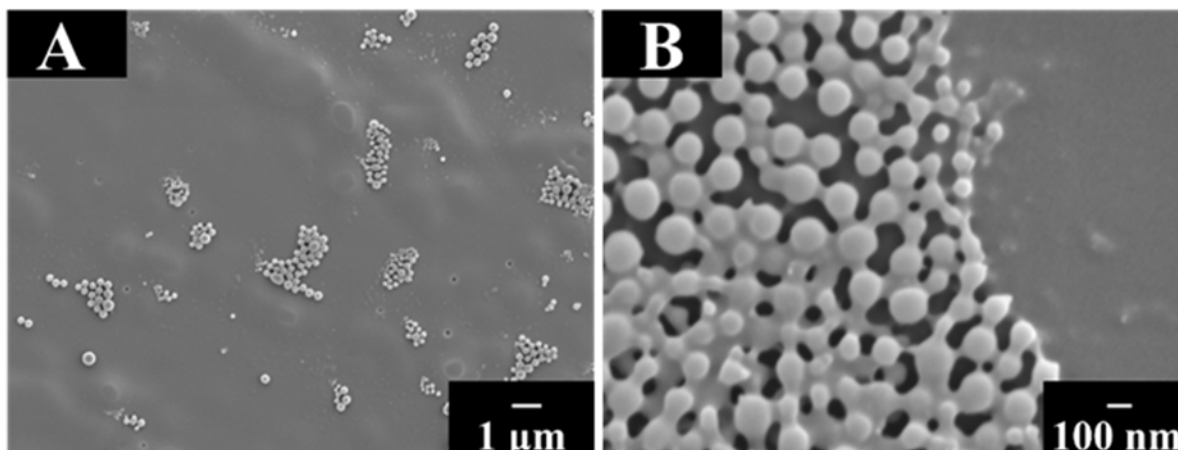


Figure 6-3 SEM images at different magnifications (A,B) of CHOLH films.

EPD was also performed from CHOLNa solutions, containing CCM, HCS, and IDM. Figure 6-4 shows microstructures of such films. The films prepared from such solutions showed different morphologies, compared to the morphology of pure CHOLH films. The films prepared from CHOLNa solutions, containing CCM showed the formation of a continuous film layer and agglomerates of particles of irregular shape with a typical size of 100–1000 nm on the top of the continuous film layer (Fig. 6-4A, B). Co-deposition from CHOLNa solutions containing HCS also resulted in the formation of a continuous film layer and agglomerates of particles with spherical and irregular shape on top of it (Fig. 6-4C, D). The continuous bottom layer of films deposited from CHOLNa solutions, containing IDM showed craters with diameter 0.1–2 μm and nearly spherical particles with a typical size in the range of 0.05–3 μm (Fig. 6-4E, F). Small particles filled some large craters. The difference in film morphologies can be attributed to co-deposition of CHOLH with drugs, which was confirmed by the results of XRD and FTIR.

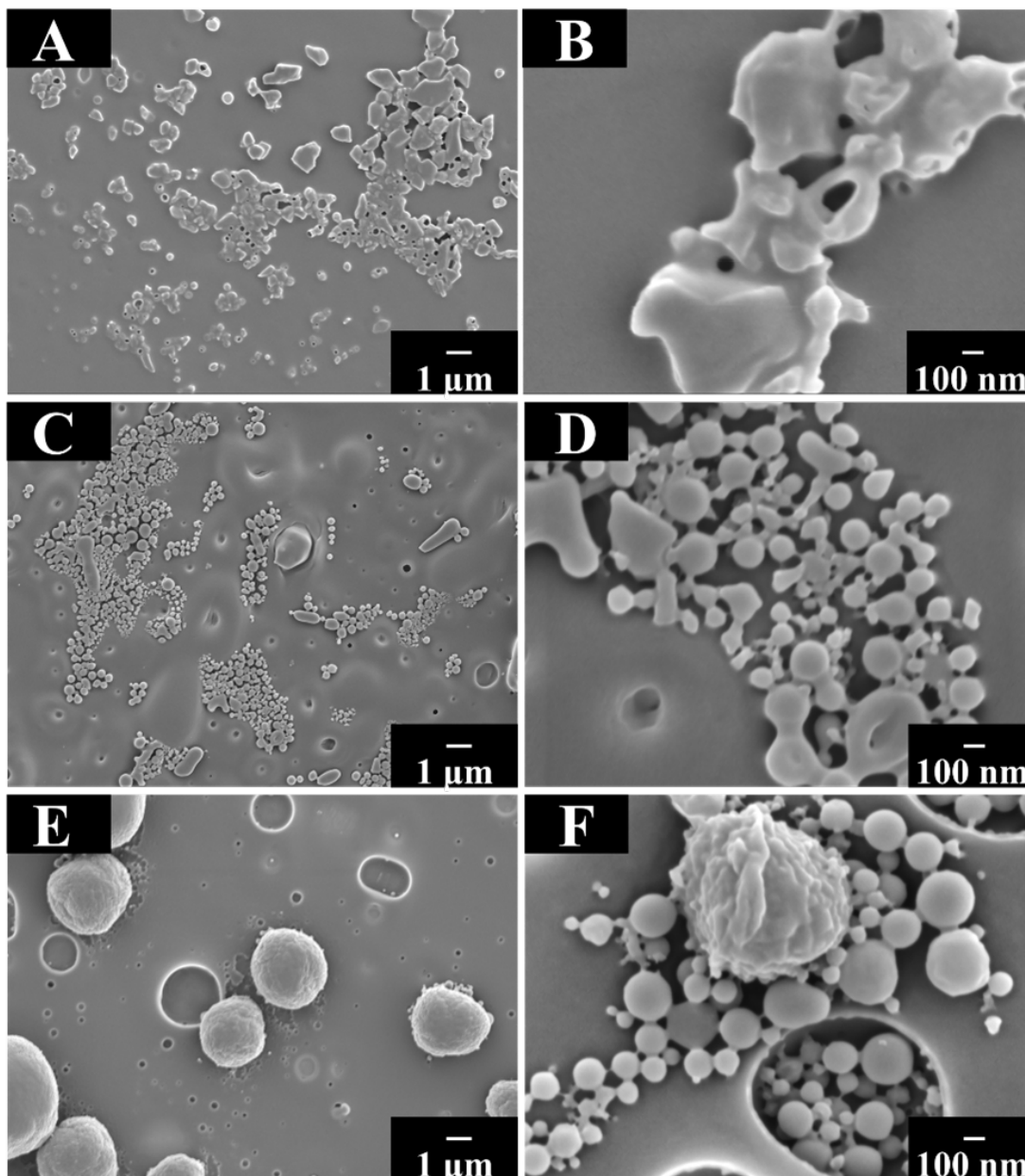


Figure 6-4 SEM images at different magnifications for films, prepared from CHOLNa solutions, containing (A,B) CCM, (C,D) HCS and (E,F) IDM.

Figure 6-5A shows X-ray diffraction patterns of pure drugs and CHOLH deposit. The diffraction patterns of CCM, HCS, and IDM showed peaks, corresponding to JCPDS files 66–1420, 15–1016, and 58–1737, respectively. The CHOLH film showed a broad peak, which resulted

from amorphous nature the deposited material. The X-ray spectra of the composites (Fig. 6-5B) showed peaks of CCM, HCS, and IDM, which indicated their co-deposition with CHOLH.

Figure 6-6A shows FTIR spectra of pure drugs and a CHOLH deposit. CCM showed absorptions due to C=O stretching [33] at 1628 and 1600 cm^{-1} , the aromatic C–C vibration peaks [33, 34] appeared at 1505 and 1453 cm^{-1} . The in-plane O–H deformation [33] for CCM was observed at 1428 cm^{-1} and the alkene CH₂ scissoring appeared at 1315 cm^{-1} , the C–O stretching peaks were observed at 1271 and 1231 cm^{-1} . Then the aromatic C–H in plane deformation [33] appeared at 1202, 1178, and 1150 cm^{-1} , the aromatic C–H out of plane deformations were observed at 1112 and 1022 cm^{-1} . The FTIR spectra of HCS showed C=O stretching [35] at 1708 cm^{-1} and the aromatic C=C stretchings at 1640, 1628, and 1609 cm^{-1} . In-plane bending bands [35] appeared in the 1300–1000 cm^{-1} region. The C–H in-plane bending vibrations [35] were observed at 1223 and 1000 cm^{-1} . The bands at 1133 and 1047 cm^{-1} were assigned to C–H out-of-plane bending and C–H in-plane bending vibrations [35], respectively. The FTIR spectrum of IDM showed characteristic bands at 1712 cm^{-1} for C=O vibrations of the COO group [36], 1612–1583 and 1475 cm^{-1} for C–C stretching of the aromatic rings, 1685 cm^{-1} for amide group, 1261–1223, and below 1012 cm^{-1} for ether group, C–H deformation, and C–C stretching modes [36]. CHOLH showed peaks related to COOH group stretching at 1703 cm^{-1} and absorptions at 1467 and 1445 cm^{-1} due to C–H and C–C vibrations [24, 37]. The spectra of composite deposits (Fig. 6-6B) showed peaks of the drugs and CHOLH and confirmed their co-deposition.

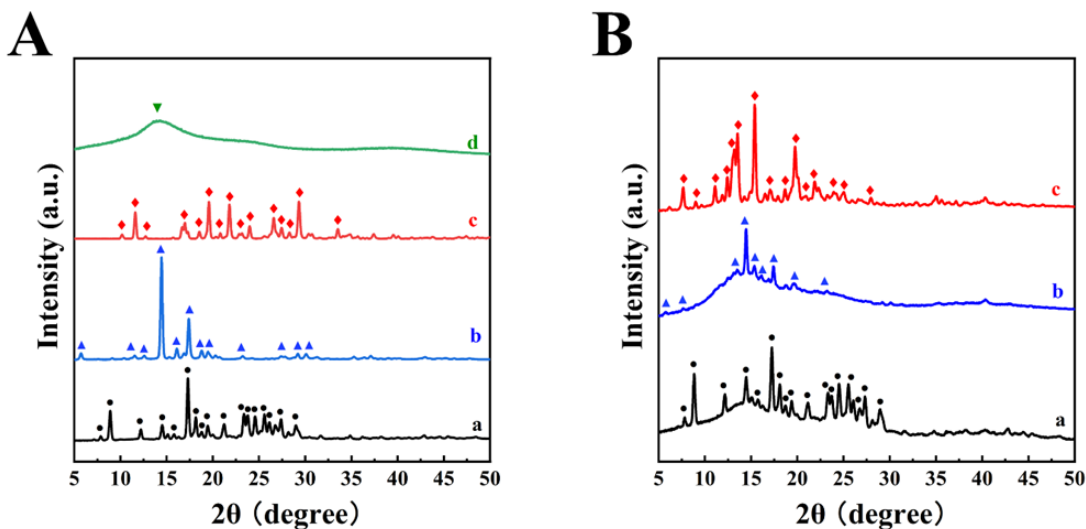


Figure 6-5 XRD patterns for A(a) CCM, A(b) HCS, A(c) IDM, A(d) CHOLH, B(a) CHOLH-CCM, B(b) CHOLH-HCS, B(c) CHOLH-IDM, ●, ▲, ◆ - labels for peaks, corresponding to JCPDS files 66-1420, 15-1016 and 58-1737, respectively.

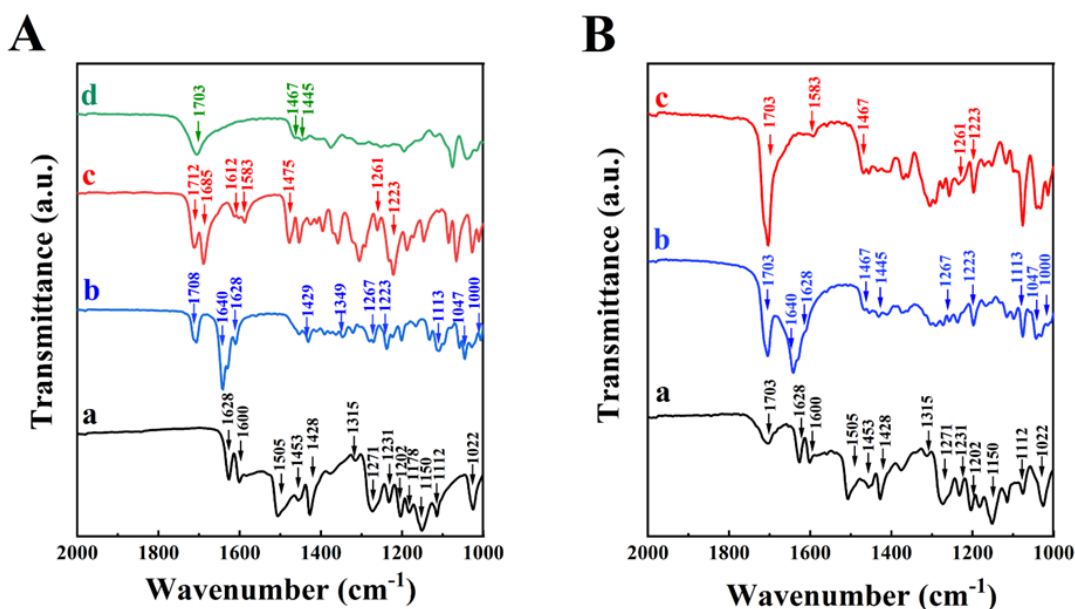


Figure 6-6 FTIR spectra for A(a) CCM, A(b) HCS, A(c) IDM, A(d) CHOLH, B(a) CHOLH-CCM, B(b) CHOLH-HCS, and B(c) CHOLH-IDM

Following the objective of this investigation, we also analyzed the feasibility of co-deposition of BSA, Hb, and HP with CHOLH. As pointed out above, BSA, Hb, and HP cannot be

deposited individually (Fig. 6-2B, C). Figure 6-7 shows SEM images of composite films, prepared from solutions containing BSA, Hb and HP and CHOLH.

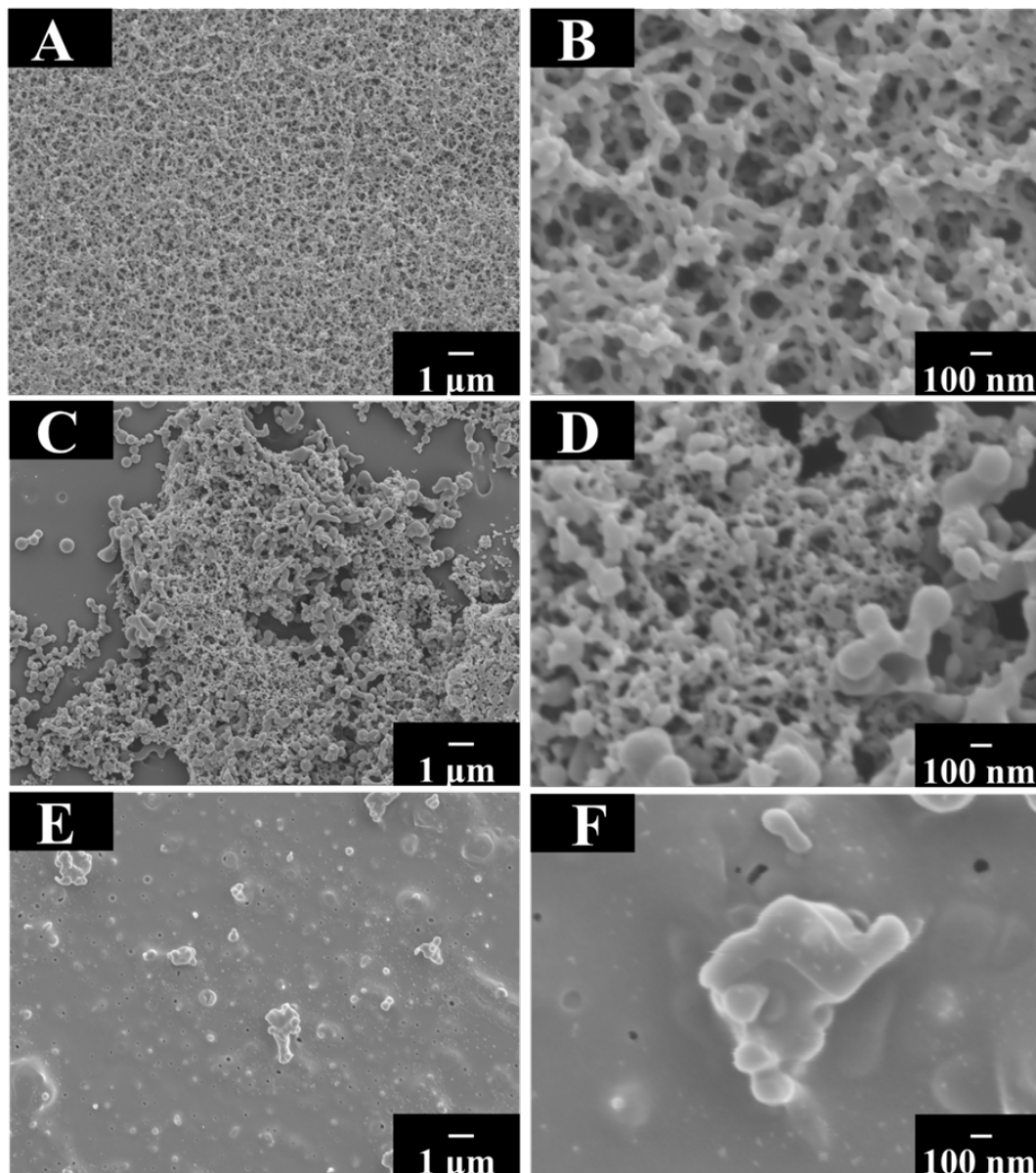


Figure 6-7 SEM images at different magnifications for films prepared from CHOLNa solutions, containing (A,B) BSA, (C,D) Hb and (E,F) HP.

The microstructure of the composite films was different from the microstructure of pure CHOLH films. The CHOLH-BSA films were porous (Fig. 6-7A, B). The SEM image at high

magnification showed a fibrous network with a typical pore size of 50–200 nm. The microstructure of CHOLH-Hb films contained a dense bottom layer and a porous top layer (Fig. 6-7B, C). The CHOL-HP films were dense and contained large particles with a size in the range of 0.1–1 μm . FTIR studies of such films provide evidence of BSA, Hb, and HP co-deposition with CHOLH. Figure 8A shows FTIR spectra of as-received BSA, Hb, and HP. The spectrum of BSA [Fig. 6-8A(a)] showed absorptions related to amide I and amide II bands[38] at 1643 and 1528 cm^{-1} , respectively. FTIR studies of Hb [Fig. 6-8A(b)] also revealed peaks related to amide I and amide II bands [39] at 1645 and 1529 cm^{-1} , respectively.

The absorption peak in the spectrum of HP [Fig. 6-8A(c)] at 1617 cm^{-1} is due to hydroxyl bending [40]. The absorption at 1418 cm^{-1} is related to the carboxylate stretching [40]. The SO_3^- asymmetric and symmetric stretchings [40] of HP resulted in peaks at 1224, 1149, and 1030 cm^{-1} . The FTIR spectra of composite films [Fig. 6-8B(a-c)] showed similar peaks of BSA, Hb, and HP. The peak at 1703 cm^{-1} is related to CHOLH in agreement with the spectrum of pure CHOLH [Fig. 6-6(d)]. EPD was performed at mild aqueous conditions without the use of chemicals, which can react with starting materials. As a result, we didn't observe any changes in the deposited materials, compared to starting materials.

The experimental results presented above indicate that CHOLNa is a versatile multifunctional material for EPD of different biomaterials. Electrically neutral materials must be dispersed and charged for EPD using charged surfactants [41, 42]. CHOLNa addresses the need in biocompatible biosurfactants for aqueous EPD of biomaterials. It is in this regard that many traditional surfactants for EPD are not biocompatible, toxic or can be used for only for non-aqueous EPD. It should be noted that many organic solvents are not chemically compatible with various biomolecules and toxic. CHOLNa can be used as a solubilizing and charging agent for electrically

neutral drug molecules of different types for their aqueous EPD. The interactions of CHOLNa with drugs and formation of mixed micelles facilitates EP of the electrically neutral drug molecules. CHOLNa possesses gel-forming, film-forming properties, and pH-dependent charge, which facilitate the fabrication of composite films by EPD. It is expected that EPD can be used for deposition of other drugs and fabrication of films for drug delivery. Moreover, other electrically neutral functional biomolecules can potentially be deposited by a similar method.

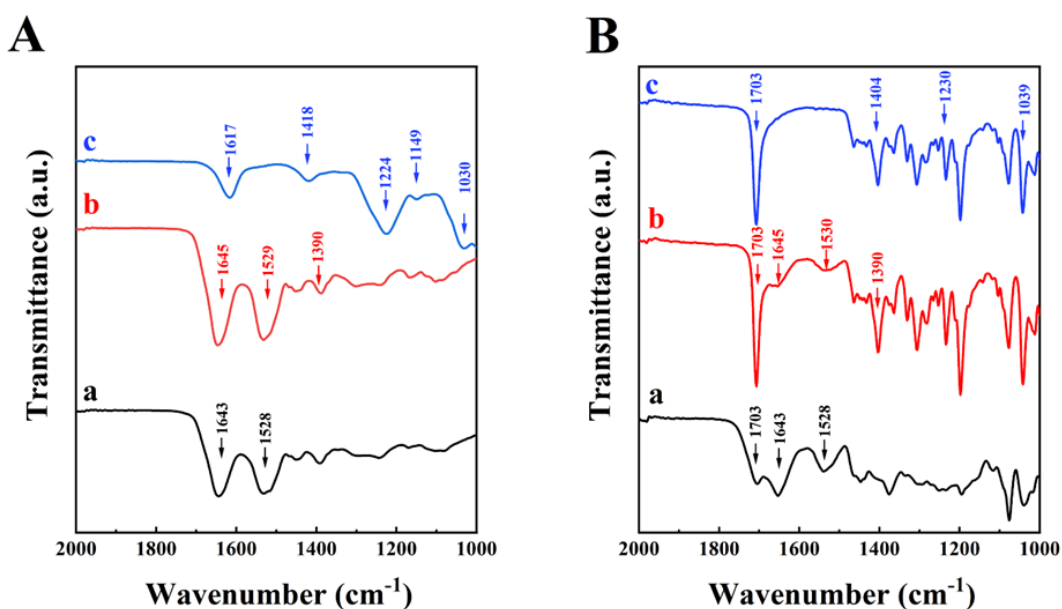


Figure 6-8 FTIR spectra of A(a) BSA, A(b) Hb, A(c) HP, B(a) CHOLH-BSA, B(b) CHOLH-Hb, B(c) CHOLH-HP.

Table 6-1 Methods for EPD of proteins

Proteins	Methods	References
Streptavidin	Co-deposition with chitosan polymer	[43]
Collagen	Deposition on a membrane in the EPD cell between cathode and anode	[44,45]
Gelatin	Co-deposit with Fmoc-phenylalanine	[46]
Bovine Serum Albumin	EPD at AC current	[47]

As pointed out above the EPD of proteins presents difficulties due to their charge reversal at isoelectric points. Table 6-1 summarized previous strategies for the deposition of proteins. Our investigation offers benefits of controlled constant voltage deposition using a charged biosurfactant. CHOLNa facilitates EPD of BSA and Hb, which exhibit pH-dependent charge with charge reversal at their isoelectric points. BSA and Hb were used as model proteins, which cannot be deposited from their pure solutions due to their charge reversal properties. The approach developed in this investigation offers benefits of mild conditions for the immobilization of proteins on inorganic surfaces. BSA is one of the most intensively studied proteins for surface modification of implants. BSA immobilization resulted in reduced bacterial adherence and anti-thrombogenic properties [48]. Hb immobilization on different surfaces is of significant interest for biotechnological applications [49, 50]. Immobilized Hb reduced inflammatory response of implants and improved biocompatibility [51, 52]. Moreover, Hb immobilization techniques are important for the development of biosensors [53]. The approach used for the immobilization of BSA and Hb can also be used for immobilization of enzymes with charge reversal properties for applications in electrochemical biosensors. It is in this regard that CHOLNa is an advanced dispersing agent for EPD of carbon nanotubes [11], which can be co-deposited and offer a benefit of improved electrical conductivity and enhanced electrochemical performance of the biosensors. To explore the possibility of other applications, we performed EPD of anionic HP molecules with pH-independent charge, which cannot be deposited individually [54]. It is known that pH-independent charge is detrimental for EPD [55] and special additives are necessary for film formation. HP is of particular interest for the EPD of composite films for the fabrication of surfaces with antithrombogenic properties [54]. The approach developed in this investigation is conceptually different from previous work on cathodic EPD of non-stoichiometric complexes of

cationic chitosan and anionic HP [54]. The approach developed in this investigation presents simple and versatile strategy for EPD of other functional organic biomolecules and their co-deposition with inorganic materials [1]. This approach can address various challenges in the development of surface modification techniques for biomedical implants and sensors [56–58].

6.5. Conclusions

The solubilization, micelle-forming and gel-forming properties of CHOLNa are key factors for the fabrication of composite films. The use of CHOLNa represents a versatile strategy for EPD of biomolecules of different types, which cannot be deposited independently due to poor solubility, electrical neutrality, charge reversal at isoelectric points, and strong pH-independent charge. The use of natural bile acid salts as multifunctional biosurfactants for deposition at mild conditions from aqueous solutions eliminates limitations of various traditional charging agents for EPD, which are toxic and cannot be used for biomedical applications. Moreover, many traditional surfactants can be used only for EPD in non-aqueous environments, which is not compatible with many functional biomolecules. The EPD mechanism involved the formation of mixed micelles and formation of composite gels at the electrode surface. The results of the XRD and FTIR studies confirmed the formation of composite films. The approach developed for EPD of drugs, proteins, and HP, which were used as model biomaterials for EPD, can be used for the fabrication of films for drug delivery, biosensors, and surface modification of biomedical implants with enhanced biocompatibility. Moreover, this approach can be further developed for co-deposition of functional organic molecules, biopolymers, and inorganic materials, which can be deposited as monolayers or multilayers.

6.6. Acknowledgements

This research was supported by the Natural Sciences and Engineering Research Council of Canada. Electron microscopy studies were performed at the Canadian Centre for Electron Microscopy.

6.7. References

1. K. Baker, R. Sikkema, W. Liang, I. Zhitomirsky, Multifunctional properties of commercial bile salts for advanced materials engineering. *Adv. Eng. Mater.* 23, 2001261 (2021)
2. K. Baker, R. Sikkema, I. Zhitomirsky, Application of bile acids for biomedical devices and sensors. *Med. Devices Sens.* 3, e10119 (2020)
3. S. Reis, C.G. Moutinho, C. Matos, B. de Castro, P. Gameiro, J.L.F.C. Lima, Noninvasive methods to determine the critical micelle concentration of some bile acid salts. *Anal. Biochem.* 334, 117–126 (2004)
4. K. Matsuoka, K. Takagi, C. Honda, Micelle formation of sodium hyodeoxycholate. *Chem. Phys. Lipid.* 172, 6–13 (2013)
5. M. Nemati, A. Fathi-Azarbayjani, H. Al-Salami, E. Roshani Asl, Y. Rasmi, Bile acid-based advanced drug delivery systems, bilosomes and micelles as novel carriers for therapeutics. *Cell Biochem. Funct.* 40, 623–635 (2022)
6. S. Glanzer, S.A. Pulido, S. Tutz, G.E. Wagner, M. Kriechbaum, N. Gubensäk, J. Trifunovic, M. Dorn, W.M. Fabian, P. Novak, Structural and functional implications of the interaction between macrolide antibiotics and bile acids. *Chem.—A Eur. J.* 21, 4350–4358 (2015)

7. T. Yadav, D. Tikariha, S. Sinha, K.K. Ghosh, Biophysical studies on the interactions between antidepressant drugs and bile salts. *J. Mol. Liq.* 233, 23–28 (2017)
8. R. Sikkema, K. Baker, I. Zhitomirsky, Electrophoretic deposition of polymers and proteins for biomedical applications. *Adv. Coll. Interface. Sci.* 284, 102272 (2020)
9. P. Lukaszczuk, E. Borowiak-Palen, M.H. Rummeli, R.J. Kalenczuk, On the efficiency of bile salt for stable suspension and isolation of single-walled carbon nanotubes—spectroscopic and microscopic investigations. *Appl. Phys. A* 100, 505–510 (2010)
10. T.-W. Tsai, G. Heckert, L.F. Neves, Y. Tan, D.-Y. Kao, R.G. Harrison, D.E. Resasco, D.W. Schmidtke, Adsorption of glucose oxidase onto single-walled carbon nanotubes and its application in layer-by-layer biosensors. *Anal. Chem.* 81, 7917–7925 (2009)
11. M.S. Ata, R. Poon, A.M. Syed, J. Milne, I. Zhitomirsky, New developments in non-covalent surface modification, dispersion and electrophoretic deposition of carbon nanotubes. *Carbon* 130, 584–598 (2018)
12. X. Pang, P. Imin, I. Zhitomirsky, A. Adronov, Amperometric detection of glucose using a conjugated polyelectrolyte complex with single-walled carbon nanotubes. *Macromolecules* 43, 10376–10381 (2010)
13. M. Zhang, S. Strandman, K.C. Waldron, X. Zhu, Supramolecular hydrogelation with bile acid derivatives: structures, properties and applications. *J. Mater. Chem. B* 4, 7506–7520 (2016)
14. D. Bariya, V. Anand, S. Mishra, Recent advances in the bile acid based conjugates/derivatives towards their gelation applications. *Steroids* 165, 108769 (2021)

15. C. Huang, X.-B. Cai, L.-L. Guo, X.-S. Qi, Q. Gao, X.-J. Wan, Drug-eluting fully covered self-expanding metal stent for dissolution of bile duct stones in vitro. *World J. Gastroenterol.* 25, 3370 (2019)
16. M. Lei, H. Liao, S. Wang, H. Zhou, Z. Zhao, G.F. Payne, X. Qu, C. Liu, Single step assembly of janus porous biomaterial by subambient temperature electrodeposition. *Small* 18, 2204837 (2022)
17. J. Li, D. Maniar, X. Qu, H. Liu, C.-Y. Tsao, E. Kim, W.E. Bentley, C. Liu, G.F. Payne, Coupling self-assembly mechanisms to fabricate molecularly and electrically responsive films. *Biomacromol* 20, 969–978 (2019)
18. E. Avcu, F.E. Baştan, H.Z. Abdullah, M.A.U. Rehman, Y.Y. Avcu, A.R. Boccaccini, Electrophoretic deposition of chitosan-based composite coatings for biomedical applications: a review. *Prog. Mater Sci.* 103, 69–108 (2019)
19. S. Awasthi, S.K. Pandey, E. Arunan, C. Srivastava, A review on hydroxyapatite coatings for the biomedical applications: experimental and theoretical perspectives. *J. Mater. Chem. B* 9, 228–249 (2021)
20. S. Singh, G. Singh, N. Bala, Electrophoretic deposition of hydroxyapatite-iron oxide-chitosan composite coatings on Ti–13Nb–13Zr alloy for biomedical applications. *Thin Solid Films* 697, 137801 (2020)
21. I. Zhitomirsky, New developments in electrolytic deposition of ceramic films. *Am. Ceram. Soc. Bull.* 79, 57–62 (2000)

22. H. Zhu, H. Liu, I. Zhitomirsky, S. Zhu, Preparation of metalorganic framework films by electrophoretic deposition method. *Mater. Lett.* 142, 19–22 (2015)
23. J. Li, I. Zhitomirsky, Cathodic electrophoretic deposition of manganese dioxide films. *Colloids Surf., A* 348, 248–253 (2009)
24. M. Ata, I. Zhitomirsky, Colloidal methods for the fabrication of carbon nanotube–manganese dioxide and carbon nanotubepolypyrrole composites using bile acids. *J. Colloid Interface Sci.* 454, 27–34 (2015)
25. N.A. Malik, Solubilization and interaction studies of bile salts with surfactants and drugs: a review. *Appl. Biochem. Biotechnol.* 179, 179–201 (2016)
26. S. Kalepu, V. Nekkanti, Insoluble drug delivery strategies: review of recent advances and business prospects. *Acta Pharmaceutica Sinica B* 5, 442–453 (2015)
27. U. Böhme, U. Scheler, Effective charge of bovine serum albumin determined by electrophoresis NMR. *Chem. Phys. Lett.* 435, 342–345 (2007)
28. Y.-Y. Zhang, X. Hu, K. Tang, G.-L. Zou, Immobilization of hemoglobin on chitosan films as mimetic peroxidase. *Process Biochem.* 41, 2410–2416 (2006)
29. M. Hashiba, H. Okamoto, Y. Nurishi, K. Hiramatsu, The zetapotential measurement for concentrated aqueous suspension by improved electrophoretic mass transport apparatus—application to Al₂O₃, ZrO₃ and SiC suspensions. *J. Mater. Sci.* 23, 2893–2896 (1988)
30. B.R. Simonović, M. Momirović, Determination of critical micelle concentration of bile acid salts by micro-calorimetric titration. *Microchim. Acta* 127, 101–104 (1997)

31. K.Y.K. Yamaguchi, K.Y.K. Yujobo, T.K.T. Kaizu, StranskiKrastranov growth of InAs quantum dots with narrow size distribution. *Jpn. J. Appl. Phys.* 39, L1245 (2000)
32. A. Baskaran, P. Smereka, Mechanisms of stranski-krastanov growth. *J. Appl. Phys.* 111, 044321 (2012)
33. S. Gunasekaran, R. Natarajan, S. Natarajan, R. Rathikha, Structural investigation on curcumin. *Asian J. Chem.* 20, 2903 (2008)
34. M.S. Ata, Y. Sun, X. Li, I. Zhitomirsky, Electrophoretic deposition of graphene, carbon nanotubes and composites using aluminon as charging and film forming agent. *Colloids Surf. A* 398, 9–16 (2012)
35. P. Manivannan, R.T. Kumar, V. Periyayagasamy, Spectral analysis of hydrocortisone. *J. Chem. Pharm. Sci* 2, 1–5 (2009)
36. A.V. Ewing, G.S. Clarke, S.G. Kazarian, Stability of indomethacin with relevance to the release from amorphous solid dispersions studied with ATR-FTIR spectroscopic imaging. *Eur. J. Pharm. Sci.* 60, 64–71 (2014)
37. L. Yang, Y. Xu, Y. Su, J. Wu, K. Zhao, J. er Chen, M. Wang, FT-IR spectroscopic study on the variations of molecular structures of some carboxyl acids induced by free electron laser. *Spectrochimica Acta Part A: Mol. Biomol. Spectrosc.* 62, 12091215 (2005)
38. J. Tang, F. Luan, X. Chen, Binding analysis of glycyrrhetic acid to human serum albumin: fluorescence spectroscopy, FTIR, and molecular modeling. *Bioorg. Med. Chem.* 14, 3210–3217 (2006)

39. M. Mahato, P. Pal, B. Tah, M. Ghosh, G. Talapatra, Study of silver nanoparticle–hemoglobin interaction and composite formation. *Colloids Surf., B* 88, 141–149 (2011)
40. A. Devlin, L. Mauri, M. Guerrini, E.A. Yates, M.A. Skidmore, The use of ATR-FTIR spectroscopy to characterise crude heparin samples by composition and structural features. *BioRxiv* (2019). <https://doi.org/10.1101/744532>
41. I. Zhitomirsky, L. Gal-Or, Formation of hollow fibers by electrophoretic deposition. *Mater. Lett.* 38, 10–17 (1999)
42. M.S. Ata, Y. Liu, I. Zhitomirsky, A review of new methods of surface chemical modification, dispersion and electrophoretic deposition of metal oxide particles. *Royal Soc. Chem. Adv.* 4, 22716–22732 (2014)
43. X.W. Shi, Y. Liu, A.T. Lewandowski, L.Q. Wu, H.C. Wu, R. Ghodssi, G.W. Rubloff, W.E. Bentley, G.F. Payne, Chitosan biotinylation and electrodeposition for selective protein assembly. *Macromol Biosci* 8, 451–457 (2008)
44. S.D. Huelin, H.R. Baker, K.M. Poduska, E.F. Merschrod, Aggregation and adsorption of type I collagen near an electrified interface. *Macromolecules* 40, 8440–8444 (2007)
45. M.R. Kumar, E.F. Merschrod, K.M. Poduska, Correlating mechanical properties with aggregation processes in electrochemically fabricated collagen membranes. *Biomacromolecules* 10, 19701975 (2009)
46. J. Alipal, S. Saidin, H.Z. Abdullah, M.I. Idris, T.C. Lee, Physicochemical and cytotoxicity studies of a novel hydrogel nanoclay EPD coating on titanium made of chitosan/gelatin/halloysite for biomedical applications. *Mater. Chem. Phys.* 290, 126543 (2022)

47. A. Braem, K. De Brucker, N. Delattin, M.S. Killian, M.B. Roeffaers, T. Yoshioka, S. Hayakawa, P. Schmuki, B.P. Cammue, S. Virtanen, K. Thevissen, B. Neirinck, Alternating current electrophoretic deposition for the immobilization of antimicrobial agents on titanium implant surfaces. *ACS Appl. Mater. Interfaces* 9, 8533–8546 (2017)

48. Y. An, G. Stuart, S. McDowell, S. McDaniel, Q. Kang, R. Friedman, Prevention of bacterial adherence to implant surfaces with a crosslinked albumin coating in vitro. *J. Orthop. Res.* 14, 846–849 (1996)

49. E. Chiancone, M. Gattoni, A. Boffi, Immobilized human hemoglobin, a versatile matrix for analytical and biotechnological applications. *J. Chromatogr. B Biomed. Sci. Appl.* 715, 81–84 (1998)

50. A. Castañeda-Miranda, V.M. Castaño, Embedded system for the analysis of thermal properties of hemoglobin. *Biomed. Mater. Devices* (2023). <https://doi.org/10.1007/s44174-023-00065-017>

51. T.L. Bonfield, E. Colton, J.M. Anderson, Plasma protein adsorbed biomedical polymers: activation of human monocytes and induction of interleukin 1. *J. Biomed. Mater. Res.* 23, 535–548 (1989)

52. Q. Wang, Q. Gao, J. Shi, Reversible intercalation of large-capacity hemoglobin into in situ prepared titanate interlayers with enhanced thermal and organic medium stabilities. *Langmuir* 20, 10231–10237 (2004)

53. J. Zhang, M. Oyama, A hydrogen peroxide sensor based on the peroxidase activity of hemoglobin immobilized on gold nanoparticles-modified ITO electrode. *Electrochim. Acta* 50, 85–90 (2004)

54. F. Sun, K. Sask, J. Brash, I. Zhitomirsky, Surface modifications of Nitinol for biomedical applications. *Colloids Surf., B* 67, 132–139 (2008)

55. X. Pang, I. Zhitomirsky, M. Niewczas, Cathodic electrolytic deposition of zirconia films. *Surf. Coat. Technol.* 195, 138–146 (2005)

56. M.M. Brigmon, R.L. Brigmon, Infectious diseases impact on biomedical devices and materials. *Biomed. Mater. Devices* (2022). <https://doi.org/10.1007/s44174-022-00035-y>

57. S. Gungordu Er, A. Kelly, S.B.W. Jayasuriya, M. Edirisinghe, Nanofiber based on electrically conductive materials for biosensor applications. *Biomed. Mater. Devices* (2022). <https://doi.org/10.1007/s44174-022-00050-z>

58. H.J. Haugen, A. Schneider, H. Schlicht, H. Wu, E. Doundoula kis, D. Wilhelm, M. Eblenkamp, E. Wintermantel, H. Feussner, Long-term in vivo response of a polyurethane gastric implant for treating gastro-oesophageal reflux diseases: a comparison of different surface treatments. *Biomed. Mater. Devices* (2022). <https://doi.org/10.1007/s44174-022-00055-8>

Chapter 7 Application of Cyrene solvent for the fabrication of polymethyl methacrylate, polyethylmethacrylate and composite films containing hydroxyapatite and diamonds

7.1. Abstract

Cyrene is a new biodegradable solvent, which represents a green alternative to many traditional toxic solvents for polymer processing. It is demonstrated that the feasibility of solubilization of polymethyl methacrylate (PMMA) and polyethyl methacrylate (PEMA) in Cyrene. The ability to form relatively concentrated solutions of the high molecular mass polymers is critical for the formation of PMMA and PEMA films using a dip coating method. The polymer coatings provide corrosion protection of stainless steel in 30 g L⁻¹ NaCl solutions. The use of Cyrene facilitates the fabrication of stable suspensions of hydroxyapatite (HA), microdiamond and nanodiamond particles. This approach addresses the issues of the dispersant selection of chemically inert diamond dispersion and biocompatible dispersants. In the meantime, HA nanorods with reduced particle size are obtained using rutin as a chelating capping agent. Composite films containing HA, microdiamond and nanodiamond in the PMMA or PEMA matrix are obtained as well, which are promising for biomedical applications. The such film's morphology, composition and microstructure are influenced by the solvent-particle-polymer interactions and processing conditions.

7.2. Introduction

Polymethyl methacrylate (PMMA) exhibits advanced properties, which were utilized in solar cells[1], batteries[2], supercapacitors[3], and optical devices[4] such as lenses[5], automotive

windcreens, solar panels and LEDs[6]. Moreover, PMMA is a material of choice for many biomedical applications, including biosensors[7], orthopaedic devices[8], and dental implants[9]. PMMA is being considered for biomedical applications due to its favourable mechanical properties, chemical stability, and biocompatibility[4]. PMMA composites have been developed and successfully applied for controlled medication delivery[10], cranioplasty[11], biomedical implants[12], bone[13] and dental cements[14].

Polyethyl methacrylate (PEMA) is another advanced polymer that exhibits good mechanical strength, thermal stability, biocompatibility, and chemical stability. PEMA has attracted significant interest for a variety of applications, including the repair of bone[15] and cartilage[16], polymer electrolytes and membranes for energy generation and storage devices[17], biodegradable antimicrobial packaging materials[18], optical[19] and electronic components[20], and corrosion protection coatings[21].

PMMA and PEMA are soluble in toxic and carcinogenic solvents, including benzene[22], toluene[23], and methyl ethyl ketone[24]. The use of such solvents represents a significant barrier to PMMA and PEMA in the biomedical applications. Other challenges include the fabrication of composites, containing various functional materials in PMMA or PEMA matrix. Of particular importance are composites, containing hydroxyapatite (HA), which has a composition similar to that of the mineral part of bones[25] and plays an important role in biomedical applications such as tissue engineering[26] and bone implants[27]. There is increasing interest in films containing diamond and nanodiamond for various biomedical applications, including blood contacting biomedical implants, sensors, drug delivery, gene therapy and biomedical imaging[28]. Diamond materials show excellent biocompatibility, cell attachment properties, good corrosion stability, mechanical hardness and wear resistance[29]. There is increasing interest in the development of

composite polymer-diamond films for biomedical applications[30]. However, challenges in the development of composite films are related to the poor dispersion[31] of diamond particles in various solvents. The use of surfactants for diamond dispersion present difficulties due to chemical inertness of the diamond, which limits surfactant adsorption.

This investigation was motivated by unique properties of a new solvent, Cyrene, which we utilized for addressing challenges in the development of PMMA, PEMA and composite films, containing HA and diamonds. Cyrene, also known as dihydrolevoglucosenone[32], has a strong polarity[33], which results from its acetal and ketone groups[34], and it can be categorized as a dipolar aprotic solvent[35]. Cyrene's significant viscosity is advantageous when creating stable dispersions. Cyrene is easily miscible with water and common organic solvents, and it has a high boiling point. This makes it possible to use Cyrene at a variety of temperatures and in blends with other solvents. Cyrene has low volatility, high flash point, low toxicity, lack of mutagenicity and it represents a significant addition to the family of green solvents. Furthermore, during its biodegradation, the Cyrene structure's lack of nitrogen or sulphur atoms prevents NO_x and SO_x from being released. This new green solvent is drawing a lot of attention due to its advantageous environmental benefits[34].

Cyrene is compatible with a wide range of chemical processes[34]. It is found that Cyrene could be used for biomass pretreatment in the biorefinery process and extraction of hesperidin and rutin from natural products[34]. Cyrene was also found to be a sustainable alternative to DMF as a medium for the construction of different metal-organic frameworks[36]. Cyrene showed advanced characteristics for processing graphene, enabling the creation of highly useful conductive graphene inks and concentrated dispersions[37]. On the other hand, Cyrene is a strong solvent that readily dissolves a wide variety of polymeric compounds and it is easily cleaned up

with a water wash. Because of this, Cyrene became the preferred solvent for the following processes: creating poly(lactic-co-glycolic acid) nanoparticles for biomedical purposes[38]; repairing membranes made of polyimide, polysulfone, polyethersulfone, polyethersulfone/graphene oxide, poly(vinylidene fluoride), and cellulose acetate; and creating cathodes with various configurations[39]. The use of Cyrene as a solvent facilitated multiwalled carbon nanotubes dispersion and eliminated the need in surfactants[39]. It also has been investigated as a solvent for biomedical applications polyhydroxyalkanoate[40].

For biomedical applications Cyrene offers antibacterial properties and exhibits solubilizing power towards common antibiotics[32]. Cyrene was applied for the fabrication of poly(D,L-lactide-co-glycolide)-based nanoparticles for efficient drug delivery[38]. Cyrene can solubilize a wide range of organic biomolecules such as aspirin, ibuprofen, salicylic acid, ferulic acid, caffeine and mandelic acid[41]. Cyrene has also demonstrated outstanding biocatalytic performance, acting as both a solvent and a catalyst[34].

The goal of this investigation was the application of Cyrene as a solvent for the fabrication of PMMA, PEMA and composite films by dip coating. It was found that PMMA and PEMA can be dissolved in Cyrene. The ability to dissolve high molecular mass PMMA and PEMA polymers and achieve relatively concentrated solutions coupled with viscosity of Cyrene facilitated film formation by a dip coating method. The films provided corrosion protection of stainless steel. Investigations revealed the influence of processing conditions on film morphology. The HAp nanoparticles prepared using a new capping agent, commercial diamond and nanodiamond powders showed good stability in Cyrene solvent, eliminating the need in a surfactant. Composite films were obtained, containing stable dispersions of HAp and diamonds in PMMA or PEMA solutions using a dip-coating method. The approach developed in this investigation opens an

avenue for the fabrication of various composites, containing different functional materials in PMMA or PEMA matrix.

7.3. Experimental

High molecular weight polymethyl methacrylate (PMMA, $M_w = 350,000$), poly(ethyl methacrylate) (PEMA, $M_w = 515,000$), Cyrene, microdiamond (size < 1), nanodiamond (size < 10 nm), rutin, NH_4OH , $\text{Ca}(\text{NO}_3)_2 \cdot 4\text{H}_2\text{O}$, and $(\text{NH}_4)_2\text{HPO}_4$ were received from the MilliporeSigma company. Stainless steel foils (304 type, $50 \times 25 \times 0.1$ mm) were used as substrates for film deposition.

HA synthesis was performed by slow adding 0.6M $(\text{NH}_4)_2\text{HPO}_4$ aqueous solution into 1.0M $\text{Ca}(\text{NO}_3)_2$ aqueous solution using rutin as a capping agent. The pH of the solutions was adjusted to 11 with NH_4OH . Stirring was performed for 7 h at 70°C . The precipitate was washed with water and dried at room temperature for 24 h.

PMMA and PEMA were dissolved in Cyrene to form 50 g L^{-1} solutions, which were used for dip coating. HA, nanodiamond and microdiamond particles were added to the polymer solutions for the fabrication of composite films for dipping 20 seconds under the room temperature. The particle concentration in the obtained suspensions was $5\text{-}20 \text{ g L}^{-1}$. The suspensions were ultrasonicated before the dip coating. And the film was dried under room temperature.

The film microstructure was examined using a scanning electron microscope[42-45] (SEM, JEOL JSM-7000F). Particle morphology was analyzed using a transmission electron microscope (TEM, Talos 200X, ThermoFisher Scientific). The starting materials and films were examined using a Bruker Smart 6000 X-ray diffractometer (XRD, CuK radiation). Electrochemical characterisation was performed using a PARSTAT 2273 (Ametek) potentiostat-impedance analyzer.

Testing was carried out in 30 g L^{-1} NaCl solution in water using a corrosion cell, containing a working electrode (coated or uncoated stainless steel), counter-electrode (Pt mesh) and a reference electrode (SCE, saturated calomel electrode). The results of potentiodynamic studies (1 mV s^{-1} rate) were presented in Tafel plots. Electrochemical impedance spectroscopy (EIS) data was obtained in the frequency range of 0.01 Hz-10 kHz and voltage amplitude of 5 mV.

7.4. Results and Discussion

PMMA and PEMA showed good solubility in Cyrene. The possibility of forming concentrated solutions of the high molecular weight polymers were key factors for the fabrication of polymer films by a dip coating method. Figure 7-1A,B shows cross section and surface of the PEMA film.

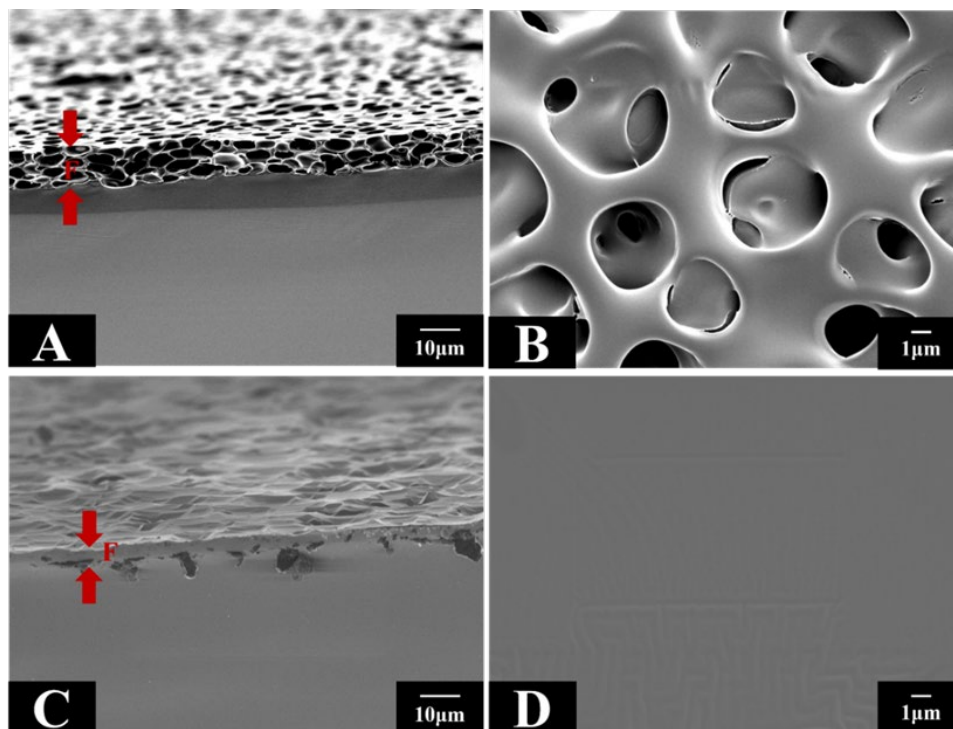


Figure 7-1 SEM images of (A) cross section (F-film) and (B) surface of as-deposited PEMA films, (C) cross section and (D) surface of annealed PMMA films, arrows show film cross section.

The as-deposited PMMA films were porous with a typical pore size of 5 μm . The film thickness was about 10 μm . Annealing of the films at 180°C resulted in relatively dense and crack-free films. As-deposited PEMA films were relatively dense and crack-free (Figure 7-2)

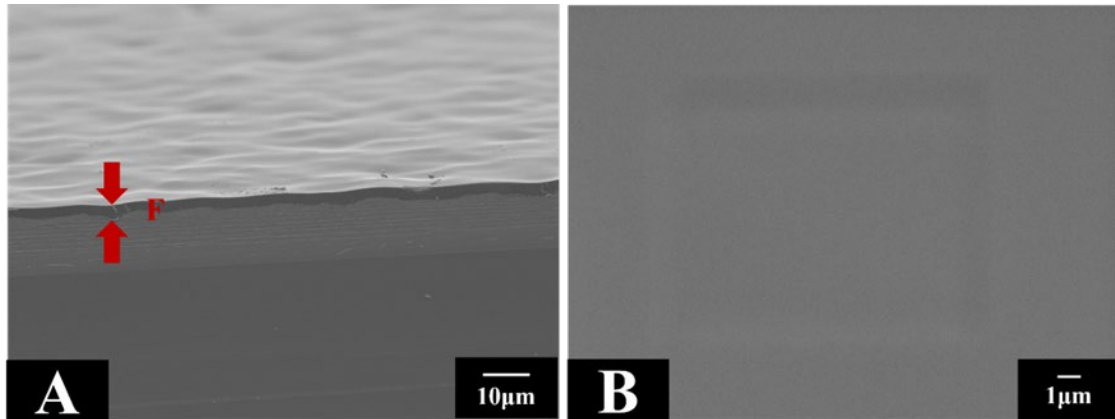


Figure 7-2 SEM images of as-deposited PEMA films: (A) cross section and (B) surface
PMMA and PEMA films provided corrosion protection of stainless steel. Figure 7-3 compares electrochemical impedance spectroscopy data for uncoated and coated stainless steel.

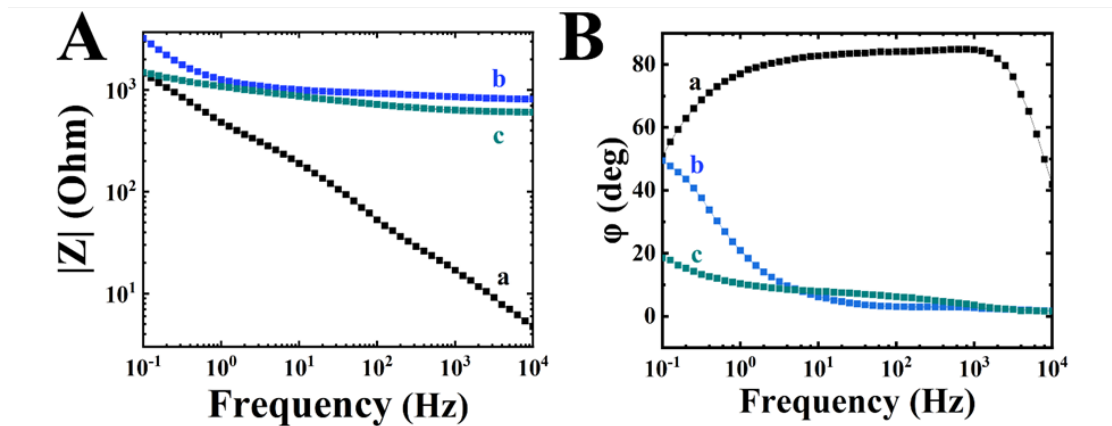


Figure 7-3 Electrochemical impedance spectroscopy data presented in Bode plots (A) absolute value of impedance $|Z|$ and (B) phase angle ϕ for (a) uncoated stainless steel, and (b) coated with PMMA and (c) coated with PEMA. The films were annealed at 180°C for 1 h.

The frequency dependence of impedance $|Z|$ for the uncoated sample showed nearly linear frequency dependence of $\text{Log } |Z|$ versus $\log f$, which indicated significant contribution of the double layer capacitance $Z=1/(C2\pi f)$ of the electrical double layer formed by the electrolyte at the electrode surface. In contrast, the frequency dependences of $|Z|$ for coated samples showed relatively small variations of $|Z|$ with frequency. This can be attributed to the limited electrolyte access to the electrode surface. The coated electrodes showed significantly higher $|Z|$ at high frequencies, compared to the uncoated electrodes. The phase angle ϕ for uncoated electrode showed values close to 80 degrees, which indicated a significant contribution of the capacitive component. In contrast, the coated samples showed significantly lower phase angles due to low capacitance and electrical resistance of the films. Therefore, the films provided a barrier for electrolyte access to the electrode surface. The analysis of potentiodynamic data presented in Tafel plots in Figure 7-4 showed increased corrosion potential of the coated samples, compared to the uncoated stainless steel.

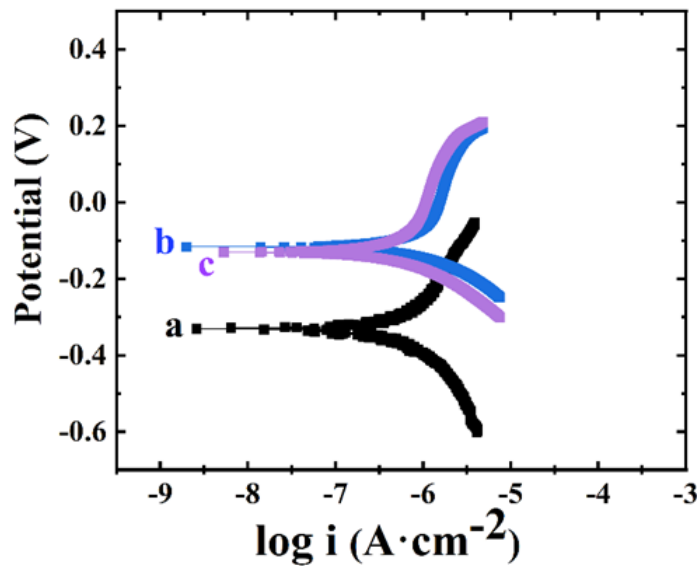


Figure 7-4 Tafel plots for (a) uncoated stainless steel and coated with (b) PMMA and (c) PEMA

Dip-coating method is a versatile technique for the fabrication of composite coatings[46]. Therefore, following the goal of this investigation we applied this method for the fabrication of composite coatings. Nanoparticles of synthesized HA, commercial nanodiamonds and microdiamonds were used. Figure 7-5 shows TEM images of HA nanoparticles prepared by a modified chemical precipitation method. In contrast to the previous investigation[47], we used rutin as a capping agent. Rutin is an important natural biosurfactant, which contains catechol ligands. It was suggested that the catechol ligand of this molecule will provide bonding to the Ca atoms of HA and the rutin adsorption will limit particle growth. The idea of using catecholates as dispersants and capping agents[48] came from the investigation of strong mussel protein adsorption on inorganic surfaces by chelating or bridging bonding of catecholate monomers of the proteins to metal atoms on the material surface.

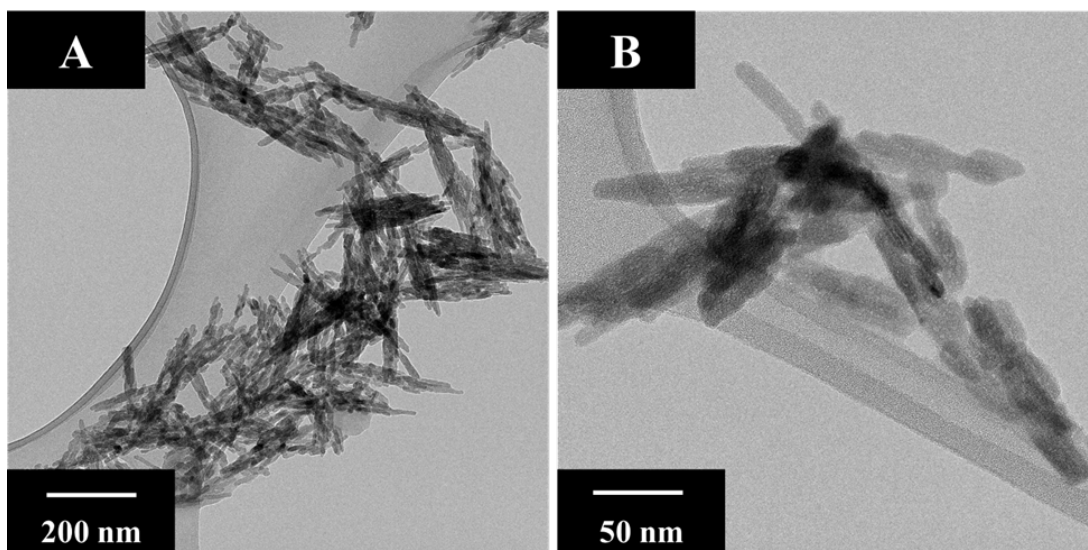


Figure 7-5 (A,B) TEM images at different magnifications of HA nanoparticles synthesized using rutin as a capping agent

Previous synthesis experiments[47] performed without capping agent resulted in HA nanorod particles with a size of 200 nm. The use of rutin as a capping agent facilitated the

formation of nanorods with reduced size of 40-70 nm. However, drying resulted in small agglomeration of the particles.

Figure 7-6A shows X-ray diffraction patterns of starting materials used in this investigation. The X-ray diffraction pattern of PMMA showed broad peaks centered at 2θ of 12, 17 and 30° . The pattern of PEMA showed broad peaks centered at 2θ of 15 and 30° . The XRD studies of microdiamond and nanodiamond showed peaks corresponding to JCPDS file 00-006-0675. The peak on nanodiamond were relatively broad due to the small particle size.

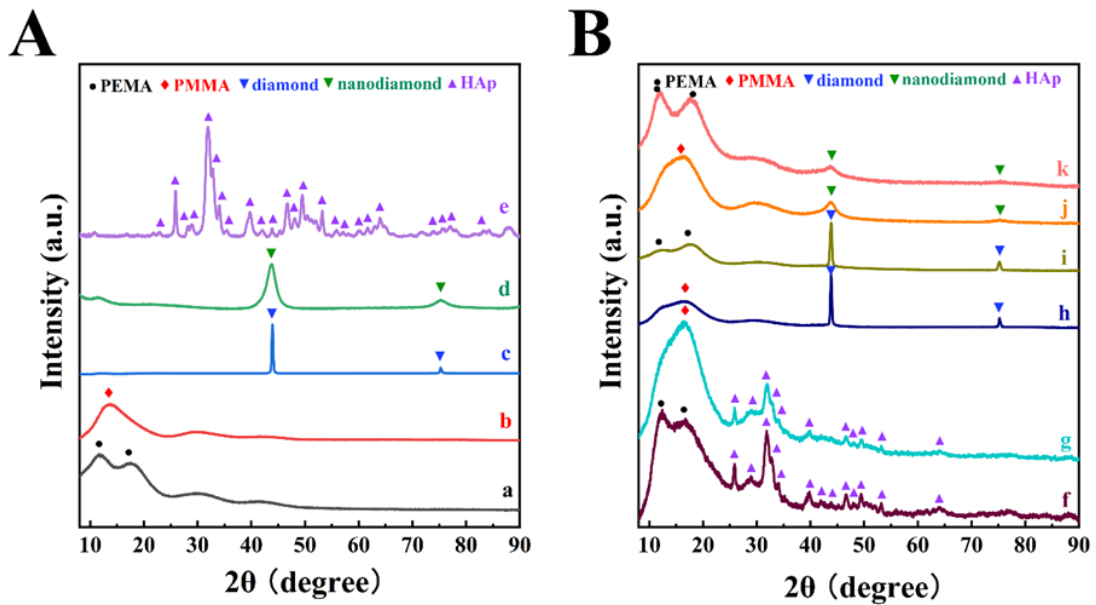


Figure 7-6 X-ray diffraction patterns of (A) starting materials: (a) PMMA, (b) PEMA, (c) microdiamond, (d) nanodiamond, (e) HA and (B) deposited composite materials (f) PMMA-HAp, (g) PEMA-HA, (h) PEMA-microdiamond, (i) PMMA-microdiamond, (j) PEMA-nanodiamond, (k) PMMA-nanodiamond (▼-peaks corresponding to JCPDS file 00-006-0675 of diamond, ▲ - peaks corresponding to JCPDS file 00-009-0432 of HA).

The X-ray diffraction peaks of the synthesized HA corresponded to the JCPDS file 00-009-0432 and confirmed successful synthesis of this material.

The use of Cyrene as a solvent facilitated the formation of stable suspensions. It is known that particle-solvent interactions play an important role in the formation of stable suspensions[49].

Therefore, Cyrene offers benefits of the formation of stable suspensions without the use of dispersants. It is in this regard that the selection of dispersants for biomedical applications presents difficulties, because some advanced dispersants for colloidal processing are toxic and cannot be used for biomedical applications[49]. It is challenging to find dispersants for chemically inert diamond particles[49]. X-ray diffraction studies confirmed co-deposition of polymers and particles (Figure 7-6B). The comparison of the diffraction patterns of individual materials (Figure 6A) and composites (Figure 7-6B) confirmed the formation of PEMA-HA, PMMA-HA, PEMA-nanodiamond, PMMA-nanodiamond, PEMA-microdiamond and PMMA-microdiamond films. The diffraction patterns of the composite films contained characteristic peaks of the individual components. The use of dip coating method offers benefits for the deposition of complex compounds, such as HA because stoichiometry of the deposited material is controlled by the stoichiometry of the starting material.

The formation of composite coatings was also confirmed by SEM. Figure 7-7 shows SEM images for PMMA-HA and PEMA-HA films obtained from suspensions with different HA concentrations. The SEM images show HA in the polymer matrix and confirm co-deposition. The increase in the particle concentration in the suspension from 5 to 20 g L⁻¹ resulted in the increased number of particles in the deposited films. Therefore, the coating composition can be varied. As pointed out above, pure PMMA coatings were porous. However, the porosity was eliminated in coatings containing HA.

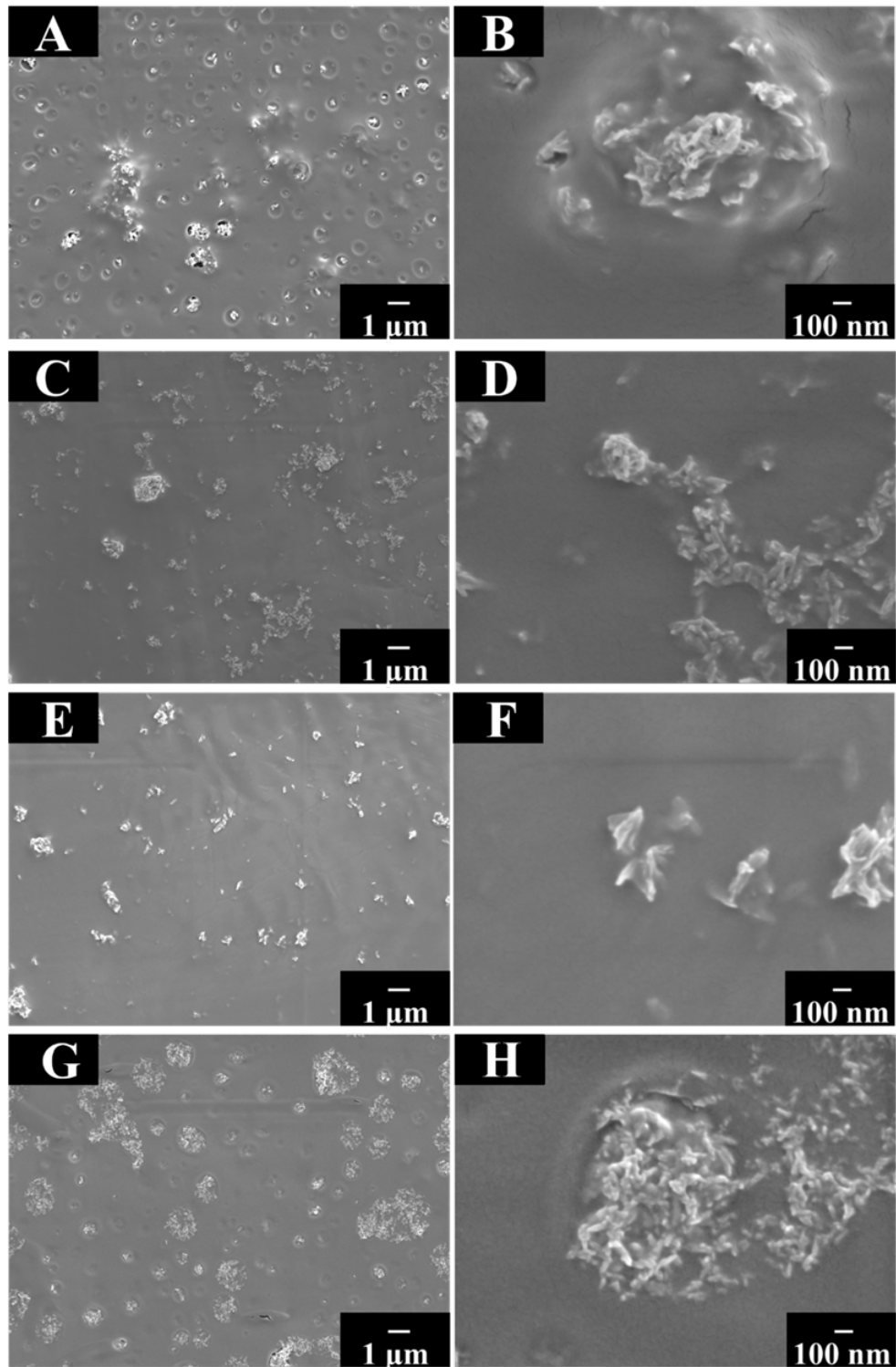


Figure 7-7 SEM images at different magnifications for films prepared from 50 g L⁻¹ PMMA solutions, containing (A,B) 5 g L⁻¹ and (C,D) 20 g L⁻¹ HA and 50 g L⁻¹ PEMA solutions, containing (E,F) 5 g L⁻¹ and (G,H) 20 g L⁻¹ HA.

Composite films containing microdiamonds were also obtained using suspensions of microdiamond in solutions of PMMA and PEMA in Cyrene. Figure 7-8 shows SEM images at different magnifications for PMMA-microdiamond and PEMA-microdiamond films. The images show microdiamond particles and confirm their co-deposition with polymers. The increase in particles concentration in suspensions resulted in increasing number of the particles in the films. The addition of microdiamond to the PMMA solution resulted in elimination of porosity in the PMMA matrix. However, small pores were observed between the particles due to their packing (Figure 7-8D).

Composite PMMA-nanodiamond and PEMA-nanodiamond films (Figure 7-9) were also obtained and showed similar features, as indicated by the incorporation of the nanodiamond particles into PMMA and PEMA films, elimination of porosity of the PMMA films and increase in nanodiamond content in the films with increasing nanodiamond concentration in the suspensions. However, the analysis of SEM images of the deposited films showed enhanced agglomeration of the nanodiamond particles.

It is suggested that the formation of composite films is governed by polymer-solvent, particle-solvent, particle-polymer, polymer-polymer and particle-particle interactions. Cyrene facilitated the dissolution of high molecular weight polymers and fabrication of concentrated suspensions, which were critically important for the deposition of the polymers by a dip-coating method. High molecular weight polymers exhibit enhanced film-forming properties. High concentration of the high molecular weight polymer promoted polymer-polymer interactions and facilitated film formation. The particle-solvent and particle-polymer interactions allowed dispersion of the HA, microdiamond and nanodiamond particles in the suspensions, containing dissolved polymers.

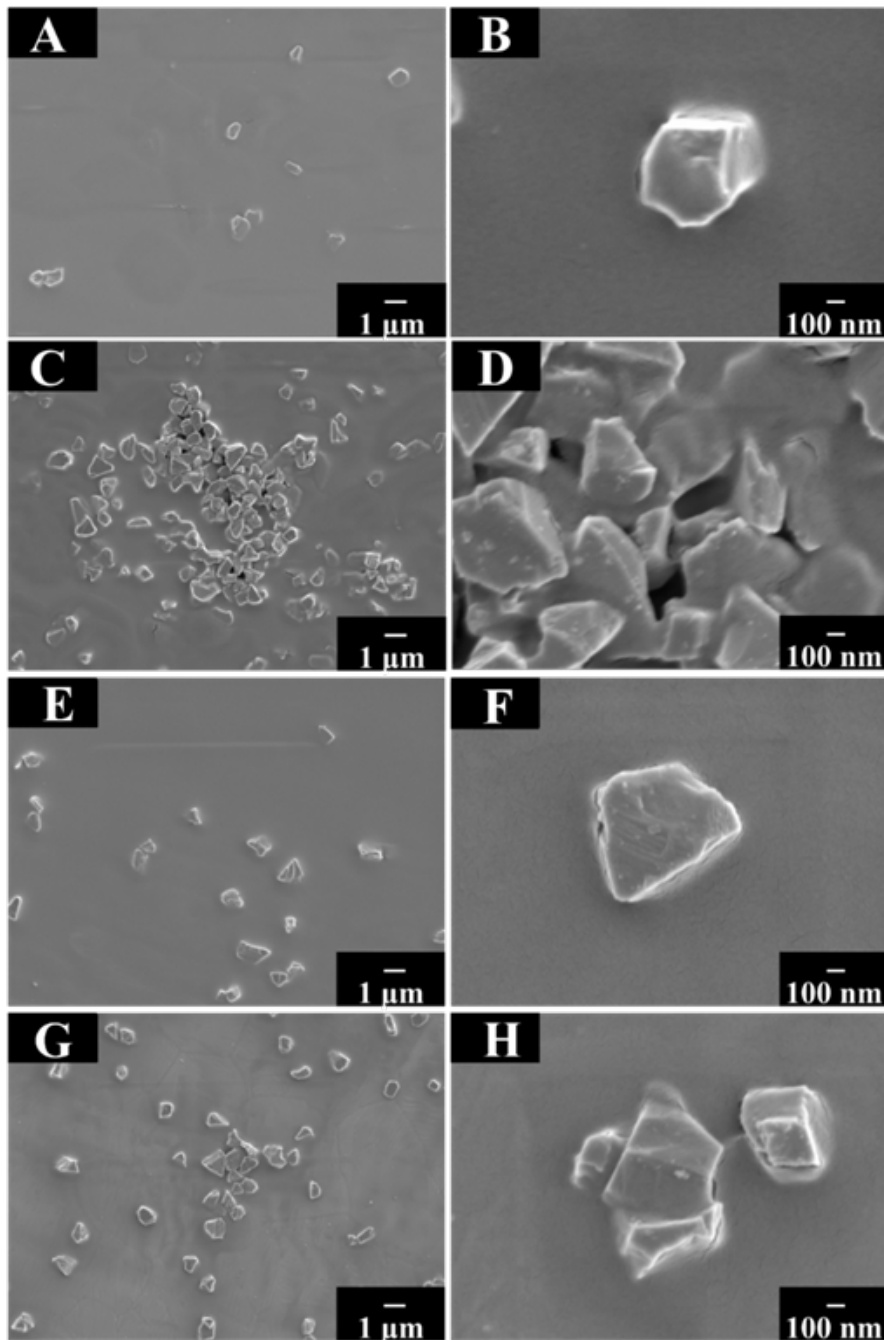


Figure 7-8 SEM images at different magnifications for films prepared from 50 g L⁻¹ PMMA solutions, containing (A,B) 5 g L⁻¹ and (C,D) 20 g L⁻¹ microdiamond and 50 g L⁻¹ PEMA solutions, containing (E,F) 5 g L⁻¹ and (G,H) 20 g L⁻¹ microdiamond.

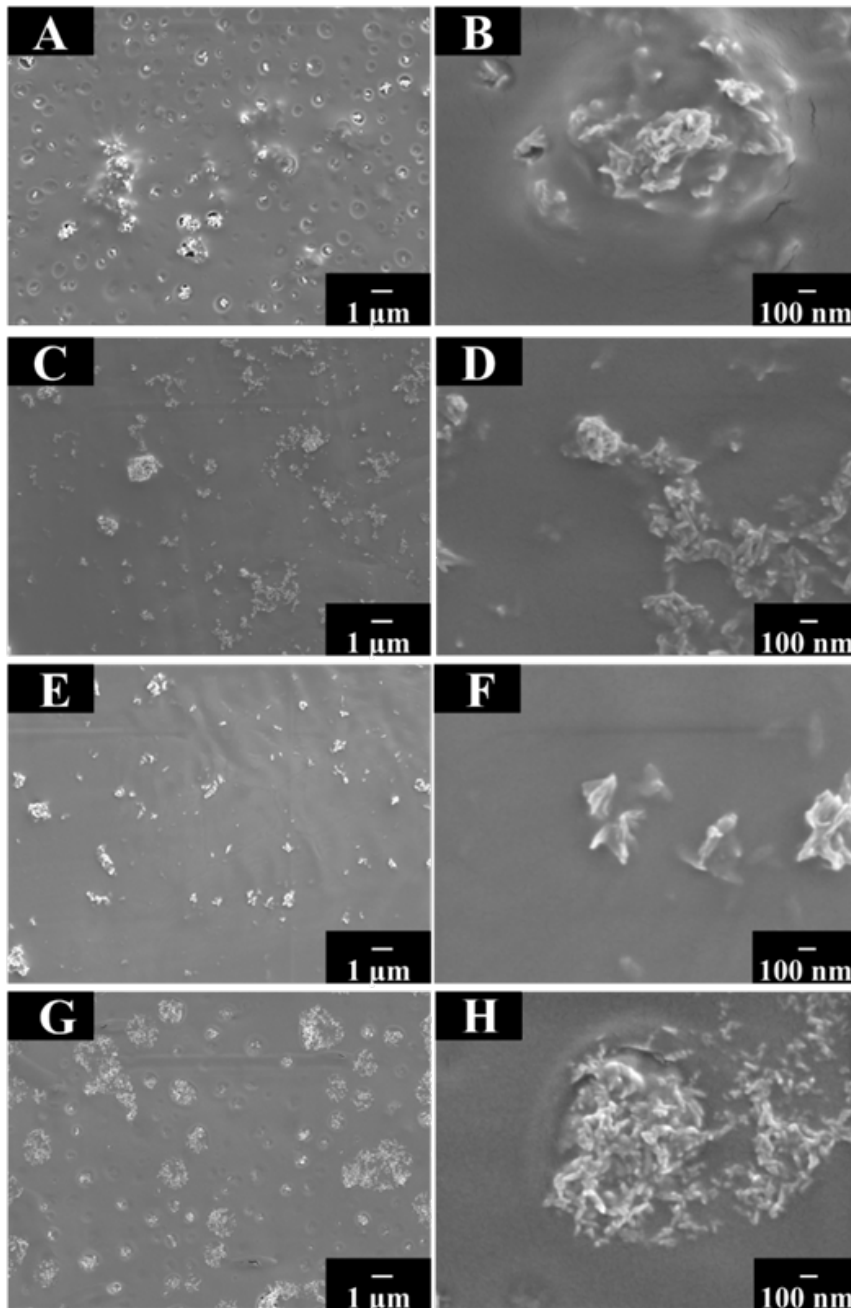


Figure 7-9 SEM images at different magnifications for films prepared from 50 g L⁻¹ PMMA solutions, containing (A,B) 5 g L⁻¹ and (C,D) 20 g L⁻¹ nanodiamond and 50 g L⁻¹ PEMA solutions, containing (E,F) 5 g L⁻¹ and (G,H) 20 g L⁻¹ nanodiamond

Such interactions facilitated co-deposition of particles and polymers. However, the SEM images (Figures 7-9) showed agglomeration of the particles in the polymer matrix, which can result from solvent evaporation, elimination of particle-solvent interactions and enhanced effect of

particle-particle interactions. It is in this regards that microdiamond particles showed enhanced agglomeration, which can result from their higher surface area. The particle-polymer interactions resulted in elimination of porosity of PMMA based composite films, which was observed in pure PMMA films. The results of this work coupled with literature data on feasibility of solubilization of various functional biomolecules[41] in Cyrene opens an avenue for the fabrication of composite films with enhanced functionality, which can be deposited as single layers, multilayers or films of graded microstructure and composition.

7.5. Conclusion

The feasibility of solubilization of PMMA and PEMA in Cyrene was demonstrated. Cyrene is a promising biodegradable solvent, which represents a green alternative to traditional solvents, which are toxic and carcinogenic. The ability to form relatively concentrated solutions of the high molecular mass polymers was a key factor for the formation of PMMA and PEMA films by a dip coating method. The polymer coatings provided corrosion protection of stainless steel in 30 g L⁻¹ NaCl solutions. The use of Cyrene facilitated the fabrication of stable suspensions of HA, microdiamond and nanodiamond particles. In this approach, the problems of the dispersant selection for dispersion of chemically inert diamond and development of biocompatible dispersants were successfully addressed. HA nanorods with reduced particle size were obtained using rutin as a chelating catecholate-type capping agent. Composite films containing HA, microdiamond and nanodiamond in the PMMA or PEMA matrix were obtained. The composite films are promising for biomedical applications. The film morphology, composition and microstructure were influenced by the solvent-particle-polymer interactions and processing conditions. The results of this work coupled with literature data on solubility of various functional

biomolecules in Cyrene open possibility for fabrication of films with advanced functionality for biomedical and other applications.

7.6. Acknowledgements

Research supported by the Natural Sciences and Engineering Research Council of Canada, grant RGPIN-2018-04014 and CRC program. Electron microscopy studies were performed at the Canadian Centre for Electron Microscopy.

7.7. References

- [1] Y. Beilei et al., "PMMA passivated CsPbI₂Br perovskite film for highly efficient and stable solar cells," *Journal of Physics and Chemistry of Solids*, vol. 153, p. 110000, 2021, doi: <https://doi.org/10.1016/j.jpics.2021.110000>.
- [2] N.-S. Choi and J.-K. Park, "New polymer electrolytes based on PVC/PMMA blend for plastic lithium-ion batteries," *Electrochimica Acta*, vol. 46, no. 10-11, pp. 1453-1459, 2001.
- [3] N. C. Abeykoon, J. S. Bonso, and J. P. Ferraris, "Supercapacitor performance of carbon nanofiber electrodes derived from immiscible PAN/PMMA polymer blends," *Rsc Advances*, vol. 5, no. 26, pp. 19865-19873, 2015.
- [4] X. Li and I. Zhitomirsky, "Deposition of poly(methyl methacrylate) and composites containing bioceramics and bioglass by dip coating using isopropanol-water co-solvent," (in en), *Progress in Organic Coatings*, vol. 148, p. 105883, 2020/11// 2020, doi: [10.1016/j.porgcoat.2020.105883](https://doi.org/10.1016/j.porgcoat.2020.105883).

[5] U. Ali, K. J. B. A. Karim, and N. A. Buang, "A Review of the Properties and Applications of Poly (Methyl Methacrylate) (PMMA)," (in en), *Polymer Reviews*, vol. 55, no. 4, pp. 678-705, 2015/10/02/ 2015, doi: 10.1080/15583724.2015.1031377.

[6] J. James et al., "Optical and physical properties of zirconium dioxide reinforced poly(methyl methacrylate) nanocomposite films," *Journal of Applied Polymer Science*, vol. 141, no. 8, p. e54977, 2023, doi: 10.1002/app.54977.

[7] S. R. Nugen, P. J. Asiello, J. T. Connelly, and A. J. Baeumner, "PMMA biosensor for nucleic acids with integrated mixer and electrochemical detection," *Biosensors and Bioelectronics*, vol. 24, no. 8, pp. 2428-2433, 2009.

[8] T. Jaeblo, "Polymethylmethacrylate: properties and contemporary uses in orthopaedics," *JAAOS-Journal of the American Academy of Orthopaedic Surgeons*, vol. 18, no. 5, pp. 297-305, 2010.

[9] M. S. Zafar, "Prosthetic applications of polymethyl methacrylate (PMMA): An update," *Polymers*, vol. 12, no. 10, p. 2299, 2020.

[10] M. Lin et al., "Structure and release behavior of PMMA/silica composite drug delivery system," *Journal of pharmaceutical sciences*, vol. 96, no. 6, pp. 1518-1526, 2007.

[11] S.-C. Lee, C.-T. Wu, S.-T. Lee, and P.-J. Chen, "Cranioplasty using polymethyl methacrylate prostheses," *Journal of clinical neuroscience*, vol. 16, no. 1, pp. 56-63, 2009.

[12] A. D'Elia, J. Deering, A. Clifford, B. E. J. Lee, K. Grandfield, and I. Zhitomirsky, "Electrophoretic deposition of polymethylmethacrylate and composites for biomedical

applications," *Colloids Surf B Biointerfaces*, vol. 188, p. 110763, Apr 2020, doi: 10.1016/j.colsurfb.2019.110763.

[13] J. Webb and R. Spencer, "The role of polymethylmethacrylate bone cement in modern orthopaedic surgery," *The Journal of Bone & Joint Surgery British Volume*, vol. 89, no. 7, pp. 851-857, 2007.

[14] M. Hossain, J. H. Jeong, T. Sultana, J. H. Kim, J. E. Moon, and S. Im, "A composite of polymethylmethacrylate, hydroxyapatite, and beta-tricalcium phosphate for bone regeneration in an osteoporotic rat model," *J Biomed Mater Res B Appl Biomater*, vol. 111, no. 10, pp. 1813-1823, Oct 2023, doi: 10.1002/jbm.b.35287.

[15] R. Wyre and S. Downes, "An in vitro investigation of the PEMA/THFMA polymer system as a biomaterial for cartilage repair," *Biomaterials*, vol. 21, no. 4, pp. 335-343, 2000.

[16] S. Rawal, "Poly (Ethyl Methacrylate) (PEMA) and its Composites for Various Applications: Background, Recent Progress, and Future challenges," *Macromolecular Symposia*, vol. 413, no. 1, p. 2300096, 2024, doi: 10.1002/masy.202300096.

[17] S. Jayanthi, S. Shenbagavalli, M. Muthuvinayagam, and B. Sundaresan, "Effect of nano TiO₂ on the transport, structural and thermal properties of PEMA-NaI solid polymer electrolytes for energy storage devices," *Materials Science and Engineering: B*, vol. 285, p. 115942, 2022.

[18] F. Mohanty and S. K. Swain, "Nano silver embedded starch hybrid graphene oxide sandwiched poly(ethylmethacrylate) for packaging application," (in en), *Nano-Structures & Nano-Objects*, vol. 18, p. 100300, 2019/04// 2019, doi: 10.1016/j.nanoso.2019.100300.

[19] S. Fares, "Influence of gamma-ray irradiation on optical and thermal degradation of poly (ethyl-methacrylate)(PEMA) polymer," *Natural Science*, vol. 4, no. 7, pp. 499-507, 2012.

[20] M. El-Sharnouby et al., "Enhanced electrical conductivity and dielectric performance of ternary nanocomposite film of PEMA/PS/silver NPs synthesized by laser ablation," *Journal of Inorganic and Organometallic Polymers and Materials*, vol. 32, no. 6, pp. 2269-2278, 2022.

[21] E. Nieuwenhuis, C. Pathmamanoharan, and A. Vrij, "Liquid-like structures in concentrated latex dispersions. a light-scattering study of pmma particles in benzene," *Journal of Colloid and Interface Science*, vol. 81, no. 1, pp. 196-213, 1981.

[22] A. R. Iyer, V. B. Mitevska, J. J. Samuelson, S. W. Campbell, and V. R. Bhethanabotla, "Sorption of Benzene, Toluene, and Ethylbenzene at Low Concentrations by Plasticized Poly (ethyl methacrylate) and Polystyrene Polymers Using a Quartz Crystal Microbalance at 298.15 K," *Journal of Chemical & Engineering Data*, vol. 66, no. 8, pp. 3354-3359, 2021.

[23] C. B. Walsh and E. I. Franses, "Ultrathin PMMA films spin-coated from toluene solutions," *Thin Solid Films*, vol. 429, no. 1-2, pp. 71-76, 2003.

[24] K. Kaur, A. R. Iyer, S. W. Campbell, and V. R. Bhethanabotla, "Sorption of benzene, toluene, and ethylbenzene by poly (ethyl methacrylate) and plasticized poly (ethyl methacrylate) AT 298.15 k using a quartz CRYSTAL Microbalance," *Journal of Chemical & Engineering Data*, vol. 65, no. 10, pp. 5046-5054, 2020.

[25] K. Gholivand, S. A. Alavinasab Ardebili, M. Mohammadpour, R. Eshaghi Malekshah, S. Hasannia, and B. Onagh, "Preparation and examination of a scaffold based on

hydroxylated polyphosphazene for tissue engineering: In vitro and in vivo studies," *Journal of Applied Polymer Science*, vol. 139, no. 20, p. 52179, 2022, doi: 10.1002/app.52179.

[26] N. Ingwattanapok, Y. Sakunrak, and N. Tangboriboon, "Bio composite of porous hydroxyapatite and collagen extracted from eggshell membrane and *Oreochromis niloticus* fish skin for bone tissue applications," *Journal of Applied Polymer Science*, vol. 140, no. 41, p. e54527, 2023, doi: 10.1002/app.54527.

[27] R. Watanabe et al., "Novel nano-hydroxyapatite coating of additively manufactured three-dimensional porous implants improves bone ingrowth and initial fixation," *J Biomed Mater Res B Appl Biomater*, vol. 111, no. 2, pp. 453-462, Feb 2023, doi: 10.1002/jbm.b.35165.

[28] P. C. Pandey, S. Shukla, G. Pandey, and R. J. Narayan, "Nanostructured diamond for biomedical applications," *Nanotechnology*, vol. 32, no. 13, p. 132001, 2021.

[29] P. A. Nistor and P. W. May, "Diamond thin films: giving biomedical applications a new shine," *Journal of the Royal Society Interface*, vol. 14, no. 134, p. 20170382 (15 pp.), 2017, doi: 10.1098/rsif.2017.0382.

[30] Z. Wang and I. Zhitomirsky, "Surfactant assisted dip-coating method for deposition of polyethylmethacrylate-diamond coatings," *Advances in Applied Ceramics. Structural, Functional and Bioceramics*, vol. 122, pp. 226-235, / 2023, doi: 10.1080/17436753.2023.2230008.

[31] I. Zhitomirsky, "Cathodic electrophoretic deposition of diamond particles," *Materials Letters*, vol. 37, no. 1, pp. 72-78, 1998/09/01/ 1998, doi: [https://doi.org/10.1016/S0167-577X\(98\)00074-3](https://doi.org/10.1016/S0167-577X(98)00074-3).

[32] D. Kong and A. V. Dolzhenko, "Cyrene: A bio-based sustainable solvent for organic synthesis," (in en), *Sustainable Chemistry and Pharmacy*, vol. 25, p. 100591, 2022/04// 2022, doi: 10.1016/j.scp.2021.100591.

[33] J. E. Camp, "Bio-available Solvent Cyrene: Synthesis, Derivatization, and Applications," (in en), *ChemSusChem*, vol. 11, no. 18, pp. 3048-3055, 2018/09/21/ 2018, doi: 10.1002/cssc.201801420.

[34] Y. Wang, M. Dai, G. Luo, J. Fan, J. H. Clark, and S. Zhang, "Preparation and Application of Green Sustainable Solvent Cyrene," (in en), *Chemistry*, vol. 5, no. 4, pp. 2322-2346, 2023/10/21/ 2023, doi: 10.3390/chemistry5040154.

[35] T. Brouwer and B. Schuur, "Dihydrolevoglucosenone (Cyrene), a Biobased Solvent for Liquid–Liquid Extraction Applications," (in en), *ACS Sustainable Chem. Eng.*, vol. 8, no. 39, pp. 14807-14817, 2020/10/05/ 2020, doi: 10.1021/acssuschemeng.0c04159.

[36] J. Zhang, G. B. White, M. D. Ryan, A. J. Hunt, and M. J. Katz, "Dihydrolevoglucosenone (Cyrene) As a Green Alternative to *N,N*-Dimethylformamide (DMF) in MOF Synthesis," (in en), *ACS Sustainable Chem. Eng.*, vol. 4, no. 12, pp. 7186-7192, 2016/12/05/ 2016, doi: 10.1021/acssuschemeng.6b02115.

[37] K. Pan et al., "Sustainable production of highly conductive multilayer graphene ink for wireless connectivity and IoT applications," (in en), *Nat Commun*, vol. 9, no. 1, p. 5197, 2018/12/05/ 2018, doi: 10.1038/s41467-018-07632-w.

[38] A. Czapka et al., "Drug delivery of 6-bromoindirubin-3'-glycerol-oxime ether employing poly(d,l-lactide-co-glycolide)-based nanoencapsulation techniques with sustainable

solvents," (in en), *J Nanobiotechnol*, vol. 20, no. 1, pp. 1-21, 2022/12// 2022, doi: 10.1186/s12951-021-01179-7.

[39] R. Poon and I. Zhitomirsky, "Application of Cyrene as a solvent and dispersing agent for fabrication of Mn₃O₄-carbon nanotube supercapacitor electrodes," (in en), *Colloid and Interface Science Communications*, vol. 34, p. 100226, 2020/01// 2020, doi: 10.1016/j.colcom.2019.100226.

[40] P. Tomietto et al., "Sustainable fabrication and pervaporation application of bio-based membranes: Combining a polyhydroxyalkanoate (PHA) as biopolymer and Cyrene™ as green solvent," (in en), *Journal of Membrane Science*, vol. 643, p. 120061, 2022/03// 2022, doi: 10.1016/j.memsci.2021.120061.

[41] M. De Bruyn et al., "Geminal Diol of Dihydrolevoglucosenone as a Switchable Hydrotrope: A Continuum of Green Nanostructured Solvents," (in en), *ACS Sustainable Chem. Eng.*, vol. 7, no. 8, pp. 7878-7883, 2019/04/15/ 2019, doi: 10.1021/acssuschemeng.9b00470.

[42] K. Vijayendra Gopal, K. R. Vijaya Kumar, J. Jayaseelan, G. Suresh, R. Vezhavendhan, and R. Ganesamoorthy, "Analyzing the Tribological Behavior of Titanium Dioxide (TiO₂) Particulate Filled Jute Fiber Reinforced Interpenetrating Polymer Network (IPNs) Composite by using Taguchi Optimization Technique," *Tribology in Industry*, vol. 45, no. 1, pp. 226-236, 2023, doi: 10.24874/ti.1448.02.23.04.

[43] K. V. Gopal, K. R. V. Kumar, G. Suresh, V. Rajasekharan, P. K. Nagarajan, and C. M. Meenakshi, "Investigation of TiO₂ Nano Filler in Mechanical, Thermal Behaviour of Sisal/Jute Fiber Reinforced Interpenetrating Polymer Network (IPN) Composites," *Materials Research*, vol. 25, 2022, doi: 10.1590/1980-5373-mr-2022-0406.

[44] R. Manikandan et al., "An investigation on thermo-mechanical characterization of activated carbon/coconut shell powder reinforced natural composites," Proceedings of the Institution of Mechanical Engineers, Part E: Journal of Process Mechanical Engineering, p. 09544089221132721, 2022.

[45] J. Rajaparthiban, G. Suresh, R. Ganesamoorthy, K. R. Padmavathi, S. H. M. Abbas, and C. M. Meenakshi, "Effect of polyurethane ratio on mechanical behavior of banana fiber/polyurethane-vinylester matrix composites," *Matéria (Rio de Janeiro)*, vol. 27, p. e13182, 2022.

[46] R. Oriňaková et al., "Biodegradable zinc-based materials with a polymer coating designed for biomedical applications," *Journal of Applied Polymer Science*, vol. 141, no. 2, p. e54773, 2023, doi: 10.1002/app.54773.

[47] X. Pang and I. Zhitomirsky, "Electrophoretic deposition of composite hydroxyapatite-chitosan coatings," *Materials Characterization*, vol. 58, no. 4, pp. 339-348, 2007/04/01/ 2007, doi: <https://doi.org/10.1016/j.matchar.2006.05.011>.

[48] M. S. Ata, Y. Liu, and I. Zhitomirsky, "A review of new methods of surface chemical modification, dispersion and electrophoretic deposition of metal oxide particles," *RSC Advances*, 10.1039/C4RA02218A vol. 4, no. 43, pp. 22716-22732, 2014, doi: 10.1039/C4RA02218A.

[49] I. Zhitomirsky, "Cathodic electrodeposition of ceramic and organoceramic materials. Fundamental aspects," *Advances in Colloid and Interface Science*, vol. 97, no. 1, pp. 279-317, 2002/03/29/ 2002, doi: [https://doi.org/10.1016/S0001-8686\(01\)00068-9](https://doi.org/10.1016/S0001-8686(01)00068-9)

Chapter 8 Strategies for alkali-free synthesis, surface modification and electrophoretic deposition of composite films for biomedical applications

8.1. Abstract

This investigation addresses increasing interest in composites for biomedical applications and advanced methods for their synthesis and electrophoretic deposition (EPD). The feasibility of preparation of hydroxyapatite (HA), titania and zirconia particles using branched polyethylenimine polymer (BPEI) or L-arginine amino acid as organic alkalizers is demonstrated. In this approach, BPEI and L-arginine are used as alkalizers-capping agents instead of inorganic alkalis. The use of BPEI facilitates synthesis of HA nanorods with reduced size. The advantages of this strategy for the fabrication of nanoparticles are discussed. Composite films are obtained by cathodic EPD using linear polyethylenimine (LPEI) as a charging and film-forming agent. A conceptually new approach is developed for anodic EPD of alginic acid polymer (AlgH) and composite films containing drug molecules in AlgH matrix. This strategy involved the use of L-arginine as an alkalizer for solubilization of drugs, which exhibit poor solubility in water. AlgH and drug molecules are solubilized in water and deposited by anodic EPD. Testing results confirm the fabrication of composite films, containing drug molecules. The synthesis and deposition methods developed in this investigation can be used for synthesis of other inorganic nanomaterials, EPD of other polymers and their co-EPD with bioceramics, drugs and other functional materials.

8.2. Introduction

Electrophoretic deposition (EPD) of materials from colloidal suspensions or polymer solutions is an important method for depositing different materials and composites[1-5]. EPD benefits include a high rate of deposition, uniform film formation on large surface area substrates, excellent control of film thickness and deposition rate [6, 7]. This method allows fabrication of thick coatings, thin films and patterned films [8]. EPD is a flexible and inexpensive method for the deposition of metal oxides, hydroxides, metals, ceramics, polymers, and other organic and inorganic materials. The high purity of the deposits makes EPD particularly important for biomedical applications[3, 4, 9].

EPD of polymers can be performed by cathodic or anodic methods[10]. Moreover, cationic and anionic polymers can be used as charging and dispersing additives for surface modification, dispersion and deposition of other materials. Polymers for cathodic or anodic deposition usually contain amino or carboxylic groups, respectively. The pH-dependent charge and solubility of such polymers are critically important for film deposition.

Polyethylenimine (PEI) has attracted significant interest for surface modification, dispersion and cathodic EPD of materials. PEI is of particular interest for various biomedical applications, such as biomedical imaging[11-14], gene delivery[15-17], controlled drug delivery[17-20], biosensors[21], antimicrobial materials[22-26], surface functionalization of biomaterials[27], biomedical scaffolds[28] and gels[29]. The chemical structure of branched PEI (BPEI) contains primary, secondary and tertiary amino groups (Figure 1A). In contrast, linear polyethylenimine (LPEI) has only secondary amino groups (Figure 1B). At room temperature, LPEI is solid (melting point 73-75°C), while BPEI is liquid (regardless of molecular weight). LPEI dissolves in ethanol, methanol, chloroform, and hot water with a low pH[16, 19, 30]. BPEI is

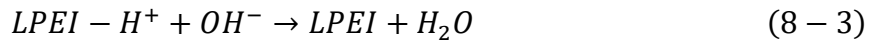
soluble in water at room temperature and forms basic solutions due to the protonation of amino groups and corresponding increase in OH⁻ concentration in the solution. BPEI is used for charging and dispersion of ceramic particles and facilitates their EPD[31-33]. However, pure BPEI films cannot be deposited by EPD due to high solubility of this polymer. In contrast, LPEI films can be deposited by cathodic EPD [34]. LPEI can be protonated and dissolved in acidic aqueous solutions:



The process of deposition involved the cataphoresis of protonated LPEI-H⁺ towards the cathode surface, where a local pH increased due to the reaction:



The deprotonation and charge neutralization of LPEI-H⁺ accumulated at the electrode surface facilitated film formation [34]:



A similar approach is used for deposition of other cationic polymers, containing amino groups, such as chitosan[4, 35], poly-l-lysine and poly-l-ornithine[36] for various biomedical applications.

Anodic deposition is used for polymers with carboxylic groups, such as alginic acid[37], hyaluronic acid[38], and polyacrylic acid[39]. Alginic acid is a naturally occurring polysaccharide derived from brown algae. The chemical structure of alginic acid (Figure 8-1C) contains blocks of α -L-guluronic acid and β -D-mannuronic acid[40]. The anionic properties of alginic acid are related to carboxylic groups. Because of its low toxicity, low cost, biocompatibility, and biodegradability, alginic acid is a very desirable polymer for biomedical applications. Alginate exhibits great

potential as a material for the encapsulation of drugs, proteins, and enzymes as well as for the fabrication of biosensors, scaffolds and coatings for biomedical implants[41]. EPD of alginate acid films was carried out using solutions of sodium alginate (AlgNa) [37]. Film formation was aided by the anodic local pH decrease in the following reaction:

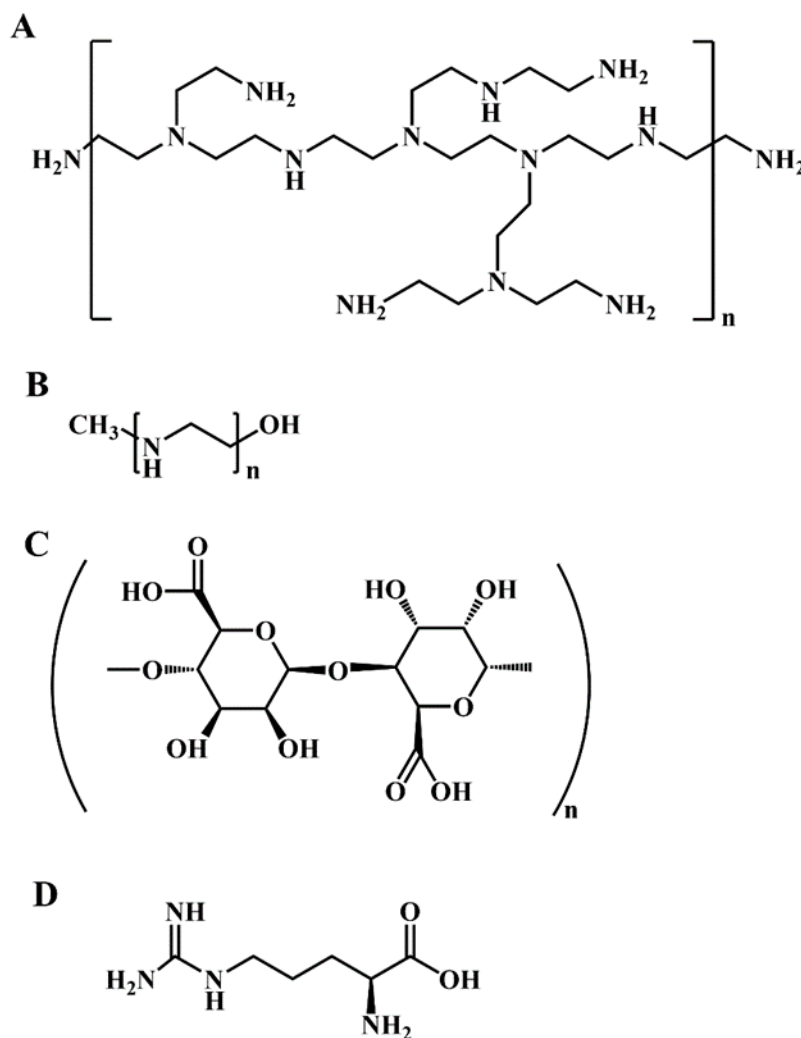
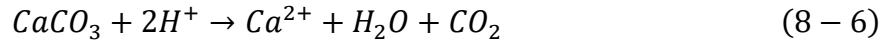


Figure 8-1 Chemical structures of (A) BPEI, (B) LPEI, (C) AlgH and (D) L-arginine.

Anionic Alg- macromolecules were accumulated at the anode surface and a local pH drop facilitated the production of water-insoluble alginate acid films[37].



EPD of AlgH and composites was demonstrated to be a viable technique for surface modification of biomedical implants [37]. Another deposition mechanism was developed for calcium alginate films[42, 43]. AlgNa solutions containing CaCO₃ particles were used for EPD. The dissolution of CaCO₃ was caused by the pH drop at the anode surface:



The interaction of Ca²⁺ and Alg⁻ facilitated the formation of calcium alginate films[42, 43]. The ability to create calcium alginate films at mild pH values is advantageous[44] for many applications.

This investigation is motivated by increasing interest in EPD of polymers and composite materials for biomedical applications and the need for the development of novel materials preparation and EPD strategies. The objective of this investigation was the development of new strategies for material preparation and EPD of composite films. LPEI and AlgH were used as model polymers for cathodic and anodic EPD, respectively. The approach was based on the use of BPEI and L-arginine as alkalizers-dispersants instead of inorganic alkalis for synthesis of bioceramic nanoparticles, such as hydroxyapatite, zirconia and titania. The use of L-arginine offers benefits for biomedical applications because it is one of the twenty amino acids that are found in proteins. In addition to the typical acid and amine groups, this molecule has a highly basic guanidinium group (Figure 8-1D). L-arginine is widely used as alkalizer for solubilization and delivery of various drugs, which exhibit poor solubility in water [45-47]. We demonstrated that the synthesis of fine bioceramic nanoparticles can be performed without the use of inorganic alkalis and described benefits of this approach. Composite LPEI-bioceramic coatings were obtained by

cathodic EPD. In another strategy, L-arginine was used for the development of new method for EPD of AlgH films. This approach is conceptually different from previous investigations [37]. It is based on the solubilization of AlgH in L-arginine solutions and formation of insoluble AlgH films in an anodic EPD process. The new approach offers benefits of high deposition rate. Moreover, it offers multiple advantages for deposition of composite films. As a step in this direction, we used L-arginine as an alkalizer for dissolution of alginic acid and an anionic drug and obtained composite film by co-EPD. The strategies developed in this investigation can be used for synthesis of other materials and EPD of other polymers and composites by cathodic and anodic methods for biomedical and other applications.

8.3.Experimental

Calcium nitrate tetrahydrate, branched polyethylenimine (BPEI, $M_w=110,000$), ammonium phosphate dibasic, zirconyl chloride octahydrate, titanium oxysulfate solution, L-arginine, alginic acid (AlgH, $M_w=200,000$) and ibuprofen were purchased from Millipore Sigma company. Linear polyethylenimine (LPEI, $M_w=250,000$) was supplied by Polysciences, Inc.

Precipitation of calcium phosphates was performed at a temperature of 60 °C by a slow addition of 0.6 M ammonium phosphate solution into 1.0 M calcium nitrate solution. The experiments were performed without pH adjustment or with adjusting pH of the individual solutions to pH=10 using BPEI or L-arginine. Stirring was performed for 1 h at 60 °C and 2 h at room temperature. The precipitates were washed with water and dried.

Synthesis of zirconia was performed using aqueous 0.005M zirconyl chloride solutions. Synthesis of titania was performed from titanium oxysulfate solutions. In this procedure, 1 mL of titanium oxysulfate solution was added to 50 mL of water. The pH of the solutions was adjusted

to pH=9 by adding PEI or L-arginine. Obtained precipitates were washed with DI water, dried and annealed for 1 h at 400 or 600 °C.

LPEI was dissolved in water by adding acetic acid [34]. Cathodic EPD of composites was performed using a mixed water-ethanol solvent (20% water). The influence of solvent composition on EPD process was discussed in a previous investigation [48]. The use of water was important for base generation in reaction (2). The use of ethanol reduced the electrical conductivity of the suspensions and allowed EPD at a higher voltage, which facilitated electrophoresis of ceramic particles. Cathodic EPD was performed from 2 g L⁻¹ LPEI solutions, containing 5 g L⁻¹ of bioceramics, such as hydroxyapatite (HA), zirconia and titania. Ultrasonication was performed for 10 min in order to obtain stable suspensions for EPD.

The use of AlgH as a starting material instead of AlgNa facilitated the fabrication of solutions with lower electrical conductivity and EPD was performed from aqueous solutions. The solutions were obtained by dissolution of AlgH in DI water in the presence of L-arginine as an alkalizer. The pH of the 1 g L⁻¹ AlgH solutions was pH=9. L-arginine facilitated dissolution of ibuprofen in the same solution. EPD was performed from 1 g L⁻¹ AlgH solutions without and with 2 g L⁻¹ ibuprofen.

A type 304 stainless steel (dimensions 25 × 30 × 0.12 mm) was used as the substrate electrode, while a platinum sheet (dimensions 25 × 30 × 0.1 mm) acted as the counter electrode, with a 17 mm spacing between them in the EPD cell. An Amersham Biosciences EPS 2A200 power supply was used for EPD. EPD was performed for 5 min at a deposition voltage of 15 V between two electrodes for cathodic deposition and 10 V for anodic deposition.

The materials were examined using a Bruker Smart 6000 X-ray diffractometer (XRD, CuK radiation). Microstructure analysis was carried out using a JEOL JSM-7000F (Tokyo, Japan) scanning electron microscope (SEM) and a Talos 200X (ThermoFisher Scientific, Waltham, MA, USA) transmission electron microscope (TEM). A Bruker Vertex 70 spectrometer was used for the Fourier Transform Infrared Spectroscopy (FTIR) experiments.

8.4. Results and Discussion

The approach developed in this investigation is based on proton-sponge effect[49] of BPEI and L-arginine, which resulted in pH increase in their solutions. Figure 8-2A shows X-ray diffraction patterns of the calcium phosphate materials synthesized without pH adjustment and using BPEI or L-arginine as alkalizers.

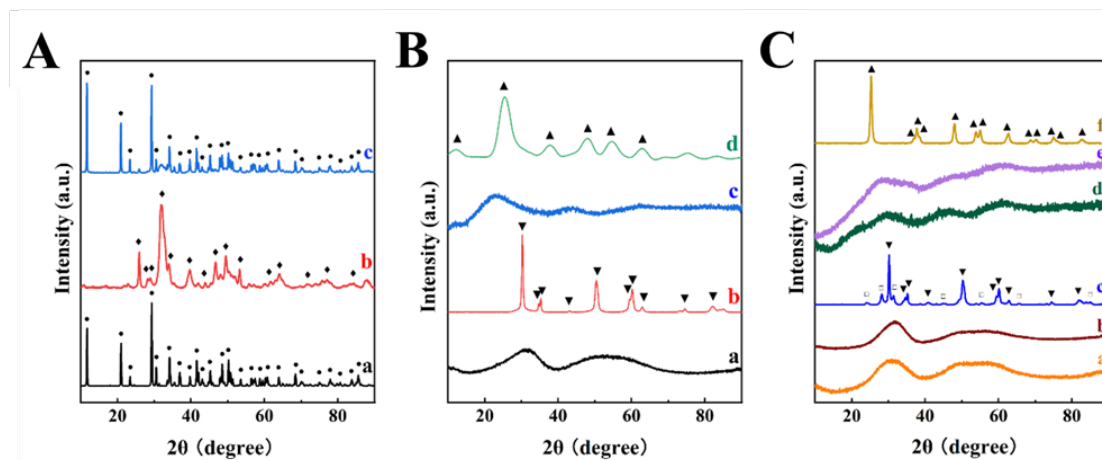


Figure 8-2 X-ray diffraction patterns of (A) calcium phosphate materials, prepared (a) without pH adjustment, (b) using BPEI for pH adjustment, (c) using L-arginine for pH adjustment, (● - peaks corresponding to JCPDS file 04-013-3344 of brushite, ◆ - peaks corresponding to JCPDS file 00-009-0432 of HA); (B) (a,b) zirconia, (c,d) titania, (a,c) as-precipitated, (b,d) annealed at 400°C for 1 h, (▼ - peaks corresponding to JCPDS file 01-075-9646 of tetragonal zirconia, ▲ – peaks corresponding to JCPDS file 04-014-5762 of anatase titania prepared using BPEI); (C) (a,b,c) zirconia, (d,e,f) titania, (a,d) as-prepared, (b,e) annealed at 400°C for 1 h, (c,f) annealed at 600°C for 1 h, (▼ - peaks corresponding to JCPDS file 01-075-9646 of tetragonal zirconia, □ – peaks corresponding to JCPDS file 00-037-1484 of monoclinic zirconia, ▲ – peaks corresponding to JCPDS file 04-014-5762 of anatase titania) prepared using L-arginine.

The precipitate obtained without pH adjustment showed XRD peaks of a brushite $\text{CaHPO}_4 \cdot 2\text{H}_2\text{O}$ phase. In contrast, the use of BPEI for pH adjustment resulted in successful synthesis of HA. Previous investigations showed that pH control during synthesis was critically important for the HA synthesis[50-52]. The pH control was achieved using NH_4OH for pH adjustment of individual 0.6 M ammonium phosphate and 1.0 M calcium nitrate solutions before their mixing. However, the use of NH_4OH for the formation of buffer solutions with fixed pH requires application of a special reactor with cooled condensers for ammonia containing vapor in a fume hood. Additional difficulties are related to the disposal of NH_4OH containing chemical waste. Such difficulties can be avoided using BPEI, which offers benefits of more environmentally friendly and very simple synthesis equipment and procedure. Therefore, the HA synthesis can be simplified, and it offers tremendous benefits for mass scale production. It will be shown below that BPEI offers additional advantages, because it also acts as a capping agent for synthesis of nanoparticles.

The fabrication procedure performed using L-arginine as an alkalizer resulted in synthesis of a brushite $\text{CaHPO}_4 \cdot 2\text{H}_2\text{O}$ phase. It is suggested that the size and adsorption of the alkalizer molecule exerts influence on the crystallization behavior. It is in this regard that BPEI and other polyelectrolytes, containing amino groups, such as chitosan and polyallylamine showed strong interaction with HA[50, 51, 53, 54]. BPEI showed strong adsorption on the HA particles[53]. The chitosan-HA interactions resulted in crystallographic orientation of HA nanorods in the composite chitosan-HA films prepared by EPD [50, 51]. Polyallylamine promoted HA synthesis inside the polyelectrolyte capsules[54].

The synthesis of zirconia and titania in the presence of BPEI and L-arginine resulted in amorphous precipitates (Figure 8-2B,C). Crystallization of tetragonal zirconia and anatase titania

phases was observed after annealing at 400°C for materials prepared using BPEI (Figure 2B). However, crystallization was observed at higher temperatures for the precipitates obtained using L-arginine (Figure 8-2C). The X-ray diffraction pattern of zirconia showed peaks of the metastable tetragonal and stable monoclinic phase after annealing of the precipitates at 600°C (Figure 8-2 C). The annealing of the titania precipitate at 600°C resulted in the formation of anatase (Figure 8-2 C). Therefore, the results of XRD studies confirmed synthesis of zirconia and titania using BPEI and L-arginine as alkalizers.

Figure 8-3 shows TEM images of precipitated powders obtained using BPEI and L-arginine. The HA particles, prepared using BPEI, showed a rod-like morphology (Figure 8-3A). The length of the nanorods was in the range of 40-80 nm. It should be noted that the size of the nanorods prepared using NH₄OH was about 200 nm [50, 51]. Therefore, the use of BPEI as an alkalizer-capping agent allowed the fabrication of nanorods with a reduced size. The titania particles formed using BPEI showed a nanorod morphology with a typical size 80-150 nm (Figure 8-3B). The zirconia particles precipitated using BPEI were very fine with a size below 10 nm (Figure 8-3C).

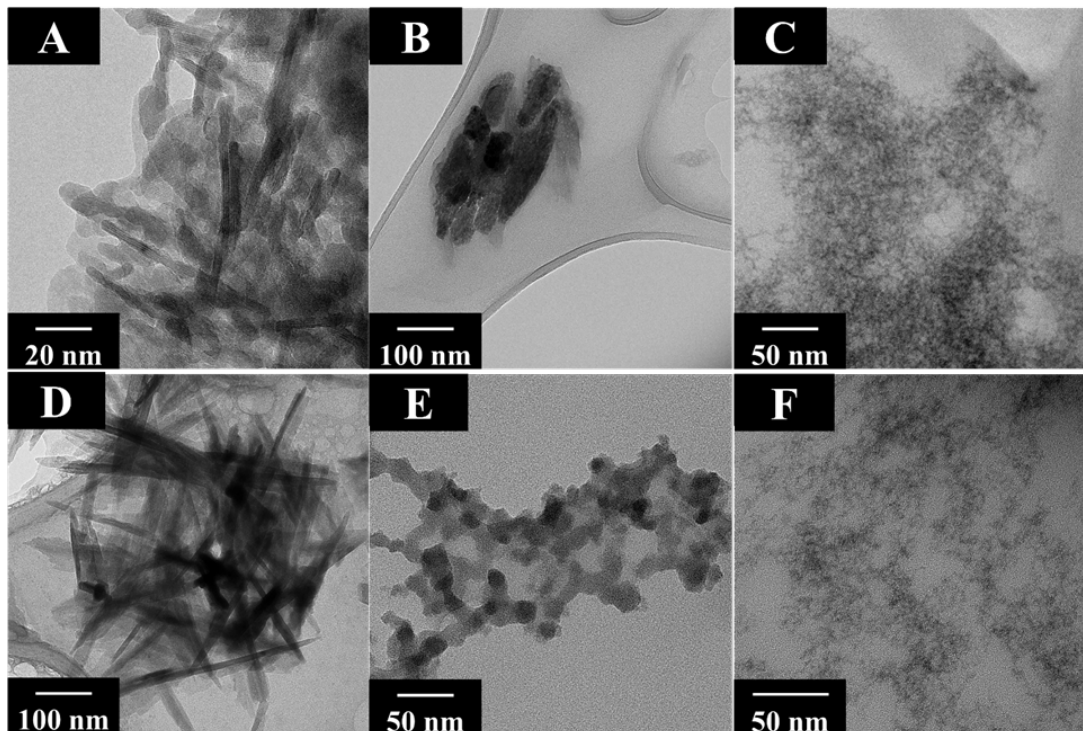


Figure 8-3 . TEM images of precipitates obtained using (A-C) BPEI and (D-F) (L-arginine), (A) HA, (D) brushite, (B,E) titania, (C, F) zirconia

The brushite particles formed in the presence of L-arginine showed a needle-shape morphology, the length of the needles was 100-300 nm (Figure 8-3D). The morphology of the titania particles formed using L-arginine was different from the morphology of the particles synthesized in the presence of BPEI. The use of L-arginine resulted in particles with nearly cubic shape and size ~ 10 nm, which showed agglomeration (Figure 8-3E). The zirconia particles precipitated in the presence of L-arginine were very fine with a typical size below 5 nm (Figure 8-3F).

As-prepared calcium phosphates, annealed zirconia and titania were used for cathodic EPD. LPEI was used as a model cationic polymer for EPD. The deposition mechanism of pure LPEI was

discussed in the Introduction section. It is based on the use of protonated LPEI. It was found that the protonated LPEI facilitated charging of the inorganic particles and allowed for the fabrication of composite films. The formation of the composite films was confirmed by SEM.

Figure 8-4 shows SEM images of composite films, containing inorganic particles synthesized using BPEI. The SEM images show the HA, titania and zirconia particles, co-deposited with LPEI. The SEM images revealed agglomeration of HA, titania and zirconia particles. It is suggested that drying of the particles and their annealing promoted agglomeration. The brushite, titania and zirconia particles prepared using L-arginine were also successfully co-deposited with LPEI. Figure 8-5 shows SEM images of the composite films. The films were crack-free and contained bioceramic particles. LPEI-titania films showed significant porosity, which resulted from packing of titania particles. The SEM images showed many titania particles. In contrast, the LPEI-zirconia films were relatively dense and contained zirconia particles in the LPEI matrix. The higher deposition yield of titania particles can result from better adsorption of LPEI on titania, which imparted a positive charge to the particles for their deposition. The annealed particles prepared using L-arginine showed smaller size and reduced agglomeration, compared to annealed particles prepared using BPEI.

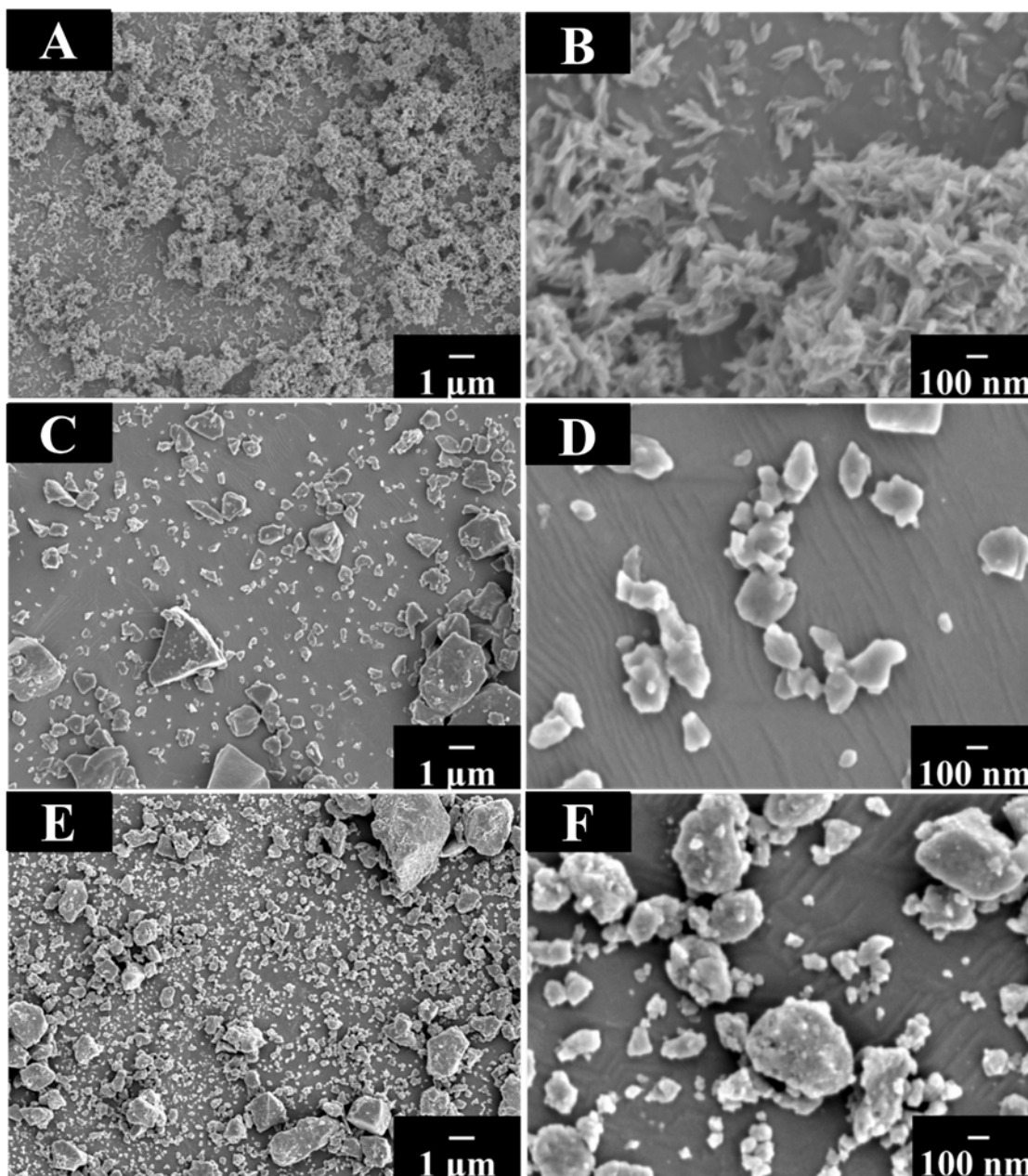


Figure 8-4 SEM images at different magnifications for composite films prepared by cathodic EPD using (A,B) as-precipitated HA, (C,D) titania annealed at 400°C for 1 h, (E,F) zirconia annealed at 400°C for 1 h, for materials synthesized using BPEI.

The approach developed in this investigation can be used for synthesis of other inorganic materials and their co-EPD with other cationic polymers.

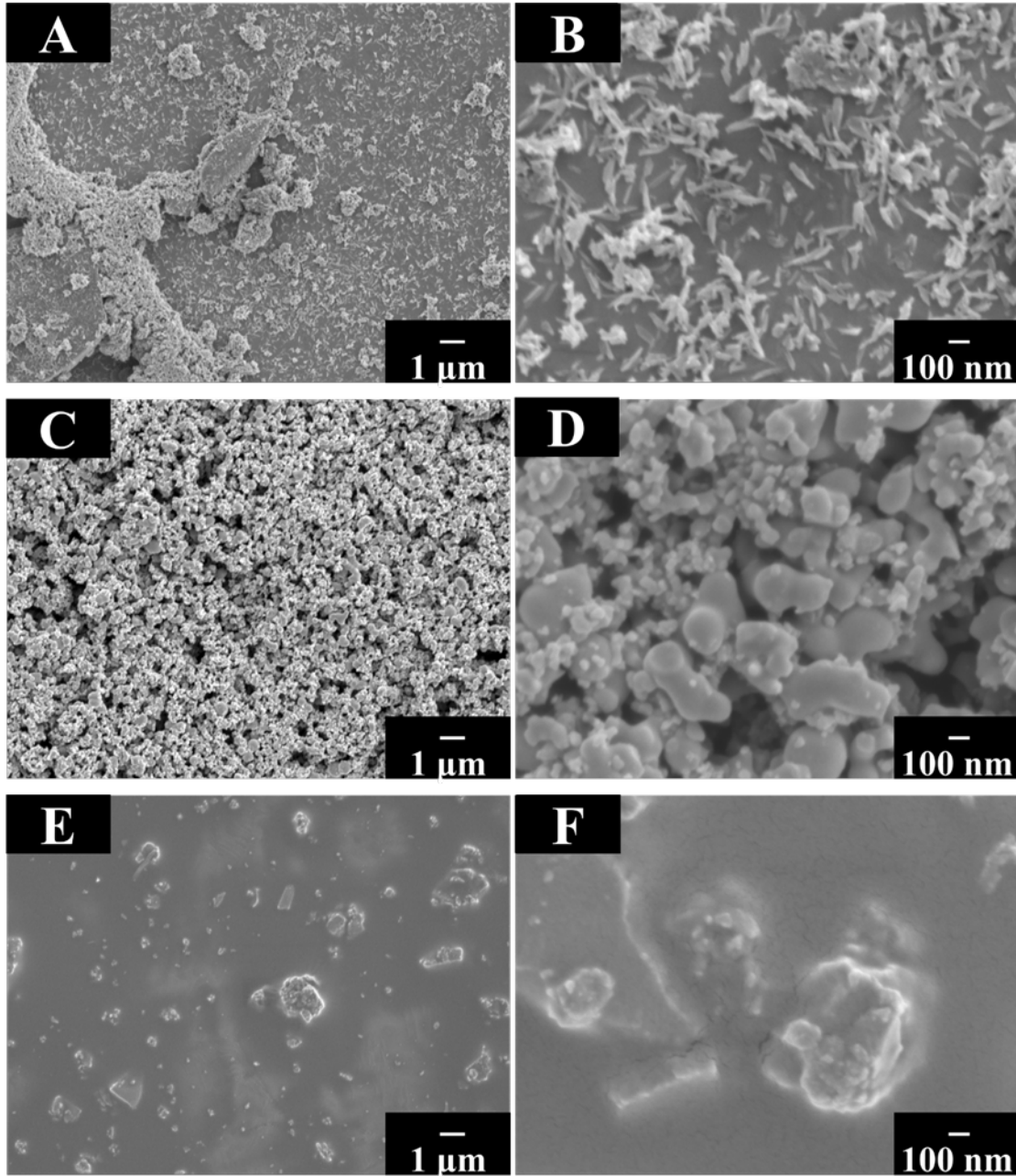


Figure 8-5 SEM images at different magnifications for composite films prepared by cathodic EPD using (A,B) as-precipitated brushite, (C,D) titania annealed at 600°C for 1 h, (E,F) zirconia annealed at 600°C for 1 h, for materials synthesized using L-arginine.

The use of L-arginine facilitated the deposition of composite coatings containing drugs. It should be noted that many drugs show poor solubility in water and significant challenges are related to their EPD[46, 55]. Such problems can be addressed using L-arginine, which is

increasingly being explored as an alkalizer for solubilization of different drugs [45-47]. The use of anionic L-arginine is beneficial for overcoming limitations of cationic PEI and other cationic polymers for drug and gene delivery[56, 57]. It is also known that AlgH is advanced polymer for drug delivery applications[58, 59]. There are excellent reviews describing drug delivery applications of AlgH in different forms, such as capsules, gels, and films[40, 60-62]. Our approach was based on solubilization of AlgH and ibuprofen drug in aqueous solutions, containing L-arginine as an alkalizer. Ibuprofen was used as a model drug, which has poor solubility in water, for the development of composite films by EPD.

It was found that AlgH and ibuprofen can be dissolved in water by the solution pH adjustment to 8.5 using L-arginine. It is suggested that the dissociation of carboxylic groups of AlgH (Figure 8-1C) and L-arginine (Figure 8-6A) facilitates their dissolution and formation of corresponding anionic species. However, investigations[46] of solubilization of drug molecules in the presence of L-arginine showed that the dissolution mechanism is more complex. It involved the formation of drug-alkalizer ion-pair complexes with low binding energy, compared to the energy of H-bonds between the drug molecules. The formation of weakly bonded ion-pair complexes facilitated the dissolution process. Another important finding was the feasibility of EPD of AlgH films from pure AlgH solutions. The deposition yield measurements showed that relatively high deposition rate of $\sim 1 \text{ mg cm}^{-2} \text{ min}^{-1}$ was achieved at a deposition voltage of 10 V. The deposition yield increased with increasing deposition voltage. However, the increase of deposition voltage above 30 V resulted in enhanced gas evolution and enhanced film porosity. Relatively smooth AlgH films were obtained at a deposition voltage of 10 V (Figure 8-7A,B) from AlgH solutions. The SEM images at different magnifications showed that the films were crack-free. Composite films were obtained from AlgH solutions containing ibuprofen. Figure 8-6B

shows X-ray diffraction patterns of deposited AlgH, as-received ibuprofen and co-deposited AlgH and ibuprofen. The X-ray diffraction pattern of AlgH showed (Figure 8-6B) broad peaks in the 2θ range of 10-25 degrees. The X-ray diffraction pattern of ibuprofen (Figure 8-6B) showed peaks corresponding to JCPDS file 00-032-1723 of this material. Similar peaks were observed in the diffraction pattern of the composite (Figure 8-6B). Therefore, X-ray diffraction studies provided evidence of co-deposition of AlgH and ibuprofen.

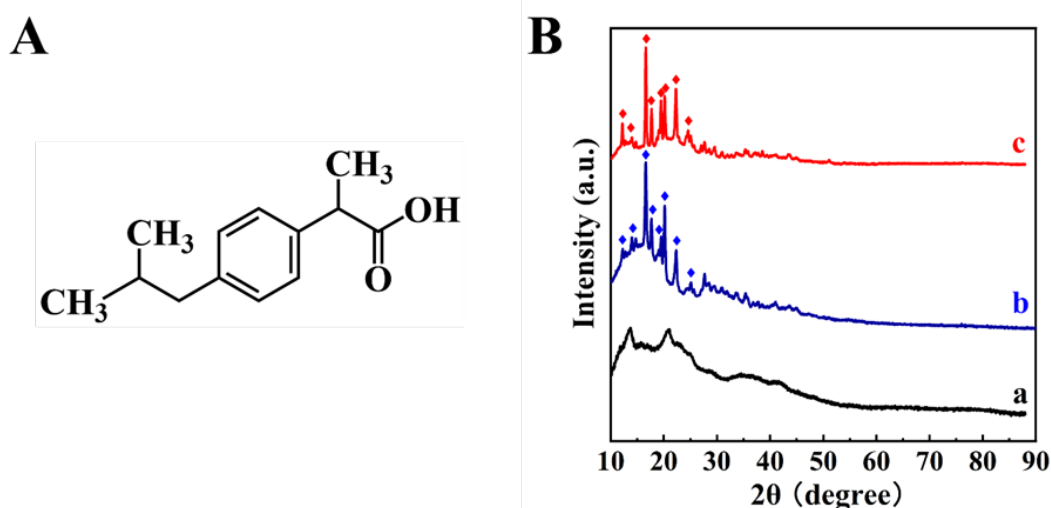


Figure 8-6 (A) chemical structure of ibuprofen, (B) X-ray diffraction patterns of (a) deposited AlgH, (b) as-received ibuprofen and (c) co-deposited AlgH and ibuprofen (♦-peaks corresponding to JCPDS file 00-032-1723 of ibuprofen).

SEM studies of the composite film showed changes in morphology of the composite AlgH-ibuprofen film, compared to pure AlgH film (Figure 8-7). The composite film showed pores with a typical size of 0.1- 0.2 μm . The analysis of SEM images at different magnifications showed that the films were crack-free and contained fibers.

FTIR studies provided additional evidence of composite film deposition. Figure 8-8 shows results of the FTIR studies.

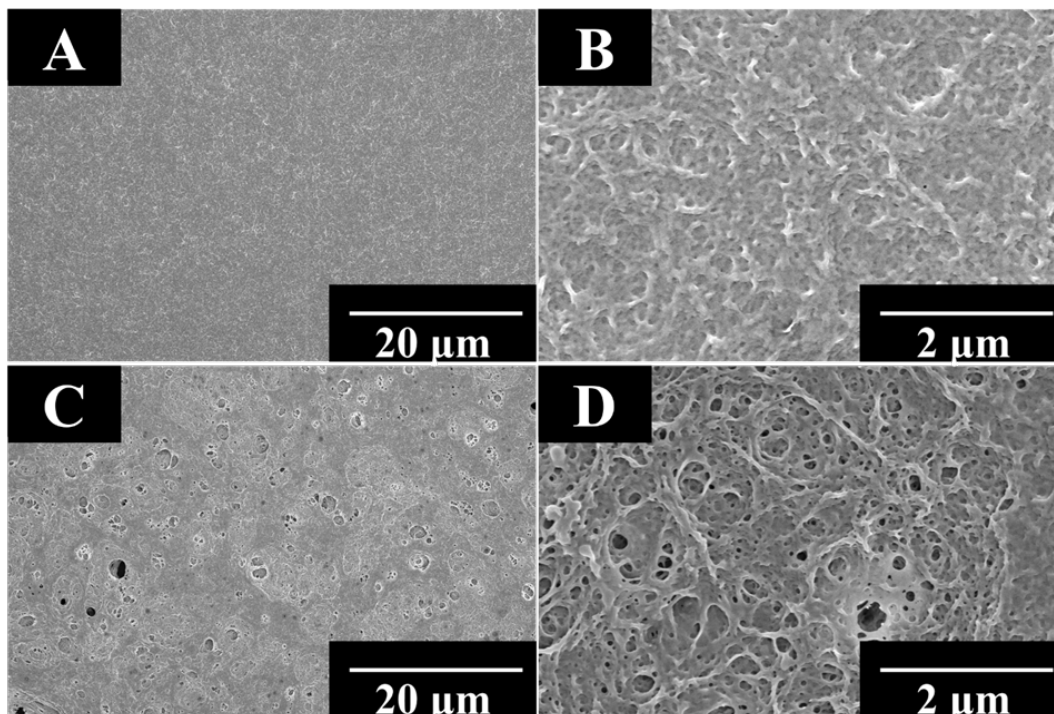


Figure 8-7 SEM images of films at different magnifications: (A,B) AlgH and (C,D) AlgH-ibuprofen

The FTIR spectrum of L-arginine agrees with literature data[63]. It contains a weak absorption due to C=O stretching at $1,672\text{ cm}^{-1}$ and a weak band due to asymmetric NH_3^+ deformation at $1,612\text{ cm}^{-1}$. The absorption peaks at $1,473\text{ cm}^{-1}$ and $1,418\text{ cm}^{-1}$ are related to COO^- vibrations modes. The peak at 1132 cm^{-1} is assigned to symmetric (C–N) stretching. Absorption at 972 cm^{-1} is due to NH_3^+ rocking vibrations and a weak peak due to C–H stretching is observed at 604 cm^{-1} .

As-received AlgH showed characteristic peaks of AlgH[64], such as absorptions due to vibrations of protonated COOH groups at 1727 cm^{-1} and peaks due to C–H and O–C–H stretching at 1233 and 1174 cm^{-1} , respectively. Strong C–O stretching vibrations produced a peak at 1031 cm^{-1} . The small peaks in the range of $922 - 735\text{ cm}^{-1}$ are related to vibrations of C–O and C–H groups, mannuronic and guluronic acid residues in agreement with literature data[64]. The

spectrum of deposited AlgH showed similar peaks. The peaks of L-arginine were not observed in the spectrum of the deposited AlgH. The FTIR studies of as-received ibuprofen showed characteristic strong peaks of this material at 1718, 1419, 1230 and 935 cm^{-1} related to COOH vibrations, C-C stretching, C-O stretching and O-H bending, respectively [65-67]. The FTIR spectrum of co-deposited AlgH and ibuprofen showed peaks of both materials and confirmed their co-deposition.

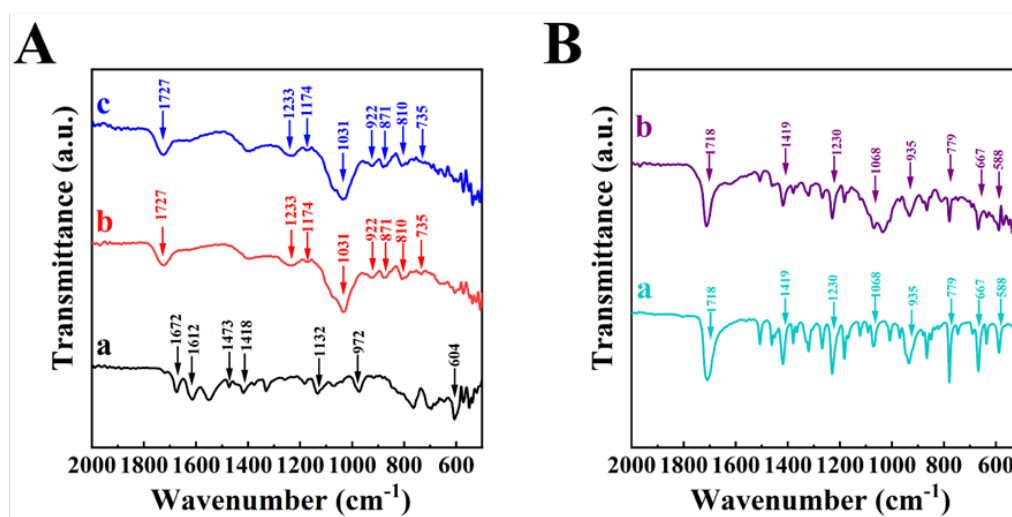


Figure 8-8 FTIR spectra of (A) (a) as-received L-arginine, (b) as-received AlgH, (c) deposited AlgH; (B) (a) as-received ibuprofen, (b) deposited AlgH-ibuprofen.

The co-deposition mechanism involved electrophoresis of anionic species of dissociated AlgH and ibuprofen, containing COO^- groups, local pH decrease at the anode surface, protonation of the COO^- groups of both materials and formation of insoluble composite films. The approach developed in this investigation can be used for EPD of other polymers for biomedical applications, such hyaluronic acid, polyacrylic acid, polygalacturonic acid and other polymers, containing carboxylic groups. Such polymers can be co-deposited with various anionic drugs and other functional molecules using L-arginine as an alkaliizer for improvement of their solubility. The

application of AlgH for deposition instead of AlgNa used in a previous investigation[37] offers benefits for co-deposition of AlgH with inorganic materials, such as bioceramics. It is challenging to obtain stable suspensions of bioceramic particles in AlgNa solutions, containing Na^+ ions, which promote precipitation and can contaminate the deposited films. In contrast, L-arginine can be adsorbed on particles[68] and facilitate their dispersion. Previous investigation[37] also showed that cathodic and anodic EPD techniques can be combined for the fabrication of multilayer and functionally graded films, containing layers of different functional materials and biopolymers. Therefore, the results of this investigations open a new and unexplored route for synthesis and EPD of different materials and composites.

8.5. Conclusion

BPEI and L-arginine can be used as organic alkalizers-capping agents for the synthesis of inorganic nanoparticles, such as HA, zirconia and titania. The use of alkalizers-capping agents offers multiple benefits, such as simple and environmentally friendly synthesis procedure and fabrication of nanoparticles of reduced size. Composite films containing LPEI and bioceramics were obtained using cathodic EPD. For the first time AlgH films were obtained by anodic EPD using L-arginine as an alkalizer, which facilitated fabrication of AlgH solutions. The use of L-arginine as an alkalizer for solubilization of AlgH and ibuprofen allowed the fabrication of composite films. The strategies developed in this investigation can be used for synthesis of other materials, anodic EPD of other advanced biopolymers, containing drugs, bioceramics and other functional materials.

8.6. Acknowledgements

Research supported by the Natural Sciences and Engineering Research Council of Canada, grant RGPIN-2018-04014 and CRC program. Electron microscopy studies were performed at the Canadian Centre for Electron Microscopy.

8.7. References

[1] H. Batili, B. Hamawandi, A.B. Ergül, M.S. Toprak, On the electrophoretic deposition of Bi₂Te₃ nanoparticles through electrolyte optimization and substrate design, *Colloids and Surfaces A: Physicochemical and Engineering Aspects* 649 (2022) 129537.

[2] O. Urrea Sanchez, J. Artigas-Arnaudas, A.J. Sánchez-Herencia, B. Ferrari, A. Ureña, M. Sánchez, Cathodic electrophoretic deposition (EPD) of two-dimensional colloidal Ni(OH)₂ and NiO nanosheets on carbon fibers (CF) for binder-free structural solid-state hybrid supercapacitor, *Journal of Energy Storage* 81 (2024) 110373.

[3] I. Corni, M.P. Ryan, A.R. Boccaccini, Electrophoretic deposition: From traditional ceramics to nanotechnology, *Journal of the European Ceramic Society* 28(7) (2008) 1353-1367.

[4] H. Yi, L.-Q. Wu, W.E. Bentley, R. Ghodssi, G.W. Rubloff, J.N. Culver, G.F. Payne, Biofabrication with Chitosan, *Biomacromolecules* 6(6) (2005) 2881-2894.

[5] P.S. Boone, S. Harris, C. Ramon, J. Shusterman, A.J. Pascall, T. Parsons-Davis, Electrophoretic deposition for improved trace element homogeneity in silica reference materials, *Materials Letters* 361 (2024) 136089.

[6] B. Ferrari, R. Moreno, EPD kinetics: A review, *Journal of the European Ceramic Society* 30(5) (2010) 1069-1078.

[7] A. Błoniarz, J. Marchewka, M. Sitarz, K. Drożdż, T. Gosiewski, M. Brzywczy-Włoch, T. Moskalewicz, Effect of adding selected carboxylic acids to the solution on electrophoretic deposition, adhesion strength, morphology and antibacterial properties of chitosan coatings on titanium, *Progress in Organic Coatings* 189 (2024) 108258.

[8] O. Ekhlasiosgouei, F. Smeacetto, S. Molin, Suspension and process parameters selection for electrophoretic deposition of Mn–Co spinel coating on steel interconnects, *International Journal of Hydrogen Energy* 60 (2024) 1054-1067.

[9] R. Sikkema, K. Baker, I. Zhitomirsky, Electrophoretic deposition of polymers and proteins for biomedical applications, *Adv Colloid Interface Sci* 284 (2020) 102272.

[10] T. Moskalewicz, M. Warcaba, A. Łukaszczyk, M. Kot, A. Kopia, Z. Hadzhieva, A.R. Boccaccini, Electrophoretic deposition, microstructure and properties of multicomponent sodium alginate-based coatings incorporated with graphite oxide and hydroxyapatite on titanium biomaterial substrates, *Applied Surface Science* 575 (2022) 151688.

[11] X. Sun, C. Cai, Q. Wang, D. Cai, J. Qian, Y. Chi, K. Zheng, X. Zhang, G. Zhang, K. Zhong, A polyethylenimine functionalized porous/hollow nanoworm as a drug delivery system and a bioimaging agent, *Physical Chemistry Chemical Physics* 18(11) (2016) 7820-7828.

[12] L. Shen, L. Zhang, M. Chen, X. Chen, J. Wang, The production of pH-sensitive photoluminescent carbon nanoparticles by the carbonization of polyethylenimine and their use for bioimaging, *Carbon* 55 (2013) 343-349.

[13] L. Shao, K. Wan, H. Wang, Y. Cui, C. Zhao, J. Lu, X. Li, L. Chen, X. Cui, X. Wang, A non-conjugated polyethylenimine copolymer-based unorthodox nanoprobe for bioimaging and related mechanism exploration, *Biomaterials science* 7(7) (2019) 3016-3024.

[14] H. Kim, R. Namgung, K. Singha, I.-K. Oh, W.J. Kim, Graphene oxide–polyethylenimine nanoconstruct as a gene delivery vector and bioimaging tool, *Bioconjugate chemistry* 22(12) (2011) 2558-2567.

[15] L. Zou, S.Y. Lee, Q. Wu, H. Zhang, A. Bastian, C. Orji, G. Payne, A. Galvez, T. Thomas, Z. Zhang, H. Dou, Facile Gene Delivery Derived from Branched Low Molecular Weight Polyethylenimine by High Efficient Chemistry, *J Biomed Nanotechnol* 14(10) (2018) 1785-1795.

[16] C.N. Lungu, M.V. Diudea, M.V. Putz, I.P. Grudzinski, Linear and Branched PEIs (Polyethylenimines) and Their Property Space, *Int J Mol Sci* 17(4) (2016) 555.

[17] U. Lungwitz, M. Breunig, T. Blunk, A. Göpferich, Polyethylenimine-based non-viral gene delivery systems, *European Journal of Pharmaceutics and Biopharmaceutics* 60(2) (2005) 247-266.

[18] S. Taghavi, A.H. Nia, K. Abnous, M. Ramezani, Polyethylenimine-functionalized carbon nanotubes tagged with AS1411 aptamer for combination gene and drug delivery into human gastric cancer cells, *International journal of pharmaceutics* 516(1-2) (2017) 301-312.

[19] A. Zakeri, M.A.J. Kouhbanani, N. Beheshtkhoo, V. Beigi, S.M. Mousavi, S.A.R. Hashemi, A. Karimi Zade, A.M. Amani, A. Savardashtaki, E. Mirzaei, S. Jahandideh, A. Movahedpour, Polyethylenimine-based nanocarriers in co-delivery of drug and gene: a developing horizon, *Nano Reviews & Experiments* 9(1) (2018) 1488497.

[20] J. Zhao, C. Lu, X. He, X. Zhang, W. Zhang, X. Zhang, Polyethylenimine-grafted cellulose nanofibril aerogels as versatile vehicles for drug delivery, *ACS applied materials & interfaces* 7(4) (2015) 2607-2615.

[21] P. Pandey, G. Pandey, R. Narayan, Polyethylenimine-mediated controlled synthesis of Prussian blue-gold nanohybrids for biomedical applications, *J Biomater Appl* 36(1) (2021) 26-35.

[22] Y. Zou, D. Li, M. Shen, X. Shi, Polyethylenimine-Based Nanogels for Biomedical Applications, *Macromolecular Bioscience* 19(11) (2019) 1900272.

[23] H. Khalil, T. Chen, R. Riffon, R. Wang, Z. Wang, Synergy between polyethylenimine and different families of antibiotics against a resistant clinical isolate of *Pseudomonas aeruginosa*, *Antimicrobial agents and chemotherapy* 52(5) (2008) 1635-1641.

[24] A.K. Tiwari, M.K. Gupta, G. Pandey, R.J. Narayan, P.C. Pandey, Molecular weight of polyethylenimine-dependent transfection and selective antimicrobial activity of functional silver nanoparticles, *Journal of Materials Research* 35(18) (2020) 2405-2415.

[25] M. Liu, J. Li, B. Li, Mannose-modified polyethylenimine: a specific and effective antibacterial agent against *Escherichia coli*, *Langmuir* 34(4) (2018) 1574-1580.

[26] N. Beyth, Y. Houry-Haddad, L. Baraness-Hadar, I. Yudovin-Farber, A.J. Domb, E.I. Weiss, Surface antimicrobial activity and biocompatibility of incorporated polyethylenimine nanoparticles, *Biomaterials* 29(31) (2008) 4157-4163.

[27] B.C. Simionescu, M. Drobot, D. Timpu, T. Vasiliu, C.A. Constantinescu, D. Rebleanu, M. Calin, G. David, Biopolymers/poly(ϵ -caprolactone)/polyethylenimine functionalized nano-hydroxyapatite hybrid cryogel: Synthesis, characterization and application in gene delivery, *Materials Science and Engineering: C* 81 (2017) 167-176.

[28] M. Delyanee, A. Solouk, S. Akbari, E. Seyedjafari, Modification of electrospun poly(L-lactic acid)/polyethylenimine

nanofibrous scaffolds for biomedical application, *International Journal of Polymeric Materials and Polymeric Biomaterials* 67(4) (2018) 247-257.

[29] Q. Li, C. Wu, B. Zhang, Hybrid hydrogels based on polyvinyl alcohol, branched polyethylenimine, polydopamine, and phosphonium-based ionic liquid for effective synergetic antibacterial applications, *Colloids and Surfaces A: Physicochemical and Engineering Aspects* 648 (2022) 129277.

[30] S. Shi, K. Shi, L. Tan, Y. Qu, G. Shen, B. Chu, S. Zhang, X. Su, X. Li, Y. Wei, Z. Qian, The use of cationic MPEG-PCL-g-PEI micelles for co-delivery of Msurvivin T34A gene and doxorubicin, *Biomaterials* 35(15) (2014) 4536-4547.

[31] Y. Zhu, X. Li, D. Zhang, H. Bao, Y. Shu, X. Guo, Y. Yin, Tuning the surface charges of MoO₃ by adsorption of polyethylenimine to realize the electrophoretic deposition of high-exothermic Al/MoO₃ nanoenergetic films, *Materials & Design* 109 (2016) 652-658.

[32] M. Mishra, Y. Sakka, C. Hu, T.S. Suzuki, T. Uchikoshi, L. Besra, Electrophoretic deposition of Ti₃SiC₂ and texture development in a strong magnetic field, *Journal of the American Ceramic Society* 95(9) (2012) 2857-2862.

[33] M. Lifshitz, A. Greenbaum, K. Sasaki, A. Gladkikh, Y. Feldman, D. Golodnitsky, Electrophoretically deposited LAGP-based electrolytes-Structure and ion transport in plasticized systems, *Journal of Power Sources* 556 (2023) 232502.

[34] Y. Sun, M.S. Ata, I. Zhitomirsky, Electrophoretic deposition of linear polyethylenimine and composite films, *Surface Engineering* 29(7) (2013-08-01).

[35] L.-Q. Wu, A.P. Gadre, H. Yi, M.J. Kastantin, G.W. Rubloff, W.E. Bentley, G.F. Payne, R. Ghodssi, Voltage-Dependent Assembly of the Polysaccharide Chitosan onto an Electrode Surface, *Langmuir* 18(22) (2002) 8620-8625.

[36] Y. Wang, X. Pang, I. Zhitomirsky, Electrophoretic deposition of chiral polymers and composites, *Colloids and Surfaces B: Biointerfaces* 87(2) (2011) 505-509.

[37] M. Cheong, I. Zhitomirsky, Electrodeposition of alginic acid and composite films, *Colloids and Surfaces A: Physicochemical and Engineering Aspects* 328(1-3) (2008) 73-78.

[38] R. Ma, R. Epanand, I. Zhitomirsky, Electrodeposition of hyaluronic acid and hyaluronic acid–bovine serum albumin films from aqueous solutions, *Colloids and Surfaces B: Biointerfaces* 77(2) (2010) 279-285.

[39] Y. Wang, I. Deen, I. Zhitomirsky, Electrophoretic deposition of polyacrylic acid and composite films containing nanotubes and oxide particles, *Journal of colloid and interface science* 362(2) (2011) 367-374.

[40] A. Sosnik, Alginate particles as platform for drug delivery by the oral route: state-of-the-art, *International Scholarly Research Notices* 2014 (2014).

[41] A.C. Hernandez-Gonzalez, L. Tellez-Jurado, L.M. Rodriguez-Lorenzo, Alginate hydrogels for bone tissue engineering, from injectables to bioprinting: A review, *Carbohydr Polym* 229 (2020) 115514.

[42] X.W. Shi, C.Y. Tsao, X. Yang, Y. Liu, P. Dykstra, G.W. Rubloff, R. Ghodssi, W.E. Bentley, G.F. Payne, Electroaddressing of Cell Populations by Co-Deposition with Calcium Alginate Hydrogels, *Advanced Functional Materials* 19(13) (2009) 2074-2080.

[43] Y. Cheng, X. Luo, J. Betz, G.F. Payne, W.E. Bentley, G.W. Rubloff, Mechanism of anodic electrodeposition of calcium alginate, *Soft Matter* 7(12) (2011).

[44] Y. Cheng, X. Luo, C.Y. Tsao, H.C. Wu, J. Betz, G.F. Payne, W.E. Bentley, G.W. Rubloff, Biocompatible multi-address 3D cell assembly in microfluidic devices using spatially programmable gel formation, *Lab Chip* 11(14) (2011) 2316-8.

[45] M. Birer, F. Acartürk, Electrospun orally disintegrating film formulation of telmisartan, *Pharmaceutical Development and Technology* 26(6) (2021) 661-672.

[46] L. Dong, Y. Mai, Q. Liu, W. Zhang, J. Yang, Mechanism and improved dissolution of glycyrrhetic acid solid dispersion by alkalizers, *Pharmaceutics* 12(1) (2020) 82.

[47] P.H.L. Tran, H.T.T. Tran, B.-J. Lee, Modulation of microenvironmental pH and crystallinity of ionizable telmisartan using alkalizers in solid dispersions for controlled release, *Journal of Controlled Release* 129(1) (2008) 59-65.

[48] I. Zhitomirsky, Cathodic electrodeposition of ceramic and organoceramic materials. Fundamental aspects, *Advances in colloid and interface science* 97(1-3) (2002) 279-317.

[49] I. Richard, M. Thibault, G. De Crescenzo, M.D. Buschmann, M. Lavertu, Ionization behavior of chitosan and chitosan–DNA polyplexes indicate that chitosan has a similar capability to induce a proton-sponge effect as PEI, *Biomacromolecules* 14(6) (2013) 1732-1740.

[50] X. Pang, I. Zhitomirsky, Electrophoretic deposition of composite hydroxyapatite-chitosan coatings, *Materials Characterization* 58(4) (2007) 339-348.

[51] X. Pang, I. Zhitomirsky, Electrodeposition of nanocomposite organic–inorganic coatings for biomedical applications, *International Journal of Nanoscience* 4(03) (2005) 409-418.

[52] X. Pang, I. Zhitomirsky, Electrodeposition of composite hydroxyapatite–chitosan films, *Materials Chemistry and Physics* 94(2-3) (2005) 245-251.

[53] X.-L. Xu, H.-Y. Yang, B. Ou, S.-D. Lin, H. Wu, W. He, Q.-C. Jiang, B.-M. Luo, G.-P. Li, Hydroxyapatite nanoparticles modified by branched polyethylenimine are effective non-viral vectors for siRNA transfection of hepatoma cells in vitro, *International Journal of Oncology* 46(5) (2015) 2138-2142.

[54] D.G. Shchukin, G.B. Sukhorukov, H. Möhwald, Biomimetic Fabrication of Nanoengineered Hydroxyapatite/Polyelectrolyte Composite Shell, *Chemistry of Materials* 15(20) (2003) 3947-3950.

[55] N.A. Malik, Solubilization and interaction studies of bile salts with surfactants and drugs: a review, *Applied biochemistry and biotechnology* 179 (2016) 179-201.

[56] Y. Zhou, S. Han, Z. Liang, M. Zhao, G. Liu, J. Wu, Progress in arginine-based gene delivery systems, *Journal of Materials Chemistry B* 8(26) (2020) 5564-5577.

[57] D.V. Patel, M.N. Patel, M.S. Dholakia, B. Suhagia, Green synthesis and properties of arginine derived complexes for assorted drug delivery systems: A review, *Sustainable Chemistry and Pharmacy* 21 (2021) 100441.

[58] J.C. Imperiale, G.B. Acosta, A. Sosnik, Polymer-based carriers for ophthalmic drug delivery, *Journal of controlled release* 285 (2018) 106-141.

[59] R. Augustine, D.L. Ashkenazi, R.S. Arzi, V. Zlobin, R. Shofti, A. Sosnik, Nanoparticle-in-microparticle oral drug delivery system of a clinically relevant darunavir/ritonavir antiretroviral combination, *Acta biomaterialia* 74 (2018) 344-359.

[60] M.J. Martín, A.C. Calpena, F. Fernández, M. Mallandrich, P. Gálvez, B. Clares, Development of alginate microspheres as nystatin carriers for oral mucosa drug delivery, *Carbohydrate polymers* 117 (2015) 140-149.

[61] D. Jain, D. Bar-Shalom, Alginate drug delivery systems: application in context of pharmaceutical and biomedical research, *Drug development and industrial pharmacy* 40(12) (2014) 1576-1584.

[62] L. Agüero, D. Zaldivar-Silva, L. Peña, M.L. Dias, Alginate microparticles as oral colon drug delivery device: A review, *Carbohydrate polymers* 168 (2017) 32-43.

[63] S. Talwatkar, A. Sunatkari, Y. Tamgadge, V. Pahunkar, G. Muley, Influence of Li⁺ and Nd³⁺ co-doping on structural and optical properties of l-arginine-passivated ZnS nanoparticles, *Applied Physics A* 118 (2015) 675-682.

[64] S.K. Papageorgiou, E.P. Kouvelos, E.P. Favvas, A.A. Sapalidis, G.E. Romanos, F.K. Katsaros, Metal–carboxylate interactions in metal–alginate complexes studied with FTIR spectroscopy, *Carbohydrate research* 345(4) (2010) 469-473.

[65] R.B. Carvalho, S.V. Joshi, Ibuprofen isobutanolammonium salt: synthesis, thermal analysis, PXRD, FTIR and solubility investigations, *Journal of Thermal Analysis and Calorimetry* 139(3) (2020) 1971-1976.

[66] M. Ibrahim, A. Nada, D.E. Kamal, Density functional theory and FTIR spectroscopic study of carboxyl group, (2005).

[67] X. Fan, L. Lin, P.B. Messersmith, Surface-initiated polymerization from TiO₂ nanoparticle surfaces through a biomimetic initiator: A new route toward polymer–matrix nanocomposites, *Composites Science and Technology* 66(9) (2006) 1198-1204.

[68] R. Sikkema, B. Keohan, I. Zhitomirsky, Hyaluronic-Acid-Based Organic-Inorganic Composites for Biomedical Applications, *Materials* 14(17) (2021) 4982.

Chapter 9 Conclusions and future work

In summary, the main goal of the research was to develop innovative methods for producing polymer and composite coatings that had advanced features for biomedical applications. The primary goal was achieved by this work. Novel approaches have been devised for the application of advanced polymers and other functional particles. Advanced functionality coatings can be manufactured using new methods, which provide processing advantages. The primary accomplishments of this dissertation can be succinctly described as follows:

1. Instead of hazardous solvents, water-isopropanol was developed to prepare PMMA and composite coatings. Dip coating has been applied as a versatile approach for making composite coatings with bioceramics, antimicrobials, and medicines. PMMA coatings with hydroxyapatite and silica may improve bioactivity and biocompatibility of biomedical implants. Composite coatings with antibacterial characteristics can be made by adding Ag₂O and ZnO to the PMMA matrix. PMMA-ZnO coating can immobilize biosensing molecules and make biosensors. Delivery of drugs is possible with PMMA-drug composite coatings.
2. GA, CFA, CA, and THB charged and dispersed PVDF allowing EPD by adsorbing on chemically inert, electrically neutral PVDF particles. PVDF deposition yield rose sequentially: THB < CFA < CA < GA. PVDF coatings protected metallic substrates against corrosion. GA can be utilized as a charged dispersant for PVDF co-deposition with nanosilica or micron-size silica and fabrication of composite films. Variations in EPD suspension silica concentration affect film composition. GA can be used as a charging co-dispersant for various materials to deposit improved organic–inorganic composites.

3. GRA and RLP can solubilize PEMA without hazardous solvents. We dissolved high molecular mass PEMA and obtained concentrated solutions. These findings helped design a dip coating process for PEMA film deposition, which is adaptable. Chemically inert diamond microparticles and nanoparticles can be dispersed, which is another key finding. GRA and RLP can solubilize PEMA and distribute diamonds, enabling composite PEMA-diamond coatings. Diamond suspension concentration affects film composition. The investigation of film morphologies demonstrated that GRA and RLP chemical structures affect their interactions with PEMA and diamonds. Expanding these investigations may lead to the development of enhanced steroid dispersants for polymer solubilization and material dispersion. Dip coating is a straightforward way to make multilayer PEMA/diamond films and alternating PEMA/diamond films.
4. CHOLNa is a versatile EPD technique for biomolecules of various types that cannot be deposited separately due to low solubility, electrical neutrality, charge reversal at isoelectric points, and high pH-independent charge. Natural bile acid salts can be employed as multifunctional biosurfactants for gentle deposition from aqueous solutions. The EPD mechanism formed mixed micelles and composite gels at the electrode surface. The EPD method for pharmaceuticals, proteins, and HP, which were utilized as model biomaterials, can be applied to make drug delivery films, biosensors, and biocompatible biomedical implant surface modifications.
5. Cyrene is a promising biodegradable solvent that could replace hazardous, carcinogenic solvents for solubilizing PMMA and PEMA. Cyrene also made stable HA, microdiamond, and nanodiamond suspensions. This strategy facilitated the

chemically inert diamond dispersion using biocompatible dispersants. Using rutin as a chelating catecholate-type capping agent produced smaller in size HA nanorods. HA, microdiamond, and nanodiamond composite films were made in PMMA or PEMA matrix. These composite films show promise for biological use. Solvent-particle-polymer interactions and processing parameters affected film shape, composition, and microstructure. This work and literature data on Cyrene solubilization of functional biomolecules allow for the production of films with increased functionality for biomedical and other purposes.

6. As organic alkalizers-capping agents, BPEI and L-arginine can synthesize inorganic nanoparticles like HA, zirconia, and titania. Alkalizer-capping agents allow for simple, ecologically friendly synthesis of smaller nanoparticles. Cathodic EPD produced LPEI-bioceramic composite films. Anodic EPD with L-arginine as an alkalizer produced AlgH films for the first time, enabling the use of AlgH solutions. As an alkalizer, L-arginine solubilized AlgH and ibuprofen to make composite films. This study's methods can be utilized to synthesize additional materials, perform anodic EPD of advanced biopolymers with medicines, bioceramics, and other functional materials.

Based on this work, these techniques can be improved to create microstructures with layers of functional materials regarding to the specific biomedical applications. For example, biocompatible materials make from PEMA/PMMA and composite coatings which are suitable for implants and sensors can be developed. This approach also helps in the combination of HA and some drugs to form implants that can be used to prevent infections and localize the therapy. Successful application of EPD and dipcoating in the preparation of biocomposites gives more

possibilities for synthesis. These methods can be expanded to co-deposit functional organic molecules, biopolymers, and inorganic materials in monolayers or multilayers.